

DISSECTING THE EXTRACELLULAR MECHANISMS OF
NODAL AND ACTIVIN SIGNALING REGULATION

By

Senem Aykul

A DISSERTATION

Submitted to
Michigan State University
in partial fulfillment of the requirements
for the degree of

Biochemistry and Molecular Biology – Doctor of Philosophy

2017

ABSTRACT

DISSECTING THE EXTRACELLULAR MECHANISMS OF NODAL AND ACTIVIN SIGNALING REGULATION

By

Senem Aykul

Transforming Growth Factor- β (TGF- β) family ligands are key regulators of multiple cellular processes including cell proliferation, differentiation, and death. Dysregulation of TGF- β family signaling thus contributes to many human diseases, including cancers, fibrosis, and musculoskeletal disorders. Because of its roles in human diseases, understanding the mechanism and regulation of TGF- β family signal transduction is essential and will help the development of new therapeutic agents that could be used to target the family for treating a number of devastating diseases.

The basic mechanisms of TGF- β family action are well established. A dimeric ligand binds two 'type I' and two 'type II' receptors to form a hexameric complex. Assembly of the ligand-receptor complex in the extracellular space leads to phosphorylation of SMAD transcription factors in the intracellular space, their translocation to the nucleus, and expression of target genes. However, beyond ligands and receptors, many additional factors contribute critically to physiological TGF- β family signaling, including membrane-bound co-receptors, secreted inhibitors, and other ligands that are present on or near the surface of a cell. Elucidating the molecular interplay of all the components that form the TGF- β signal transduction system of a particular cell type or tissue is essential for understanding TGF- β signaling in a cellular context. The goal of my thesis was to investigate the extracellular regulation mechanisms of the TGF- β family ligands, Nodal and Activin using biophysical approaches and to define the physiological consequences using cell-based approaches.

In the first chapter of my dissertation, I introduced the TGF- β family and described how I expressed and purified TGF- β family ligands, receptors, and extracellular regulators. I also introduced a powerful technique called Surface Plasmon Resonance (SPR) that I used to determine the binding modes between TGF- β family members. In the second chapter of my dissertation, I elucidated the molecular function of TGF- β family signaling co-receptor Cripto-1 and its homolog. I demonstrated that soluble Cripto-1 inhibits ligand induced signaling, but the membrane-anchored form potentiates the signaling, suggesting an extracellular capture and endocytic trafficking mechanism. In the third chapter of my dissertation, I characterized the function of the TGF- β family ligand Nodal and its natural inhibitor Cerberus in breast cancer cell lines. I found that Cerberus significantly suppresses migration, invasion, and colony formation of Nodal expressing breast cancer cells. In the fourth chapter of my dissertation, I defined the function of human Cerberus in TGF- β family signaling. I showed that full-length and short forms of human Cerberus share TGF- β family ligand binding and inhibition mechanism, but only full-length Cerberus suppresses MDA-MB-231 breast cancer cell migration. In the fifth chapter of my dissertation, I evaluated how the population of different ligands affects signaling outcomes. I demonstrated that high affinity TGF- β family ligands compete with low affinity ligands for receptor binding and antagonize low affinity ligand signaling. In the sixth chapter of my dissertation, I discussed the possible future directions for this project. Collectively, the results of these experiments provide new information about TGF- β family signaling and regulation, and potentially lead to evaluation of new therapeutics targeting family members in different diseases.

ACKNOWLEDGEMENTS

First and foremost, I would like to thank my supervisor, Dr. Erik Martinez Hackert for his guidance, encouragement, and patience throughout the six years of my PhD studies. He guided me with his great ideas and expertise, but he also taught me how to approach a scientific problem, interpret and criticize the results. His working ethics, open-mindedness, intelligence, scientific vision and passion for science have always motivated me. I am very fortunate to have an amazing advisor like him.

I also want to thank all previous and current members of the Dr. Martinez lab. Especially, I would like to thank Dr. Washington Mutatu. He taught me all the basic techniques when I first joined the lab, but he also has been a really good friend supporting me all the time. Special thanks to all undergraduate assistants worked in the lab, specifically Wendi Ni, Wongsirikul Will, Jake Reske, Elisa Chaparro, Sabeth Dalbo, Alice Chu and Melissa Meschkewitz.

I would like to thank my committee members, Dr. Leslie Kuhn, Dr. Min Hao Kuo, Dr. David Weliky and Dr. Shelagh Ferguson-Miller. Each of them was available to share their expertise and made me think about my research in a new and deeper way.

Finally, my most heartfelt appreciation goes to my mom and dad, and the rest of my family. Their presence, support, love, and encouragement are invaluable important for me. I owe them everything I have. I also would like to thank Asim Addemir and Dilek Addemir for considering me as a member of their family and supporting me all the time since I came to the USA.

TABLE OF CONTENTS

LIST OF TABLES	viii
LIST OF FIGURES	ix
KEY TO ABBREVIATIONS	xi
CHAPTER 1 - INTRODUCTION	1
Discovery of the TGF- β family	2
TGF- β family ligands and receptors	3
Extracellular regulation of TGF- β family signaling	7
Why is it important to study TGF- β family signaling?	11
A general approach for expression of TGF- β family ligands and receptors	12
A general approach to examine the interactions between TGF- β family signaling components	16
REFERENCES	20
CHAPTER 2 – BIOCHEMICAL AND CELLULAR ANALYSIS REVEAL LIGAND BINDING SPECIFICITIES, A MOLECULAR BASIS FOR LIGAND RECOGNITION, AND MEMBRANE ASSOCIATION DEPENDENT ACTIVITIES OF CRIPTO-1 AND CRYPTIC	
Abstract	31
Introduction	32
Materials and Methods	32
TGF- β family ligands	34
Expression plasmids	34
Protein purification	35
Cell lines	35
Surface plasmon resonance	36
Cross-linking	37
Reporter assays	37
Immunoblotting	39
Statistics	39
Results	39
Production of soluble Cripto-1 and Cryptic	39
Cripto-1 and Cryptic bind distinct ligands	42
All Cripto-1 domains are required for ligand binding	45
Cripto-1 glycosylation is necessary for ligand binding	46
Soluble Cripto-1 does not bind type I receptors strongly	47
Cripto-1 and Cryptic block ligand association with type II and some type I receptors	51
Soluble Cripto-1 and Cryptic inhibit signaling	55
Membrane associated Cripto-1 potentiates BMP-4 signaling	57

Discussion	60
REFERENCES	65

CHAPTER 3 –HUMAN CERBERUS PREVENTS NODAL-RECEPTOR BINDING, INHIBITS NODAL SIGNALING, AND SUPPRESSES

NODAL-MEDIATED BREAST CANCER PHENOTYPES	73
Abstract	74
Introduction	74
Materials and Methods	78
Materials	78
Construction of expression plasmids	78
Protein purification	78
Cell lines	79
Immunoblotting	79
Surface plasmon resonance	81
Migration assay	82
Invasion assay	82
Soft agar colony formation assay	83
Reporter assay	83
Statistics	83
Results	84
Nodal binds ALK4, BMPRII and Cripto-1	84
Human Cerberus binds Nodal with high affinity	87
Human Cerberus prevents Nodal interactions and inhibits Nodal signaling	90
Nodal is expressed in invasive breast cancer cell lines and induces invasion	93
Cerberus suppresses aggressive phenotypes of Nodal expressing breast cancer cells	95
Discussion	100
REFERENCES	105

CHAPTER 4 – NEW LIGAND BINDING FUNCTION OF HUMAN CERBERUS AND ROLE OF PROTEOLYTIC PROCESSING IN REGULATING LIGAND RECEPTOR INTERACTIONS AND ANATGONISTIC ACTIVITY

112	
Abstract	113
Introduction	114
Materials and Methods	116
Materials	116
Construction of expression plasmids	116
Protein purification	117
Surface plasmon resonance	117
Cell lines	118
Reporter assays	119
Wound healing	119
Statistics	120

Results	120
The design of Cerberus constructs	120
Different forms of Cerberus have similar ligand binding profiles	124
Cerberus prevents ligand binding to both type I and type II receptors	128
Cerberus inhibits intracellular SMAD signaling	132
Only full-length Cerberus can inhibit migration of MDA-MB-231 breast cancer cells	134
Discussion	138
REFERENCES	142

CHAPTER 5 – TRANSFORMING GROWTH FACTOR- β FAMILY
LIGANDS CAN FUNCTION AS ANTAGONISTS BY COMPETING FOR
TYPE II RECEPTOR BINDING

.....	147
Abstract	148
Introduction	148
Materials and Methods	151
TGF- β family ligands	151
Receptor-Fc constructs	151
Receptor-Fc purification	152
Surface plasmon resonance	152
Cell lines	153
Reporter assays	153
Immunoblotting	154
Statistics	155
Results	155
Type II receptors bind multiple ligands with high affinity	155
Ligands have distinctive, cell-line specific signaling profiles	159
Activin A antagonizes BMP-2 and BMP-7 signaling	162
BMP-2 and BMP-7 signaling is antagonized by high affinity ligands	165
ActRIIA-Fc and Follistatin, but not SB-431542, inhibit Activin A antagonism	168
Activin A inhibits BMP-7 – ActRIIA binding	172
BMP-10 is a weak Activin A antagonist	174
Discussion	174
REFERENCES	180

CHAPTER 6 - FUTURE PERSPECTIVES	188
Discover how Cerberus suppresses breast cancer cell migration and invasion	189
Establish the effect of Cerberus <i>in vivo</i>	190
Determine how EGF-CFC family members recognize TGF- β family ligands	190

LIST OF TABLES

Table 2-1. Binding rate and equilibrium dissociation constants	45
Table 2-2. Half-maximal inhibitory concentration (IC_{50})	57
Table 3-1. Equilibrium dissociation and binding rate constants	87
Table 3-2. Sequence comparison between TGF- β family proteins of different species	89
Table 4-1. Equilibrium dissociation and rate constants	127
Table 4-2. IC_{50} values for SPR binding inhibition and reporter assays	131
Table 5-1. Ligand binding to ActRIIA-Fc, single injection	157
Table 5-2. Ligand binding to ActRIIB-Fc, single injection	157
Table 5-3. Ligand binding to BMPRII-Fc, single injection	158
Table 5-4. Ligand binding to TGF β RII-Fc, single injection	158

LIST OF FIGURES

Figure 1-1. Domain organizations of TGF- β family ligands and receptors	4
Figure 1-2. The overview of TGF- β family signaling	6
Figure 1-3. Expression constructs to make TGF- β family ligands	14
Figure 1-4. Expression constructs to make TGF- β family signaling partners	16
Figure 1-5. SPR approaches to characterize complex interactions	18
Figure 2-1. Construct design and purification	41
Figure 2-2. Ligand binding specificity	44
Figure 2-3. Cripto-1 and Cryptic – receptor interactions	50
Figure 2-4. Mapping of Cripto-1 – ligand interaction	52
Figure 2-5. Mapping of Cryptic – ligand interaction	54
Figure 2-6. Signaling inhibition by soluble Cripto-1 and Cryptic	56
Figure 2-7. Signal-potentiating activities of membrane associated Cripto-1	59
Figure 2-8. Molecular basis of ligand binding	62
Figure 3-1. The Nodal signaling pathway	77
Figure 3-2. Nodal-receptor interactions	85
Figure 3-3. Cerberus ligand binding	88
Figure 3-4. Cerberus inhibition of Nodal interactions	91
Figure 3-5. Nodal inhibition with Cerberus in cell lines	92
Figure 3-6. Nodal induces breast cancer cell invasion	95
Figure 3-7. Cerberus inhibits breast cancer cell migration	98
Figure 3-8. Cerberus suppresses breast cancer cell colony-forming ability	99

Figure 3-9. Proposed mechanism of Cerberus inhibition	102
Figure 4-1. Construct design and purification	122
Figure 4-2. Cerberus ligand binding comparison	125
Figure 4-3. Cerberus ligand binding affinities	126
Figure 4-4. Cerberus inhibition of ligand-type II receptor interactions	129
Figure 4-5. Cerberus inhibition of SMAD2/3 and SMAD1/5/8 signaling	133
Figure 4-6. Cerberus inhibition of breast cancer cell migration	136
Figure 4-7. The effect of different TGF- β family inhibitor on MDA-MB-231 breast cancer cell migration	137
Figure 5-1. Type II receptors bind a range of TGF- β family ligands with high affinity	156
Figure 5-2. TGF- β family signaling activity is cell line dependent	160
Figure 5-3. Activin A antagonizes BMP signaling	164
Figure 5-4. Antagonism of low affinity BMP-2 and BMP-7 signaling is common	167
Figure 5-5. The extracellular Activin A signaling inhibitor ActRIIA-Fc rescues BMP-7 activity	169
Figure 5-6. Activin A role in BMP-2 signal transduction and inhibition with BMP-10.....	171
Figure 5-7. Follistatin suppresses Activin A antagonism	173
Figure 5-8. Model of ligand antagonism	175

KEY TO ABBREVIATIONS

ActRIIA	Activin receptor type IIA
ActRIIB	Activin receptor type IIB
ALK 1	Activin like kinases 1
ALK 2	Activin like kinases 2
ALK 3	Activin like kinases 3
ALK 4	Activin like kinases 4
ALK 5	Activin like kinases 5
ALK 6	Activin like kinases 6
ALK 7	Activin like kinases 7
AMHRII	Anti-muellerian hormone receptor type II
ATCC	The American type culture collection
BMD	Bone mineral density
β ME	Beta mercaptoethanol
BMP	Bone morphogenetic protein
BMPRII	Bone morphogenetic receptor type II
CHO	Chinese hamster ovary
Co-IP	Co-immunoprecipitation
DAN-family	The differential screening-selected gene in neuroblastoma
ECD	Extracellular domain
EGF	Epidermal growth factor
EGF-CFC	Epidermal growth factor-Cripto/FRL-1/Cryptic

EMT	Epithelial-to-mesenchymal transition
ESC	Embryonic stem cell
FBS	Fetal bovine serum
GDF	Growth and differentiation factor
gLuc	Gaussia Luciferase
GPI	Glycosylphosphatidylinositol
GS domain	Glycine serine rich domain
HIC	Hydrophobic interaction chromatography
IC ₅₀	Half-maximal inhibitory concentration
k_a	Association rate constant
k_d	Dissociation rate constant
K_d	Equilibrium dissociation constant
kDa	Kilodalton
LAP	Latency associated peptide
LABP	Latency associated binding protein
MIS	Muellerian inhibiting substance
PAH	Pulmonary arterial hypertension
PBS	Phosphate-buffered saline
PCR	Polymerase chain reaction
P/S	Penicillin/streptavidin
RGM	Repulsive guidance molecule
RLU	Relative luciferase units
RPC	Reverse phase chromatography

RU	Response units
SDS-PAGE	Sodium dodecyl sulfate polyacrylamide gel electrophoresis
SE	Standard error
SEC	Size exclusion chromatography
SGF	Sarcoma growth factor
Smurf1	E3 ubiquitin protein ligase 1
SP	Signal peptide
SPR	Surface plasmon resonance
TBS	Tris buffered saline
TEV	Tobacco etch virus
TGF- β	Transforming growth factor-beta
TGF β RII	Transforming growth factor-beta receptor type II

CHAPTER 1 –
INTRODUCTION

Discovery of the TGF- β family

The transforming growth factor beta (TGF- β) family is composed of multifunctional growth and differentiation factors. Before the discovery of TGF- β in 1978, Dr. Michael Bishop and Dr. Harold Varmus published in 1976 the Nobel Prize winning breakthrough, which gave rise to the identification of TGF- β a few years later (1, 2). Dr. Bishop and Dr. Varmus found that a single viral gene (*v-src*, oncogene) causes neoplastic transformation of a normal cell (2, 3). In the same year, Dr. George Todaro proposed that murine viruses transform normal cells by inducing the secretion of an endogenous, epidermal growth factor (EGF) related molecule with transforming activity (later known as autocrine secretion) (2, 3). In 1979, Dr. De Larco and Dr. Todaro found that secreted growth factors cause normal fibroblast cells to form colonies in soft agar (anchorage-independent growth *in vitro* is correlated with malignant cell growth *in vivo*) (2,4). In contrast to the *v-src* oncogene, secreted factors, but not genetic change, caused the phenotypic transformation (2, 4). Dr. Larco and Dr. Todaro identified these growth factors from Moloney sarcoma virus transformed fibroblast cells (NRK-2B normal fibroblast cells) and called them sarcoma growth factor (SGF) (5). In 1981, Dr. Harold Moses (at Mayo Clinic), and Dr. Michael Sporn and Dr. Anita Roberts (at National Cancer Institute) tried to purify SGF to homogeneity (2, 6, 7). They found that certain fractions didn't have the colony forming ability when they were added to fibroblast cells. However, this property could be rescued with EGF (6, 7). At the end, both groups published that SGF was composed of two different molecules: TGF- α , a member of the EGF family that binds to EGF receptors, and TGF- β , which does not bind EGF receptors (2, 8). Dr. Roberts and Dr. Moses found that TGF- β in combination with EGF

was required for the forming activity (2, 8). From the discovery of first TGF- β family member to today, there are ~100,000 published research papers (2, 9, 10).

TGF- β family ligands and receptors

The transforming growth factor beta (TGF- β) family ligands are key regulators of animal cell physiology (11-14). TGF- β family is composed of two main subfamilies: the TGF- β /Activin/Nodal and the BMP (bone morphogenetic protein)/GDF (growth and differentiation factor)/MIS (muellerian inhibiting substance) subfamilies (11-14). In mammals, TGF- β family consists of 33 ligand genes. These are secreted proteins which are stored in the extracellular matrix. Generally, the active form of the ligand is a disulfide-linked homodimer where each protomer is characterized by a 'cystine knot' structure. A cystine knot is characterized by 3-4 intramolecular disulfide bonds (11-16). TGF- β family ligands are synthesized as precursors that consist of a signal peptide, an approximately 300 amino acid 'pro-' domain, and an approximately 100 amino acid 'mature' domain. The pro-domain is required for effective folding and secretion of the mature domain (17-19). The precursors are processed by Furin family proteases (PACE), which cleave the polypeptide at the junction between pro- and mature domains. Furin family proteases are endoproteases cleaving after a basic RXXR amino acid motif (11, 13, 17, 20). After processing, the pro-domain remains noncovalently bound to the mature domain (17-19). Some mature ligands are inactive or latent when complexed with their pro-domains; others have signaling activity while they are stably associated with their pro-domains (11, 13, 17-19). However, the mature disulfide-linked dimeric ligand is usually considered as an active form of the protein.

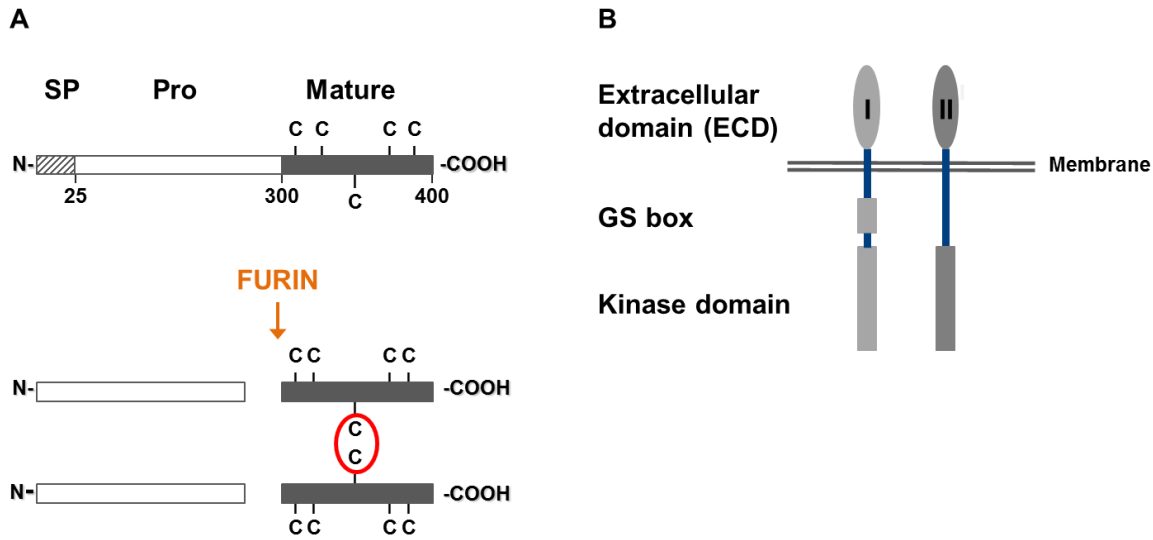


Figure 1-1. Domain organizations of TGF- β family ligands and receptors.

(A) TGF- β family ligands are synthesized as precursors consisting of an N-terminal signal peptide, a pro-domain and a mature domain. Proteolytic processing by Furin family proteases occurs at the junction between pro-domain and mature domains. A disulfide-linked dimeric mature domain is the active form of the protein. (B) TGF- β family signaling type I and type II receptors are composed of an N-terminal signal peptide, an extracellular ligand binding domain, a single span transmembrane domain and a cytoplasmic kinase domain. An intracellular GS (glycine/serine rich) domain is a characteristic of TGF- β family type I receptors.

TGF- β family ligands signal by binding type I and type II receptor serine/threonine kinases on the cell surface (11-15, 18, 21-23). There are five type II receptors (Activin receptor type IIA or ActRIIA; Activin receptor type IIB or ActRIIB; Bone morphogenetic protein receptor type II or BMPRII; Transforming growth factor beta receptor type II or TGF β RII; Anti-muellerian hormone receptor type II or AMHRII) and seven type I receptors (Activin like kinases 1-7, ALK1-7) which are utilized by TGF- β family ligands for signaling. Both type I and type II receptors are composed of an N-terminal extracellular ligand binding domain, a transmembrane domain, and a C-terminal cytoplasmic serine/threonine kinase domain. A dimeric TGF- β family ligand initiates a signaling cascade by binding to two type I

and two type II receptors to form a hexameric complex on the cell surface (11-15, 18, 21-24). Type I receptors contain a 'GS domain' (glycine serine rich domain, SGSGSG sequence), which is located at the N-terminus of the serine/threonine kinase domain. When a TGF- β family forms a signaling complex, the constitutively active serine/threonine kinase type II receptor phosphorylates the GS domain of a type I receptor. This activated type I receptor initiates intracellular signal transduction by phosphorylating receptor SMAD (R-SMAD) transcription factors. R-SMADs are averagely 500 amino acid proteins. In mammals, there are eight SMAD proteins: receptor SMADs (R-SMADs), SMAD1, 2, 3, 5, 8; common SMAD (Co-SMAD), SMAD4; inhibitory SMADs (I-SMAD), SMAD6, 7 (12, 13, 15, 16, 24). There are two canonical signaling pathways that TGF- β family ligands activate; SMAD2/3 and SMAD1/5/8. Two phosphorylated (activated) R-SMADs form a complex with a common SMAD (Co-SMAD), SMAD4. This SMAD complex translocates to the nucleus and interacts with other transcription factors to modulate expression of target genes. R-SMADs and Co-SMAD are composed of N-terminal MH1 and C-terminal MH2 domains connected with a linker region. Only R-SMADs have SXS motif at the C-terminus of the MH2 domain which can be phosphorylated by type I receptor kinases (12, 13, 24). The MH2 domain is responsible for receptor binding and homo/hetero oligomerization, but both MH1 and MH2 domains interact with DNA binding proteins to regulate expression of target genes. Under standard conditions, R-SMADs are mostly found in the cytoplasm, I-SMADs mostly found in the nucleus, and Co-SMAD is found in both. I-SMADs (SMAD6 and SMAD7) are composed of a non-conserved N-terminal domain and an MH2 domain. I-SMADs are negative regulators of TGF- β family signaling (12-14). There are different mechanisms suggested for the action of I-SMADs. In order to end TGF- β family signaling, I-SMADs

might move to the cytoplasm and compete with R-SMADs for receptor binding. SMAD7 can also make complexes with the ‘SMAD Specific E3 Ubiquitin Protein Ligase 1 or 2’ (Smurf1 or Smurf2) to induce degradation of SMAD complexes and type I receptors by ubiquitinating them. In addition, SMAD6 can compete with SMAD1 for SMAD4 binding and this property makes SMAD6 serve as a more specific inhibitor of SMAD1/5/8 signaling.

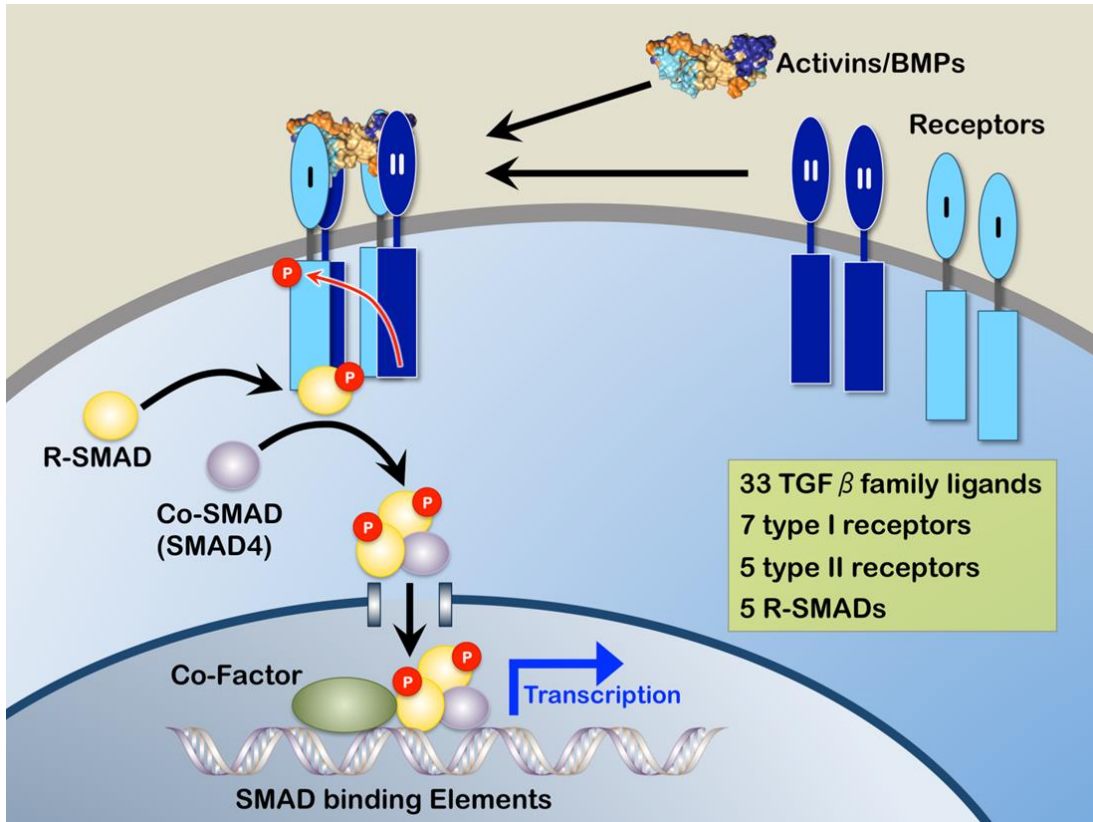


Figure 1-2. The overview of TGF-β family signaling.

TGF-β family pathways are activated when a dimeric ligand (molecular model) binds two ‘type I’ (light blue) and two ‘type II’ receptors (dark blue) to form a signaling complex. This leads to phosphorylation of R-SMAD transcription factors, their translocation to the nucleus, and expression of target genes. Ligands may require accessory ‘co-receptors’ for signaling.

Extracellular regulation of TGF- β family signaling

In TGF- β family, ligand accessibility to receptors and the consequent signaling outcomes are highly controlled (13, 15, 16, 21-25). TGF- β family signaling regulation begins at the ligand activation level. Ligands are synthesized as inactive precursors (11-13, 16, 17, 19). Inactive precursors (pre-pro-polypeptide) are composed of a pro-domain and a mature domain. There is a multistep regulatory process to release the active ligand. Firstly, the covalent bond between pro-domain and mature domain has to be cleaved by proteases like Furin convertase to release the biologically active form of the protein (11-13, 17, 20). However, pro-domain stays associated with the mature domain noncovalently (noncovalently associated prodomain is called as latency associated peptide, LAP) and secreted as a complex after intracellular cleavage by Furin protease. In the extracellular matrix, pro-complexes can be associated with different proteins, such as latency associated binding protein (LTBP) and fibrillin (11-13, 16-19). The activity of the cleaved pro-domain bound form depends on a ligand. For example, cleaved pro-Activin A complex (pro-domain bound Activin A) has the full activity like mature Activin A (12, 13, 17), but cleaved pro-TGF- β -1 (pro-domain bound TGF- β -1) has no activity (latent) (12, 13, 19). In this case, pro-domain of TGF- β -1 keeps mature domain inactive by preventing its binding to receptors. The removal of the prodomain depends on extracellular factors (i.e. the extracellular context), such as proteases, pH of the environment, K_d (equilibrium dissociation constant) between pro-domain and mature domain, the presence of Integrin (transmembrane receptor) to create a physical pulling force by binding the pro-domain, and the presence of other high affinity molecules for the mature domain binding.

Once active TGF- β family ligands are produced, there are also natural antagonists that bind to ligands and inhibit their access to type I and type II receptors. These antagonists are generally soluble extracellular molecules (11, 13, 16, 26, 27). There are four main families of extracellular regulators: The Follistatin, Noggin, Chordin, and DAN- (the differential screening-selected gene in neuroblastoma) families. Each family is composed of several members, but the common feature of these extracellular regulators is blocking one or both receptor binding surfaces to neutralize the activity of a TGF- β family ligand. These regulators have differential affinities for different TGF- β family ligands. For example, Cerberus (a member of DAN-family) binds Activin B and Nodal with high affinity ($K_d \sim 1.0$ nM), but binds BMP-6 with 20 fold lower affinity ($K_d \sim 20.0$ nM) (28, 29). Especially during embryonic development, extracellular regulators have major roles (13, 16, 26, 27, 30). For example, in mouse development, deletion of the *Cerberus* gene caused defects in primitive streak formation as a result of Nodal signaling inhibition (26, 27, 30, 31). In addition to their differential expression profile, the diffusion of these regulators creates a signaling gradient where cells respond differently to the local concentration of a signaling molecule (13, 16, 26, 27, 30).

In addition to these secreted antagonists, there are also membrane anchored accessory proteins (co-receptors) that mediate ligand accessibility to receptors (13, 16, 32). There are four types of co-receptors, which are utilized by TGF- β family ligands: BAMBI, RGMs (repulsive guidance molecule), TGF β RIII (betaglycan), and Cripto-like. Co-receptors are either GPI (glycosylphosphatidylinositol) anchored or have a transmembrane region and a short cytoplasmic domain, which doesn't have kinase activity. Soluble extracellular domains of co-receptors can be released from the membrane-anchored form in the presence of certain

enzymes like metalloproteases. These soluble co-receptor forms regulate TGF- β family signaling either by binding to ligands or their signaling type I and type II receptors. Originally, their role was identified as enhancing signaling by promoting ligand binding to receptors. However, recent studies have shown that co-receptors have a broader role in TGF- β family signaling regulation. For instance, in 2015, Dr. Christian Siebold's group published the crystal structure of RGMC in complex with BMP-2 (a TGF- β family BMP subgroup ligand) (33). This crystal structure in combination with other biochemical studies demonstrated that RGMC binds the type I receptor binding surface of BMP-2. The soluble form of RGMC inhibits BMP-2 induced SMAD1/5/8 signaling by competing with type I receptor binding (BMPRI1A). By contrast, the membrane bound form of RGMC potentiates BMP-2 induced SMAD1/5/8 signaling (33-36). This and other evidence from co-receptor functional studies (including our lab) have supported a generalized model that co-receptors have dual functions (32, 33, 37-40). Like other factors in TGF- β family signaling, the role of co-receptors is context dependent, and their expression is critical for the normal development of the vertebrate embryo, but their misregulated expression is also observed in many diseases (32, 41-46). For example, Cripto-1 knockout is embryonically lethal, and its overexpression is associated with breast, colon, pancreas, and several other cancers (43-46, 49, 50). Generally, co-receptors are more selective for ligand binding than type I or type II receptors and their activities depend on their localization (32, 37). On one hand, membrane anchored forms can potentiate signaling, possibly by directing ligand internalization (32, 37, 51). On the other hand, soluble forms can act as signaling antagonists by making stable complexes with ligands and blocking their binding to their type I or type II receptors (32, 37-39).

The current population of ligands in the extracellular space is also a crucial factor in the TGF- β family signaling regulation. TGF- β family ligands can bind several different receptors, and receptors can bind multiple distinct ligands (11, 13, 16, 18). Significantly, receptor-ligand binding affinities vary greatly (15, 21-23, 25). As a rule, it is suggested that Activins, Inhibins, and TGF- β s first bind type II receptors with high affinity, and then recruit low affinity type I receptor for the signaling complex assembly. On the other hand, it has been proposed that BMPs and GDFs first bind type I receptor with high affinity, and then recruit low affinity type II receptor for signaling complex assembly. This mechanism is called as sequential signaling complex assembly model. There are also exceptional ligands (such as BMP-10) that bind both type I and type II receptors with high affinity. Based on existing ligand-receptor crystal structures, it is well established that high affinity and low affinity ligands bind the same type II receptors at the same epitope (18, 22, 25). Originally, it was believed that the signaling of low affinity BMP and GDF subgroup ligands is independent of the one of high affinity ligands because low affinity ligands uniquely utilize BMPRII as signaling type II receptor (13, 23, 52, 53). However, recently, we and other groups have shown that there are also high affinity ligands for BMPRII (28, 54). In addition, we and other groups have established that high affinity ligands compete with low affinity ligands for type II receptor binding, and they can shut down the signaling mechanism of low affinity ligands and induce theirs. This cross-inhibition mechanism has proved that ligands can also act as antagonists, and added an extra level to the regulation of TGF- β family signaling (55, 56).

Why is it important to study TGF- β family signaling?

TGF- β family proteins are critically important for human health (11-14, 30). Family members regulate cell differentiation, proliferation and maintain homeostasis in healthy tissues (57, 58), but mutations or misexpression cause many fatal human diseases, including cancers, Pulmonary Arterial Hypertension (PAH), and bone loss (57-63).

For example, recent studies have shown that expression of the TGF- β family ligand Nodal is strongly associated with tumorigenesis and metastasis of several human cancers, including glioma, melanoma, breast, pancreatic, and prostate cancers (64-70). Nodal is a key regulator of embryonic development (30, 31). However, Nodal is mostly absent in the adult tissues. This differential expression pattern makes Nodal an attractive target to create potential therapeutics for treating different cancers (66, 70-73).

Another example showing the importance of the TGF- β family in human diseases is BMPRII (one of the 'type II' TGF- β family receptors). Heterozygous loss-of-function mutations in BMPRII are highly correlated with heritable form of Pulmonary Arterial Hypertension (PAH) (74-76), a fatal lung disease characterized by remodeling of pulmonary arteries that leads to elevated pulmonary arterial pressure and ultimately heart failure (77). 80% of heritable PAH and 40% of acquired PAH patients have identified with BMPRII mutations localized throughout the entire gene (13, 57, 58, 74-77). PAH causing mutations lead to reduced BMPRII signaling, leading to PAH onset and progression (74-78). Finding new ways to rescue the reduced BMPRII signaling is important to develop new therapeutics to treat this fatal disease.

Clearly, much evidence shows that targeting the TGF- β family for therapeutic purposes is important. However, development of therapeutics has been challenging. One

underlying reason is that although TGF- β family signaling mechanism seems straightforward, the regulation is highly complex and depends on the context (i.e. the network of receptors, membrane-bound co-receptors, secreted inhibitors, and other ligands that are present on or near the surface of a cell). This complexity makes target identification and drug discovery very challenging. Clarifying the complexity underlying TGF- β family action in normal cell physiology and disease will greatly help the development of new therapeutics for treating cancers, PAH and many other devastating diseases.

Notably, there is currently several advanced clinical developments that target TGF- β family signaling (79-81). Many of these agents inhibit specific TGF- β family ligands. For example, Luspatercept (or ACE-536) (developed by Acceleron Pharma) is a potential drug consisting of a modified extracellular domain of ActRIIB (one of the TGF- β family type II receptors) fused to the Fc domain of human immunoglobulin G1. Luspatercept is currently in phase III clinical trials to treat anemia. Luspatercept specifically targets the TGF- β family ligand, GDF-11 (82, 83). GDF-11 is known as a negative regulator of blood cell differentiation. Luspatercept binds free GDF-11, blocks GDF-11 binding to its signaling receptor, and as a consequence, it inhibits SMAD2/3 signaling. This is an example of the therapeutic significance of TGF- β family.

A general approach for expression of TGF- β family ligands and receptors

Because of its important roles in human diseases, the TGF- β family has enormous therapeutic potential and many biotechnology companies have worked to develop therapeutic agents that target the family. However, it is essential to overcome the difficulty in producing TGF- β family ligands to be more successful in the development of therapeutics. By this way, we can obtain more information about functional, structural and biological characterizations

and, as a result, understand more deeply the specific roles of individual members of the TGF- β family in cell physiology and in human diseases. Several important features of the TGF- β family have to be considered to produce biologically active ligands. First, the mature domain contains a disulfide rich core and generally exists as a disulfide-linked dimer, making the expression of a biologically active protein in prokaryotic systems extremely unreliable, even after refolding from inclusion bodies (11, 13, 18, 84). Second, the C-terminus of the mature domain is highly conserved and buried at the dimer interface, which rules out the introduction of purification tags at the C-terminus of the mature domain (85). Third, TGF- β family ligands require a functional signal peptide for secretion, restricting the use of purification tags at the N-terminus of the pro-domain. Fourth, TGF- β family proteins are processed by Furin family proteases, often necessitating co-expression with these enzymes for proper maturation (11-14, 20, 86-89). And fifth, glycosylation might be required for the stability or the full activity of the growth factor moiety.

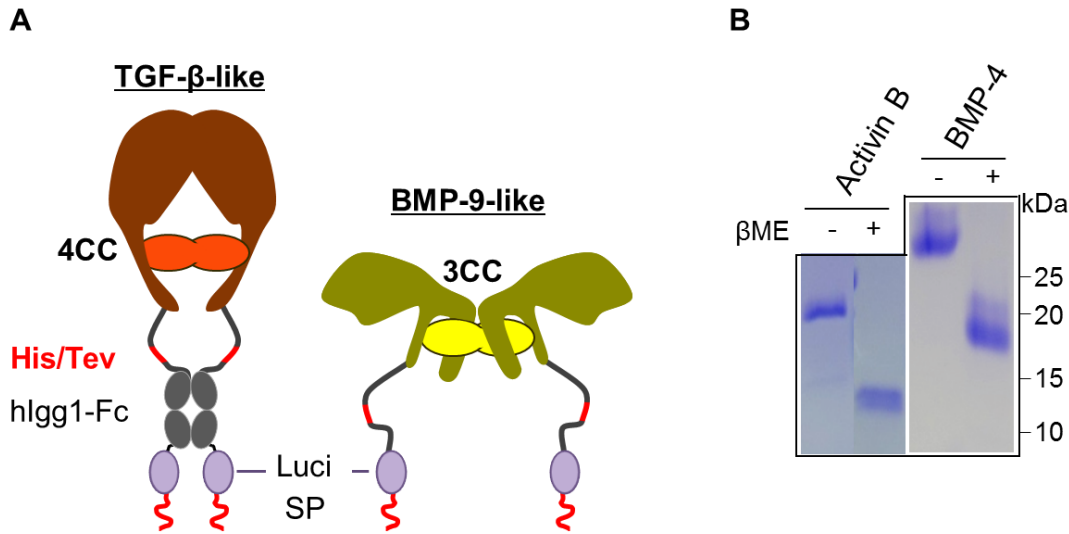


Figure 1-3. Expression constructs to make TGF- β family ligands.

(A) Ligands are synthesized as precursors consisting of pro- and mature domains. According to the crystal structure of ligands in pro-domain bound forms, pro-domains are categorized into TGF- β -like (left, brown) and BMP-9-like (right, green) ones. Mature domains (orange oval represents TGF- β -like mature domains, yellow oval represents BMP-9 like mature domain) lose activity when tagged at the C-terminus. Therefore, purification tags are introduced at the N-terminus of the pro-domain. TGF- β -like ligands have Fc tags, but BMP-9-like ligands only have an 8XHis tag. Gaussia luciferase (Luci) helps secretion and tracing. **(B)** An SDS-PAGE gel shows purified mature domain of Activin B and BMP-4 under reducing and non-reducing conditions (with and without β ME).

In order to overcome these obstacles, we engineered a mammalian expression and purification tag after taking into consideration pro-domain bound crystal structure of TGF- β -1 (19, 86) and BMP-9 (90). TGF- β -1 has four intramolecular disulfide bonds and has a more constrained structure in the pro-domain bound form. BMP-9 has three intramolecular disulfide bonds and has a more flexible structure in the pro-domain bound form. For ligands that have four intramolecular disulfide bonds, the tag includes, from N- to C-terminus, Gaussia Luciferase (gLuc) for secretion, human IgG1-Fc (Fc) for purification, a Tobacco Etch Virus (TEV) protease cleavage site, a hexahistidine tag, and the full-length ligand. For ligands that have three intramolecular disulfide bonds, the tag includes, from N- to C-terminus, gLuc for

secretion, a hexahistidine tag for purification, a TEV protease cleavage site, and the full-length ligand. We found that it was not beneficial to use Fc tag for the expression of ligands having three intramolecular disulfide bonds, speculating that dimerization of Fc tag constrains these molecules, preventing their proper folding and secretion. We express TGF- β family ligands in CHO (Chinese Hamster Ovary) cells. Generally, the mature domain remains stably associated with the pro-domain throughout purification for most of the ligands, and it can only be removed by acidification, urea or guanidine hydrochloride treatment and reversed phase chromatography (RPC). If the molecule has an Fc tag, it is captured from conditioned medium with a Protein A column, and further purified with RPC in the presence of denaturing urea or guanidine hydrochloride. If the molecule doesn't have an Fc tag, it is captured from conditioned medium with heparin or anion/cation exchange column, and further purified with phenyl sepharose column (hydrophobic interaction chromatography, HIC) and/or RPC in the presence of urea or guanidine hydrochloride. The buffer of RPC purified samples is removed in speedvac and samples are reconstituted in 0.1 M acetic acid, and stored at -80 °C. By following this approach, we have obtained biologically active Activin A, Activin B, TGF- β -1, GDF-8, and BMP-4 (Nodal and Lefty-1 purifications are ongoing). Yields of active, mature growth factor range between 0.5 mg/L and 2.0 mg/L culture.

In contrast to TGF- β family ligands, expression and purification of other TGF- β family members, such as type I receptors, type II receptors, co-receptors, and antagonists are comparatively easy. For these molecules, we engineered a mammalian expression construct consisting of (from N- to C-terminus) signal peptide for secretion, the extracellular domain of the protein, TEV protease cleavage site, and an Fc tag for purification. We also express TGF- β family signaling partners in CHO cells. The secreted Fc fusion molecules are purified from

conditioned medium by Protein A affinity capture, and further purified with size exclusion chromatography (SEC). Yields (after SEC) range between 30 mg/L and 300 mg/L. The Fc tag can be removed by cleaving the fusion protein with TEV protease. In that case, cleaved protein is passed over Protein A column to remove Fc tag, and then further purified with SEC. SEC purified protein is dialyzed in 1X PBS, filter-sterilized and stored at -80 °C.

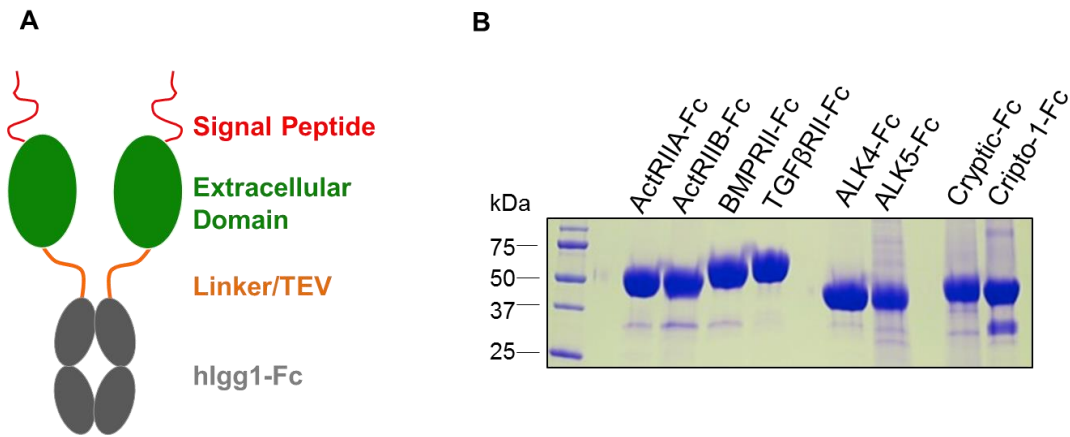


Figure 1-4. Expression constructs to make TGF-β family signaling partners.

(A) Extracellular domains of TGF-β family signaling receptors and co-receptors are fused to human Igg1-Fc via a linker containing a TEV site. (B) An SDS-PAGE shows protein A column purified TGF-β family signaling partners under reducing conditions (with βME).

A general approach to examine the interactions between TGF-β family signaling components

In order to investigate the interactions between TGF-β family signaling components, early research studies mostly relied on co-immunoprecipitation (Co-IP). Although Co-IP is a very useful approach, it might give ambiguous results as a consequence of high concentrations of overexpressed proteins, poorly defined material composition and activity, and the presence of other interacting proteins in the medium. Co-IP has been mostly the preferred approach due to the fact that pure, active TGF-β family ligands and receptors are exceptionally difficult to obtain. Because we have been using a reliable CHO cell expression

system to obtain active TGF- β family ligands and signaling partners, Surface Plasmon Resonance (SPR) has been our main approach to analyze the TGF- β family interaction network. SPR can identify the interactions between ligand-receptor/co-receptor and ligand-antagonist complexes, and how good these interactions are (91). In a standard SPR binding-experiment, one binding partner (the ‘ligand’ in SPR lingo) is immobilized or captured on a sensor chip while the other binding partner (the ‘analyte’ in SPR lingo) is injected over the sensor chip surface. If analyte binds to the ligand, the SPR response increases with increasing analyte concentration until the surface is saturated by the analyte. Binding is detected by measuring changes in the refractive index at the sensor chip surface. The refractive index increases as mass accumulate due to ‘analyte’ binding to the captured ‘ligand’. Changes in the refractive index reveal the association and dissociation of molecules, informing on the kinetic rates of an interaction. Equilibrium binding constants can be derived from these kinetic rates. As SPR is extremely sensitive, it requires relatively small quantities of a test material. Importantly, test proteins do not require molecular labels which can affect their activity. Taken together, these characteristics make SPR especially useful and powerful for studying the TGF- β family interaction network.

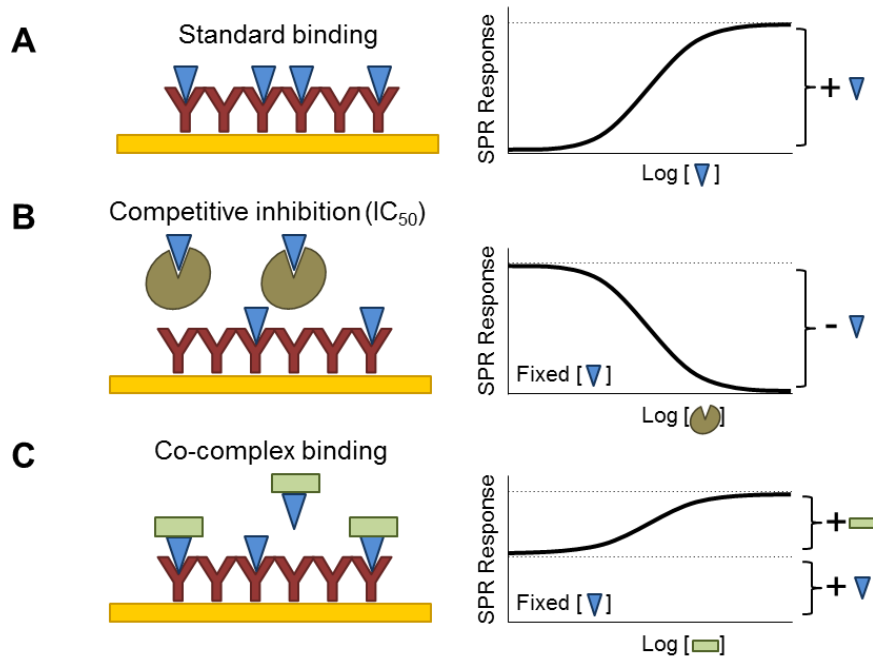


Figure 1-5. SPR approaches to characterize complex interactions.

(A) In a typical SPR binding experiment (left panel), the ‘analyte’ (blue triangle, an example: TGF- β family ligand) is injected at increasing concentrations over the captured ‘ligand’ (an example: Fc fusion TGF- β family signaling partner). If analyte binds to the ligand, the SPR response increases with increasing analyte concentration until the surface is saturated by the analyte. The representative binding isotherm for this model is shown in the right panel. (B) In the competitive inhibitor format (left panel), the analyte concentration is fixed at a level that results in $\sim 80\%$ saturation. The injected sample is preincubated with increasing concentrations of ‘inhibitor’ (dark green circle, an example: Fc-free natural antagonist). The analyte mediated SPR response decreases with increasing inhibitor concentration. The representative binding isotherm for this model is shown in the right panel. (C) If the putative inhibitor forms a complex with the analyte that can bind the captured ligand (left panel), the starting SPR response corresponds to the free analyte response. The SPR response increases with increasing concentration of the co-binder (light green square) until all analyte is captured in a complex. The representative binding isotherm for this model is shown in the right panel.

In addition to this traditional use of SPR, we have also used it to characterize co-operative or inhibitory interactions in the TGF- β family (28, 29, 37, 92). In order to analyze co-operative and inhibitory interactions, one binding partner (the ‘ligand’ in SPR lingo) is immobilized or captured on a sensor chip surface and the fixed concentration of binding

partner (the ‘analyte’ in SPR lingo) preincubated with increasing concentrations of agonist or antagonist (the agent) is injected over the sensor chip surface. Increasing concentrations of the agent are also injected over the ‘ligand’ immobilized surface alone (without the ‘analyte’) to be used as a blank. If there is an increase in the SPR response with increasing agent concentration, this shows that the agent works as an agonist, but if there is a decrease with increasing agent concentration, this shows that the agent works as an antagonist. In this setup, SPR can be used to determine half-maximal inhibitory concentration (IC_{50} , how much of a specific pharmacologic agent is required to inhibit a given biological activity by half) between a specific TGF- β family ligand and an inhibitor (or ligand trap) (91-93). Although IC_{50} values are generally obtained from whole cell system (94-95), it is also very informative to know the efficacy of blocking a specific interaction because TGF- β family signaling is context dependent and regulatory components in different contexts may vary significantly. By comparing theoretical and experimental IC_{50} values from different approaches, we have found that simple plotting of normalized RU values from the association phase (any time point) of SPR as a function of an inhibitor concentration using the non-linear regression algorithm for log (concentration) versus normalized response implemented in GraphPad gives very accurate IC_{50} values for blocking specific interactions (92).

REFERENCES

REFERENCES

1. Stehelin, D., Varmus, H. E., Bishop, J. M., and Vogt, P. K. (1976) DNA related to the transforming gene(s) of avian sarcoma viruses is present in normal avian DNA. *Nature* **260**, 170-173.
2. Moses, H. L., Roberts, A. B., and Derynck, R. (2016) The discovery and early days of TGF- β : A historical perspective. *Cold Spring Harbor Perspectives in Biology* **8**, a021865.
3. Todaro, G. J., De Larco, J. E., and Cohen, S. (1976) Transformation by murine and feline sarcoma viruses specifically blocks binding of epidermal growth factor to cells. *Nature* **264**, 26-31.
4. Todaro, G. J., De Larco, J. E., Marquardt, H., Bryant, M. L., Sherwin, S. A., and Sliski, A. H. (1979) Polypeptide growth factors produced by tumor cells and virus-transformed cells: A possible growth advantage for the producer cells. *Hormones and Cell Culture. Cell Proliferation Conference* **6**, 113–127.
5. De Larco, J. E., and Todaro, G. J. (1980) Sarcoma growth factor (SGF): Specific binding to epidermal growth factor (EGF) membrane receptors. *Journal of Cellular Physiology* **102**, 267-277.
6. Roberts, A. B., Anzano, M. A., Lamb, L. C., Smith, J. M., and Sporn, M. B. (1981) New class of transforming growth factors potentiated by epidermal growth factor: Isolation from non-neoplastic tissues. *Proceedings of the National Academy of Sciences of the United States of America* **78**, 5339-5343.
7. Moses, H. L., Branum, E. L., Proper, J. A., and Robinson, R. A. (1981) Transforming growth factor production by chemically transformed cells. *Cancer Research* **41**, 2842-2848.
8. Anzano, M. A., Roberts, A. B., Smith, J. M., Sporn, M. B., and De Larco, J. E. (1983) Sarcoma growth factor from conditioned medium of virally transformed cells is composed of both type α and type β transforming growth factors. *Proceedings of the National Academy of Sciences of the United States of America* **80**, 6264-6268.
9. Wahl, S. M. (1994) Transforming growth factor β : The good, the bad, and the ugly. *The Journal of Experimental Medicine* **180**, 1587-1590.
10. Garber, K. (2009) Companies waver in efforts to target transforming growth factor β in cancer. *Journal of the National Cancer Institute* **101**, 1664-1667.

11. Massague, J. (1990) The transforming growth factor-beta family. *Annual Review of Cell Biology* **6**, 597-641.
12. Massague, J. (1998) TGF-beta signal transduction. *Annual Review of Biochemistry* **67**, 753-791.
13. Shi, Y., and Massague, J. (2003) Mechanisms of TGF-beta signaling from cell membrane to the nucleus. *Cell* **113**, 685-700.
14. Massague, J. (2012) TGF- β signalling in context. *Nature Reviews. Molecular Cell Biology* **13**, 616-630.
15. Groppe, J., Hinck, C. S., Samavarchi-Tehrani, P., Zubieta, C., Schuermann, J. P., Taylor, A. B., Schwarz, P. M., Wrana, J. L., and Hinck, A. P. (2008) Cooperative assembly of TGF-beta superfamily signaling complexes is mediated by two disparate mechanisms and distinct modes of receptor binding. *Molecular Cell* **29**, 157-168.
16. Zhu, H. J., and Burgess, A. W. (2008) Regulation of transforming growth factor- β signaling. *Molecular Cell Biology Research Communications* **4**, 321-330.
17. Wang, X., Fischer, G., and Hyvonen, M. (2016) Structure and activation of pro-activin A. *Nature Communications* **7**, 12052.
18. Lin, S. J., Lerch, T. F., Cook, R. W., Jardetzky, T. S., and Woodruff, T. K. (2006) The structural basis of TGF- β , bone morphogenetic protein, and activin ligand binding. *Reproduction* **132**, 179-190.
19. Shi, M., Zhu, J., Wang, R., Chen, X., Mi, L., Walz, T., and Springer, T. A. (2011) Latent TGF- β structure and activation. *Nature* **474**, 343-349.
20. Thomas, G. (2002) Furin at the cutting edge: From protein traffic to embryogenesis and disease. *Nature Reviews Molecular Cell Biology* **3**, 753-766.
21. Sako, D., Grinberg, A. V., Liu, J., Davies, M. V., Castonguay, R., Maniatis, S., Andreucci, A. J., Pobre, E. G., Tomkinson, K. N., Monnell, T. E., Ucran, J. A., Martinez-Hackert, E., Pearsall, R. S., Underwood, K. W., Sehra, J., and Kumar, R. (2010) Characterization of the ligand binding functionality of the extracellular domain of activin receptor type IIB. *The Journal of Biological Chemistry* **285**, 21037-21048,
22. Townson, S. A., Martinez-Hackert, E., Greppi, C., Lowden, P., Sako, D., Liu, J., Ucran, J. A., Liharska, K., Underwood, K. W., Sehra, J., Kumar, R., and Grinberg, A. V. (2012) Specificity and structure of a high affinity activin receptor-like kinase 1 (ALK1) signaling complex. *The Journal of Biological Chemistry* **287**, 27313-27325.

23. Mueller, T. D., and Nickel, J. (2012) Promiscuity and specificity in BMP receptor activation. *FEBS Letters* **586**, 1846-1859.
24. Nishimura, R., Hata, K., Ikeda, F., Matsubara, T., Yamashita, K., Ichida, F., and Yoneda, T. (2003) The role of SMADs in BMP signaling. *Frontiers in Bioscience* **8**, 275-284.
25. Khalil, A. M., Dotimas, H., Kahn, J., Lamerdin, J. E., Hayes, D. B., Gupta, P., and Franti, M. (2016) Differential binding activity of TGF- β family proteins to select TGF- β receptors. *The Journal of Pharmacology and Experimental Therapeutics* **358**, 423-430.
26. Chang, C. (2016) Agonists and antagonists of TGF- β family ligands. *Cold Spring Harbor Perspectives in Biology*, 10.1101.
27. Nolan, K., and Thompson, T. B. (2014) The DAN family: Modulators of TGF- β signaling and beyond. *Protein Science* **23**, 999-1012.
28. Aykul, S., Ni, W., Mutatu, W., and Martinez-Hackert, E. (2015) Human cerberus prevents nodal-receptor binding, inhibits nodal signaling, and suppresses nodal-mediated phenotypes. *PLoS One* **10**, e0114954.
29. Aykul, S., and Martinez-Hackert, E. (2016) New ligand binding function of human cerberus and role of proteolytic processing in regulating ligand-receptor interactions and antagonist activity. *Journal of Molecular Biology* **428**, 590-602.
30. Oshimori, N., and Fuchs, E. (2012) The harmonies played by TGF-beta in stem cell biology. *Cell Stem Cell* **11**, 751-764.
31. Schier, A. F. (2003) Nodal signaling in vertebrate development. *Annual Review of Cell and Developmental Biology* **19**, 589-621.
32. Kirkbride, K. C., Ray, B. N., and Blobe, G. C. (2005) Cell-surface co-receptors: Emerging roles in signaling and human disease. *Trends in Biochemical Sciences* **30**, 611-621.
33. Healey, E. G., Bishop, B., Elegheert, J., Bell, C. H., Padilla-Parra, S., and Siebold, C. (2015) Repulsive guidance molecule is a structural bridge between neogenin and bone morphogenetic protein. *Nature Structural and Molecular Biology* **22**, 458-465.
34. Babitt, J. L., Zhang, Y., Samad, T. A., Xia, Y., Tang, J., Campagna, J. A., Schneyer, A. L., Woolf, C. J., and Lin, H. Y. (2005) Repulsive guidance molecule (RGMa), a DRAGON homologue, is a bone morphogenetic protein co-receptor. *The Journal of Biological Chemistry* **280**, 29820-29827.

35. Mueller, T. D. (2015) RGM co-receptors add complexity to BMP signaling. *Nature Structural and Molecular Biology* **22**, 439-440.
36. Wu, Q., Sun, C. C., Lin, H. Y., and Babitt, J. L. (2012) Repulsive Guidance Molecule (RGM) Family Proteins Exhibit Differential Binding Kinetics for Bone Morphogenetic Proteins (BMPs). *PLoS One* **7**, e46307.
37. Aykul, S., Parenti, A., Chu, K. Y., Reske, J., Floer, M., Ralston, A., and Martinez-Hackert, E. (2017) Biochemical and cellular analysis reveal ligand binding specificities, a molecular basis for ligand recognition, and membrane association dependent activities of cripto-1 and cryptic. *The Journal of Biological Chemistry* **292**, 4138-4151.
38. Gray, P. C., Harrison, C. A., and Vale, W. (2003) Cripto forms a complex with activin and type II activin receptors and can block activin signaling. *Proceedings of the National Academy of Sciences of the United States of America* **100**, 5193-5198.
39. Kelber, J. A., Shani, G., Booker, E. C., Vale, W. W., and Gray, P. C. (2008) Cripto is a noncompetitive activin antagonist that forms analogous signaling complexes with activin and nodal. *The Journal of Biological Chemistry* **283**, 4490-4500.
40. Watanabe, K., Nagaoka, T., Lee, J. M., Bianco, C., Gonzales, M., Castro, N. P., Rangel, M. C., Sakamoto, K., Sun, Y., Callahan, R., and Salomon, D. S. (2009) Enhancement of notch receptor maturation and signaling sensitivity by cripto-1. *The Journal of Cell Biology* **187**, 343-353.
41. Ciccodicola, A., Dono, R., Obici, S., Simeone, A., Zollo, M., and Persico, M. G. (1989) Molecular characterization of a gene of the 'EGF family' expressed in undifferentiated human NTERA2 teratocarcinoma cells. *Embo Journal* **8**, 1987-1991.
42. Ciardiello, F., Dono, R., Kim, N., Persico, M. G., and Salomon, D. S. (1991) Expression of cripto, a novel gene of the epidermal growth factor gene family, leads to in vitro transformation of a normal mouse mammary epithelial cell line. *Cancer Research* **51**, 1051-1054.
43. Bianco, C., Strizzi, L., Normanno, N., Khan, N., and Salomon, D. S. (2005) Cripto-1: an oncofetal gene with many faces. *Current Topics Developmental Biology* **67**, 85-133.
44. Klauzinska, M., Castro, N. P., Rangel, M. C., Spike, B. T., Gray, P. C., Bertolette, D., Cuttitta, F., and Salomon, D. (2014) The multifaceted role of the embryonic gene cripto-1 in cancer, stem cells and epithelial-mesenchymal transition. *Seminars in Cancer Biology* **29**, 51-58.
45. Strizzi, L., Bianco, C., Normanno, N., and Salomon, D. (2005) Cripto-1: A multifunctional modulator during embryogenesis and oncogenesis. *Oncogene* **24**, 5731-5741.

46. Xu, C. H., Sheng, Z. H., Hu, H. D., Hao, K. K., Wang, Q. B., and Yu, L. K. (2014) Elevated expression of cripto-1 correlates with poor prognosis in non-small cell lung cancer. *Tumor Biology* **35**, 8673-8678.
47. Yan, Y. T., Gritsman, K., Ding, J., Burdine, R. D., Corrales, J. D., Price, S. M., Talbot, W. S., Schier, A. F., and Shen, M. M. (1999) Conserved requirement for EGF-CFC genes in vertebrate left-right axis formation. *Genes and Development* **13**, 2527-2537.
48. Bamford, R. N., Roessler, E., Burdine, R. D., Saplakoglu, U., dela Cruz, J., Splitt, M., Goodship, J. A., Towbin, J., Bowers, P., Ferrero, G. B., Marino, B., Schier, A. F., Shen, M. M., Muenke, M., and Casey, B. (2000) Loss-of-function mutations in the EGF-CFC gene CFC1 are associated with human left-right laterality defects. *Nature Genetics* **26**, 365-369.
49. Castro, N. P., Fedorova-Abrams, N. D., Merchant, A. S., Rangel, M. C., Nagaoka, T., Karasawa, H., Klauzinska, M., Hewitt, S. M., Biswas, K., Sharan, S. K., and Salomon, D. S. (2015) Cripto-1 as a novel therapeutic target for triple negative breast cancer. *Oncotarget* **6**, 11910-11929.
50. Miyoshi, N., Ishii, H., Mimori, K., Sekimoto, M., Doki, Y., and Mori, M. (2010) TDGF1 is a novel predictive marker for metachronous metastasis of colorectal cancer. *International Journal of Oncology* **36**, 563-568.
51. Blanchet, M. H., Le Good, J. A., Oorschot, V., Baflast, S., Minchiotti, G., Klumperman, J., and Constam, D. B. (2008) Cripto localizes nodal at the limiting membrane of early endosomes. *Science Signaling* **1**, ra13.
52. Rosenzweig, B. L., Imamura, T., Okadome, T., Cox, G. N., Yamashita, H., ten Dijke, P., Heldin, C. H., and Miyazono, K. (1995) Cloning and characterization of a human type II receptor for bone morphogenetic proteins, *Proceedings of the National Academy of Sciences of the United States of America* **92**, 7632-7636.
53. Hinck, A. P. (2012) Structural studies of the TGF-betas and their receptors - insights into evolution of the TGF-beta superfamily, *FEBS Letters* **586**, 1860-1870.
54. Rejon, C. A., Hancock, M. A., Li, Y. N., Thompson, T. B., Hebert, T. E., and Bernard, D. J. (2013) Activins bind and signal via bone morphogenetic protein receptor type II (BMPRII) in immortalized gonadotrope-like cells, *Cellular Signalling* **25**, 2717-2726.
55. Aykul, S., and Martinez-Hackert, E. (2016) Transforming growth factor-beta family ligands can function as antagonists by competing for type II receptor binding. *The Journal of Biological Chemistry* **291**, 10792-10804.

56. Olsen, O. E., Wader, K. F., Hella, H., Mylin, A. K., Turesson, I., Nesthus, I., Waage, A., Sundan, A., and Holien, T. (2015) Activin A inhibits BMP-signaling by binding ACVR2A and ACVR2B. *Cell Communication and Signaling* **13**, 27.
57. Gordon, K. J., and Blobel, G. C. (2008) Role of transforming growth factor- β superfamily signaling pathways in human disease. *Biochimica et Biophysica Acta* **1782**, 197-228.
58. Massagué, J., Blain, S. W., and Lo, R. S. (2000) TGF- β signaling in growth control, cancer, and heritable disorders. *Cell* **103**, 295-309.
59. Antsiferova, M., and Werner, S. (2012) The bright and the dark sides of activin in wound healing and cancer. *Journal of Cell Science* **125**, 3929-3937.
60. Chen, J. L., Walton, K. L., Winbanks, C. E., Murphy, K. T., Thomson, R. E., Makanji, Y., Qian, H., Lynch, G. S., Harrison, C. A., and Gregorevic, P. (2014) Elevated expression of activins promotes muscle wasting and cachexia. *Faseb Journal* **28**, 1711-1723.
61. Hatsell, S. J., Idone, V., Wolken, D. M., Huang, L., Kim, H. J., Wang, L., Wen, X., Nannuru, K. C., Jimenez, J., Xie, L., Das, N., Makhoul, G., Chernomorsky, R., D'Ambrosio, D., Corpina, R. A., Schoenherr, C. J., Feeley, K., Yu, P. B., Yancopoulos, G. D., Murphy, A. J., and Economides, A. N. (2015) ACVR1R206H receptor mutation causes fibrodysplasia ossificans progressiva by imparting responsiveness to activin A. *Science Translational Medicine* **7**, 303ra137.
62. Guglielmo, G. M., Roy, C. L., Goodfellow, A. F., and Wrane, J. L. (2003) Distinct endocytic pathways regulate TGF- β receptor signaling and turnover. *Nature Cell Biology* **5**, 410-421.
63. Hartung, A., Bitton-Worms, K., Rechtman, M. M., Wenzel, V., Boergemann, J. H., Hassel, S., Henis, Y. I., and Petra, K. (2006) Different routes of bone morphogenic protein (BMP) receptor endocytosis influence BMP signaling. *Molecular and Cellular Biology* **26**, 7791-7805.
64. Strizzi, L., Hardy, K. M., Kirschmann, D. A., Ahrlund-Richter, L., and Hendrix, M. J. (2012) Nodal expression and detection in cancer: experience and challenges. *Cancer Research* **72**, 1915-1920.
65. Strizzi, L., Postovit, L. M., Margaryan, N. V., Seftor, E. A., Abbott, D. E., Seftor, R. E., Salomon, D. S., and Hendrix, M. J. (2008) Emerging roles of nodal and cripto-1: from embryogenesis to breast cancer progression. *Breast Disease* **29**, 91-103.

66. Lawrence, M. G., Margaryan, N. V., Loessner, D., Collins, A., Kerr, K. M., Turner, M., Seftor, E. A., Stephens, C. R., Lai, J., Postovit, L. M., Clements, J. A., and Hendrix, M. J. (2011) Reactivation of embryonic nodal signaling is associated with tumor progression and promotes the growth of prostate cancer cells. *Prostate* **71**, 1198-1209.
67. Topczewska, J. M., Postovit, L. M., Margaryan, N. V., Sam, A., Hess, A. R., Wheaton, W. W., Nickoloff, B. J., Topczewski, J., and Hendrix, M. J. (2006) Embryonic and tumorigenic pathways converge via nodal signaling: role in melanoma aggressiveness. *Nature Medicine* **12**, 925-932.
68. Lee, C. C., Jan, H. J., Lai, J. H., Ma, H. I., Hueng, D. Y., Lee, Y. C., Cheng, Y. Y., Liu, L. W., Wei, H. W., and Lee, H. M. (2010) Nodal promotes growth and invasion in human gliomas. *Oncogene* **29**, 3110-3123.
69. Lonardo, E., Hermann, P. C., Mueller, M. T., Huber, S., Balic, A., Miranda-Lorenzo, I., Zagorac, S., Alcalá, S., Rodríguez-Arabaolaza, I., Ramirez, J. C., Torres-Ruiz, R., Garcia, E., Hidalgo, M., Cebrian, D. A., Heuchel, R., Lohr, M., Berger, F., Bartenstein, P., Aicher, A., and Heeschen, C. (2011) Nodal/Activin signaling drives self-renewal and tumorigenicity of pancreatic cancer stem cells and provides a target for combined drug therapy. *Cell Stem Cell* **9**, 433-446.
70. Quail, D. F., Zhang, G., Walsh, L. A., Siegers, G. M., Dieters-Castator, D. Z., Findlay, S. D., Broughton, H., Putman, D. M., Hess, D. A., and Postovit, L. M. (2012) Embryonic morphogen nodal promotes breast cancer growth and progression. *PLoS One* **7**, e48237.
71. Strizzi, L., Postovit, L. M., Margaryan, N. V., Lipavsky, A., Gadiot, J., Blank, C., Seftor, R. E., Seftor, E. A., and Hendrix, M. J. (2009) Nodal as a biomarker for melanoma progression and a new therapeutic target for clinical intervention. *Expert Review of Dermatology* **4**, 67-78.
72. Adkins, H. B., Bianco, C., Schiffer, S. G., Rayhorn, P., Zafari, M., Cheung, A. E., Orozco, O., Olson, D., De Luca, A., Chen, L. L., Miatkowski, K., Benjamin, C., Normanno, N., Williams, K. P., Jarpe, M., LePage, D., Salomon, D., and Sanicola, M. (2003) Antibody blockade of the cripto CFC domain suppresses tumor cell growth in vivo. *The Journal of Clinical Investigation* **112**, 575-587.
73. Kelly, R. K., Olson, D. L., Sun, Y., Wen, D., Wortham, K. A., Antognetti, G., Cheung, A. E., Orozco, O. E., Yang, L., Bailly, V., and Sanicola, M. (2011) An antibody-cytotoxic conjugate, BIIB015, is a new targeted therapy for cripto positive tumours. *European Journal of Cancer* **47**, 1736-1746.

74. International, P. P. H. C., Lane, K. B., Machado, R. D., Pauciulo, M. W., Thomson, J. R., Phillips, J. A., 3rd, Loyd, J. E., Nichols, W. C., and Trembath, R. C. (2000) Heterozygous germline mutations in *BMP2*, encoding a TGF-beta receptor, cause familial primary pulmonary hypertension. *Nature Genetics* **26**, 81-84.
75. Deng, Z., Morse, J. H., Slager, S. L., Cuervo, N., Moore, K. J., Venetos, G., Kalachikov, S., Cayanis, E., Fischer, S. G., Barst, R. J., Hodge, S. E., and Knowles, J. A. (2000) Familial primary pulmonary hypertension (gene PPH1) is caused by mutations in the bone morphogenetic protein receptor-II gene. *The American Journal of Human Genetics* **67**, 737-744.
76. Yang, X., Long, L., Southwood, M., Rudarakanchana, N., Upton, P. D., Jeffery, T. K., Atkinson, C., Chen, H., Trembath, R. C., and Morrell, N. W. (2005) Dysfunctional SMAD signaling contributes to abnormal smooth muscle cell proliferation in familial pulmonary arterial hypertension. *Circulation Research* **96**, 1053-1063.
77. Simonneau, G., Robbins, I. M., Beghetti, M., Channick, R. N., Delcroix, M., Denton, C. P., Elliott, C. G., Gaine, S. P., Gladwin, M. T., Jing, Z. C., Krowka, M. J., Langleben, D., Nakanishi, N., and Souza, R. (2009) Updated clinical classification of pulmonary hypertension. *Journal of the American College of Cardiology* **54**, S43-54.
78. West, J., Austin, E., Fessel, J. P., Loyd, J., and Hamid, R. (2014) Rescuing the *BMP2* signaling axis in pulmonary arterial hypertension. *Drug Discovery Today* **19**, 1241-1245.
79. Huang, C. (2009) Receptor-Fc fusion therapeutics, traps, and mimetibody technology. *Current Opinion in Biotechnology* **20**, 692-699.
80. Economides, A. N., and Stahl, N. (2013) Receptor-Fc and ligand traps as high-affinity biological blockers: Development and clinical applications. *Fusion Protein Technologies for Biopharmaceuticals: Applications and Challenges*, 10.1002/9781118354599.ch9.
81. Adams, T. E., Koziolk, E. J., Hoyne, P. H., Bentley, J. D., Lu, L., Lovrecz, G., Ward, C. W., Lee, F. T., Scott, A. M., Nash, A. D., Rothacker, J., Nice, E. C., Burgess, A. W., and Johns, T. G. (2009) A truncated soluble epidermal growth factor receptor-Fc fusion ligand trap displays anti-tumor activity in vivo. *Growth Factors* **27**, 141-154.

82. Giagounidis, A., Platzbecker, U., Germing, U., Gotze, K., Kiewe, P., Mayer, K. T., Ottmann, O., Radsak, M., Wolff, T., Haase, D., Hankin, M., Wilson, D., Zhang, X., Laadem, A., Sherman, M. L., and Attie, K. M. (2015) Luspatercept Treatment Leads to Long Term Increases in Hemoglobin and Reductions in Transfusion Burden in Patients with Low or Intermediate-1 Risk Myelodysplastic Syndromes (MDS): Preliminary Results from the Phase 2 PACE-MDS Extension Study. *Blood* **126**, 92.
83. Suragani, R. N, Cadena, S. M., Cawley, S. M., Sako, D., Mitchell, D., Li, R., Davies, M. V., Alexander, M. J., Devine, M., Loveday, K S., Underwood, K. W., Grinberg, A. V., Quisel, J. D., Chopra, R., Pearsall, R. S., Seehra, J., and Kumar, R. (2014) Transforming growth factor- β superfamily ligand trap ACE-536 corrects anemia by promoting late-stage erythropoiesis. *Nature Medicine* **20**, 408-414.
84. de Marco, A. (2009) Strategies for successful recombinant expression of disulfide bond-dependent proteins in Escherichia coli. *Microbial Cell Factories* **8**, 26.
85. Wakefield, L. M., Kondaiiah, P., Hollands, R. S., Winokur, T. S., and Sporn, M. B. (1991) Addition of a C-terminal extension sequence to transforming growth factor-beta 1 interferes with biosynthetic processing and abolishes biological activity. *Growth Factors* **5**, 243-253.
86. Gray, A. M., and Mason, A. J. (1990) Requirement for activin A and transforming growth factor--beta 1 pro-regions in homodimer assembly. *Science* **247**, 1328-1330.
87. Cui, Y., Jean, F., Thomas, G., and Christian, J. L. (1998) BMP-4 is proteolytically activated by furin and/or PC6 during vertebrate embryonic development. *Embo Journal* **17**, 4735-4743.
88. Dubois, C. M., Blanchette, F., Laprise, M. H., Leduc, R., Grondin, F., and Seidah, N. G. (2001) Evidence that furin is an authentic transforming growth factor-beta1-converting enzyme. *American Journal of Pathology* **158**, 305-316.
89. Constam, D. B., and Robertson, E. J. (1999) Regulation of bone morphogenetic protein activity by pro domains and proprotein convertases. *The Journal of Cell Biology* **144**, 139-149.
90. Mi, L. Z., Brown, C. T., Gao, Y., Tian, Y., Le, V. Q., Walz, T., and Springer, T. A. (2015) Structure of bone morphogenetic protein 9 procomplex. *Proceedings of the National Academy of Sciences of the United States of America* **112**, 3710-3715.
91. Olaru, A., Bala, C., Jaffrezic-Renault, N., and Aboul-Enein, H. Y. (2015) Surface plasmon resonance (SPR) biosensors in pharmaceutical analysis. *Critical Reviews in Analytical Chemistry* **45**, 97-105.

92. Aykul, S., and Martinez-Hackert, E. (2016) Determination of half-maximal inhibitory concentration using biosensor-based protein interaction analysis. *Analytical Biochemistry* **508**, 97-103.
93. Castonguay, R., Werner, E. D., Matthews, R. G., Presman, E., Mulivor, A. W., Solban, N., Sako, D., Pearsall, R. S., Underwood, K. W., Seehra, J., Kumar, R., and Grinberg, A. V. (2011) Soluble endoglin specifically binds bone morphogenetic proteins 9 and 10 via its orphan domain, inhibits blood vessel formation, and suppresses tumor growth. *The Journal of Biological Chemistry* **286**, 30034-30046.
94. Cortes, A., Cascante, M., Cardenas, M. L., and Cornish-Bowden, A. (2001) Relationships between inhibition constants, inhibitor concentrations for 50% inhibition and types of inhibition: new ways of analyzing data. *Biochemical Journal* **357**, 263-268.
95. Cheng, Y., and Prusoff, W. H. (1973) Relationship between the inhibition constant (K₁) and the concentration of inhibitor which causes 50 per cent inhibition (I₅₀) of an enzymatic reaction. *Biochemical Pharmacology* **22**, 3099-3108.

CHAPTER 2 -

BIOCHEMICAL AND CELLULAR ANALYSIS REVEAL LIGAND BINDING SPECIFICITIES, A MOLECULAR BASIS FOR LIGAND RECOGNITION, AND MEMBRANE ASSOCIATION DEPENDENT ACTIVITIES OF CRIPTO-1 AND CRYPTIC¹

¹The work described in this chapter was published as the following manuscript: Senem Aykul, Anthony Paranti, Kit Y. Chu, Jake Raske, Monique Floer, Amy Ralston, and Erik M. Hackert. (2017) Biochemical and cellular analysis reveal ligand binding specificities, a molecular basis for ligand recognition, and membrane association dependent activities of Cripto-1 and Cryptic. *The Journal of Biological Chemistry* **292**, 4138-4151.

Abstract

Epidermal Growth Factor-Cripto/FRL-1/Cryptic (EGF-CFC) proteins are membrane-associated regulators of TGF- β family signaling. Although their biological functions have been widely studied, their molecular functions remain speculative. For example, it is unclear how many TGF- β family ligands the mammalian EGF-CFC family homologs Cripto-1 and Cryptic regulate, or what their mechanism of action is. Here we show using highly purified human Cripto-1 and mouse Cryptic produced in mammalian cells that these two homologs have distinct, highly specific ligand binding activities. Both Cripto-1 and Cryptic can block ligand binding to the type II Activin Receptors 2A and 2B (ActRIIA and ActRIIB), the type II Bone Morphogenetic Protein (BMP) Receptor 2 (BMPRII), and the type I Activin-Like Receptor Kinase 3 (ALK3). These findings suggest both Cripto-1 and Cryptic contact receptor binding-surfaces on ligands and thus could function as inhibitors of their cognate ligands. Indeed, soluble Cripto-1 and Cryptic inhibited ligand signaling in various cell-based assays, including SMAD mediated luciferase reporter gene expression, and multipotent XEN cell differentiation (data not shown). But the membrane bound form of Cripto-1 potentiated signaling as previously reported, revealing a critical role of membrane association for biological function. In conclusion, our biochemical studies clarify the molecular mechanism of ligand recognition by this enigmatic family of membrane-anchored TGF- β family signaling regulators and link membrane association with their signal potentiating activities.

Introduction

The mammalian ‘Epidermal Growth Factor-Cripto/FRL-1/Cryptic’ (EGF-CFC) family proteins Cripto-1 and Cryptic are membrane-anchored regulators of TGF- β family

signaling that have key roles in early embryonic development (1-6). Cripto-1 (a.k.a. TDGF1) is a marker of stem cell pluripotency that is implicated in embryonic patterning (7-11). Cryptic (CFC1) is associated with heart morphogenesis and left-right asymmetry specification (12-14). Biological functions beyond embryogenesis are not known, but both play major roles in human diseases. Cripto-1 is associated with colon, breast, pancreatic, ovarian, lung and other cancers (15-18). Cryptic is associated with heterotaxy syndromes and other laterality defects (19-21).

Molecular genetic studies have established a functional link between Cripto-1 and the TGF- β family ligand Nodal (4, 22): Nodal co-IPed with Cripto-1 and required Cripto-1 for signaling (9, 13, 23-29). These findings have supported the idea that Cripto-1 and the EGF-CFC family are obligate Nodal ‘co-receptors’ that potentiate Nodal signaling (3, 30, 31). However, the fundamental requirement of Cripto-1 for this function is not certain, as some studies indicated that Nodal can bind its receptors and can have signaling activities without Cripto-1 (8, 25-27, 32, 33). Intriguingly, a number of studies discovered a seemingly contradicting function. Namely, Cripto-1 blocked signaling by the TGF- β family ligands Activin A, Activin B and TGF- β 1, indicating Cripto-1 could also act as antagonist of some ligands (28, 34-36). Together, these findings indicate that the function of Cripto-1 remains unclear. And while Cripto-1 has been widely investigated, less is known about Cryptic, except that it is also implicated in Nodal signaling (13, 29, 30).

To clarify the functions of Cripto-1 and Cryptic, we examined their molecular mechanisms in TGF- β family signaling. Using purified proteins expressed in mammalian cells and protein-protein interaction analysis, we showed human Cripto-1 binds Nodal as expected, but not Activin A or Activin B as previously suggested. Notably, we discovered

Cripto-1 also binds BMP-4 with high affinity, revealing a new regulatory function. By contrast, mouse Cryptic only bound Activin B, indicating its biological activities are different from Cripto-1. We also investigated how Cripto-1 and Cryptic recognize ligands. Using a surface plasmon resonance competition assay (37), we discovered both Cripto-1 and Cryptic inhibited ligand-receptor binding, indicating that they contact the type I and type II receptor recognition surfaces on ligands (38). As both Cripto-1 and Cryptic blocked ligand-receptor binding, we speculated they could inhibit signaling. Using reporter gene expression assays, and an extraembryonic endoderm stem (XEN) cell differentiation assay (data not shown) (39, 40), we demonstrated that soluble forms of Cripto-1 and Cryptic respectively inhibited BMP-4 and Activin B signaling in a cellular context. But in agreement with earlier reports on the role of Cripto-1 in Nodal function, membrane bound Cripto-1 potentiated BMP-4 signaling. This finding reveals a potentially critical role for membrane association in signal potentiation. In sum, we provide a molecular framework that helps explain the function of these enigmatic TGF- β family signaling-regulators. While soluble Cripto-1 and Cryptic can act as inhibitors, membrane-anchored forms could exploit this ligand capture function and localize ligands to endosomal vesicles as a way to potentiate signaling (41, 42).

Materials and Methods

TGF- β family ligands

Activin A (338-AC/CF), Activin B (659-AB/CF) and TGF- β 1 (240-B/CF) were purchased from R&D Systems or produced in house. Nodal (3218-ND/CF), GDF-1 (6937- GD/CF), GDF-3 (958-G3/CF), GDF-8 (788-G8/CF), GDF-11 (1958-GD/CF), GDF-15 (957-GD/CF), BMP-4 (314-BP/CF), and BMP-9 (3209-BP/CF) were purchased from R&D Systems. BMP-2 (C-67309), BMP-6 (C-67307), BMP-7 (C-67319), BMP-10 (C-67317), TGF- β 2 (C-63498),

and TGF- β 3 (C-63508) were purchased from PROMOCCELL. We note both BMP-4 and GDF-3 lose activity within 8 weeks of reconstitution.

Expression plasmids

Synthetic Cripto-1-hIgg-Fc, and Cryptic-hIgg-Fc genes were obtained from GeneArt. Full-length fusion constructs included the human Cryptic signal peptide (1-25), and the extracellular domains (ECD) of human Cripto-1 (amino acid 31-163) and mouse Cryptic (amino acid 36-175). Functional domains were linked to human IgG1-Fc via a 22 amino acid long linker containing a TEV cleavage site, a glycine/serine rich region, and a FLAG-tag. Domain deletion constructs were generated by PCR or were purchased from GeneArt.

Protein purification

Proteins were expressed using stably transfected Chinese Hamster Ovary (CHO) cell pools. The secreted fusion constructs were captured from condition medium using protein A affinity chromatography, eluted with 100 mM Glycine pH 3.0, subjected to size-exclusion chromatography (SEC), dialyzed into phosphate-buffered saline, pH 7.5, and stored at -20 °C or -80 °C. For inhibition assays, cleaved Fc was removed using TEV protease followed by protein A affinity chromatography and SEC. Purity was determined with SDS-PAGE.

Cell lines

CHO cells were obtained from Life Technologies. HepG2 cells (HB-8065) and NTERA2 cl.D1 (NT2/D1) cells (CRL-1973) were obtained from ATCC (American Type Culture Collection) and maintained as indicated by the manufacturer. Briefly, HepG2 and NT2/D1 cells were grown in Eagle's Minimum Essential Medium supplemented with 10% FBS and 1% P/S at 37 °C in 5% CO₂ and 10% CO₂, respectively. Cells were passaged at least three times before performing assays. Passage number did not exceed 15. XEN cell lines were

cultured as described (43).

Surface plasmon resonance

Binding affinities and inhibition were determined using the Biacore 2000. Anti-human IgG (Fc) antibody was immobilized onto four channels of a CM5 chip using amine coupling chemistry. 200-300 RU of purified Cripto-1-Fc, Cryptic-Fc, ActRIIA-Fc, ActRIIB-Fc, BMPRII-Fc, ALK3-Fc or ALK4-Fc were captured on the experimental channels. A reference channel was monitored to account for nonspecific binding, drift, and bulk shifts. To determine ligand-binding specificity, 80 nM of each ligand (see ligands above) was injected over captured Cripto-1 or Cryptic. For analysis of Cripto-1/Cryptic binding to receptors, Fc-free forms at concentrations up to 24 μ M were injected over captured receptors. For ligand binding kinetics, a concentration series of interacting ligands (BMP-4, Activin B or GDF-3) was injected over captured Cripto-1 or Cryptic. To determine if Fc dimerization causes difference in ligand binding, 4000 RU of Cripto-1 was cross-linked on the experimental channel and a concentration series of BMP-4 was injected over immobilized Cripto-1. For inhibition analysis, BMP-4 or Activin B at one concentration preincubated with various concentrations of Fc-free Cripto-1 or Cryptic was injected over captured receptors. To determine if the presence of a ligand affects the interaction between Cripto-1 and receptors, BMP-4 or Nodal at one concentration were preincubated with Fc-free Cripto-1 or Alk4 and injected over captured receptors. For deglycosylation experiments, Cripto-1 constructs were treated with PNGase F and Sialidase and captured on the sensor chip. SDS-PAGE was used to evaluate the glycosylation status. All experiments were carried out at 25 °C. HBS-EPS buffer (0.01 M HEPES, 0.5 M NaCl, 3 mM EDTA, 0.005% (v/v) Tween 20, pH 7.4) containing 0.1 % BSA was used as running buffer at a flow rate of 50 μ l/min. Nodal

containing samples were kept without BSA, as it causes rapid inactivation. After each binding cycle, the antibody surface was regenerated to base line. Sensograms were analyzed by double referencing. To obtain kinetic rate constants, the processed data was fitted to 1:1 ‘two-state reaction model’ using BiaEvaluation software. The equilibrium dissociation constant K_d was determined by calculating the ratio of binding rate constants k_d/k_a . Results are summarized in Table 2-1. For Cripto-1 – ALK4 binding, we used BiaEvaluation and GraphPad Prism Version 6.0h. We obtained best-fit curves by nonlinear curve fitting using a ‘one-site total binding’ model. We determined B_{max} , K_d and non-specific (NS) binding contributions. For competition experiments, we obtained a best-fit inhibition curve using a non-linear regression algorithm for log(antagonist) versus normalized response model (37).

Cross-linking

Approximately 4 μ g of protein samples were cross-linked with 0.01% or 0.02% glutaraldehyde for 20 min at room temperature. Native cross-linking reactions were performed in PBS. The cross-linking reaction was quenched with Tris buffer pH 8 (final concentration: 200 mM). Samples were analyzed by 12% SDS-PAGE under reducing conditions.

Reporter assays

For standard reporter assays, ~ 10,000 HepG2 cells/well in complete medium (Eagle's Minimum Essential Medium supplemented with 10% FBS and 1% P/S) were seeded in a 96-well plate and grown overnight. Each well was transfected with 0.25 μ l lipofectamine 2000, 200 ng of the SMAD1/5/8 responsive reporter plasmid pGL3 [luc2P/BRE] or the SMAD3 responsive reporter plasmid pGL4.48 [luc2P/SBE] and 2 ng of the [Luc2P/hRluc/TK] vector (control luciferase reporter plasmid, Promega, E6921). Transfection medium was removed

the following day, and replaced with assay medium (FBS free growth medium with 0.1% BSA) containing BMP-4, Activin B, Cripto-1-Fc, Cryptic-Fc and/or ActRIIA-Fc was preincubated at 37 °C for 1 h before adding to cells. For Cripto-1 overexpression studies, ~ 10,000 HepG2 cells/well were seeded in a 96-well plate and grown overnight. Each well was transfected with 0.4 µl lipofectamine 2000, 100 ng of human TDGF-1 natural ORF mammalian expression plasmid (Sino Biological, HG10908-UT) or 100 ng of empty pCMV control vector, 100 ng of the SMAD1/5/8 responsive reporter plasmid and 1 ng of the control reporter plasmid. Transfection medium was removed the following day, and replaced with assay medium containing a concentration series of BMP-4, BMP-2 and/or Cripto-1-Fc. Assay medium was preincubated at 37 °C for 1 h before adding to cells. For Cripto-1 knockdown assays, ~ 10,000 NT2/D1 cells in complete medium were seeded in each well of a 96-well plate and grown overnight. Each well was transfected with 0.3 µl lipofectamine 3000, 100 ng of

of	TDGF1	shRNA	
			(5'-

CCGGACAGCACAGTAAGGAGCTAAACTCGAGTTTAGCTCCTTACTGTGCTGTTTTT
TT-3') (Sigma-Aldrich, SHCLNG-NM-003212) or scrambled TRC1 control vector, 100 ng of the SMAD1/5/8 responsive reporter plasmid and 1 ng of the control reporter plasmid. Transfection medium was removed the following day, and replaced with assay medium. After 48 h, assay medium was replaced with fresh assay medium containing 0, 1 and 10 nM BMP-4. After addition of assay medium, cells were incubated for 16 h at 37 °C, luciferase activity was detected using a homemade dual-glow luciferase assay (44). Luminescence was determined using a FluoStar Omega plate reader. Relative luciferase units were calculated by dividing firefly luciferase units with renilla luciferase units. To obtain IC₅₀ values, we used a non-linear regression algorithm for log(antagonist) versus normalized response model

(GraphPad). Data are expressed as mean of four independent measurements. Error bars correspond to SE of four biological replicates.

Immunoblotting

Cell lysates were prepared in RIPA buffer as previously described (44). Protein concentration of total cell lysate was determined with the Bradford assay. 10 µg of cell lysate were loaded on 12% SDS-polyacrylamide gels under reducing conditions. Western blot analysis was performed with antibodies specific for Cripto-1 (Abcam, ab108391) and beta-actin (Cell Signaling, 8H10D10). WesternBright Sirius HRP substrate was used for detection (Advansta, K-12043-D10). Western blots were visualized by exposing the membrane to autoradiography film.

Statistics

Cell-based assays were performed in quadruplicates and were repeated at least two different times. Statistical significance was determined using a two-tailed T-test. P values < than 0.05 were considered statistically significant.

Results

Production of soluble Cripto-1 and Cryptic

A critical bottleneck in the molecular analysis of mammalian Cripto-1 and Cryptic has been the lack of purified, active proteins. Several complicating factors contribute to this problem. Both Cripto-1 and Cryptic are expressed as secreted precursors that attach to the membrane via a glycosyl-phosphatidylinositol (GPI) anchor, both have six disulfide bonds distributed between two separate domains, and both may require post-translational fucosylation for biological activity (5, 46-48). To obtain active Cripto-1 and Cryptic we used stably transfected CHO cells, as they can carry out the required modifications. We created a

Cripto-1 expression construct that included the Cryptic signal peptide and human Cripto-1 extracellular (ecto)-domain amino acids 31-163. We also created a mouse Cryptic expression construct that included the native signal peptide plus ecto-domain amino acids 36-175 (Fig. 2-1A). Both fragments were fused at their C-terminus, which is near the predicted GPI processing site, to human IgG1-Fc (Fig. 2-1A, B). Fusion proteins were purified from conditioned medium by protein A affinity capture. A size exclusion chromatography step was further required to remove inactive aggregates (Fig. 2-1C). Overall, we obtained approximately ~ 150 mgs highly purified hCripto-1-Fc and ~ 50 mgs mCryptic-Fc per liter culture. Notably, the C-terminus was critical for expression, as constructs that ended near the C-terminal cysteine were more highly aggregated, and constructs that ended at the putative GPI processing site failed to secrete.

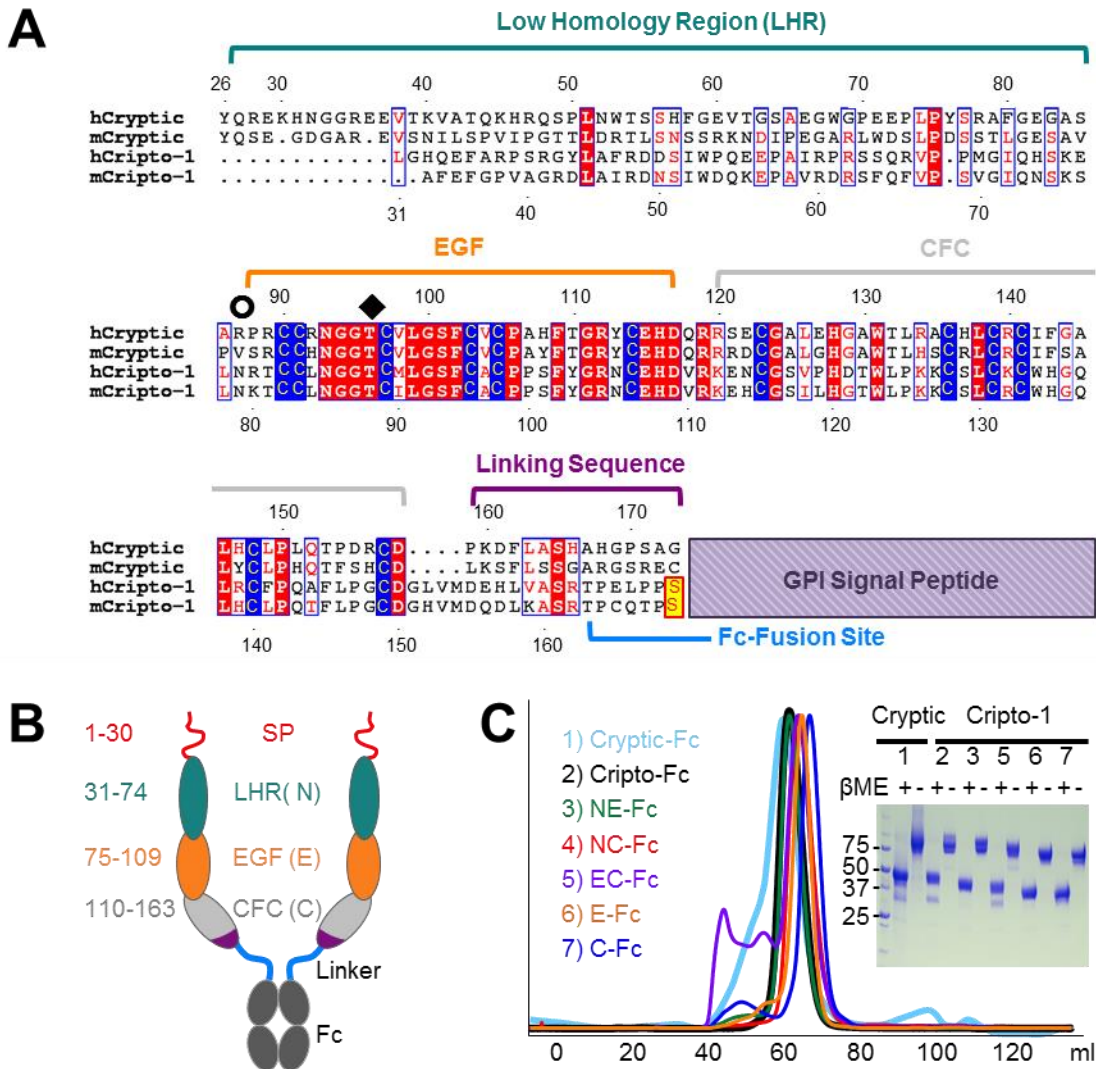


Figure 2-1. Construct design and purification.

(A) Multiple sequence alignment of human and mouse Cryptic and Cripto-1. Both molecules have a signal peptide for secretion (not shown in the alignment), a Low Homology Region (LHR, teal), an Epidermal Growth-Factor-like domain (EGF, orange), a Cripto-1-FRL-Cryptic domain (CFC, grey), and a Glycophosphatidylinositol (GPI) signal peptide (represented by the purple box). The Cripto-1 GPI signal peptide is cleaved after Ser169 (residues in yellow box). Cryptic of mouse origin has a canonical GPI signal peptide, whereas Cryptic of primate origin has a large, non-canonical GPI signal peptide. The GPI modification site of Cryptic is not known. For expression constructs, human Cripto-1 and mouse Cryptic were truncated at the ‘Fc-Fusion site’ (light blue). The open circle marks the N-linked glycosylation site. The black diamond marks the O-linked fucosylation site. Numbering represents amino acid positions of human Cryptic (top) and human Cripto-1 (bottom). (B) Domain organization of Cryptic/Cripto-1 constructs colored as in A. Both were fused to human IgG1-Fc via a 22 amino acid linker at the ‘Fc-Fusion site’. Numbering

Figure 2-1 (cont'd)

represents amino acid positions of human Cripto-1. (C) Purification of Cripto-1-Fc and Cryptic-Fc fusion forms expressed in CHO cells. Fc-fusion form constructs were captured from conditioned medium using protein A affinity chromatography and further purified using SEC. Constructs migrate as a single, well-defined peak in a size exclusion chromatographic column. The molecular weight of the protein corresponds to the dimeric species. Non-reducing and reducing SDS-PAGE gels show the disulfide-linked dimeric species and the reduced, monomeric species. Dimerization occurs via free cysteine in the Fc region.

Cripto-1 and Cryptic bind distinct ligands

Genetic and co-immunoprecipitation studies have indicated that Cripto-1 and Cryptic interact with the TGF- β family ligands Nodal and Activin A (9, 13, 28, 35). Using SPR, we confirmed earlier that Cripto-1 binds Nodal with high affinity (33), but we did not detect Activin A binding to Cripto-1 or Nodal binding to Cryptic. These findings indicated that previously proposed ligand-binding and regulatory activities of Cripto-1 and Cryptic are inaccurate. To identify ligands that interact directly with (and thus are regulated by) Cripto-1 or Cryptic, we used a high-throughput, SPR-based binding-assay. We captured purified human Cripto-1-Fc or mouse Cryptic-Fc on an SPR sensor chip cross-linked with an anti-Fc antibody and injected 16 different TGF- β family ligands at an 80 nM concentration (Fig. 2-2A, B). Cripto-1-Fc bound Nodal and to a lesser degree GDF-3, but not Activin A as had been proposed. Notably, we discovered that Cripto-1-Fc interacts very strongly with BMP-4 (Fig. 2-2A). By contrast, mouse Cryptic-Fc did not bind Nodal, Activin A, BMP-4 or GDF-3, but interacted very specifically with Activin B (Fig. 2-2B). We did not observe appreciable binding of any other tested TGF- β family ligand to either Cripto-1 or Cryptic, including TGF- β 1, TGF- β 2, TGF- β 3, GDF-8, GDF-11, GDF-15, BMP-2, BMP-3, BMP-6, BMP-7, BMP-9 or BMP-10. We confirmed our single injection findings with systematic ligand titrations and obtained kinetic rate and equilibrium binding constants for BMP-4, GDF-3 and

Activin B (Fig. 2-2C-F, Table 2-1). To determine if the Fc moiety affects ligand binding, we cross-linked Fc-free Cripto-1 directly on the sensor chip. Notably, Cripto-1 captured in this way bound BMP-4 with approximately 40-fold lower affinity, indicating that the Fc moiety or the capture method impact ligand binding (Fig. 2-2C, D). We speculate three factors could contribute to the difference in affinity: 1) a loss of avidity due to use of the Fc-free, monomeric form, 2) a loss in binding activity due to chemical modification of lysine residues on Cripto-1, and/or 3) a gradual loss in binding activity caused by repeated regeneration of the Cripto-1 bound surface. In spite of the observed differences in binding rates, our findings show that Cripto-1 binds BMP-4 with high affinity regardless of capture method. In conclusion, we have identified two new TGF- β family ligands that are bound (and thus regulated) by Cripto-1 or Cryptic, namely BMP-4 and Activin B. Importantly, we show Cripto-1 and Cryptic interact with different ligands, indicating that they have markedly distinct biological functions.

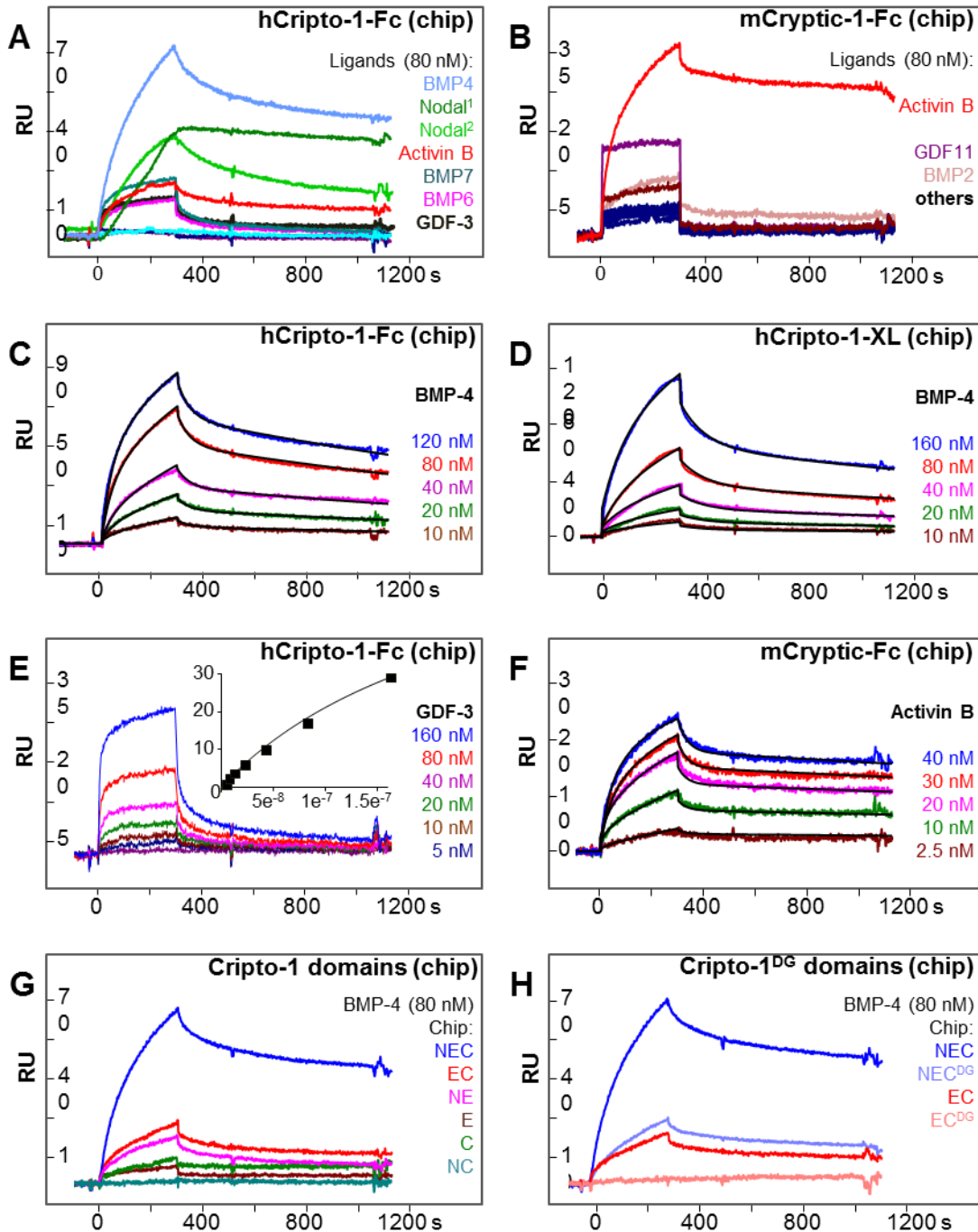


Figure 2-2. Ligand binding specificity.

Approximately 250 response units (RU) of (A) Cripto-1-Fc or (B) Cryptic-Fc were captured on an SPR sensor chip, and 80 nM Activin A, Activin B, GDF-1, GDF-3, GDF-8, GDF-11, TGF- β 1, TGF- β 2, TGF- β 3, BMP-2, BMP-3, BMP-4, BMP-6, BMP-7, BMP-9, BMP-10, or Nodal (lot 1 and lot 2) were injected. Ligands that elicited an SPR response are shown in relevant panels. Ligand name and corresponding binding curves are color-matched.

Figure 2-2 (cont'd)

(C) Human Cripto-1-Fc was captured on the sensor chip and different concentrations of BMP-4 as shown were injected. (D) Human Cripto-1 was cross-linked to the sensor chip and different concentrations of BMP-4 as shown were injected. (E) Human Cripto-1-Fc was captured on the sensor chip and different concentrations of GDF-3 as shown were injected. The inserted panel shows the equilibrium-binding analysis. (F) Mouse Cryptic-Fc was captured on the sensor chip and different concentrations of Activin B as shown were injected. Colors of injection curves are matches with corresponding concentrations. Fitted curves (black lines) are superimposed over all experimental curves. Calculated binding rate constants and equilibrium dissociation rate constants are shown in Table 2-1. (G) Cripto-1-Fc domain deletion constructs were captured on the sensor chip and 80 nM BMP-4 was injected. Cripto-1 constructs are named according to their domain composition, i.e N constructs have the N-terminal Low Homology Region, E constructs have the EGF domain and C constructs have the CFC domain. Injection curves are color-matched with corresponding constructs. (H) Glycosylated and deglycosylated (DG) full-length Cripto-1 (NEC) and N-terminal domain deletion construct (EC) were captured on the sensor chip and 80 nM BMP-4 was injected. Injection curves are color-matched with corresponding constructs and glycosylation status.

Table 2-1. Binding rate and equilibrium dissociation constants

Analyte	Chip	k_a	k_d	K_d	Chi^2	R^2
BMP-4	Cripto-1-Fc	8.390×10^4	4.000×10^{-4}	4.770	0.710	-
BMP-4	Cripto-1-XL	1.930×10^4	3.650×10^{-3}	189	1.490	-
GDF-3	Cripto-1-Fc	-	-	256	0.637	-
Activin B	mCryptic-Fc	1.260×10^4	1.410×10^{-4}	1.120	0.221	-
ALK4	Cripto-1-Fc	N.D.	N.D.	1307	-	0.989
ALK4	Cripto CFC-Fc	N.D.	N.D.	750.4	-	0.996
Cripto-1	ALK4-Fc	N.D.	N.D.	725.2	-	0.998

Note: Units are: k_a ($M^{-1}s^{-1}$), k_d (s^{-1}), K_d (nM), Chi^2 (RU²).

All Cripto-1 domains are required for ligand binding

EGF-CFC family proteins comprise three structural domains, an N-terminal low homology region (N), an epidermal growth factor (E)-like motif, and a C-terminal Cripto-FRL1-Cryptic (C) domain (Fig. 2-1A). The molecular functions of individual domains have been investigated, but results are inconclusive. For example, some studies indicate the EGF domain is required for signaling, while others suggest it is not (26, 30). Some indicate the

EGF domain binds Nodal, while others indicate it does not (30, 42, 49). Some suggest the CFC domain interacts with ALK4, while others indicate it may not (26, 30). To clarify the contribution of Cripto-1 domains in ligand interactions, we created constructs that consisted of two domains (NE, EC and NC) or single domains (N, E or C) and compared their ability to bind ligands with that of full-length Cripto-1-Fc (NEC). We expressed and purified the six domain deletion constructs as described for the full-length form, and tested their ability to bind BMP-4 using single injection SPR binding. Of the six constructs, five were readily expressed and purified. The N-terminal domain construct (N) was severely degraded and thus was not used in these studies. Both two-domain constructs that included the EGF region (NE and EC) bound BMP-4, although binding was significantly weaker compared with full-length Cripto-1-Fc (Fig. 2-2G). Single domain constructs did not bind BMP-4. Taken together, these findings indicate all three Cripto-1 domains are required for the BMP-4 interaction. However, whether all three domains contact BMP-4 directly or whether they help support a Cripto-1 conformation that recognizes BMP-4 remains to be determined. We did not test Cripto-1 domain functions against Nodal, as we do not have consistently active Nodal (Fig. 2-2A). But we expect Nodal to parallel our BMP-4 findings.

Cripto-1 glycosylation is necessary for ligand binding

Human Cripto-1 is glycosylated at asparagine 79. This glycosylation site appears to be conserved across all mammalian species (Fig. 2-1A), indicating the glycan moiety may have functional relevance. To determine if N79 glycosylation has a role in ligand binding, we enzymatically processed Cripto-1 with the endoglycosydases PNGase F or ENDO-F3. PNGase F removes the entire glycan. ENDO-F3 leaves the N-acetylglucosamine moiety on the protein. Strikingly, both PNGase F and ENDO-F3 treated Cripto-1-Fc lost the ability to

bind BMP-4, indicating N79 glycosylation is critical for Cripto-1 function (Fig. 2-2H). Importantly, this finding supports our previous conclusion that Cripto-1 – ligand recognition requires multiple structural features. However, whether N79 glycosylation is directly involved in ligand binding or whether it plays a structural role remains to be determined. Notably, N79 is at the junction between N and E domains. Only three of our domain constructs, NE, EC and E, carried this glycosylation site. NE and EC constructs also lose their binding activity after deglycosylation (Fig. 2-2H).

Soluble Cripto-1 does not bind type I receptors strongly

The commonly accepted model of Cripto-1 action is that it binds both Nodal and the type I TGF- β family receptor ALK4 to stabilize Nodal-ALK4 complexes and thus potentiate Nodal signaling (26, 30, 49, 50). Specifically, it is suggested the EGF domain contacts Nodal and the CFC domain contacts ALK4, thus linking Nodal with its type I receptor and stabilizing an active signaling complex (51, 52). But our previous findings show the function of Cripto-1 is more complex. Namely, ligand binding necessitates all three domains, including the CFC domain (Fig. 2-2G). To investigate the function of Cripto-1 in ligand-receptor complex stabilization, we first examined if Cripto-1 binds TGF- β family receptors directly. We captured the type I receptors ALK2, ALK3 and ALK4, or the type II receptors ActRIIA, ActRIIB, BMPRII and T β RII on a sensor chip, as these receptors interact with the cognate Cripto-1/Cryptic ligands Nodal, BMP-4 and Activin B (44). We injected 6 μ M Fc-free Cripto-1 or Cryptic (Fig. 2-3A). Cripto-1 elicited a strong SPR response when injected over ALK4. But the response was dominated by extremely fast on- and off-rates, indicating it is dominated by significant bulk-shift or non-specific binding components (Fig. 2-3A). A weaker response with similarly fast kinetics could also be observed with other receptors. In

contrast to Cripto-1, Cryptic did not elicit an SPR response with any captured receptors (data not shown).

To identify the source of the SPR response, we evaluated the Cripto-1 – ALK4 dose-response relationship. We titrated Fc-free Cripto-1 over ALK4 at concentrations ranging from 46 nM to 24 μ M (Fig. 2-3B). As anticipated from our single injection studies, the SPR response increased with Cripto-1 concentrations. But the SPR response did not follow Langmuir adsorption kinetics (Fig. 2-3B). Thus, we fit our binding data using a “one-site total binding” model and obtained a K_d of \sim 750 nM with a maximum specific binding value (B_{\max}) of 62.5 RU (Fig. 2-3B) (53). Based on this analysis and the observation that Cripto-1 caused small SPR responses with other tested receptors (Fig. 2-3A), we propose that the Cripto-1 – ALK4 interaction is weak, and that Cripto-1 can interact non-specifically with receptors. Notably, when we injected ALK4 over captured Cripto-1, we observed a similar response dominated by bulk shift and kinetic rate constants (data not shown).

Earlier studies indicated the CFC domain interacts directly with ALK4 (54). To assess this observation, we captured domain deletion constructs on a sensor chip and injected 24 μ M ALK4. We speculated constructs that include the CFC domain bind ALK4, but constructs that lack the CFC domain do not. As anticipated, we observed an SPR response with all CFC domain constructs, but not with constructs lacking this domain (Fig. 2-3C). However, responses were again dominated by bulk shift, indicating the interaction is weak and has significant non-specific elements. To obtain an independent measure of Cripto-1 – ALK4 binding, we used glutaraldehyde cross-linking approach. We hypothesized that a cross-linking product would show if Cripto-1 – ALK4 complexes are stable. But we failed to detect adducts using this approach (Fig. 2-3D).

To determine if ligands help stabilize Cripto-1 – ALK4 or other Cripto-1 – receptor complexes, we performed two independent SPR experiments. First, we captured ALK4-Fc, ActRIIA-Fc or ActRIIB-Fc on the sensor chip and injected Nodal or Nodal preincubated with Fc-free Cripto-1 (Fig. 2-3E, F). Strikingly, while Cripto-1 did not have a noticeable effect on the Nodal–ALK4 interaction, indicating Cripto-1 does not stabilize Nodal–ALK4 complexes in this format (Fig. 2-3F), Cripto-1 prevented binding of Nodal to the type II receptors ActRIIA and ActRIIB (Fig. 2-3E). In a second experiment, we captured Cripto-1-Fc and injected Nodal alone or preincubated with ALK4 (Fig. 2-3F). ALK4 did not enhance Cripto-1 – Nodal complexation. We therefore conclude that Cripto-1 – ALK4 complexes are weak and that a direct interaction between these two proteins may not be consequential.

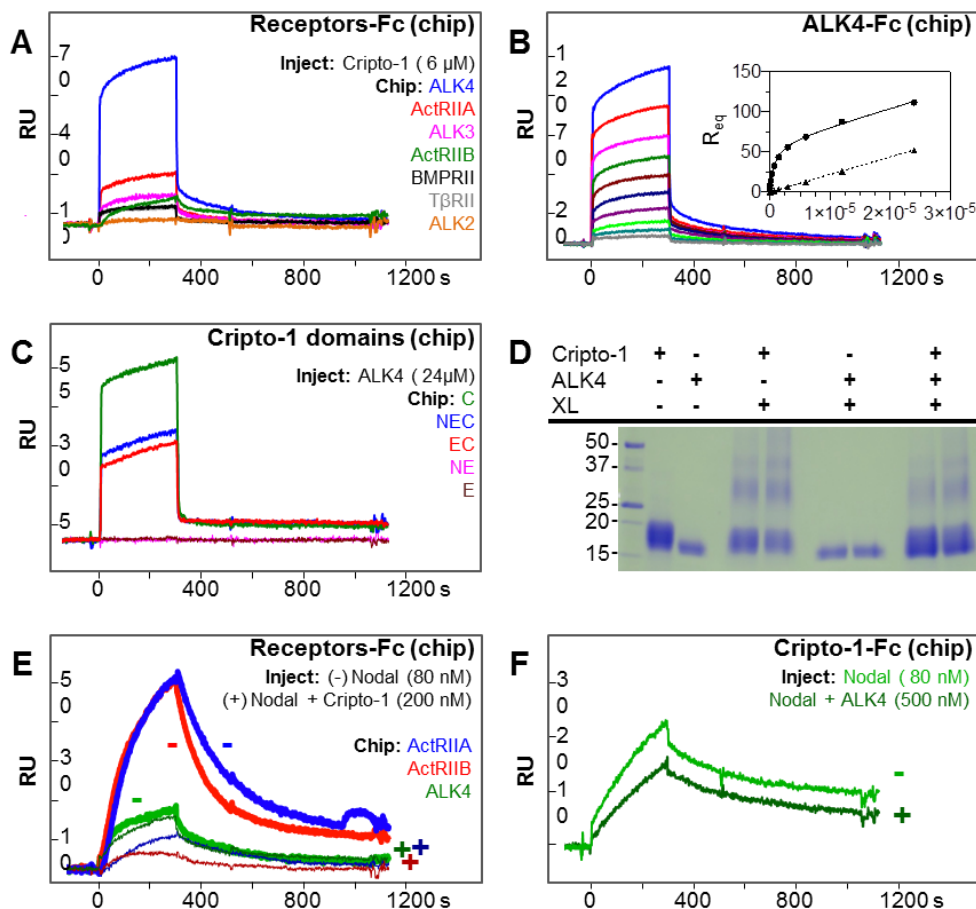


Figure 2-3. Cripto-1 and Cryptic – receptor interactions.

(A) Binding of Cripto-1 to TGF- β family receptors. Type I receptors ALK2-Fc, ALK3-Fc, and ALK4-Fc, or type II receptors ActRIIA-Fc, ActRIIB-Fc, BMPRII-Fc, and T β RII-Fc were captured on the sensor chip. 6 μ M Fc-free Cripto-1 or Cryptic was injected. Receptors and corresponding binding curves are color-matched. Cryptic binding curves are not shown, as Cryptic did not elicit an SPR response. (B) ALK4 – Cripto-1 interaction analysis. ALK4-Fc was captured and Fc-free Cripto-1 was injected (blue = 24.0 μ M, red = 12.0 μ M, magenta = 6.0 μ M, green = 3.0 μ M, maroon = 1.5 μ M, dark blue = 750.0 nM, purple = 375.0 nM, light green = 187.5 nM, teal = 93.75 nM, and grey = 46.875 nM). Nonlinear curve fitting using a ‘one-site total binding’ model was inserted (solid line, circles). B_{max} , K_d and non-specific contribution were determined. The theoretically determined non-specific contribution is also shown (insert, dotted line, triangles). (C) Binding of ALK4 to Cripto-1 domain deletion constructs. Deletion constructs were captured on the sensor chip and 6 μ M Fc-free ALK4 was injected. Constructs and corresponding binding curves are color-matched. (D) Glutaraldehyde cross-linking of Cripto-1 and ALK4. The SDS-PAGE gel shows Cripto-1, ALK4, cross-linked (XL) Cripto-1, cross-linked ALK4 and cross-linked complexes. 0.01% (left lane) and 0.02% (right lane) glutaraldehyde was used. Molecular weight markers are shown on the right side. (E) Binding of Nodal \pm Cripto-1 to Nodal receptors ActRIIA (blue),

Figure 2-3 (cont'd)

ActRIIB (red) and ALK4 (green). The minus sign denotes curves obtained with Nodal only (thick, light colored lines), the plus sign denotes curves obtained with Nodal preincubated with Cripto-1 (thin, dark colored lines). A Cripto-1 – ALK4 injection was subtracted from the Nodal – Cripto-1 – ALK4 injection to eliminate the non-specific Cripto-1 – ALK4 binding contribution. **(F)** Binding of Nodal \pm ALK4 (green) to Cripto-1. The presence of ligand does not appear to alter the SPR signal obtained for Cripto-1 and ALK4 significantly.

Cripto-1 and Cryptic block ligand association with type II and some type I receptors

It is well established that Cripto-1 and Cryptic interact with TGF- β family ligands (9, 26, 33, 34), but how they bind ligands is not clear. Based on molecular knowledge about the TGF- β family ligand–receptor interaction (38), we hypothesized Cripto-1 and Cryptic either contact ligand surfaces that overlap with receptor binding sites (and thus compete with receptors for ligand binding), or they contact ligand surfaces that don't overlap with receptor binding sites (and thus form multimeric complexes with ligands and receptors, as is suggested). To test this hypothesis we used an SPR based co-binding/inhibition assay (37). In this format, receptor-Fc fusion constructs were captured on the sensor chip and a constant concentration of ligand preincubated with increasing concentrations of Cripto-1 or Cryptic was injected. If Cripto1/Cryptic and receptors occupy the same ligand surface, the SPR signal is expected to decrease with increasing Cripto-1/Cryptic concentrations. But, if Cripto1/Cryptic and receptors occupy different ligand surfaces, the SPR signal is expected to increase with increasing Cripto-1/Cryptic concentrations (37).

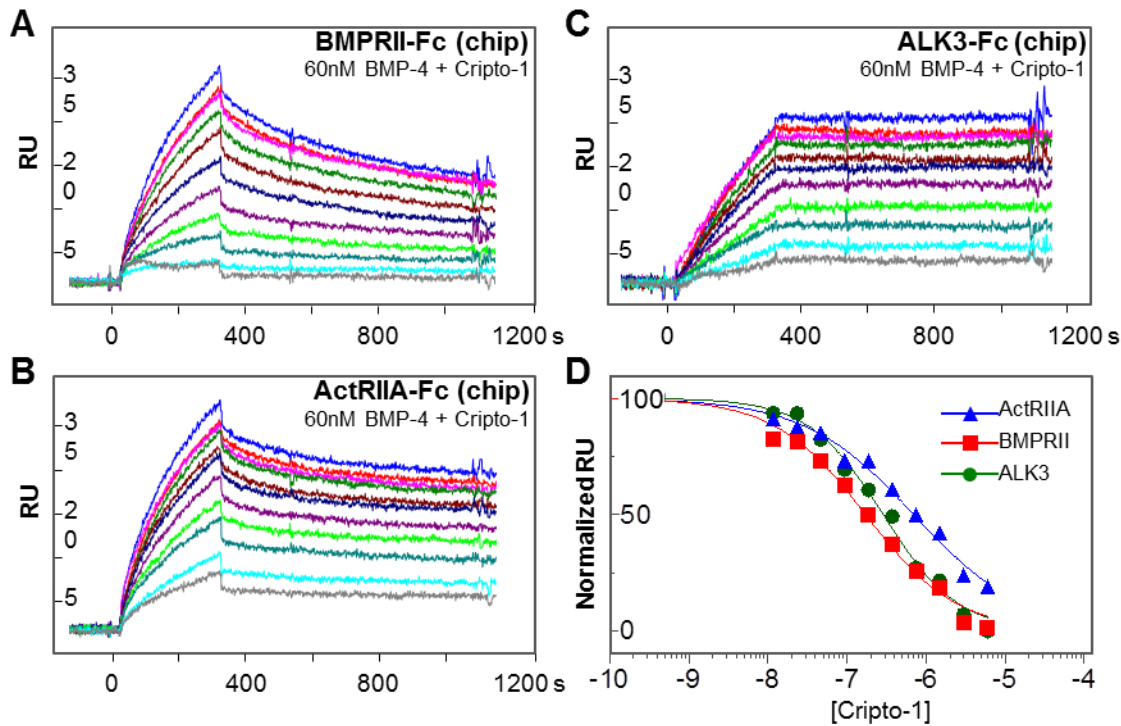


Figure 2-4. Mapping of Cripto-1 – ligand interaction.

(A) BMPRII-Fc, (B) ActRIIA-Fc and (C) ALK3-Fc were captured on the sensor chip. 60 nM BMP-4 was preincubated with 0 nM (blue), 11.72 nM (red), 23.44 nM (magenta), 46.88 nM (dark green), 93.75 nM (maroon), 187.5 nM (dark blue), 375.0 nM (purple), 750.0 nM (bright green), 1500.0 nM (teal), 3000.0 nM (cyan), and 6000.0 nM (grey) Fc-free Cripto-1. Cripto-1 – BMP-4 mixtures were injected over the sensor chip. (D) IC₅₀ determination. Raw RU values at 150 seconds post injection were taken for each Cripto-1 concentration. RU values were normalized and fitted using the non-linear regression algorithm implemented in GraphPad. Standard errors (SEs) are small and were omitted for clarity (37).

Using this approach, we discovered soluble Cripto-1 prevents BMP-4 binding to the type I receptor ALK3 and the type II receptors ActRIIA and BMPRII in a concentration dependent manner (Fig. 2-4A-C), replicating our earlier observation with Nodal (Fig. 2-3E). The reaction followed a sigmoidal inhibition curve (Fig. 2-4D), indicating Cripto-1 competitively inhibited BMP-4 binding to its receptors. Based on the changing SPR response (37), we calculated IC₅₀ values for inhibition of BMP-4 binding to ActRIIA (705 nM), BMPRII (164 nM) and ALK3 (288 nM). Soluble Cryptic showed a similar behavior (Fig. 2-

5A, B). But its effect was more sensitive, as it blocked Activin B binding to the type II receptor BMPRII much more effectively than to ActRIIA (Fig. 2-5C) we calculated IC_{50} values for inhibition of Activin B binding to BMPRII (288 nM) and ActRIIA (1024 nM). We did not investigate the function of Cryptic in the Activin B–type I receptor interaction, as type I receptors for Activin B are not known. Significantly, Cripto-1 also prevented Nodal binding to type II receptors (Fig. 2-3E), but these findings are preliminary, as the activity of currently available Nodal is not consistent. Even so, our studies support the conclusion that Cripto-1 and Cryptic contact ligands at or near their type I and type II receptor binding sites.

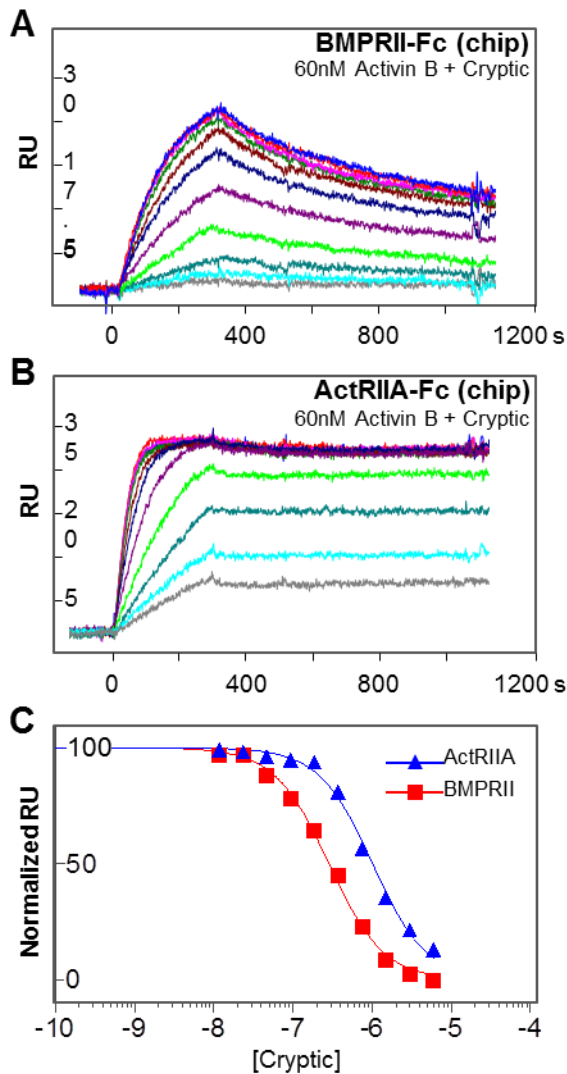


Figure 2-5. Mapping of Cryptic – ligand interaction.

(A) BMPRII-Fc and (B) ActRIIA-Fc were captured on the sensor chip. 10 nM Activin B was preincubated with 0 nM (blue), 11.72 nM (red), 23.44 nM (magenta), 46.88 nM (dark green), 93.75 nM (maroon), 187.5 nM (dark blue), 375.0 nM (purple), 750.0 nM (bright green), 1500.0 nM (teal), 3000.0 nM (cyan), and 6000.0 nM (grey) Fc-free Cryptic. Activin B - Cryptic mixtures were injected over the sensor chip. (C) IC_{50} determination. Raw RU values from SPR measurements were taken for each Cryptic concentration at 150 seconds post injection. RU values were normalized and fitted using the non-linear regression algorithm implemented in GraphPad. Standard errors (SEs) are small and were omitted for clarity (37).

Soluble Cripto-1 and Cryptic inhibit signaling

As Cripto-1 and Cryptic inhibited ligand – receptor binding, we hypothesized that they could also inhibit ligand signaling. To test this hypothesis, we used reporter gene expression assays. We transfected HepG2 hepatocellular carcinoma cells with control plasmid pGL4.74 [hRluc] and the SMAD3 responsive reporter plasmid pGL4.48 [luc2P/SBE] or the SMAD1/5/8 responsive reporter plasmid pGL3 [luc2P/BRE] (Fig. 2-6) (55, 56). We treated transfected cells with 10 ng/ml BMP-4 or Activin B and increasing concentrations of Cripto-1-Fc or Cryptic-Fc (0-5000 nM). Both ligands induced luciferase reporter activity and both Cripto-1-Fc and Cryptic-Fc reduced the luciferase signal in a concentration dependent manner. Cripto-1-Fc abrogated the BMP-4 mediated SMAD1/5/8 response completely (Fig 2-6A). Cryptic-Fc exhibited an intriguing behavior. It blocked Activin B mediated SMAD1/5/8 signaling completely. But inhibition followed a biphasic dose response (Fig. 2-6C), indicating it blocks at least two distinct Activin B signaling complexes with different potency. Notably it only inhibited the Activin B induced SMAD2/3 signal by about half (Fig. 2-6D), suggesting signaling is activated differentially by type II receptors and that Cryptic-Fc may block activation by one receptor (BMPRII) much better than activation by another (ActRIIA, ActRIIB).

To validate Cripto-1 domain functions, we also evaluated their inhibitory potency (Fig. 2-6B). We treated transfected HepG2 cells with 10 ng/ml BMP-4 and 1000 nM Cripto-1-Fc domain constructs. Matching our SPR results (Fig. 2-2E), only full-length Cripto-1-Fc (NEC-Fc) exhibited full inhibitory potency (a 5-fold reduction in signaling from 30 RLU to 6 RLU). Both two-domain constructs (NE-Fc and EC-Fc) showed residual inhibitory activity, but were far weaker than the full-length construct. They reduced signaling only from 30 RLU to

about 20 RLU. Single domains (E-Fc and C-Fc) did not inhibit signaling.

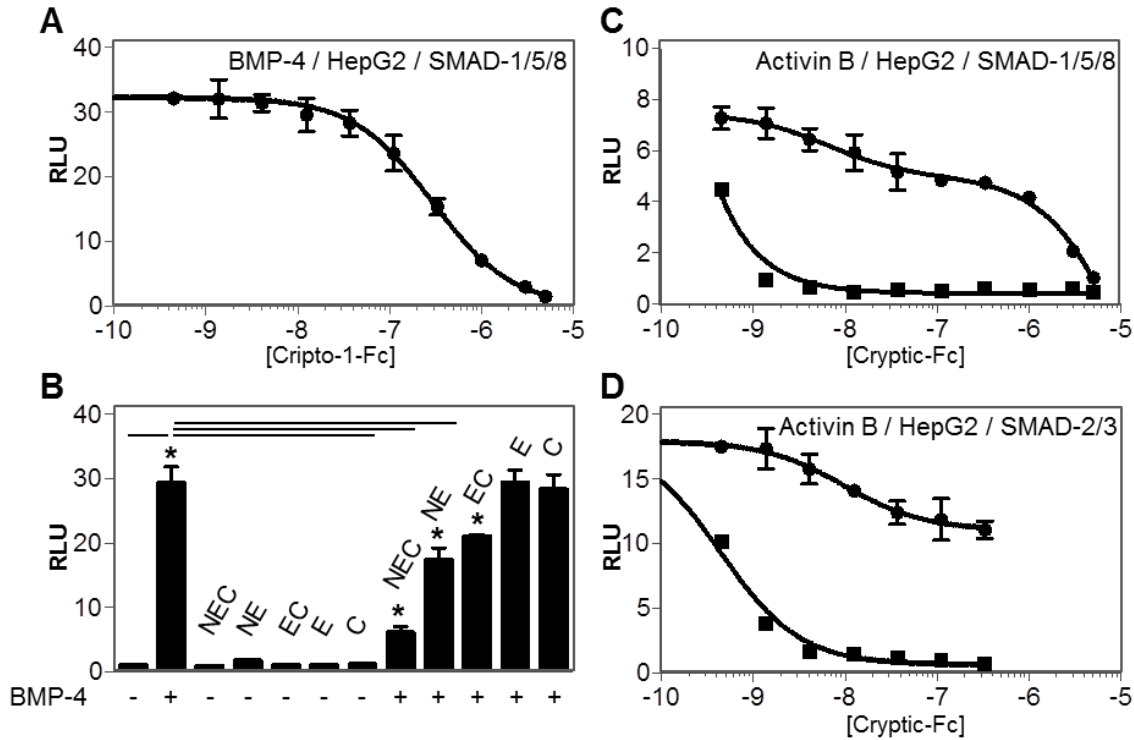


Figure 2-6. Signaling inhibition by soluble Cripto-1 and Cryptic.

(A) Cripto-1-Fc suppresses BMP-4 signaling. BMP-4 (10 ng/ml) induces expression of a SMAD1/5/8-responsive luciferase reporter. Cripto-1-Fc inhibits the BMP-4 dependent luciferase signal in a concentration dependent manner. The Y-axis shows RLU (relative luciferase units). The X-axis shows Cripto-1 concentration in log scale (M). (B) Individual Cripto-1 domains lack inhibitory potency. BMP-4 (10 ng/ml) induces expression of a SMAD1/5/8-responsive luciferase reporter. Full-length Cripto-1-Fc (NEC) almost completely inhibits BMP-4 signaling, Cripto-1 constructs that comprise two domains (NE and EC) reduce BMP-4 signaling but are much less potent than the full-length (NEC) form. Single domain constructs (E and C) do not inhibit BMP-4 signaling. Statistically significant differences are marked by an asterisk and are linked to the comparison value by a black bar. (C, D) Cryptic-Fc suppresses Activin B signaling. 10 ng/ml Activin B induces expression of both SMAD2/3 (C) and SMAD1/5/8 (D) responsive luciferase reporters. Cryptic-Fc (triangles) inhibits the Activin B dependent luciferase signal in a concentration dependent manner. Inhibition follows a biphasic curve and inhibits SMAD1/5/8 pathways more effectively more effectively than SMAD2/3 pathways. Standard errors of biphasic curve-fitting are not calculated. For comparison, inhibition of Activin B signaling by ActRIIA-Fc (squares) is also shown. The Y-axis shows RLU (relative luciferase units). The X-axis shows the Cryptic-Fc concentration in log scale (M). All values are shown as average of 4 biological replicates. Error bars correspond to standard error. Errors from ActRIIA-Fc inhibition are less than 5% and thus are not shown.

Table 2-2. Half-maximal inhibitory concentrations (IC₅₀)

*SPR-BINDING (IC₅₀ (nM))		Chip		
Analyte	Inhibitor	ActRIIA-Fc	BMPRII-Fc	ALK3-Fc
BMP-4	Cripto-1	705.1 ± 74.5	172.9 ± 19.0	288.8 ± 28.5
Activin B	mCryptic	1024 ± 60.9	288.2 ± 14.5	-

**REPORTER-SIGNALING (IC₅₀ (nM))				
Ligand	Reporter	Inhibitor	IC₅₀-1st phase	IC₅₀-2nd phase
BMP-4	SMAD1/5/8	Cripto-1-Fc	207.1 ± 34.3	-
Activin B	SMAD1/5/8	mCryptic-Fc	6.400	13061.7
Activin B	SMAD2	mCryptic-Fc	N.D.	N.D.
Activin B	SMAD1/5/8	ActRIIA-Fc	0.4220 ± 0.011	-
Activin B	SMAD2	ActRIIA-Fc	0.5100 ± 0.035	-

Note: 10 concentrations of inhibitor were used. *SPR-study was performed in duplicate, **Reporter-gene expression study was performed in quadruplicate.

Membrane associated Cripto-1 potentiates BMP-4 signaling

Endogenously expressed, membrane-anchored Cripto-1 is known for its ability to potentiate Nodal signaling (26, 30, 49, 50). By contrast, we discovered soluble Cripto-1-Fc inhibits Nodal and BMP-4 signaling. To reconcile these two opposing activities we examined how endogenously expressed and overexpressed Cripto-1 affects BMP-4 signaling (Fig. 2-7). We found Cripto-1 was efficiently overexpressed in transiently transfected HepG2 cells (Figs. 2-7A, B) and strongly knocked down by shRNA in endogenously expressing NT2/D1 cells (Fig. 2-7C). Consistent with the potentiating activity of membrane-anchored Cripto-1, BMP-4 signaling was 2- to 3-fold higher in HepG2 cells transfected with Cripto-1 expression vector compared with HepG2 cells transfected with control vector (Fig. 2-7D). But Cripto-1

did not potentiate signaling by the BMP-4 homolog BMP-2, which we found does not bind Cripto-1 (Fig. 2-2A). In agreement with our earlier findings, soluble Cripto-1-Fc neutralized the potentiating activity of membrane associated Cripto-1 in HepG2 cells (Fig. 2-7E), revealing key functional differences between soluble and membrane bound forms. In support of our findings using HepG2 cells and Cripto-1 overexpression, BMP-4 signaled effectively in NT2/D1 cells transfected with scrambled shRNA vector, while Cripto-1 shRNA knockdown strongly suppressed BMP-4 signaling activities (Fig. 2-7F). Taken together, our findings indicate that membrane-anchored Cripto-1 can potentiate signaling by its cognate ligands, whereas the soluble form can inhibit signaling and outweigh the activities of the membrane-anchored form.

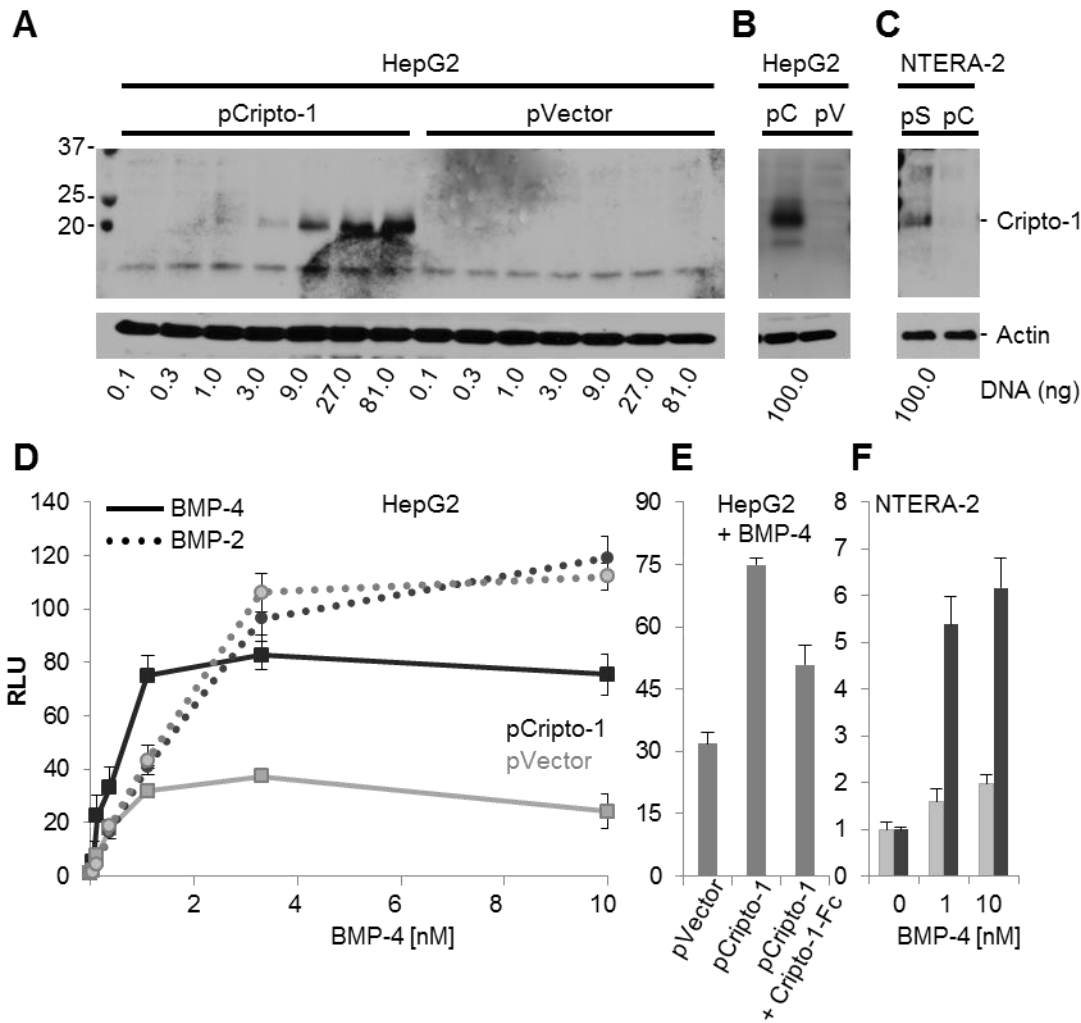


Figure 2-7. Signal-potentiating activities of membrane associated Cripto-1.

(A) Western blot of Cripto-1 overexpression in HepG2 cells. Cells were transfected with a control (*pVector*) or Cripto-1 (*pCripto-1*) expression vector at indicated concentrations. Expression of membrane associated (GPI-anchored) Cripto-1 was detected using the monoclonal anti-Cripto-1 antibody ab108391. (B) Western blot of Cripto-1 overexpression in HepG2 cells as used for reporter assay (D and E). Cells were transfected with 100 ng control (*pV*) or Cripto-1 (*pC1*) expression vector. (C) Western blot of Cripto-1 knockdown in NT2/D1 cells as used for the reporter assay (see F). Cells were transfected with 100 ng scrambled (*pSs*) or Cripto-1 (*pC1s*) shRNA vector. (D) Comparison of BMP-4 signaling (squares, solid lines) and BMP-2 signaling (circles, dotted lines) in HepG2 cells transfected with Cripto-1 expression vector (dark shade) or control vector (light shade). Signaling was induced with increasing concentrations of BMP-4 or BMP-2 as shown. Membrane bound Cripto-1 potentiates BMP-4 but not BMP-2 signaling. (E) Inhibition of signal potentiation with soluble Cripto-1. HepG2 cells transfected with control (*pVector*) or Cripto-1 (*pCripto-1*) expression vector were treated with 1 nM BMP-4 or with 1 nM BMP-4 and 500 nM Cripto-1-Fc.

Figure 2-7 (cont'd)

Fc. Soluble Cripto-1-Fc inhibits BMP-4 signaling even with co-expression of membrane bound Cripto-1. **(F)** Signal potentiation in Cripto-1 expressing NT2/D1 cells. Cells were transfected with 100 ng Cripto-1 shRNA vector (sC-1, light grey bars) or scrambled shRNA vector (sSc, dark grey bars). Cells were treated with 1 or 10 nM BMP-4. Cripto-1 knockdown (light grey bars) reduces BMP-4 signaling relative to the scrambled shRNA control (dark grey bars). Data are expressed as mean \pm SE of four biological replicates. Of note, previous studies have demonstrated that the magnitude of the luciferase signal is cell line dependent (44).

Discussion

The EGF-CFC family proteins Cripto-1 and Cryptic are essential regulators of TGF- β family signaling (2). They appear to have dual functions: as co-receptors of Nodal related ligands (3, 30, 31), and as antagonists of Activins and TGF- β s (28, 34-36). To reconcile these dichotomous activities, we undertook to elucidate their mechanism of action. Using recombinant human Cripto-1 and mouse Cryptic, we discovered that both molecules interact with a limited number of TGF- β family ligands. Cripto-1 interacted with Nodal and BMP-4, Cryptic interacted with Activin B. Notably, it has been suggested that Cripto-1 and Cryptic have similar, possibly redundant functions. But our biophysical evidence indicates there are clear functional differences between the two molecules. Thus, we propose Cripto-1 and Cryptic have distinct, non-overlapping ligand binding and regulatory functions.

Previous studies have indicated Cripto-1 binds the TGF- β family receptor ALK4. This interaction is thought to be critical for the Cripto-1 co-receptor function and for Nodal signaling (26, 28, 50). To evaluate its functional significance, we investigated whether Cripto-1 or Cryptic bind ALK4 or other TGF- β family receptors directly. Using SPR, we detected a response when probing Cripto-1 binding to ALK4. However, although these results appear to confirm an interaction, they are not conclusive as the response is dominated

by a non-specific binding component. Significantly, Cripto-1 did not cross-link with ALK4 in solution or improve Nodal–ALK4 complexation. We therefore conclude that the direct interaction between soluble Cripto-1 and ALK4 is weak, possibly non-specific and of limited consequence.

But our findings do not exclude a role for Cripto-1 in ALK4-dependent Nodal signaling. Previously, this interaction was investigated by co-IP. These studies showed Cripto-1 co-precipitated with ALK4. It is possible that the cell-based approach masked a more complex behavior. Namely, Cripto-1 – ALK4 binding could have been bridged by ligands that are present in the cell-growth medium. Alternatively, cell-surface proteins like LRP5, LRP6 or glypican could have facilitated Cripto-1 – ALK4 complexation (57, 58). Or ALK4 could have contacted the GPI linker, which is not present in the Fc fusion forms. While we show that the direct Cripto-1 – ALK4 ectodomain interaction is weak and possibly non-specific, whether Cripto-1 interacts with ALK4 indirectly and what the function of this complex is, remains to be determined.

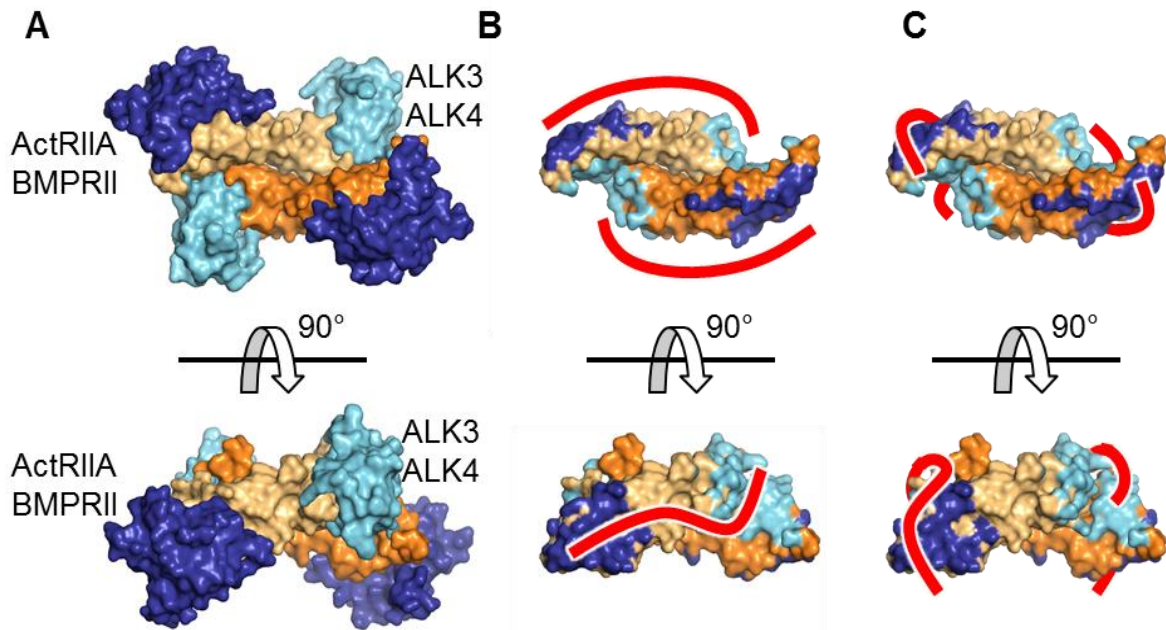


Figure 2-8. Molecular basis of ligand binding.

(A) Ligand-receptor complex based on the BMP-9-ALK1-ActRIIB structure (59). The disulfide-linked homodimeric ligand (center, orange) binds the extracellular domains of type I Activin receptor-like kinases (light blue) and type II Activin and BMP receptors (dark blue). Cripto-1 prevents ligand binding to type I and type II receptors indicating it contacts the receptor interaction surfaces on ligands. (B) Ipsilateral binding model. Receptor binding surfaces on the homodimeric ligand (orange) are shown. Light blue surfaces contact type I receptors, dark blue surfaces contact type II receptors. In this binding model, a Cripto-1/Cryptic protomer (red) contacts one side of the dimeric ligand. (C) Contralateral binding model. Receptor binding surfaces on the ligand are shown. Light blue surfaces contact type I receptors, dark blue surfaces contact type II receptors. In this model, a Cripto-1/Cryptic protomer (red) contacts both interaction surfaces of one ligand protomer.

The most widely recognized function of Cripto-1 is as Nodal ‘co-receptor’ (2). It is suggested Cripto-1 binds Nodal and potentiates Nodal signaling by stabilizing Nodal–ALK4 complexes (9, 23, 25, 26, 30). But Cripto-1 also antagonizes Activin and TGF- β signaling (28, 35, 36). To reconcile these divergent functions, we investigated how Cripto-1 and Cryptic recognize ligands. We speculated that molecular knowledge of this interaction could help clarify their biological functions. Using an SPR based approach that enables binding site

mapping (37), we discovered Cripto-1 and Cryptic contact ligand surfaces that are also recognized by type I or by type II receptors (Fig. 2-8). Although unexpected, these findings are not surprising, as ligands are small and a large fraction of their surface is covered by receptors when they form signaling complexes (38, 59). As our findings indicated there is significant overlap between the Cripto-1, Cryptic and receptor binding sites on ligands, we hypothesized soluble Cripto-1 and Cryptic could function as inhibitors of their cognate ligands *in vitro*. As predicted, Cripto-1-Fc inhibited BMP-4-dependent reporter gene expression. By contrast, Cryptic-Fc inhibited Activin B dependent reporter gene expression, supporting the conclusion that Cripto-1 and Cryptic have differing activities. Strikingly, the Cryptic-Fc reaction revealed a biphasic dose-response. As Cryptic-Fc was a far more effective inhibitor of Activin B – BMPRII than of Activin B – ActRIIA binding, we propose the biphasic response reflects differential inhibition of BMPRII and ActRIIA signaling complexes *in vitro*.

Taken together, our biophysical and *in vitro* studies show Cripto-1 and Cryptic can compete with receptors for ligand binding, thus revealing the molecular basis of their interaction with ligands. As Cripto-1 and Cryptic appear to bind ligands at or near receptor binding sites (Fig. 2-8), it is not surprising that the soluble Fc-fusion forms effectively inhibit signaling by their cognate ligands. But our findings raise critical questions about the co-receptor function. How can Cripto-1 or Cryptic potentiate signaling when their soluble forms prevent ligand-receptor complex formation? We submit that this mechanism has precedent in the repulsive guidance molecule (RGM) family of GPI anchored co-receptors (60-62). Like Cripto-1 and Cryptic, membrane-anchored RGMs potentiate BMP signaling, while their soluble forms inhibit BMP signaling (63). Recent crystal structures explain the inhibitory

function of RGMs: Similar to Cripto-1 and Cryptic, they occupy type I receptor binding-sites on ligands and thus inhibit signaling (64). To reconcile the RGM co-receptor and inhibitor functions, the authors propose RGMs help target BMP ligands into endosomes (64), which are enriched with TGF- β family receptors (65). By promoting internalization into receptor-rich endosomes, RGMs could help potentiate signaling. We propose Cripto-1 and Cryptic could have similar trafficking functions, which are mediated by GPI dependent membrane attachment and endosomal membrane localization (42). Indeed, overexpression of GPI anchored Cripto-1 on the cell surface potentiates BMP-4 signaling, whereas knockdown of endogenously expressed Cripto-1 reduces BMP-4 signaling, revealing a distinct, but critical function of the membrane associated forms. We propose that Cripto-1 and Cryptic may provide a mechanism for ligand capture at the cell surface and help target cognate ligands into receptor rich endosomes for signal potentiation.

In conclusion, we have elucidated the molecular basis of ligand recognition by the EGF-CFC family co-receptors Cripto-1 and Cryptic. Our findings reveal an unexpected molecular function that may be paralleled by the RGM family of GPI-anchored co-receptors. Namely, like RGMs, Cripto-1 and Cryptic contact receptor interaction-surfaces on TGF- β family ligands. Thus, their soluble forms can function as inhibitors of ligand-receptor binding. But our findings also raise many new questions. Does the inhibitor function have a biological role? Does endocytosis or trafficking explain how membrane-anchored Cripto-1 and Cryptic potentiate signaling (41, 42)? Can the co-receptor and inhibitor functions be reconciled?

REFERENCES

REFERENCES

1. Ciccodicola, A., Dono, R., Obici, S., Simeone, A., Zollo, M., and Persico, M. G. (1989) Molecular characterization of a gene of the 'EGF family' expressed in undifferentiated human NTERA2 teratocarcinoma cells. *Embo Journal* **8**, 1987-1991.
2. Shen, M. M., and Schier, A. F. (2000) The EGF-CFC gene family in vertebrate development. *Trends in Genetics* **16**, 303-309.
3. Salomon, D. S., Bianco, C., Ebert, A. D., Khan, N. I., De Santis, M., Normanno, N., Wechselberger, C., Seno, M., Williams, K., Sanicola, M., Foley, S., Gullick, W. J., and Persico, G. (2000) The EGF-CFC family: Novel epidermal growth factor-related proteins in development and cancer. *Endocrine Related Cancer* **7**, 199-226.
4. Schier, A. F. (2003) Nodal signaling in vertebrate development. *Annual Review of Cell and Developmental Biology* **19**, 589-621.
5. Minchiotti, G., Parisi, S., Liguori, G., Signore, M., Lania, G., Adamson, E. D., Lago, C. T., and Persico, M. G. (2000) Membrane-anchorage of cripto protein by glycosylphosphatidylinositol and its distribution during early mouse development. *Mechanisms of Development* **90**, 133-142.
6. Watanabe, K., Hamada, S., Bianco, C., Mancino, M., Nagaoka, T., Gonzales, M., Bailly, V., Strizzi, L., and Salomon, D. S. (2007) Requirement of glycosylphosphatidylinositol anchor of cripto-1 for trans activity as a nodal co-receptor. *The Journal of Biological Chemistry* **282**, 35772-35786.
7. Xu, C., Liguori, G., Persico, M. G., and Adamson, E. D. (1999) Abrogation of the cripto gene in mouse leads to failure of postgastrulation morphogenesis and lack of differentiation of cardiomyocytes. *Development* **126**, 483-494.
8. Ding, J., Yang, L., Yan, Y. T., Chen, A., Desai, N., Wynshaw-Boris, A., and Shen, M. M. (1998) Cripto is required for correct orientation of the anterior-posterior axis in the mouse embryo. *Nature* **395**, 702-707.
9. Gritsman, K., Zhang, J., Cheng, S., Heckscher, E., Talbot, W. S., and Schier, A. F. (1999) The EGF-CFC protein one-eyed pinhead is essential for nodal signaling. *Cell* **97**, 121-132.
10. Bhattacharya, B., Miura, T., Brandenberger, R., Mejido, J., Luo, Y., Yang, A. X., Joshi, B. H., Ginis, I., Thies, R. S., Amit, M., Lyons, I., Condie, B. G., Itskovitz-Eldor, J., Rao, M. S., and Puri, R. K. (2004) Gene expression in human embryonic stem cell lines: Unique molecular signature. *Blood* **103**, 2956-2964.

11. International Stem Cell, I., Adewumi, O., Aflatoonian, B., Ahrlund-Richter, L., Amit, M., Andrews, P. W., Beighton, G., Bello, P. A., Benvenisty, N., Berry, L. S., Bevan, S., Blum, B., Brooking, J., Chen, K. G., Choo, A. B., Churchill, G. A., Corbel, M., Damjanov, I., Draper, J. S., Dvorak, P., Emanuelsson, K., Fleck, R. A., Ford, A., Gertow, K., Gertsenstein, M., Gokhale, P. J., Hamilton, R. S., Hampl, A., Healy, L. E., Hovatta, O., Hyllner, J., Imreh, M. P., Itskovitz-Eldor, J., Jackson, J., Johnson, J. L., Jones, M., Kee, K., King, B. L., Knowles, B. B., Lako, M., Lebrin, F., Mallon, B. S., Manning, D., Mayshar, Y., McKay, R. D., Michalska, A. E., Mikkola, M., Mileikovsky, M., Minger, S. L., Moore, H. D., Mummery, C. L., Nagy, A., Nakatsuji, N., O'Brien, C. M., Oh, S. K., Olsson, C., Otonkoski, T., Park, K. Y., Passier, R., Patel, H., Patel, M., Pedersen, R., Pera, M. F., Piekarczyk, M. S., Pera, R. A., Reubinoff, B. E., Robins, A. J., Rossant, J., Rugg-Gunn, P., Schulz, T. C., Semb, H., Sherrer, E. S., Siemen, H., Stacey, G. N., Stojkovic, M., Suemori, H., Szatkiewicz, J., Turetsky, T., Tuuri, T., van den Brink, S., Vintersten, K., Vuoristo, S., Ward, D., Weaver, T. A., Young, L. A., and Zhang, W. (2007) Characterization of human embryonic stem cell lines by the International Stem Cell Initiative. *Nature Biotechnology* **25**, 803-816.
12. Shen, M. M., Wang, H., and Leder, P. (1997) A differential display strategy identifies cryptic, a novel EGF-related gene expressed in the axial and lateral mesoderm during mouse gastrulation. *Development* **124**, 429-442.
13. Yan, Y. T., Gritsman, K., Ding, J., Burdine, R. D., Corrales, J. D., Price, S. M., Talbot, W. S., Schier, A. F., and Shen, M. M. (1999) Conserved requirement for EGF-CFC genes in vertebrate left-right axis formation. *Genes and Development* **13**, 2527-2537.
14. Gaio, U., Schweickert, A., Fischer, A., Garratt, A. N., Muller, T., Ozcelik, C., Lankes, W., Strehle, M., Britsch, S., Blum, M., and Birchmeier, C. (1999) A role of the cryptic gene in the correct establishment of the left-right axis. *Current Biology* **9**, 1339-1342.
15. Strizzi, L., Bianco, C., Normanno, N., and Salomon, D. (2005) Cripto-1: A multifunctional modulator during embryogenesis and oncogenesis. *Oncogene* **24**, 5731-5741.
16. Cocciadiferro, L., Miceli, V., Kang, K. S., Polito, L. M., Trosko, J. E., and Carruba, G. (2009) Profiling cancer stem cells in androgen-responsive and refractory human prostate tumor cell lines. *Annals of the New York Academy of Science* **1155**, 257-262.
17. Miyoshi, N., Ishii, H., Mimori, K., Sekimoto, M., Doki, Y., and Mori, M. (2010) TDGF1 is a novel predictive marker for metachronous metastasis of colorectal cancer. *International Journal of Oncology* **36**, 563-568.

18. Xu, C. H., Sheng, Z. H., Hu, H. D., Hao, K. K., Wang, Q. B., and Yu, L. K. (2014) Elevated expression of cripto-1 correlates with poor prognosis in non-small cell lung cancer. *Tumor Biology* **35**, 8673-8678.
19. Bamford, R. N., Roessler, E., Burdine, R. D., Saplakoglu, U., dela Cruz, J., Splitt, M., Goodship, J. A., Towbin, J., Bowers, P., Ferrero, G. B., Marino, B., Schier, A. F., Shen, M. M., Muenke, M., and Casey, B. (2000) Loss-of-function mutations in the EGF-CFC gene CFC1 are associated with human left-right laterality defects. *Nature Genetics* **26**, 365-369.
20. Goldmuntz, E., Bamford, R., Karkera, J. D., dela Cruz, J., Roessler, E., and Muenke, M. (2002) CFC1 mutations in patients with transposition of the great arteries and double-outlet right ventricle. *The American Journal of Human Genetics* **70**, 776-780.
21. Sutherland, M. J., and Ware, S. M. (2009) Disorders of left-right asymmetry: heterotaxy and situs inversus. *American Journal of Medical Genetics. Part C, Seminars in Medical Genetics* **151C**, 307-317.
22. Shen, M. M. (2007) Nodal signaling: developmental roles and regulation. *Development* **134**, 1023-1034.
23. Kumar, A., Novoselov, V., Celeste, A. J., Wolfman, N. M., ten Dijke, P., and Kuehn, M. R. (2001) Nodal signaling uses activin and transforming growth factor-beta receptor-regulated SMADs. *The Journal of Biological Chemistry* **276**, 656-661.
24. Minchiotti, G., Manco, G., Parisi, S., Lago, C. T., Rosa, F., and Persico, M. G. (2001) Structure-function analysis of the EGF-CFC family member cripto identifies residues essential for nodal signalling. *Development* **128**, 4501-4510.
25. Reissmann, E., Jornvall, H., Blokzijl, A., Andersson, O., Chang, C., Minchiotti, G., Persico, M. G., Ibanez, C. F., and Brivanlou, A. H. (2001) The orphan receptor ALK7 and the activin receptor ALK4 mediate signaling by nodal proteins during vertebrate development. *Genes and Development* **15**, 2010-2022.
26. Yeo, C., and Whitman, M. (2001) Nodal signals to SMADs through cripto-dependent and cripto-independent mechanisms. *Molecular Cell* **7**, 949-957.
27. Chen, C., and Shen, M. M. (2004) Two modes by which lefty proteins inhibit nodal signaling. *Current Biology* **14**, 618-624.
28. Kelber, J. A., Shani, G., Booker, E. C., Vale, W. W., and Gray, P. C. (2008) Cripto is a noncompetitive activin antagonist that forms analogous signaling complexes with activin and nodal. *The Journal of Biological Chemistry* **283**, 4490-4500.

29. Fuerer, C., Nostro, M. C., and Constam, D. B. (2014) Nodal.Gdf1 heterodimers with bound prodomains enable serum-independent nodal signaling and endoderm differentiation. *The Journal of Biological Chemistry* **289**, 17854-17871.
30. Yan, Y. T., Liu, J. J., Luo, Y., E, C., Haltiwanger, R. S., Abate-Shen, C., and Shen, M. M. (2002) Dual roles of cripto as a ligand and coreceptor in the nodal signaling pathway. *Molecular and Cellular Biology* **22**, 4439-4449.
31. Cheng, S. K., Olale, F., Bennett, J. T., Brivanlou, A. H., and Schier, A. F. (2003) EGF-CFC proteins are essential coreceptors for the TGF-beta signals Vg1 and GDF-1. *Genes and Development* **17**, 31-36.
32. Liguori, G. L., Borges, A. C., D'Andrea, D., Liguoro, A., Goncalves, L., Salgueiro, A. M., Persico, M. G., and Belo, J. A. (2008) Cripto-independent nodal signaling promotes positioning of the A-P axis in the early mouse embryo. *Developmental Biology* **315**, 280-289.
33. Aykul, S., Ni, W., Mutatu, W., and Martinez-Hackert, E. (2015) Human cerberus prevents nodal-receptor binding, inhibits nodal signaling, and suppresses nodal-mediated phenotypes. *PLoS One* **10**, e0114954.
34. Adkins, H. B., Bianco, C., Schiffer, S. G., Rayhorn, P., Zafari, M., Cheung, A. E., Orozco, O., Olson, D., De Luca, A., Chen, L. L., Miatkowski, K., Benjamin, C., Normanno, N., Williams, K. P., Jarpe, M., LePage, D., Salomon, D., and Sanicola, M. (2003) Antibody blockade of the cripto CFC domain suppresses tumor cell growth in vivo. *The Journal of Clinical Investigation* **112**, 575-587.
35. Gray, P. C., Harrison, C. A., and Vale, W. (2003) Cripto forms a complex with activin and type II activin receptors and can block activin signaling. *Proceedings of the National Academy of Sciences of the United States of America* **100**, 5193-5198.
36. Gray, P. C., Shani, G., Aung, K., Kelber, J., and Vale, W. (2006) Cripto binds transforming growth factor beta (TGF-beta) and inhibits TGF-beta signaling. *Molecular and Cellular Biology* **26**, 9268-9278.
37. Aykul, S., and Martinez-Hackert, E. (2016) Determination of half-maximal inhibitory concentration using biosensor-based protein interaction analysis. *Analytical Biochemistry* **508**, 97-103.
38. Hinck, A. P. (2012) Structural studies of the TGF-betas and their receptors - insights into evolution of the TGF-beta superfamily. *FEBS Letters* **586**, 1860-1870.
39. Artus, J., Douvaras, P., Piliszek, A., Isern, J., Baron, M. H., and Hadjantonakis, A. K. (2012) BMP4 signaling directs primitive endoderm-derived XEN cells to an extraembryonic visceral endoderm identity. *Developmental Biology* **361**, 245-262.

40. Paca, A., Seguin, C. A., Clements, M., Ryczko, M., Rossant, J., Rodriguez, T. A., and Kunath, T. (2012) BMP signaling induces visceral endoderm differentiation of XEN cells and parietal endoderm. *Developmental Biology* **361**, 90-102.
41. Blanchet, M. H., Le Good, J. A., Mesnard, D., Oorschot, V., Baflast, S., Minchiotti, G., Klumperman, J., and Constam, D. B. (2008) Cripto recruits furin and PACE4 and controls nodal trafficking during proteolytic maturation. *Embo Journal* **27**, 2580-2591.
42. Blanchet, M. H., Le Good, J. A., Oorschot, V., Baflast, S., Minchiotti, G., Klumperman, J., and Constam, D. B. (2008) Cripto localizes nodal at the limiting membrane of early endosomes. *Science Signaling* **1**, ra13.
43. Parenti, A., Halbisen, M. A., Wang, K., Latham, K., and Ralston, A. (2016) OSKM induce extraembryonic endoderm stem cells in parallel to induced pluripotent stem cells. *Stem Cell Reports* **6**, 447-455.
44. Aykul, S., and Martinez-Hackert, E. (2016) Transforming growth factor-beta family ligands can function as antagonists by competing for type II receptor binding. *The Journal of Biological Chemistry* **291**, 10792-10804.
45. Gjidoda, A., Tagore, M., McAndrew, M. J., Woods, A., and Floer, M. (2014) Nucleosomes are stably evicted from enhancers but not promoters upon induction of certain pro-inflammatory genes in mouse macrophages. *PLoS One* **9**, e93971.
46. Schiffer, S. G., Foley, S., Kaffashan, A., Hronowski, X., Zichittella, A. E., Yeo, C. Y., Miatkowski, K., Adkins, H. B., Damon, B., Whitman, M., Salomon, D., Sanicola, M., and Williams, K. P. (2001) Fucosylation of cripto is required for its ability to facilitate nodal signaling. *The Journal of Biological Chemistry* **276**, 37769-37778.
47. Watanabe, K., Bianco, C., Strizzi, L., Hamada, S., Mancino, M., Bailly, V., Mo, W., Wen, D., Miatkowski, K., Gonzales, M., Sanicola, M., Seno, M., and Salomon, D. S. (2007) Growth factor induction of cripto-1 shedding by glycosylphosphatidylinositol-phospholipase D and enhancement of endothelial cell migration. *The Journal of Biological Chemistry* **282**, 31643-31655.
48. Shi, S., Ge, C., Luo, Y., Hou, X., Haltiwanger, R. S., and Stanley, P. (2007) The threonine that carries fucose, but not fucose, is required for cripto to facilitate nodal signaling. *The Journal of Biological Chemistry* **282**, 20133-20141.
49. Calvanese, L., Marasco, D., Doti, N., Saporito, A., D'Auria, G., Paolillo, L., Ruvo, M., and Falcigno, L. (2010) Structural investigations on the nodal-cripto binding: A theoretical and experimental approach. *Biopolymers* **93**, 1011-1021.

50. Bianco, C., Adkins, H. B., Wechselberger, C., Seno, M., Normanno, N., De Luca, A., Sun, Y., Khan, N., Kenney, N., Ebert, A., Williams, K. P., Sanicola, M., and Salomon, D. S. (2002) Cripto-1 activates nodal- and ALK4-dependent and -independent signaling pathways in mammary epithelial cells. *Molecular and Cellular Biology* **22**, 2586-2597.
51. Whitman, M. (2001) Nodal signaling in early vertebrate embryos: Themes and variations. *Developmental Cell* **1**, 605-617.
52. Lin, S. J., Lerch, T. F., Cook, R. W., Jardetzky, T. S., and Woodruff, T. K. (2006) The structural basis of TGF-beta, bone morphogenetic protein, and activin ligand binding. *Reproduction* **132**, 179-190.
53. Myszka, D. G., Jonsen, M. D., and Graves, B. J. (1998) Equilibrium analysis of high affinity interactions using BIACORE. *Analytical Biochemistry* **265**, 326-330.
54. Calvanese, L., Saporito, A., Oliva, R., G. D. A., Pedone, C., Paolillo, L., Ruvo, M., Marasco, D., and Falcigno, L. (2009) Structural insights into the interaction between the Cripto CFC domain and the ALK4 receptor. *Journal of Peptide Science* **15**, 175-183.
55. Korchynskyi, O., and ten Dijke, P. (2002) Identification and functional characterization of distinct critically important bone morphogenetic protein-specific response elements in the Id1 promoter. *The Journal of Biological Chemistry* **277**, 4883-4891.
56. Zawel, L., Dai, J. L., Buckhaults, P., Zhou, S., Kinzler, K. W., Vogelstein, B., and Kern, S. E. (1998) Human SMAD3 and SMAD4 are sequence-specific transcription activators. *Molecular Cell* **1**, 611-617.
57. Nagaoka, T., Karasawa, H., Turbyville, T., Rangel, M. C., Castro, N. P., Gonzales, M., Baker, A., Seno, M., Lockett, S., Greer, Y. E., Rubin, J. S., Salomon, D. S., and Bianco, C. (2012) Cripto-1 enhances the canonical wnt/beta-catenin signaling pathway by binding to LRP5 and LRP6 co-receptors. *Cell Signaling* **25**, 178-189.
58. Bianco, C., Strizzi, L., Rehman, A., Normanno, N., Wechselberger, C., Sun, Y., Khan, N., Hirota, M., Adkins, H., Williams, K., Margolis, R. U., Sanicola, M., and Salomon, D. S. (2003) A nodal- and ALK4-independent signaling pathway activated by cripto-1 through glypican-1 and c-Src. *Cancer Research* **63**, 1192-1197.
59. Townson, S. A., Martinez-Hackert, E., Greppi, C., Lowden, P., Sako, D., Liu, J., Ucran, J. A., Liharska, K., Underwood, K. W., Sehra, J., Kumar, R., and Grinberg, A. V. (2012) Specificity and structure of a high affinity activin receptor-like kinase 1 (ALK1) signaling complex. *The Journal of Biological Chemistry* **287**, 27313-27325.

60. Babitt, J. L., Zhang, Y., Samad, T. A., Xia, Y., Tang, J., Campagna, J. A., Schneyer, A. L., Woolf, C. J., and Lin, H. Y. (2005) Repulsive guidance molecule (RGMa), a DRAGON homologue, is a bone morphogenetic protein co-receptor. *The Journal of Biological Chemistry* **280**, 29820-29827.
61. Andriopoulos, B., Jr., Corradini, E., Xia, Y., Faasse, S. A., Chen, S., Grgurevic, L., Knutson, M. D., Pietrangelo, A., Vukicevic, S., Lin, H. Y., and Babitt, J. L. (2009) BMP-6 is a key endogenous regulator of hepcidin expression and iron metabolism. *Nature Genetics* **41**, 482-487.
62. Samad, T. A., Rebbapragada, A., Bell, E., Zhang, Y., Sidis, Y., Jeong, S. J., Campagna, J. A., Perusini, S., Fabrizio, D. A., Schneyer, A. L., Lin, H. Y., Brivanlou, A. H., Attisano, L., and Woolf, C. J. (2005) DRAGON, a bone morphogenetic protein co-receptor. *The Journal of Biological Chemistry* **280**, 14122-14129.
63. Corradini, E., Babitt, J. L., and Lin, H. Y. (2009) The RGM/DRAGON family of BMP co-receptors. *Cytokine Growth Factor Reviews* **20**, 389-398.
64. Healey, E. G., Bishop, B., Elegheert, J., Bell, C. H., Padilla-Parra, S., and Siebold, C. (2015) Repulsive guidance molecule is a structural bridge between neogenin and bone morphogenetic protein. *Nature Structural and Molecular Biology* **22**, 458-465.
65. Hartung, A., Bitton-Worms, K., Rechtman, M. M., Wenzel, V., Boergemann, J. H., Hassel, S., Henis, Y. I., and Knaus, P. (2006) Different routes of bone morphogenetic protein (BMP) receptor endocytosis influence BMP signaling. *Molecular and Cellular Biology* **26**, 7791-7805.

CHAPTER 3 -

HUMAN CERBERUS PREVENTS NODAL-RECEPTOR BINDING, INHIBITS NODAL SIGNALING, AND SUPPRESSES NODAL-MEDIATED BREAST CANCER PHENOTYPES²

²The work described in this chapter was published as the following manuscript: Senem Aykul, Wendi Ni, Washington Mutatu, and Erik M. Hackert. (2015) Human Cerberus Prevents Nodal-Receptor Binding, Inhibits Nodal Signaling, and Suppresses Nodal-Mediated Phenotypes. *PLoS ONE* **10**, e0114954.

Abstract

The Transforming Growth Factor- β (TGF- β) family ligand Nodal is an essential embryonic morphogen that is associated with progression of breast and other cancers. It has therefore been suggested that Nodal inhibitors could be used to treat breast cancers where Nodal plays a defined role. As secreted antagonists, such as Cerberus, tightly regulate Nodal signaling during embryonic development, we undertook to produce human Cerberus, characterize its biochemical activities, and determine its effect on human breast cancer cells. Using quantitative methods, we investigated the mechanism of Nodal signaling, we evaluated binding of human Cerberus to Nodal, and we characterized the mechanism of Nodal inhibition by Cerberus. Using cancer cell assays, we examined the ability of Cerberus to suppress aggressive breast cancer cell phenotypes. We found that human Cerberus binds Nodal with high affinity, blocks binding of Nodal to its signaling partners, and inhibits Nodal signaling. Moreover, we demonstrated that Cerberus profoundly suppresses migration, invasion, and colony forming ability of Nodal expressing and Nodal supplemented breast cancer cells. Taken together, our studies provide mechanistic insights into Nodal signaling and Nodal inhibition with Cerberus and highlight the potential value of Cerberus as anti-Nodal therapeutic.

Introduction

The Transforming Growth Factor- β (TGF- β) family ligand Nodal is an essential regulator of vertebrate embryonic development that plays a critical role in formation of the primary body axes and in germ layer specification (1–3). Beyond embryogenesis, the

biological roles of Nodal appear to be limited and, in mammals, Nodal is thought to be largely absent from adult tissues, with exception of some adult stem cell populations and highly dynamic reproductive tissues (4–7). However, a number of recent studies have shown that Nodal is re-expressed in various metastatic carcinomas, including melanoma and breast cancers, and that Nodal plays a critical role in promoting cancer progression (8–12). For example, Nodal has been shown to be expressed by aggressive melanoma cells and contributes to their tumorigenicity and plasticity (8), Nodal levels correlate with invasive phenotypes in several breast cancer cell lines (4, 10, 12), and Nodal is significantly overexpressed in tissue samples from patients diagnosed with advanced stage, invasive breast disease (11).

Nodal knockdown, pharmacologic inhibition of Nodal signaling, and Nodal blockade with polyclonal antibodies or with Embryonic Stem Cell (ESC) conditioned medium have been shown to suppress the invasive and tumorigenic phenotype of Nodal expressing, melanoma and breast cancer cells *in vitro* and *in vivo* (4, 8–10, 12–14). Thus, Nodal is a potential therapeutic target in treatment of melanoma and breast cancers. However, Nodal inhibition is currently not a feasible clinical option, as existing small molecule inhibitors suffer from poor bioavailability and/or inadequate specificity (15, 16), and function-blocking anti-Nodal monoclonal antibodies have yet to be identified.

During fish, frog, chick and mouse embryonic development, Nodal signaling is regulated by the secreted proteins Lefty and Cerberus (1). Both Lefty and Cerberus co-immunoprecipitate (co-IP) with Nodal and antagonize Nodal signaling (17–23). In addition, Lefty blocks Nodal receptor complex formation (17). Thus, it has been suggested that these embryonic Nodal-signaling antagonists could serve as Nodal inhibitors and potential anti-

Nodal therapeutics (24). Indeed, Lefty purified from stem cell conditioned medium inhibited the colony forming ability of Nodal-expressing human melanoma cells *in vitro* and decreased tumor cell proliferation and increased tumor cell apoptosis when injected into tumors formed from Nodal-expressing human melanoma cells *in vivo* (4). In contrast to Lefty, the embryonic Nodal antagonist Cerberus is less well understood and its molecular role during development as well as its potential as Nodal inhibitor in cancers have yet to be explored. We therefore undertook to elucidate, using purified, recombinant human proteins, the mechanism of Nodal signaling and Cerberus inhibition, and to characterize biological activities of human Cerberus in several human breast cancer cell lines.

Like all members of the TGF- β family, Nodal signals by binding the extracellular domains of ‘type I’ and ‘type II’ receptor kinases, thus initiating a phosphorylation cascade that leads to SMAD2/3 mediated expression of Nodal target genes (25–31). In addition, Nodal signaling during development requires membrane-anchored ‘co-receptors’ (5, 26, 32, 33) (Fig. 3-1). Here, using human proteins, we identified receptors and co-receptors that associate with Nodal. We showed that Cerberus binds Nodal with high affinity, blocks binding of Nodal to its receptors and co-receptors, and we demonstrated that Cerberus inhibits Nodal signaling. In addition, we discovered that Cerberus profoundly suppresses aggressive phenotypes in Nodal expressing, human breast cancer cell lines. Taken together, our studies demonstrate that human Cerberus is an inhibitor of Nodal and a potential therapeutic for treatment of breast cancers where Nodal plays a role.

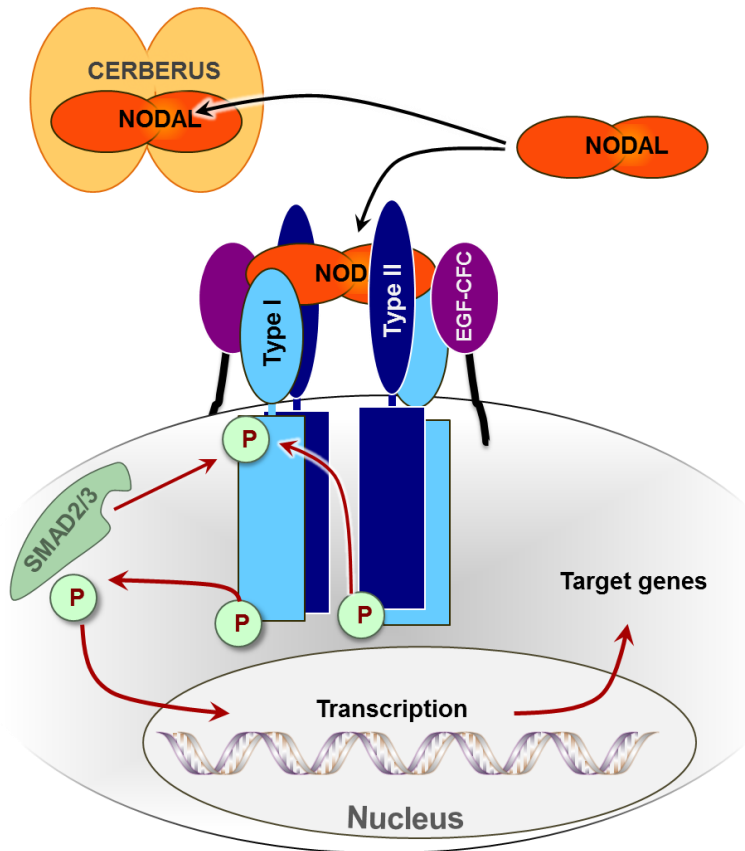


Figure 3-1. The Nodal signaling pathway.

Genetic interaction and co-immunoprecipitation (co-IP) studies have shown that the TGF- β family ligand Nodal (orange) interacts with the extracellular domains of type I Activin receptor-like kinases, including ALK4 and/or ALK7 (light blue), and type II Activin receptor kinases, including ActRIIA and/or ActRIIB (dark blue). Simultaneous binding of Nodal to both receptors initiates a phosphorylation cascade that leads to translocation of phosphorylated SMAD2 or SMAD3 (light green) transcription factors to the nucleus and expression of Nodal target genes. Nodal signaling also requires the EGF-CFC ‘co-receptors’ Cripto-1 and/or Cryptic (purple) during embryonic development. Co-IP studies have shown that EGF-CFC co-receptors interact with Nodal. The secreted protein Cerberus (light orange) binds Nodal and inhibits Nodal signaling.

Materials and Methods

Materials

Recombinant Activin A, GDF-8, GDF-11, GDF-1, TGF- β 1, BMP-2, BMP-9, ALK7-Fc and BMPRII-Fc were obtained from R&D Biosystems or Life Technologies. Activin A was also produced in-house.

Construction of expression plasmids

Synthetic human Cerberus-hIgg-Fc, human ActRIIA-hIgg-Fc, human ActRIIB-hIgg-Fc, human ALK4-hIgg-Fc and human Cryptic-hIgg-Fc genes were obtained from GeneArt. Fusion constructs included full-length Cerberus (amino acid 1–267), extracellular domains (ECD) of human ActRIIA (amino acid 1–120), ActRIIB (amino acid 1–120), ALK4 (amino acid 1–110), and Cryptic (amino acid 1–158). Functional domains (Cerberus and ECDs) were linked to human IgG1-Fc via a 22 amino acid long linker containing a TEV cleavage site, a glycine/serine rich region, and a FLAG-tag. Cripto-1 was cloned from cDNA obtained from Thermo Scientific. An amplicon encompassing Cripto-1 (amino acid 1–151) was fused to hIgg1-Fc domain using PCR.

Protein purification

All proteins were expressed using CHO cells. Cerberus-Fc, ActRIIA-Fc, ActRIIB-Fc, Cryptic-Fc, and Cripto-1-Fc were purified from condition medium using Protein A capture. Proteins were eluted with 100 mM Glycine, pH 3.0 and immediately neutralized with 2 M Tris, pH 8.5. Proteins were further purified or analyzed by SEC to ascertain monodispersity. Purified proteins were dialyzed PBS, pH 7.5 and stored at -20°C. The purity of the proteins was checked with SDS-PAGE under reducing and non-reducing conditions. The Fc portion

from recombinant Cerberus-Fc was removed using TEV protease followed by protein A affinity and SEC.

Cell lines

MDA-MB-231 (HTB-26), BT549 (HTB-122), Hs578t (HTB-125), MCF-7 (HTB-22) and T47D (HTB-133) were purchased from ATCC by Michigan State University researchers Kathleen Gallo and Chengfeng Yang and made available for these studies (34, 35). Cell lines were maintained according to ATCC culture conditions. Briefly, MDA-MB-231 cells were grown in DMEM/F12 medium supplemented with 5% FBS (Corning, 35-010-CV) and 1% P/S. MCF-7 and Hs578t cells were maintained in DMEM medium supplemented with 10% FBS and 1% P/S. BT549 cells were maintained in RPMI medium supplemented with 6% FBS and 1% P/S. T47D cells were maintained in RPMI medium supplemented with 10% FBS, 0.2 units/ml bovine insulin (SigmaAldrich, 11070-73-8) and 1% P/S. All cell lines were grown at 37°C under humidified, 5% CO₂ atmosphere. Freshly thawed cells were passaged at least three times before performing assays.

Immunoblotting

Cells were grown to 80% confluency, washed with 1X PBS and grown for an additional 24 h in fresh medium. Protein lysate was prepared by using ice cold RIPA lysis buffer (150mM NaCl, 1% NP40, 0.1% SDS, 50mM Tris, pH 8.0, protease inhibitor cocktail (Roche, 11836153001)). Cells were harvested in lysis buffer and stored at -80°C. Protein concentration of lysates was determined using Bradford. For Western blot, equal amounts of protein were separated on SDS-PAGE gels under reducing conditions and transferred to Hybond-P membranes. Membranes were blocked with 5% dry milk and incubated with primary Nodal antibody (Santa Cruz Biotechnology, sc-28913) at 1:1000 dilution followed

by incubation with Horseradish peroxidase conjugated secondary antibody at 1:5000 dilution. For Cerberus immunoblots, purified Cerberus was separated on SDS-PAGE and transferred to Hybond-P membranes. Membranes were probed with 1 ug/ml primary Cerberus antibody (RnD Systems, AF1075) followed by incubation with Horseradish peroxidase conjugated secondary antibody at 1:1000 dilution. For p-SMAD2 immunoblots, $\sim 1.0 \times 10^5$ cells were plated to 24-well plate and grown to 80% confluency in complete media, washed with 1X PBS, starved overnight and grown for an additional 24 h in serum free medium+0.1%BSA with or without 178 nM Cerberus-Fc. For p-SMAD2 immunoblots of T47D cells, $\sim 2.0 \times 10^5$ cells were plated to 24-well plate and grown to 80% confluency in complete media, washed with 1X PBS, starved overnight and grown for additional 24 h in serum free medium with or without 39 nM Nodal and/or 17.8 or 178 nM Cerberus. Protein lysate was prepared by using ice cold RIPA lysis buffer (150mM NaCl, 1% NP40, 0.1% SDS, 0.5% sodium deoxycholate, 50mM Tris pH 8.0, 1X 'Recom ProteaseArrest' protease inhibitor cocktail (G-Biosciences, 786-436) and 2X 'PhosphataseArrest' phosphatase inhibitor cocktail (G-Biosciences, 786-450)). Cells were harvested in lysis buffer and cell lysis supernatant was stored at -80°C . Protein concentration of lysates was determined using Bradford Assay. Equal amounts of protein were separated on SDS-PAGE and transferred to Hybond-P membranes. Membranes were blocked with 5% BSA and incubated with primary p-SMAD2 (Cell Signaling, 3108S), SMAD2 (Cell Signaling, 5339S) antibodies at 1:1000 dilution and followed by incubation with Horseradish peroxidase conjugated secondary antibody at 1:2000 dilution. WesternBright ECL HRP substrate was used for detection (Advansta, K-12043-D20). Western blots were visualized by exposing the gel to autoradiography film or by using a Bio-

Rad ChemiDoc imaging system. Quantification of immunoblots was done by using ImageJ software.

Surface plasmon resonance

Receptor-ligand binding affinities were determined by SPR using the Biacore 2000. Anti-human IgG (Fc) antibody was immobilized onto four channels of a CM5 chip using amine coupling chemistry. 200–300 RU of purified Cerberus-Fc, ActRIIA-Fc, ActRIIB-Fc, ALK4-Fc or Cripto-1-Fc was captured on the experimental flow channels. A reference channel was monitored to account for nonspecific binding, drift, and bulk shifts. For kinetic analysis, a concentration series of Nodal and other ligands (Activin A, GDF-8, GDF-11, GDF-1, TGF- β 1, BMP-2 and BMP-9) was injected over experimental and control flow channels at 50 μ l/min flow rate. Associations were performed for 300 seconds and dissociations were performed for 750. For selected concentrations, dissociations were also performed for 4000 seconds. Only 750 second dissociations are shown in figures. For inhibition analysis 80 nM Nodal was combined with 0 nM, 40 nM or 400 nM Fc-free Cerberus. The pre-assembled Nodal/Cerberus complexes were injected over experimental and control flow channels at 50 μ l/min flow rate. After each binding cycle, the antibody surface was regenerated to base line. All experiments were carried out at 25°C in HBS-EPS buffer (0.01 M HEPES, 0.5 M NaCl, 3 mM EDTA, 0.005% (v/v) Tween 20, pH 7.4). Receptors and ligands, except Nodal, were kept in running buffer containing 0.5mg/ml BSA (Sigma-Aldrich, A3059). Nodal containing samples were kept without BSA, as the presence of BSA causes rapid inactivation of recombinant human Nodal. Running buffer for all experiments, except those involving Nodal, contained 0.5 mg/ml BSA. Sensograms were analyzed by double referencing. To obtain kinetic rate constants, the processed data was fitted to 1:1 Langmuir interaction model

using Scrubber or BiaEvaluation software. The equilibrium dissociation constant K_d was determined by calculating the ratio of binding rate constants k_d/k_a . Binding rate constants are summarized in Table 3-1.

Migration assay

MCF-7, Hs578t, BT549, and MDA-MB-231 cells were seeded in an Ibidi insert (Ibidi GmbH, 81176) in complete growth medium. Once cells reached ~ 80% confluence, the insert was removed and medium was replaced with complete medium containing 2.5 $\mu\text{g/ml}$ Mitomycin C and 17.8, or 178 nM Cerberus-Fc or no Cerberus control. Cells were monitored for up to 48 h and images were taken using an inverted microscope with 10X magnification at 0 h and 24 h. Migration was quantified using Vimages software (Ibidi).

Invasion assay

Experiments were performed using a Cultrex 96 Well Basement Membrane Extract (BME) Cell Invasion Assay kit (Trevigen) and medium containing 2.5 $\mu\text{g/ml}$ Mitomycin C. For Nodal induction, ~ 50,000 T47D cells in serum free medium containing 0, or 39 nM (500 ng/ml) Nodal were seeded in the top chamber of the BME coated Boyden chamber plate. Serum free medium containing 0.2 units/ml bovine insulin was added to the bottom chamber. For Cerberus inhibition, ~10,000 MCF-7, Hs578t, BT549, and MDA-MB-231 cells in serum free medium were seeded in the top chamber of the BME coated Boyden chamber plate. Complete medium was added to the bottom chamber. Top and bottom chamber contained 0 nM, 17.8 nM, or 178 nM Cerberus-Fc and 2.5 $\mu\text{g/ml}$ Mitomycin C. Cell invasion was determined after 24 h by monitoring Calcein-AM fluorescence in the bottom chamber.

Soft agar colony formation assay

MCF-7 or MDA-MB-231 cells (~ 2,500) were resuspended in 0.35% SeaPlaque agarose (Lonza, 50101) in complete medium containing 0 nM, 17.8 nM, or 178 nM Cerberus-Fc and plated on a layer of 0.7% SeaPlaque agarose containing complete medium. Cells were fed twice weekly with complete medium and the corresponding concentrations of Cerberus-Fc. After three weeks, cells were stained with 0.005% crystal violet and images were taken. Cell clusters were quantified using ImageJ software. Colony forming ability was calculated by dividing the number of colonies by the number of initial cells. Percent colony forming ability was determined by dividing the number of colonies formed with Cerberus-Fc relative to no Cerberus-Fc control.

Reporter assay

~ 50,000 T47D cells in complete medium were seeded in each well of a 96-well plate and grown overnight. The next day, each was transfected with a solution containing 200 ng of the pSBE4-luc (experimental luciferase reporter plasmid, firefly luciferase), 2 ng of the pRL-CMV-luc (control luciferase reporter plasmid, renilla luciferase) and 0.25 μ l Lipofectamine 2000 (Life Technologies). Transfection reagent containing medium was removed the following day, and medium was replaced with serum free RPMI medium containing test proteins. After 16 h incubation at 37°C, luciferase activity was detected with the Dual-Glo Luciferase Assay System (Promega). Relative luciferase units were calculated by dividing firefly luciferase units with renilla luciferase units.

Statistics

2D cell-based assays with exception of cell migration were performed in quadruplicates and were repeated at least three different times. Colony forming assays were performed in

triplicate. Statistical significance was determined using a two-tailed T-test. P values < than 0.05 marked *, P values < than 0.01 were marked **. Cell invasion assays were performed at least three different times.

Results

Nodal binds ALK4, BMPRII and Cripto-1

Mouse, frog and fish Nodal have been shown to signal and/or co-IPs with the ‘type I’ Activin receptor-like kinases ALK4 and ALK7, the ‘type II’ receptor kinases ActRIIA and ActRIIB, and the co-receptors Cripto-1 and Cryptic (26, 27, 32). To confirm that the homologous human receptors and co-receptors interact with Nodal, we examined their binding to Nodal using purified human-hIggFc fusion proteins and SPR. We captured receptor/co-receptor extracellular domain-Fc (ECD-Fc) fusion proteins by immobilizing an anti-hIggFc antibody on a CM5 SPR sensor chip and we injected recombinant Nodal (RnD Systems) over the captured human receptor and co-receptor extracellular domains.

Our SPR sensograms showed that Nodal binds both ActRIIB and ActRIIA (Fig. 3-2A, B); however, the interaction between Nodal and ActRIIA is very weak by TGF- β -family ligand/receptor standards ($K_d \sim 100$ nM). ActRIIB appears to bind Nodal more stably, as reflected in the slow dissociation of this complex ($k_d = 4.9 \times 10^{-4}$ (s⁻¹), Fig. 3-2A, Table 3-1); however, we were unable to obtain a satisfactory kinetic model to describe this interaction. Thus, our data indicate that Nodal binds ActRIIB over ActRIIA, but neither receptor interacts with Nodal in a manner that is characteristic of cognate TGF- β family ligand-type II receptors complexes (36–38). These unexpected findings led us to ask whether other type II receptors may interact with Nodal in a more characteristic manner. We therefore tested binding of Nodal to the type II TGF- β family receptors TGF β RII and BMPRII. We found

that Nodal alone does not bind TGF β RII (data not shown). By contrast, we discovered that Nodal binds BMPRII with very high affinity (Fig. 3-2D, Table 3-1). This interaction can be described satisfactorily with a standard kinetic model and the resulting binding rate constants are consistent with those determined for other TGF- β family ligands and their cognate type II receptors ($k_a = 3.1 \times 10^5 \text{ (M}^{-1}\text{s}^{-1})$, $k_d = 4.6 \times 10^{-5} \text{ (s}^{-1})$, $K_d = 0.15 \text{ nM}$) (36–38).

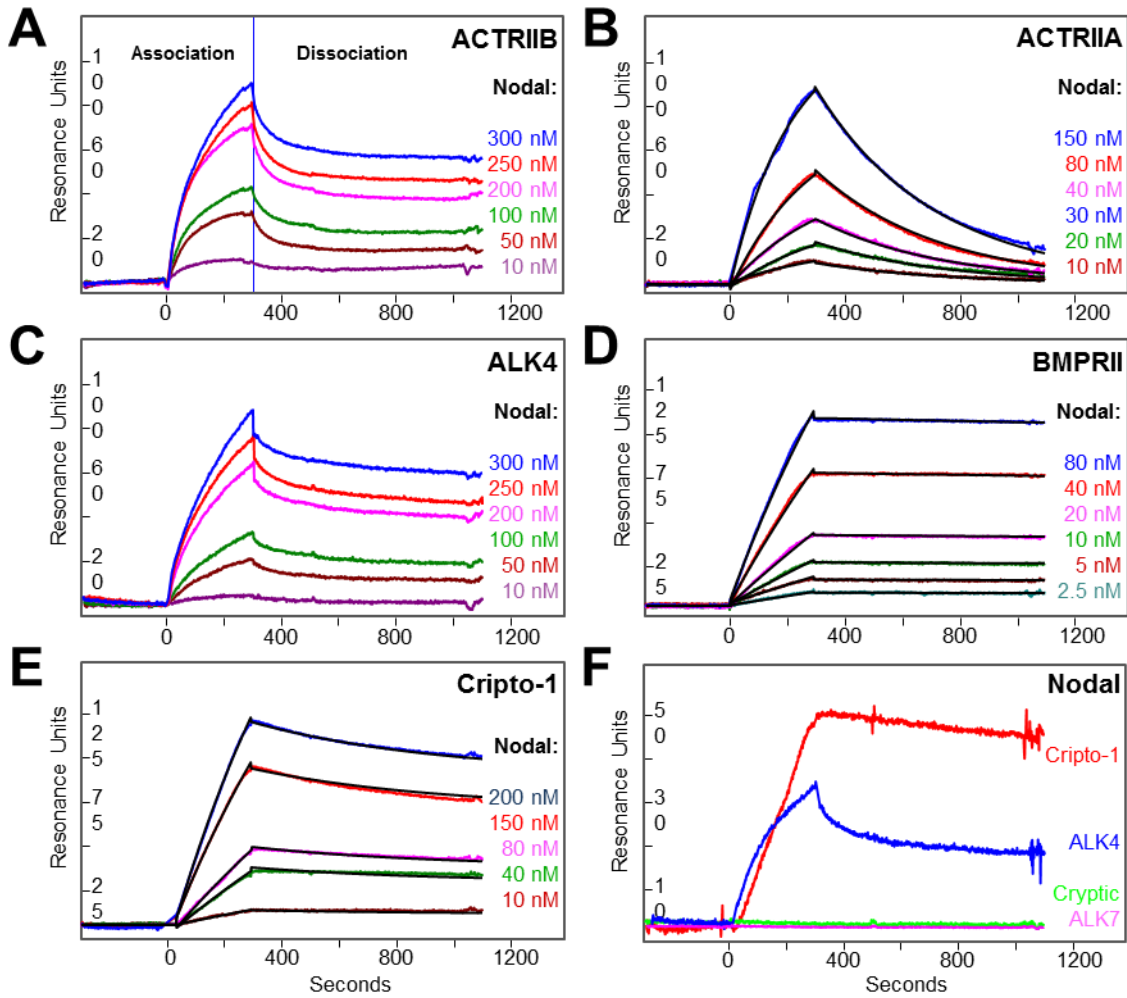


Figure 3-2. Nodal-receptor interactions.

Nodal binding to (A) ActRIIB-Fc, (B) ActRIIA-Fc, (C) ALK4-Fc, (D) BMPRII-Fc, (E) Cripto-1-Fc. (A-E) ActRIIB-Fc, ActRIIA-Fc, ALK4-Fc, BMPRII-Fc and Cripto-1-Fc were immobilized on an SPR sensor chip and different concentrations of Nodal were injected as

Figure 3-2 (cont'd)

shown. Fitted curves (orange lines) are superimposed over experimental curves. **(F)** Comparison of Nodal binding to Cripto-1, Cryptic, ALK4 and ALK7. Equal amounts of Fc fusion proteins as determined by SPR response units were immobilized on the SPR sensor chip and 80 nM Nodal was injected. Cripto-1 (red) binds Nodal as co-receptor, but not Cryptic (green). ALK4 (blue) binds Nodal as type I receptor, but not ALK7 (purple).

Our SPR sensograms further revealed that Nodal binds ALK4, but not ALK7 (Fig. 3-2C, F). The interaction between Nodal and ALK4 (Fig. 3-2C); however, is not as well defined or as strong as, for example, the interaction between Activin A and ALK4, which fits a standard kinetic model very well (data not shown, Table 3-1). Concerning co-receptors, Nodal binds strongly the co-receptor Cripto-1, whereas Nodal doesn't bind Cryptic (Fig. 3-2E, F). Significantly, Nodal binding to Cripto-1 is stable and can be described well with a standard kinetic model (Fig. 3-2E, Table 3-1). In summary, we conclude that, in humans, the cognate type II receptor for Nodal is BMPRII and to a lesser degree ActRIIB (Fig. 3-2A, D), that the cognate type I receptor for Nodal is ALK4 and not ALK7 (Fig. 3-2C, F), and that the primary co-receptor is Cripto-1 and not Cryptic (Fig. 3-2E, F).

Table 3-1. Equilibrium dissociation and binding rate constants

Ligand	Interacting	k_a ($M^{-1}s^{-1}$)	k_d (s^{-1})	K_d (nM)
Nodal	ActRIIA	2.0×10^4	2.0×10^{-3}	100
	ActRIIB	4.9×10^4 (est)	4.9×10^{-4} (est)	10 (est)
	BMPRII	3.1×10^5	4.6×10^{-5}	0.149
	ALK4	4.6×10^4 (est)	3.2×10^{-4} (est)	15 (est)
	ALK7		No Binding	
	Cripto-1	1.0×10^4	2.6×10^{-4}	16
	Cryptic		No Binding	
Activin A	ActRIIA	1.1×10^6	2.5×10^{-5}	0.023
	ActRIIB	1.5×10^6	2.7×10^{-5}	0.018
	ALK4	2.0×10^5	4.8×10^{-4}	2.4
Nodal	Cerberus	1.3×10^4	1.4×10^{-5}	1.1
GDF-11	Cerberus	$\sim 1.2 \times 10^3$	~ 0.014	$\sim 5,800^\dagger$
BMP-2	Cerberus	$\sim 2.4 \times 10^4$	~ 0.072	$\sim 3,000^\dagger$

(est): Binding rates were calculated by separately fitting association and dissociation rate constants for each concentration and taking the average of the calculated binding rate constants.

†: Binding rates were calculated by fitting each individual concentration and taking the average of the calculated binding rate constants.

Human Cerberus binds Nodal with high affinity

The secreted protein Cerberus is a negative regulator of Nodal signaling during frog and mouse embryonic development and co-IPs with frog Nodal (Xnr1) (18, 22, 23, 40). To demonstrate that human Cerberus binds human Nodal and inhibits Nodal signaling, we expressed it as fusion protein with human Igg1-Fc (Cerberus-Fc) (Fig. 3-3A). We purified Cerberus-Fc to homogeneity (Fig. 3-3B), and examined binding of Nodal to Cerberus by SPR (Fig. 3-3C). Our sensograms showed that Nodal bound immobilized Cerberus-Fc with low nanomolar affinity ($K_d = 1.1$ nM, Fig. 3-3C, Table 1). Its slow dissociation rate ($k_d = 1.4 \times 10^{-5}$ (s^{-1})) indicates that this complex is very stable.

Cerberus from different species has been shown to interact with Nodal and with other TGF- β family ligands. For example, functional antagonism, co-IP, or direct binding studies in

frog and mouse showed that Cerberus interacts with BMP-2, and Activin A (18, 23, 41–43). We therefore examined by SPR binding of human Cerberus-Fc to these ligands. We also tested binding of TGF- β family ligands that interact with ActRIIB, including GDF-8, GDF-11, and BMP-9. Our sensograms revealed that of all tested TGF- β family ligands only BMP-2 and GDF-11 also bound Cerberus-Fc; however, both molecules bound Cerberus-Fc considerably more weakly than Nodal (K_d 3,000 and 5,800 nM, respectively, Table 3-1). In contrast, human Cerberus-Fc did not bind any other tested TGF- β family ligand with consequential affinity. We therefore conclude that human Cerberus binds Nodal with high affinity and Cerberus seems to be more specific relatively to TGF- β family receptors.

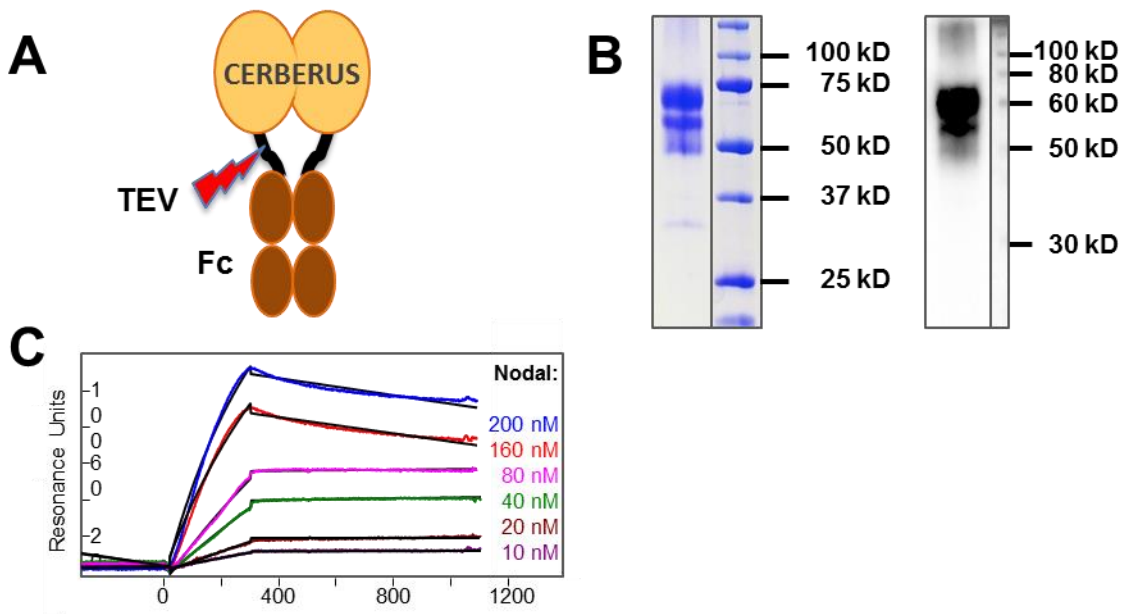


Figure 3-3. Cerberus ligand binding.

(A) Recombinant Cerberus construct. Full length human Cerberus was fused at the C-terminus to a human IgG1-Fc fragment via a linker containing a TEV cleavage site. (B) Coomassie Blue stained SDS-PAGE of Cerberus shown on the left side of the panel, Western blot using anti-Cerberus antibody is shown on the right side of the panel. Recombinant Cerberus is purified from CHO cell conditioned medium using protein A capture. Overall, Cerberus-Fc is pure; size heterogeneity may be introduced by variations in glycan structure. The observed smaller Cerberus-Fc fragment could correspond is likely a proteolytic product.

Figure 3-3 (cont'd)

(C) Nodal-Cerberus interaction. Cerberus-Fc was immobilized on an SPR sensor chip and different concentrations of Nodal were injected as shown. Fitted curves (black lines) are superimposed over experimental curves.

As others have shown by single SPR injection that BMP-2 stably associates with mouse Cerberus (Cer1) (42), we were surprised to discover that the human Cerberus-BMP-2 complex is not very stable. This can be seen in its fast dissociation rate ($k_d = 0.072 \text{ (s}^{-1}\text{)}$). To resolve this unexpected observation, we compared the amino acid sequences of Cerberus and several TGF- β family ligands and receptors from different species (Table 3-2). As expected, we found that sequence conservation in TGF- β family ligands and receptors is very high throughout a wide range of vertebrate species. For example, mature domains of TGF- β family ligands are essentially identical between mice and humans (98–100% sequence identity). By comparison, the primary sequence of Cerberus differs significantly between species and shows only 69% identity between mice and humans. We propose that considerable variations in amino acid sequence could result in unique binding specificities and function of Cerberus in different species.

Table 3-2. Sequence comparison between TGF- β family proteins of different species

	Mouse	Chick	Xenopus	Zebrafish
Cerberus	69	47 (Caronte)	51	29 (DAND5)
Nodal	98	63	60	68 (NR2)
BMP-4	98	95	96	89
BMP-2	100	96	96	82
Activin A	100	98	87	80
GDF-11	100	89 (GDF-8)	99	97
ActRIIB ^{ecd}	99	87	77	74
ALK4 ^{ecd}	93	75	65	57
Cripto-1	73	49	45	36 (OEP)

Note: Mature ligand and receptor/co-receptor ecto domains were compared. Identities were calculated relative to the human proteins over the entire conserved region.

Human Cerberus prevents Nodal interactions and inhibits Nodal signaling

Cerberus is an inhibitor of Nodal signaling and Nodal mediated phenotypes during mouse, chick and frog embryonic development (18, 22, 23, 40, 43, 44). To elucidate the mechanism of Cerberus inhibition, we tested by SPR binding of pre-formed Nodal-Cerberus complexes to Nodal receptors and co-receptors. This format enabled us to identify specific Nodal interactions that Cerberus blocks. We immobilized the Nodal interacting proteins ActRIIB-Fc, BMPRII-Fc, ALK4-Fc and Cripto-1-Fc on an SPR sensor chip and flew Nodal or pre-assembled Nodal-Cerberus complexes over the receptor or co-receptor bound sensor chip. In this format, we kept the Nodal concentration constant at 80 nM. Our SPR sensograms revealed that Cerberus effectively blocks binding of Nodal to ActRIIB, ALK4 and Cripto-1 in a concentration dependent manner (Fig. 3-4A-D). Cerberus also blocks binding of Nodal to its high affinity receptor BMPRII, however, this inhibition is not as efficient or complete as that of Nodal binding to ActRIIB (Fig. 3-4A, B) and appears to be driven primarily by a change in interaction kinetics. To evaluate if Cerberus-Fc is a competitive Nodal inhibitor, we determined the K_d of Nodal binding to ActRIIB, BMPRII, ALK4 and Cripto-1 in the presence of Cerberus-Fc. We found that for ActRIIB, ALK4 and Cripto-1, Cerberus-Fc obeys a competitive inhibitor binding-model (data not shown).

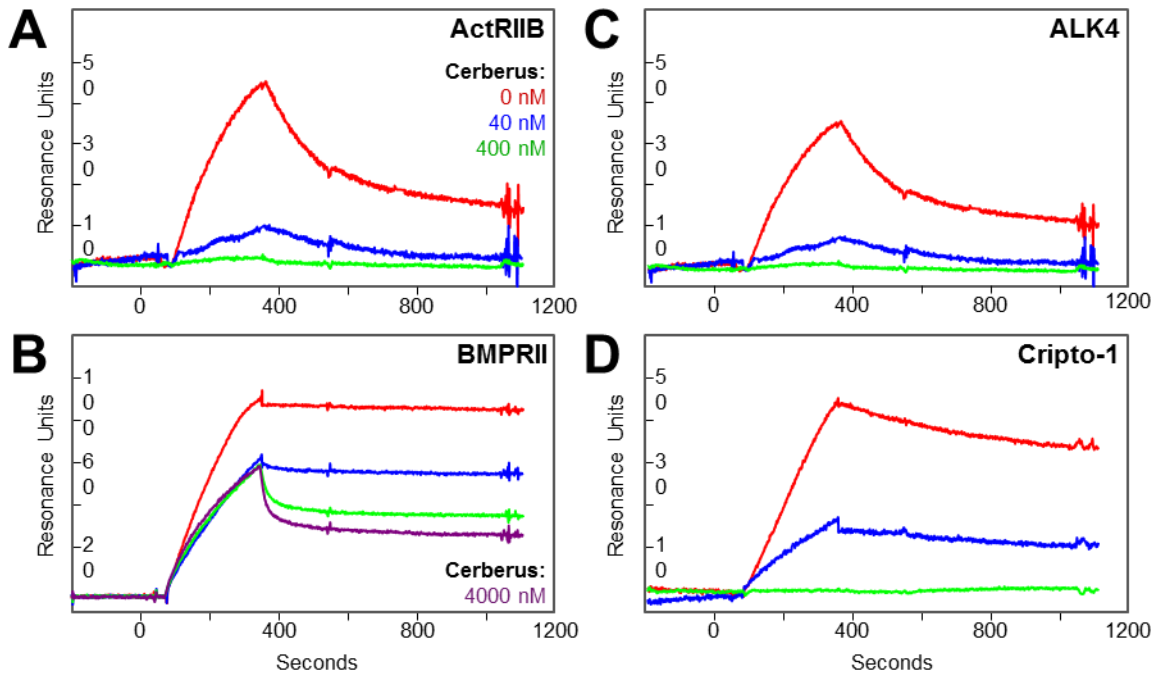


Figure 3-4. Cerberus inhibition of Nodal interactions.

(A) Cerberus inhibition of Nodal-ActRIIB binding. (B) Cerberus inhibition of Nodal-BMPRII binding. (C) Cerberus inhibition of Nodal-ALK4 binding. (D) Cerberus inhibition of Nodal-Cripto-1 binding. ActRIIB-Fc, ALK4-Fc, BMPRII-Fc or Cripto-1-Fc was immobilized on an SPR sensor chip. (A-D) 80 nM Nodal was preincubated with 0 nM (red), 40 nM (blue), 400 nM (green), or 4000 nM (purple) Cerberus. Preformed Nodal-Cerberus complexes were injected over the sensor chip. (A, C, D) Cerberus prevents binding of Nodal to ActRIIB, ALK4, and Cripto-1, as seen in the complete loss of an SPR response at the 400 nM Cerberus concentration (green). (B) Cerberus destabilizes the Nodal-BMPRII interaction, as seen in the altered curve shapes at 4000 nM Cerberus (purple).

As binding of Nodal to its cognate receptor kinases has been shown to initiate a phosphorylation cascade that leads to SMAD2/3 mediated gene expression (Fig. 3-1) (31), we undertook to demonstrate using a SMAD2/3 sensitive reporter gene assay that Cerberus suppresses Nodal mediated gene expression. We transfected T47D human breast cancer cells with pSBE4-luc (45) as SMAD2/3 responsive reporter, and pRL-CMV-luc as control. We treated transfected cells with Nodal and/or Cerberus-Fc to final concentrations of 39 nM and 178 nM, respectively. Our reporter assay showed that Nodal induces luciferase activity

approximately 2.2 fold relative to control and that Cerberus-Fc strongly inhibits the Nodal dependent luciferase signal (Fig. 3-5A). To demonstrate that this effect is linked with SMAD2/3 phosphorylation, we performed a phospho-SMAD2 Western blot (Fig. 3-5B). We treated T47D cells with 39 nM Nodal and/or 178 nM Cerberus-Fc. Consistent with the reporter assay results, Nodal alone causes a small increase in SMAD2 phosphorylation. Cerberus-Fc alone has no effect on SMAD2 phosphorylation in T47D cells. However, Cerberus-Fc reverses Nodal mediated SMAD2 phosphorylation. Together, our results support the conclusion that Cerberus prevents binding of Nodal to its receptors and co-receptors and thus suppresses Nodal dependent transcriptional programs.

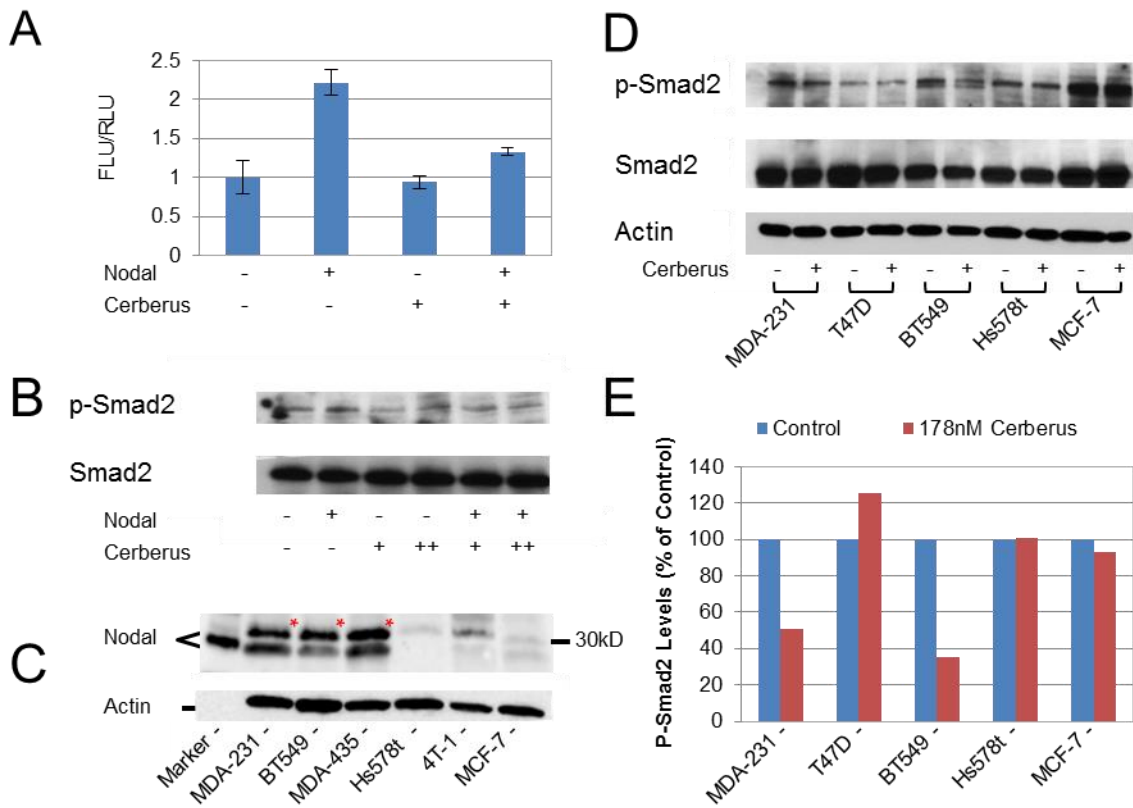


Figure 3-5. Nodal inhibition with Cerberus in cell lines.

(A) Nodal induced gene expression. T47D cells were transfected with the pSBE4-luc reporter plasmid and the pRL-CMV-luc control plasmid. Cells were treated with 39 nM Nodal, and/or

Figure 3-5 (cont'd)

178 nM Cerberus. Nodal signaling was detected by firefly luciferase activity and normalized against renilla luciferase activity. **(B)** Nodal induced SMAD2 phosphorylation. T47D cells were treated with 39 nM Nodal, and/or 17.8 or 178 nM Cerberus. 10 µg of whole cell lysate per lane were loaded on an SDS-PAGE gel and probed with an anti-p-SMAD2 antibody. A small increase in SMAD2 phosphorylation can be seen when recombinant Nodal is added. Cerberus inhibits Smad2 phosphorylation. **(C)** Western blot detection of Nodal in five breast cancer cell lines. 10 µg of whole cell lysate per lane were loaded on an SDS-PAGE gel and probed with an anti-Nodal antibody. MCF-7, Hs578t, BT549 and MDA-MB-231 human breast cancer cells were tested. Human MDA-MB-435 melanoma derived cells and mouse 4T-1 breast cancer cells were also probed. **(D)** Western blot detection of SMAD2 phosphorylation in five breast cancer cell lines. Cells were grown in serum free medium with or without 178 nM Cerberus. 5 µg of whole cell lysate per lane were loaded on an SDS-PAGE gel. The gels were probed with an anti-SMAD2 antibody. Total SMAD2 and Actin were used as controls. **(E)** Quantitation of p-SMAD2 western. The image shown in Fig. 3-5D was scanned and quantitated using ImageJ. SMAD2 phosphorylation is normalized with untreated cells. Both MDA-MB-231 and BT549 cells show a significant decrease in SMAD2 phosphorylation when treated with Cerberus. By contrast Hs578t, T47D and MCF-7 SMAD2 phosphorylation is not affected by Cerberus.

Nodal is expressed in invasive breast cancer cell lines and induces invasion

Nodal expression has been found to be elevated in invasive and poorly differentiated breast cancer cell lines and Nodal has been shown to promote aggressive breast cancer cell phenotypes (10–13, 46, 47). To evaluate Cerberus as Nodal inhibitor in human breast cancers, we examined by Western blotting Nodal expression in several human breast cancer cell lines that exhibit different invasive properties *in vitro* and *in vivo*, including MDA-MB-231, BT549, Hs578t, and MCF-7. In agreement with previous studies, we found that triple negative, highly invasive and metastatic MDA-MB-231 breast cancer cells express high levels of Nodal and that hormone receptor positive, weakly invasive and non-metastatic MCF-7 breast cancer cells express low levels of Nodal (Fig. 3-5C) (10, 11, 13, 48, 49). In addition, we found that Nodal is expressed in triple negative, highly invasive and metastatic BT549 breast cancer cells, in MDA-MB-435 melanoma cells, but not in triple negative, invasive but non-metastatic Hs578t human or in 4T1 mouse breast cancer cells. To test

whether Cerberus-Fc can directly impact Nodal mediated SMAD2/3 signaling in Nodal expressing breast cancer cells, we performed a phospho-SMAD2 Western blot (Fig. 3-5D, E). We grew breast cancer cells in serum free medium with or without 178 nM Cerberus-Fc. Consistent with our Nodal Western blot results (Fig. 3-5C), we found that Cerberus-Fc reduced p-SMAD2 levels in Nodal expressing breast cancer cell lines, including MDA-MB-231 and BT549, but not in cell lines where we did not detect a Nodal signal, including T47D, MCF-7 and Hs578t. Quantification of our Western blot results shows that Cerberus-Fc reduces SMAD2 phosphorylation by almost 50% in MDA-MB-231 cells and 75% in BT549 cells.

To demonstrate that Nodal mediates aggressive phenotypes in breast cancer cell lines, we examined the ability of recombinant Nodal to induce invasion in well differentiated, hormone receptor positive T47D human breast cancer cells, which are weakly invasive and express Nodal at low levels (10, 12, 13). We performed a transwell invasion assay to characterize Nodal induced cell invasion. We seeded T47D cells supplemented with Mitomycin C in the top chamber of a Boyden chamber plate and we quantified cell invasion through a Basement Membrane Extract (BME) coated filter by measuring Calcein-AM fluorescence in the bottom chamber. We found that 39 nM recombinant Nodal causes an approximately two fold increase in cell invasion relative to control (Fig. 3-6A). Thus, our results provide further evidence supporting the conclusion that Nodal is expressed in invasive, poorly differentiated human breast cancers, that Nodal can induce breast cancer cell invasion, and that Cerberus-Fc inhibits Nodal mediated SMAD2 phosphorylation.

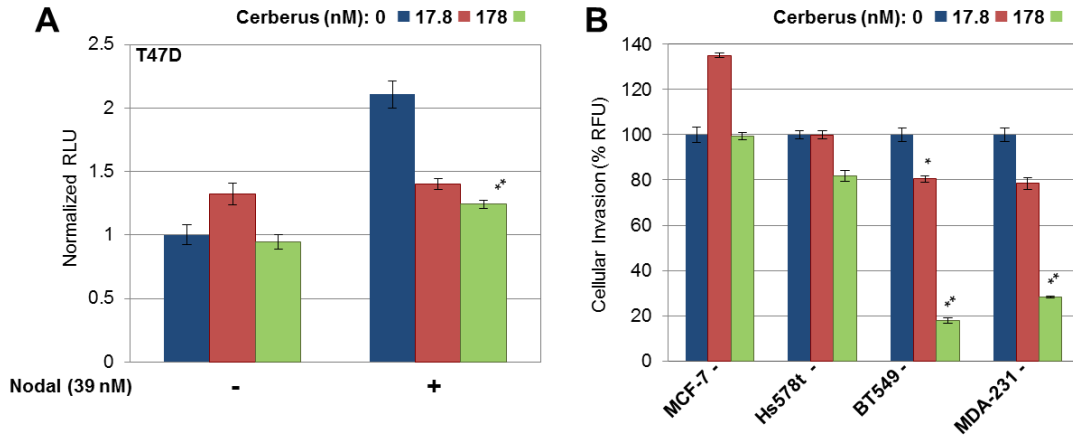


Figure 3-6. Nodal induces breast cancer cell invasion.

(A) Nodal induced cell invasion. T47D cells were grown for 24 h in a Boyden Chamber. Growth medium contained 2.5 $\mu\text{g/ml}$ Mitomycin C, 0 nM (left) or 39 nM (right) Nodal and 0 nM (blue), 17.8 nM (red), or 178 nM (green) Cerberus-Fc. A Cultrex Basement Membrane Extract (BME) coated filter separated the upper and lower chambers. Cell invasion was quantified using Calcein-AM fluorescence. (B) Cerberus inhibits invasion of Nodal expressing human breast cancer cells. MCF-7, Hs578t, BT549, and MDA-MB-231, were placed in the top well of Boyden chamber in serum free medium containing 0 nM (blue), 17.8 nM (red) or 178 nM (green) Cerberus and 2.5 $\mu\text{g/ml}$ Mitomycin C. The bottom chamber was filled with matching medium supplemented with serum. The filter separating top and bottom chambers was coated with BME. Cell invasion was quantified using Calcein-AM fluorescence.

Cerberus suppresses aggressive phenotypes of Nodal expressing breast cancer cells

Nodal knockdown and pharmacologic inhibition of Nodal signaling in highly invasive MDA-MB-231 breast cancer cell lines profoundly suppresses invasion and migration (13). We therefore undertook to evaluate the ability of Cerberus to suppress Nodal mediated cell invasion, migration, and colony forming ability in several human breast cancer cells. For these studies, we selected five human breast cancer cell lines that exhibit an array of characteristics, including invasive and metastatic breast cancer cell lines, which express high levels of Nodal (MDA-MB-231, BT549), invasive, weakly metastatic cell lines that express low levels of Nodal (Hs578t), as well as non-invasive breast cancer cell lines that express low

levels of Nodal (MCF-7, T47D) (Fig. 3-5C). To demonstrate that Cerberus suppresses invasion of Nodal expressing breast cancer cells, we characterized cell migration through a transwell filter coated with BME. We plated cells in the top well of a Boyden chamber and incubated cells for 24 h in serum free medium with 2.5 $\mu\text{g/ml}$ Mitomycin C and 0, 17.8, or 178 nM Cerberus-Fc. The bottom chamber contained complete medium as chemoattractant, Mitomycin C and Cerberus-Fc matching the concentration of the top chamber. Our data showed that invasion by the Nodal expressing cell lines MDA-MB-231 and BT549 is profoundly suppressed by 17.8 nM and 178 nM Cerberus-Fc relative to untreated control samples (Fig. 3-6B). Indeed, at 178 nM Cerberus-Fc we observed a greater than 70% and 80% reduction in cells that invaded the lower chamber for MDA-MB-231 and BT549, respectively (Fig. 3-6B). By comparison, Cerberus-Fc only minimally affected Hs578t, and MCF-7 cell invasion, resulting in approximately 20% and 0% reductions respectively in invading cells relative to control samples (Fig. 3-6B).

To demonstrate that the observed effects are due to Nodal inhibition by Cerberus, we performed invasion assay using the non-invasive T47D breast cancer cell line. We supplemented growth medium with 39 nM recombinant Nodal to induce T47D invasion (Fig. 3-6A). In addition, we supplemented growth medium with 17.8 or 178 nM Cerberus-Fc to inhibit Nodal and Nodal mediated phenotypes. Our results showed that Cerberus-Fc suppressed Nodal induced invasion in a concentration dependent manner. Indeed, at 178 nM Cerberus-Fc we observed a substantial reduction in Nodal induced invasion relative to control (Fig. 3-6A).

To show that Cerberus inhibits migration of Nodal-expressing breast cancer cells, we performed a wound-healing assay (Fig. 3-7). We plated cells in an Ibidi culture insert. When

cells reached 80% confluence, we removed the insert to create a 500 μm gap and replaced medium with medium containing 2.5 $\mu\text{g/ml}$ Mitomycin C and 0, 17.8, or 178 nM of Cerberus-Fc. Our results showed that the invasive cell lines MDA-MB-231, BT549, and Hs578t completely close the wound within 24 h when grown without Cerberus-Fc (Fig. 3-7A, B). When grown in medium supplemented with 17.8 nM Cerberus-Fc, the Nodal expressing cell lines MDA-MB-231 and BT549 did not close the wound. At a Cerberus-Fc concentration of 178 nM, we failed to detect any meaningful wound closure over the course of 48 h (not shown). In contrast, Hs578t and MCF-7 migration was not appreciably affected by Cerberus-Fc and the extent of gap closure did not change relative to untreated control samples.

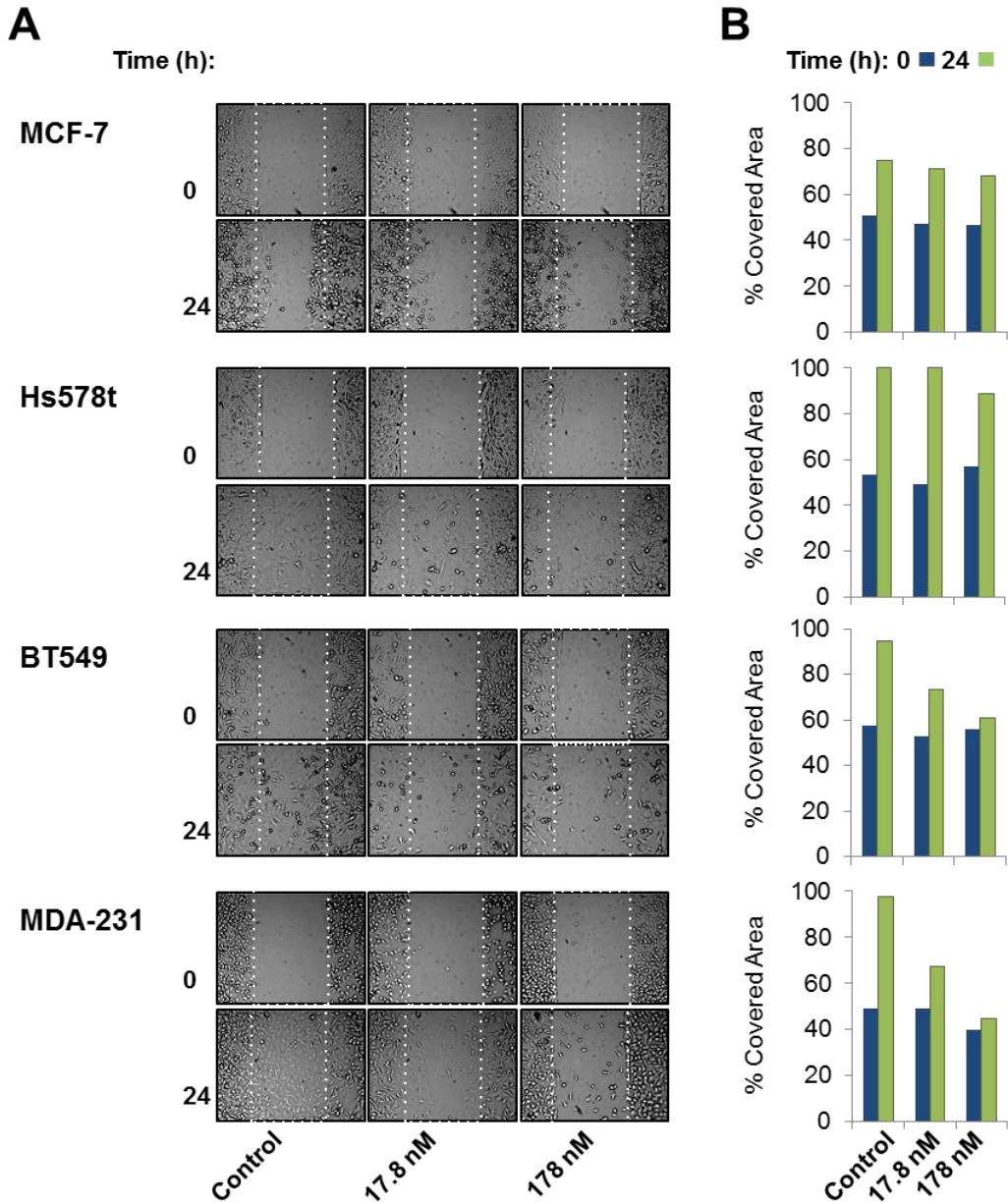


Figure 3-7. Cerberus inhibits breast cancer cell migration.

(A) Cerberus prevents wound closure of Nodal expressing breast cancer cells. MCF-7, Hs578t, BT549 and MDA-MB-231 cells were plated in Ibidi culture insert dishes. Cells were grown in complete medium to 80% confluence, inserts were removed to create a gap and medium was replaced with complete medium supplemented with 2.5 $\mu\text{g/ml}$ Mitomycin C and 0 nM (left panel), 17.8 nM (middle panel), or 178 nM (right panel) Cerberus. Images were taken at 0 h and 24 h after removing insert. (B) Wound closure evaluation. Images taken at 0 h (blue) and 24 h (green) were analyzed using Wimasis software (Ibidi) to quantify cell migration. Graphs within a panel correspond to experiments carried out with 0 nM (left), 17.8 nM (middle), or 178 nM (right) Cerberus.

To evaluate the potential *in vivo* response of Nodal expressing breast cancer cells to Cerberus inhibition, we examined the effect of Cerberus-Fc on colony forming ability of two human breast cancer cells, MCF-7 and MDA-MB-231. We grew cells for 3 weeks in agarose containing growth medium lacking or supplemented with 17.8, or 178 nM Cerberus-Fc and determined the number of colonies formed. Our data showed that MDA-MB-231 and MCF-7 cells formed colonies when grown without Cerberus-Fc (Fig. 3-8A, B); however, the colony forming ability of MDA-MB-231 cells was significantly reduced when cells were grown with Cerberus-Fc. Indeed, less than 20% colonies formed when MDA-MB-231 cells were treated with 178 nM Cerberus-Fc relative to control (Fig. 3-8A, B). By comparison, the colony forming ability of MCF-7 cells was not changed when cells were grown with 178 nM Cerberus-Fc. Thus, we conclude that Cerberus can suppress proliferation, invasion, migration, and colony forming ability of Nodal expressing or Nodal supplemented human breast cancer cell lines.

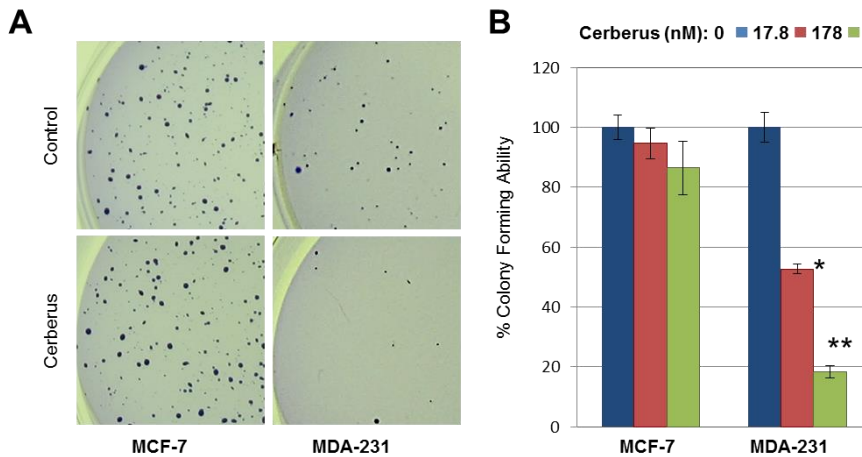


Figure 3-8. Cerberus suppresses breast cancer cell colony-forming ability.

(A) Representative images of colony formation assay for MCF-7 (left) and MDA-MB-231 cells (right) (10X magnification). Cells were grown in serum containing medium supplemented with 0 nM (top, control), 17.8 nM (not shown) or 178 nM (bottom) Cerberus. (B) Analysis of colony formation assay for MCF-7 (right) and MDA-MB-231 (left) cells.

Figure 3-8 (cont'd)

Images were analyzed using ImageJ to determine number of colonies. Experiments were carried out with 0 nM (blue), 17.8 nM (red), or 178 nM (green) Cerberus. Colony formation assays were performed in triplicates in 6-well plates.

Discussion

Our goal for this work was to demonstrate that the embryonic Nodal antagonist Cerberus could suppress Nodal-mediated phenotypes. To demonstrate that human Cerberus functionally inhibits Nodal, we first dissected the mechanism of Nodal signaling using quantitative methods and purified human proteins (50). Our studies showed that recombinant Nodal binds the type I Activin receptor-like kinase ALK4 and the co-receptor Cripto-1 as expected (50). The Nodal-ALK4 interaction is weak compared to the analogous Activin A-ALK4 interaction (Table 3-1), but is consistent with the observation that many TGF- β family ligands interact with type I receptors with intermediate or low affinities (51). On the other hand, the putative type I Nodal receptor ALK7, which we obtained commercially, does not bind Nodal as tested and may not directly contribute to Nodal signaling. By comparison, Nodal forms a stable complex with the co-receptor Cripto-1. The co-receptor Cryptic, on the other hand, doesn't bind Nodal, which would suggest that human Cryptic doesn't play a significant role in the Nodal signaling pathway in humans. Surprisingly, we found that recombinant Nodal does not bind its expected type II receptors ActRIIA and ActRIIB with affinities and kinetics that are characteristic of ligand-cognate type II receptor complexes. Many TGF- β family ligands bind their cognate type II receptors with picomolar equilibrium dissociation constants (K_d) and slow dissociation rate constants (k_d) (36–38), whereas Nodal binds ActRIIA and ActRIIB with mid nanomolar dissociation constants and fast dissociation rate constants. This suggested to us that ActRIIA and ActRIIB are not the dominant, Nodal

interacting type II receptors. We therefore tested binding of Nodal to other type II receptors and we discovered that Nodal binds BMPRII with characteristically high affinity and standard kinetics. This finding indicates that BMPRII is the dominant Nodal-interacting human type II receptor. Moreover, this finding identifies for the first time a high affinity ligand for BMPRII, which until now has been thought to bind exclusively to BMP ligands with low affinity. While this finding was unexpected, a recent study showed that BMPRII-Fc co-IP's with Nodal and that BMPRII-Fc inhibits Nodal signaling, while ActRIIA-Fc and ActRIIB-Fc do not (55). That BMPRII has high affinity ligands is of great consequence for the TGF- β family and needs to be explored further.

As Nodal has been shown to promote aggressive breast cancer phenotypes and as Nodal knockdown has been shown to reduce tumor incidence and blunt tumor growth in animal models of human breast cancer (8, 10, 11), we undertook to identify and develop a Nodal antagonist that could potentially inhibit Nodal in breast cancers. We hypothesized that the secreted human protein Cerberus could work as Nodal inhibitor, as its frog and mouse homologs co-IP with frog Nodal (Xnr1) and suppress Nodal mediated phenotypes during embryogenesis (18, 22, 23). To establish the inhibitory activity of human Cerberus, we characterized its interaction with Nodal and its mechanism of inhibition. We found that human Cerberus forms a stable, high affinity complex with Nodal. To elucidate the mechanism of Cerberus antagonism, we examined the ability of Cerberus to inhibit binding of Nodal to its signaling partners. We found that Cerberus blocks binding of Nodal to its receptors ALK4, ActRIIB and BMPRII, as well as to its co-receptor Cripto-1. As structural conservation within the TGF- β family indicates that the type I and type II receptor binding sites lie on opposite sides of a Nodal protomer (Fig. 3-9A, B) (56), our inhibition data

suggested that the homodimeric Cerberus could wrap around the Nodal homodimer and cover both receptor interacting surfaces at once (Fig. 3-9C, D). However, while Cerberus completely blocked Nodal binding to the type II receptor ActRIIB, Cerberus only appeared to destabilize Nodal binding to the type II receptor BMPRII by lowering the association rate and increasing the dissociation rate. This suggests that Cerberus is more effective at inhibiting the Nodal-ActRIIB interaction than the Nodal-BMPRII interaction. While this finding may reflect only the different affinities between Nodal and its type II receptors, it is also possible that BMPRII binds Nodal at a site that is distinct from that of ActRIIA/ActRIIB, which would cause BMPRII to behave differently from ActRIIB (56, 57).

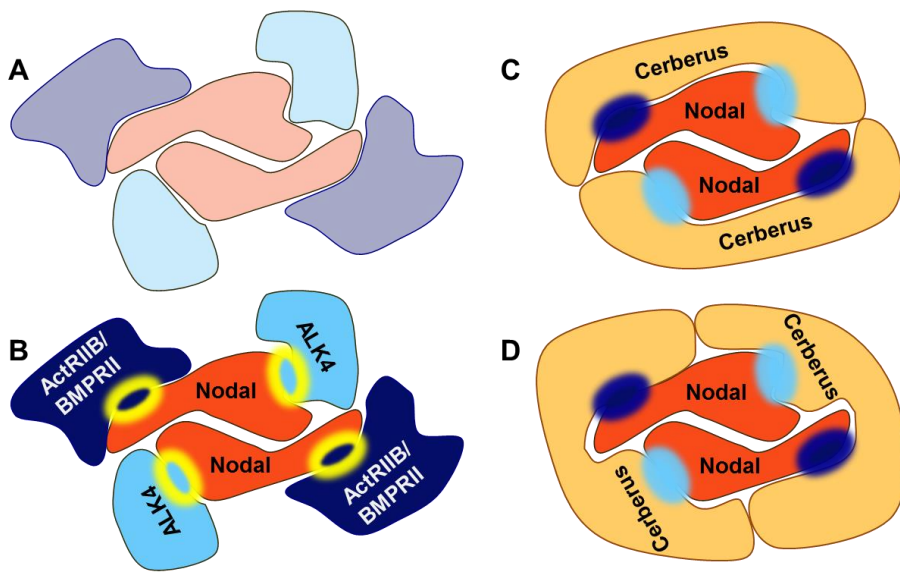


Figure 3-9. Proposed mechanism of Cerberus inhibition.

(A) Structure of BMP-9/ALK1/ActRIIB complex (37). The disulfide-linked BMP-9 homodimer (center, orange) simultaneously binds the extracellular domains of the type I Activin receptor-like kinase ALK1 (light blue) and the type II Activin receptor kinase ActRIIB (dark blue). (B) Molecular model of Nodal-receptor interactions based on the BMP-9/ALK1/ActRIIB structure. The disulfide-linked Nodal homodimer (center, orange) binds the extracellular domains of the type I Activin receptor-like kinase ALK4 (light blue) and the type II Activin receptor kinase ActRIIB or BMPRII (dark blue), likely using canonical interaction surfaces (yellow lined circles). (C-D) Cerberus forms a stable homodimer in

Figure 3-9 (cont'd)

solution (58), binds Nodal and prevents binding of Nodal to both receptors. Thus Cerberus blocks simultaneously the ALK4 interaction surface (light blue circle) and the ActRIIB interaction surface (dark blue circle). We propose that one Cerberus protomer could block interaction surfaces within one Nodal protomer (C) or two protomers (D). We expect the overall stoichiometry of this complex to be 2:2.

Previous studies showed that Nodal expression is elevated in breast cancer cell lines that are invasive and poorly differentiated, including MDA-MB-231 (10, 11, 13, 48, 49). Significantly, Nodal knockdown, small molecule Nodal receptor inhibitors and Nodal blockade with an anti-Nodal polyclonal antibody suppresses MDA-MB-231 invasion, proliferation and colony forming ability (10, 11, 13). As we demonstrated that human Cerberus is a functional Nodal antagonist, we undertook to evaluate its effect on breast cancer cells that express Nodal. We therefore investigated Nodal expression in human breast cancer cell lines that exhibit different characteristics. Based on previous studies (10, 11), we expected to find that Nodal levels are higher in invasive breast cancer cell lines. Indeed, our Western blot data confirmed that Nodal expression is higher in breast cancer cell lines that are invasive and that have the ability to metastasize *in vivo*, whereas Nodal levels are low in weakly or non-invasive and non-metastatic breast cancer cell lines. Within this limited panel of breast cancer cell lines, it appears that Nodal expression is elevated in triple negative breast cancer cells (10).

Next, we examined the effect of Cerberus on Nodal expressing breast cancer cells. We showed that Cerberus-Fc profoundly inhibited invasion, and migration of Nodal expressing MDA-MB-231 and BT549 cells. In contrast, the effect of Cerberus on breast cancer cells that don't express Nodal and aren't induced with recombinant Nodal, including Hs578t, MCF-7 and T47D, is minor. Similarly, we showed that Cerberus profoundly

suppresses the colony forming ability of the Nodal expressing MDA-MB-231 cells, whereas MCF-7 cells are minimally affected. Significantly, we confirmed that the Cerberus effect is directly related to Nodal inhibition, as Cerberus suppresses invasion induced with recombinant Nodal in well-differentiated and weakly invasive T47D cells. Taken together, our breast cancer cell line studies demonstrated that Cerberus could suppress Nodal-mediated, aggressive breast cancer phenotypes *in vitro*, including in physiologically predictive 3D culture assays, indicating that Cerberus could be an effective inhibitor of Nodal-mediated, aggressive breast cancers *in vivo*.

REFERENCES

REFERENCES

1. Shen, M. M. (2007) Nodal signaling: Developmental roles and regulation. *Development* **134**, 1023-1034.
2. Zhou, X., Sasaki, H., Lowe, L., Hogan, B. L., and Kuehn, M. R. (1993) Nodal is a novel TGF-beta-like gene expressed in the mouse node during gastrulation. *Nature* **361**, 543-547.
3. Varlet, I., Collignon, J., and Robertson, E. J. (1997) Nodal expression in the primitive endoderm is required for specification of the anterior axis during mouse gastrulation. *Development* **124**, 1033-1044.
4. Postovit, L. M., Margaryan, N. V., Seftor, E. A., Kirschmann, D. A., Lipavsky, A., and et al. (2008) Human embryonic stem cell microenvironment suppresses the tumorigenic phenotype of aggressive cancer cells. *Proceedings of the National Academy of Sciences of the United States of America* **105**, 4329-4334.
5. Bianco, C., Adkins, H. B., Wechselberger, C., Seno, M., Normanno, N., and et al. (2002) Cripto-1 activates Nodal- and ALK4-dependent and -independent signaling pathways in mammary epithelial cells. *Molecular and Cellular Biology* **22**, 2586-2597.
6. Papageorgiou, I., Nicholls, P. K., Wang, F., Lackmann, M., Makanji, Y., and et al. (2009) Expression of Nodal signalling components in cycling human endometrium and in endometrial cancer. *Reproductive Biology and Endocrinology : RB&E* **7**, 122.
7. Herrera, M. B., Bruno, S., Buttiglieri, S., Tetta, C., Gatti, S., and et al. (2006) Isolation and characterization of a stem cell population from adult human liver. *Stem Cells* **24**, 2840-2850.
8. Topczewska, J. M., Postovit, L. M., Margaryan, N. V., Sam, A., Hess, A. R., and et al. (2006) Embryonic and tumorigenic pathways converge via Nodal signaling: role in melanoma aggressiveness. *Nature Medicine* **12**, 925-932.
9. Lonardo, E., Hermann, P. C., Mueller, M. T., Huber, S., Balic, A., and et al. (2011) Nodal/Activin signaling drives self-renewal and tumorigenicity of pancreatic cancer stem cells and provides a target for combined drug therapy. *Cell Stem Cell* **9**, 433-446.
10. Quail, D. F., Zhang, G., Walsh, L. A., Siegers, G. M., Dieters-Castator, D. Z., and et al. (2012) Embryonic morphogen Nodal promotes breast cancer growth and progression. *PLoS One* **7**, e48237.

11. Strizzi, L., Hardy, K. M., Margaryan, N. V., Hillman, D. W., Seftor, E. A., and et al. (2012) Potential for the embryonic morphogen Nodal as a prognostic and predictive biomarker in breast cancer. *Breast Cancer Research* **14**, R75.
12. Strizzi, L., Postovit, L. M., Margaryan, N. V., Seftor, E. A., Abbott, D. E., and et al. (2008) Emerging roles of Nodal and Cripto-1: from embryogenesis to breast cancer progression. *Breast Disease* **29**, 91-103.
13. Quail, D. F., Zhang, G., Findlay, S. D., Hess, D. A., and Postovit, L. M. (2013) Nodal promotes invasive phenotypes via a mitogen-activated protein kinase-dependent pathway. *Oncogene* **33**, 461-473.
14. Fang, R., Zhang, G., Guo, Q., Ning, F., Wang, H., and et al. (2013) Nodal promotes aggressive phenotype via snail-mediated epithelial-mesenchymal transition in murine melanoma. *Cancer Letters* **333**, 66-75.
15. Petersen, M., Thorikay, M., Deckers, M., van Dinther, M., Grygielko, E. T., and et al. (2008) Oral administration of GW788388, an inhibitor of TGF-beta type I and II receptor kinases, decreases renal fibrosis. *Kidney International* **73**, 705-715.
16. Inman, G. J., Nicolas, F. J., Callahan, J. F., Harling, J. D., Gaster, L. M., and et al. (2002) SB-431542 is a potent and specific inhibitor of transforming growth factor-beta superfamily type I activin receptor-like kinase (ALK) receptors ALK4, ALK5, and ALK7. *Molecular Pharmacology* **62**, 65-74.
17. Chen, C., and Shen, M. M. (2004) Two modes by which lefty proteins inhibit nodal signaling. *Current Biology : CB* **14**, 618-624.
18. Piccolo, S., Agius, E., Leys, L., Bhattacharyya, S., Grunz, H., and et al. (1999) The head inducer cerberus is a multifunctional antagonist of nodal, BMP and wnt signals. *Nature* **397**, 707-710.
19. Meno, C., Gritsman, K., Ohishi, S., Ohfuji, Y., Heckscher, E., and et al. (1999) Mouse lefty2 and zebrafish antivin are feedback inhibitors of nodal signaling during vertebrate gastrulation. *Molecular Cell* **4**, 287-298.
20. Sakuma, R., Ohnishi Yi, Y., Meno, C., Fujii, H., Juan, H., and et al. (2002) Inhibition of nodal signalling by lefty mediated through interaction with common receptors and efficient diffusion. *Genes to Cells : Devoted to Molecular and Cellular Mechanisms* **7**, 401-412.
21. Marques, S., Borges, A. C., Silva, A. C., Freitas, S., Cordenonsi, M., and et al. (2004) The activity of the nodal antagonist cerl-2 in the mouse node is required for correct L/R body axis. *Genes and Development* **18**, 2342-2347.

22. Bertocchini, F., and Stern, C. D. (2002) The hypoblast of the chick embryo positions the primitive streak by antagonizing nodal signaling. *Developmental Cell* **3**, 735-744.
23. Belo, J. A., Bachiller, D., Agius, E., Kemp, C., Borges, A. C., and et al. (2000) Cerberus-like is a secreted BMP and nodal antagonist not essential for mouse development. *Genesis* **26**, 265-270.
24. Hendrix, M. J., Seftor, E. A., Seftor, R. E., Kasemeier-Kulesa, J., Kulesa, P. M., and et al. (2007) Reprogramming metastatic tumour cells with embryonic microenvironments. *Nature Reviews Cancer* **7**, 246-255.
25. Massague, J. (1998) TGF-beta signal transduction. *Annual Review of Biochemistry* **67**, 753-791.
26. Yeo, C., and Whitman, M. (2001) Nodal signals to SMADs through cripto-dependent and cripto-independent mechanisms. *Molecular Cell* **7**, 949-957.
27. Reissmann, E., Jornvall, H., Blokzijl, A., Andersson, O., Chang, C., and et al. (2001) The orphan receptor ALK7 and the Activin receptor ALK4 mediate signaling by nodal proteins during vertebrate development. *Genes and Development* **15**: 2010-2022.
28. Vallier, L., Mendjan, S., Brown, S., Chng, Z., Teo, A., and et al. (2009) Activin/Nodal signalling maintains pluripotency by controlling nanog expression. *Development* **136**, 1339-1349.
29. Zhang, C., and Klymkowsky, M. W. (2009) Unexpected functional redundancy between twist and slug (snail2) and their feedback regulation of NF-kappaB via nodal and cerberus. *Developmental Biology* **331**, 340-349.
30. Brown, S., Teo, A., Pauklin, S., Hannan, N., Cho, C. H., and et al. (2011) Activin/Nodal signaling controls divergent transcriptional networks in human embryonic stem cells and in endoderm progenitors. *Stem Cells* **29**, 1176-1185.
31. Kumar, A., Novoselov, V., Celeste, A. J., Wolfman, N. M., ten Dijke, P., and et al. (2001) Nodal signaling uses activin and transforming growth factor-beta receptor-regulated Smads. *The Journal of Biological Chemistry* **276**, 656-661.
32. Yan, Y. T., Liu, J. J., Luo, Y., E, C., Haltiwanger, R. S., and et al. (2002) Dual roles of cripto as a ligand and coreceptor in the nodal signaling pathway. *Molecular and Cellular Biology* **22**, 4439-4449.
33. Gritsman, K., Zhang, J., Cheng, S., Heckscher, E., Talbot, W. S., and et al. (1999) The EGF-CFC protein one-eyed pinhead is essential for nodal signaling. *Cell* **97**, 121-132.

34. Wu, X., and Gallo, K. A. (2013) The 18-kDa translocator protein (TSPO) disrupts mammary epithelial morphogenesis and promotes breast cancer cell migration. *PLoS One* **8**, e71258.
35. Humphries, B., Wang, Z., Oom, A. L., Fisher, T., Tan, D., and et al. (2014) MicroRNA-200b targets protein kinase calpha and suppresses triple-negative breast cancer metastasis. *Carcinogenesis* **35**, 2254-2263.
36. Sako, D., Grinberg, A. V., Liu, J., Davies, M. V., Castonguay, R., and et al. (2010) Characterization of the ligand binding functionality of the extracellular domain of activin receptor type IIB. *The Journal of Biological Chemistry* **285**, 21037-21048.
37. Townson, S. A, Martinez-Hackert, E., Greppi, C., Lowden, P., Sako, D., and et al. (2012) Specificity and structure of a high affinity activin receptor-like kinase 1 (ALK1) signaling complex. *The Journal of Biological Chemistry* **287**, 27313-27325.
38. De Crescenzo, G., Pham, P. L., Durocher, Y., and O'Connor-McCourt, M. D. (2003) Transforming growth factor-beta (TGF-beta) binding to the extracellular domain of the type II TGF-beta receptor: Receptor capture on a biosensor surface using a new coiled-coil capture system demonstrates that avidity contributes significantly to high affinity binding. *Journal of Molecular Biology* **328**, 1173-1183.
39. Gray, P. C., Harrison, C. A., and Vale, W. (2003) Cripto forms a complex with activin and type II activin receptors and can block activin signaling. *Proceedings of the National Academy of Sciences of the United States of America* **100**, 5193-5198.
40. Yu, X., He, F., Zhang, T., Espinoza-Lewis, R. A., Lin, L., and et al. (2008) Cerberus functions as a BMP agonist to synergistically induce nodal expression during left-right axis determination in the chick embryo. *Developmental Dynamics* **237**, 3613-3623.
41. Hsu, D. R., Economides, A. N., Wang, X., Eimon, P. M., and Harland, R. M. (1998) The *Xenopus* dorsalizing factor gremlin identifies a novel family of secreted proteins that antagonize BMP activities. *Molecular Cell* **1**, 673-683.
42. Chi, L., Saarela, U., Railo, A., Prunskaitė-Hyyryläinen, R., Skovorodkin, I., and et al. (2011) A secreted BMP antagonist, cer1, fine tunes the spatial organization of the ureteric bud tree during mouse kidney development. *PLoS One* **6**, e27676.
43. Cai, W., Albin, S., Wei, K., Willems, E., Guzzo, R. M., and et al. (2013) Coordinate nodal and BMP inhibition directs Baf60c-dependent cardiomyocyte commitment. *Genes and Development* **27**, 2332-2344.
44. Foley, A. C., Korol, O., Timmer, A. M., and Mercola, M. (2007) Multiple functions of cerberus cooperate to induce heart downstream of nodal. *Developmental Biology* **303**, 57-65.

45. Zawel, L., Dai, J. L., Buckhaults, P., Zhou, S., Kinzler, K. W., and et al. (1998) Human SMAD3 and SMAD4 are sequence-specific transcription activators. *Molecular Cell* **1**, 611-617.
46. Quail, D. F., Walsh, L. A., Zhang, G., Findlay, S. D., Moreno, J., and et al. (2012) Embryonic protein nodal promotes breast cancer vascularization. *Cancer Research* **72**, 3851-3863.
47. Strizzi, L., Hardy, K. M., Kirschmann, D. A., Ahrlund-Richter, L., and Hendrix, M. J. (2012) Nodal expression and detection in cancer: Experience and challenges. *Cancer Research* **72**, 1915-1920.
48. Sheridan, C., Kishimoto, H., Fuchs, R. K., Mehrotra, S., Bhat-Nakshatri, P., and et al. (2006) CD44+/CD24- breast cancer cells exhibit enhanced invasive properties: An early step necessary for metastasis. *Breast Cancer Research* **8**, R59.
49. Sommers, C. L., Byers, S. W., Thompson, E. W., Torri, J. A., and Gelmann, E. P. (1994) Differentiation state and invasiveness of human breast cancer cell lines. *Breast Cancer Research and Treatment* **31**, 325-335.
50. Schier, A. F. (2003) Nodal signaling in vertebrate development. *Annual Review of Cell and Developmental Biology* **19**, 589-621.
51. Shi, Y., and Massague, J. (2003) Mechanisms of TGF-beta signaling from cell membrane to the nucleus. *Cell* **113**, 685-700.
52. Calvanese, L., Saporito, A., Oliva, R., G, D. A., Pedone, C., and et al. (2009) Structural insights into the interaction between the cripto CFC domain and the ALK4 receptor. *Journal of Peptide Science : An Official Publication of the European Peptide Society* **15**, 175-183.
53. Kelber, J. A., Shani, G., Booker, E. C., Vale, W. W., and Gray, P. C. (2008) Cripto is a noncompetitive activin antagonist that forms analogous signaling complexes with activin and nodal. *The Journal of Biological Chemistry* **283**, 4490-4500.
54. Adkins, H. B., Bianco, C., Schiffer, S. G., Rayhorn, P., Zafari, M., and et al. (2003) Antibody blockade of the cripto CFC domain suppresses tumor cell growth in vivo. *The Journal of Clinical Investigation* **112**, 575-587.
55. Fuerer, C., Nostro, M. C., and Constam, D. B. (2014) Nodal.Gdf1 heterodimers with bound prodomains enable serum-independent nodal signaling and endoderm differentiation. *The Journal of Biological Chemistry* **289**, 17854-17871.
56. Hinck, A. P. (2012) Structural studies of the TGF-betas and their receptors - insights into evolution of the TGF-beta superfamily. *FEBS Letters* **586**, 1860-1870.

57. Groppe, J., Hinck, C. S., Samavarchi-Tehrani, P., Zubieta, C., Schuermann, J.P., and et al. (2008) Cooperative assembly of TGF-beta superfamily signaling complexes is mediated by two disparate mechanisms and distinct modes of receptor binding. *Molecular Cell* **29**, 157-168.
58. Nolan, K., Kattamuri, C., Luedeke, D. M., Deng, X., Jagpal, A., and et al. (2013) Structure of protein related to dan and cerberus: Insights into the mechanism of bone morphogenetic protein antagonism. *Structure* **21**, 1417-1429.

CHAPTER 4 -

NEW LIGAND BINDING FUNCTION OF HUMAN CERBERUS AND ROLE OF PROTEOLYTIC PROCESSING IN REGULATING LIGAND RECEPTOR INTERACTIONS AND ANTAGONISTIC ACTIVITY³

³The work described in this chapter was published as the following manuscript: Senem Aykul, and Erik M. Hackert. (2016) New Ligand Binding Function of Human Cerberus and Role of Proteolytic Processing in Regulating Ligand Receptor Interactions and Antagonistic Activity. *Journal of Molecular Biology* **428**, 590-602.

Abstract

Cerberus is a key regulator of vertebrate embryogenesis. Its biological function has been studied extensively in frog and mouse embryos. Its ability to bind and antagonize the transforming growth factor- β (TGF- β) family ligand Nodal is well established. Strikingly, the molecular function of Cerberus remains poorly understood. The underlying reason is that Cerberus is a complex, multifunctional protein: It binds and inhibits multiple TGF- β family ligands, it may bind and inhibit some Wnt family members, and two different forms with distinct activities have been described. In addition, sequence homology between frog and mammalian Cerberus is low, suggesting that previous studies, which analyzed frog Cerberus function, may not accurately describe the function of mammalian Cerberus. We therefore undertook to determine the molecular activities of human Cerberus in TGF- β family signaling. Using purified proteins, surface plasmon resonance, and reporter gene assays, we discovered that human Cerberus bound and inhibited the TGF- β family ligands Activin B, BMP-4, BMP-6, and BMP-7, but not the frog Cerberus ligand BMP-2. Notably, full-length Cerberus successfully blocked ligand binding to type I and type II receptors, but the short form was less effective in type II receptor binding inhibition. In addition, full-length Cerberus suppressed breast cancer cell migration but the short form did not. Thus, our findings expand the roles of Cerberus as TGF- β family signaling inhibitor, provide a molecular rationale for the function of the N-terminal region, and support the idea that Cerberus could have regulatory activities beyond direct inhibition of TGF- β family signaling.

Introduction

Cerberus is a secreted antagonist of Transforming Growth Factor- β (TGF- β) family signaling that belongs to the DAN family of cystine knot proteins (1, 2). It plays an important role in head formation and cardiogenesis during vertebrate embryonic development (3-8). Overexpression of frog Cerberus (xCer) in frog embryos induced formation of ectopic heads (3, 9), and Cerberus knockdown in mouse Embryonic Stem Cells prevented cardiac lineage specification (7). Beyond embryogenesis and cardiogenic progenitor cells, Cerberus functions are not known. However, mutations in the Cerberus gene are well correlated with an increased risk of low bone mineral density (BMD) in premenopausal women and osteoporosis in postmenopausal women (10-12). Significantly, how Cerberus regulates head formation, cardiac lineage commitment, and BMD is not well understood, because its molecular activities are poorly defined. The common view is that Cerberus is a multifunctional protein that binds and inhibits the TGF- β family ligands Nodal, BMP-2, BMP-4 and Activin A, as well as some members of the Wnt family (1, 13); however, contradicting activities have also been reported. For example, frog Cerberus inhibited frog Nodal (Xnr1 and Xnr2), BMP-2, BMP-4, and XWnt8 (frog Wnt8) (1), whereas mouse and human Cerberus only inhibited Nodal (13-15).

A possible reason for the different observations is limited sequence conservation between Cerberus from different species (13, 15). Human and mouse Cerberus, respectively, only share 35.7% and 33.8% sequence identity with frog Cerberus. Even between human and mouse Cerberus sequence identity is only 67.2% (2, 15). Notably, sequence identity in the C-terminal cystine knot domain is

approximately 50% between the mammalian and the frog species, whereas conservation in the N-terminal half of the sequence is nearly negligible. In addition, two forms of frog Cerberus with potentially distinct functions have been described (1). A long form (xCer-L) inhibited Xnr2, BMP-2, BMP-4 and XWnt8, whereas a short form (xCer-S), which is likely generated by proteolytic processing of xCer-L, only inhibited Xnr2 (1). Taken together, these findings indicate that the molecular functions of mammalian Cerberus need to be defined. Knowing which signaling pathways mammalian Cerberus regulates and how the long and short forms of Cerberus differ is critically important for elucidating the cellular programs that lead to head formation in developing embryos, to differentiation of mouse cardiogenic progenitors, and to low BMD and osteoporosis in women that carry the mutant Cerberus alleles.

To clarify the function of human Cerberus in TGF- β family signaling, we investigated its ligand binding specificity and its ability to inhibit signaling. Using purified proteins and SPR, we discovered three new TGF- β family ligands that bind human Cerberus with high-affinity: Activin B, BMP-6 and BMP-7. Using SPR and reporter gene assays, we showed that human Cerberus prevented type I and type II receptor binding and signaling by these ligands, but not by its putative ligands BMP-2, or Activin A, indicating that the activity of human Cerberus differs from the activity reported for frog Cerberus (1). Notably, full-length and short-form Cerberus bound and inhibited ligands equivalently, but the two forms differed in their ability to prevent ligand binding to type II receptors, suggesting that the cleavable, N-terminal region could play a role in blocking the type II receptor-

binding surface. In addition, full-length Cerberus profoundly suppressed migration of MDA-MB-231 breast cancer cells, whereas short form Cerberus did not, suggesting that the different forms of Cerberus could have distinct biological activities, such as regulation of Wnt signaling via the cleavable, N-terminal region. Indeed, full-length frog Cerberus (Cer-L) co-immunoprecipitated with the Wnt family ligand XWnt8, but the short form (Cer-S) did not (1). In conclusion, we have identified new TGF- β family signaling ligands that are antagonized by human Cerberus and we have elucidated molecular and biological activities of full-length and short-form Cerberus.

Materials and Methods

Materials

Recombinant human Activin A RnD, Activin B RnD, GDF-8 RnD, Nodal RnD, TGF- β 1 RnD, TGF- β 2 PC, TGF- β 3 PC, GDF-1 RnD, GDF-3 RnD, BMP-2 LT, BMP-4 RnD, BMP-6 PC, BMP-7 PC, BMP-9 PC, and BMP-10 PC were obtained from R&D Biosystems (RnD) or PROMOCCELL (PC). Activin A, Activin B, GDF-8, and TGF- β 1 were also produced in-house.

Construction of expression plasmids

Synthetic genes consisting of human Cerberus (O95813), ActRIIA (P27037) and ActRIIB (Q13705) fused to human IgG1-Fc were obtained from GeneArt. Human BMPRII (Q13873) was cloned from cDNA and fused to human IgG1-Fc by PCR. NCBI-protein accession numbers are shown in parenthesis. Cerberus fusion constructs included the full-length gene (amino acid 1-267, wtCer), a full-length construct with two mutations (amino acid 1-267, R82G and C206A, mutCer) and a truncated form (amino acid 1-17 Δ 83-267, C206A, CerS).

Mutants and deletions were obtained by PCR. Receptor fusion constructs included extracellular domains (ECD) of human ActRIIA (amino acid 1-120), ActRIIB (amino acid 1-120), and BMPRII (amino acid 1-136). Extracellular domains were linked to human IgG1-Fc via a 22 amino acid long linker containing a TEV cleavage site.

Protein purification

Proteins were expressed using CHO cells. wtCer-Fc, mutCer-Fc, CerS-Fc, ActRIIA-Fc, ActRIIB-Fc, and BMPRII-Fc were purified from condition medium using Protein A capture. Proteins were eluted with 100 mM Glycine, pH 3.0 and immediately neutralized by adding 2 M Tris, pH 8.5. To evaluate monodispersity, proteins were analyzed by SEC. For inhibition assays, the Fc portion of Cerberus constructs was removed using TEV protease. Cleaved Fc was removed with one step of protein A capture, followed by SEC. Purified proteins were dialyzed into PBS, pH 7.5 and stored at -20 °C or -80 °C. The purity of the proteins was checked with SDS-PAGE under reducing and non-reducing conditions.

Surface plasmon resonance

Ligand binding affinities and binding inhibition were determined by SPR using the Biacore 2000. All experiments were carried out at 25 °C. HBS-EPS buffer (0.01 M HEPES, 0.5 M NaCl, 3 mM EDTA, 0.005% (v/v) Tween 20, pH 7.4) containing 0.1 % BSA (SigmaAldrich,) was used as running buffer. To capture Fc fusion proteins, including wtCer-Fc, mutCer-Fc, CerS-Fc, ActRIIA-Fc, ActRIIB-Fc and BMPRII-Fc, anti-human IgG (Fc) antibody was immobilized onto four channels of a CM5 chip using amine-coupling chemistry. To characterize ligand binding specificity of Cerberus, different ligands at a concentration of 80 nM were injected, including Nodal, Activin A, Activin B, GDF-8, GDF-11, TGF- β 1, TGF- β 2, TGF- β 3, BMP-2, BMP-4, BMP-6, BMP-7, BMP-9, and BMP-10. For kinetic analysis of

ligands that bound Cerberus, a series of concentrations was injected over experimental and control flow channels. To minimize mass transport artifacts, a high flow rate (50 $\mu\text{l}/\text{min}$) was used and low levels of purified wtCer-Fc, mutCer-Fc, or CerS-Fc (approximately 200-300 RU) were captured on the experimental flow channels. A reference channel was monitored to account for nonspecific binding, drift, and bulk shifts. To obtain kinetic rate constants, the processed data was fitted to a 1:1 Langmuir interaction model using BiaEvaluation software. Equilibrium dissociation constants (K_d) were determined by calculating the ratio of binding rate constants. After each binding cycle, the antibody surface was regenerated to base line by injecting 3 M MgCl_2 . For SPR inhibition analysis, ActRIIA-Fc, ActRIIB-Fc, or BMPRII-Fc were captured on the sensor chip. Activin B and BMP-6 at certain concentration were preincubated with different concentrations of Fc-free wtCer, mutCer or CerS. Preformed complexes were injected over experimental and control flow channels. Sensograms were analyzed by double referencing. IC_{50} values for SPR inhibition data were determined using GraphPad. Results are summarized in Table 4-2.

Cell lines

A-204 rhabdomyosarcoma cells (HTB-82) and HepG2 cells (HB-8065) were obtained from ATCC. Cells were maintained according to ATCC culture conditions. A-204 cells were grown in McCoy's 5A medium supplemented with 10% FBS and 1% P/S. HepG2 cells were grown in Eagle's Minimum Essential Medium supplemented with 10% FBS and 1% P/S. Cells were grown at 37 °C under humidified, 5% CO_2 atmosphere. Freshly thawed cells were passaged at least three times before performing assays.

Reporter assays

~ 50,000 A-204 or ~ 10,000 HepG2 cells in complete medium were seeded in each well of a 96-well plate and grown overnight. For transfection, each well was transfected with 0.2 μ l lipofectamine 2000, 2 ng pGL4.48 [Luc2P/hRluc/TK] vector (control luciferase reporter plasmid, Promega, E6921) and 200 ng of the SMAD3 responsive reporter plasmid pGL4.48 [luc2P/SBE] or the SMAD1/5/8 responsive reporter plasmid pGL3 [luc2P/BRE]. Transfection medium was removed the following day, and medium was replaced with assay medium (growth medium supplemented with 0.1% BSA) containing test proteins, including Activin A, Activin B, BMP-2 and BMP-6 (all 10 ng/ml) and/or the Cerberus-Fc constructs (0-10,000 ng/ml). Assay medium containing test proteins was incubated at 37 °C for 1 h before adding to cells. After addition of medium, A-204 cells were incubated for 6 h and HepG2 cells were incubated for 16 h at 37 °C. Luciferase activity was detected with the Dual-Glo Luciferase Assay System (Promega) or a homemade version of that assay (34). Luminescence was determined using FluoStar Omega plate reader. Relative luciferase units (RLU) were calculated by dividing firefly luciferase units with renilla luciferase units. IC₅₀ values were determined using GraphPad. Results are summarized in Table 4-2.

Wound healing

MDA-MB-231 human breast cancer cells (HTB-26) were seeded in an Ibidi insert in standard growth medium. Once cells reached 80% confluence, the insert was removed and medium was replaced with complete medium containing 2.5 μ g/ml Mitomycin C and 17.8 nM wtCer-Fc, mutCer-Fc CerS-Fc or no Cerberus control. Cells were monitored for up to 24 h and images were taken using an inverted microscope with 10X magnification at 0 h and 24 h. Cellular migration was quantified using Vimages software (Ibidi).

Statistics

Reporter gene assays were performed in quadruplicates and were repeated two different times. Statistical significance was determined by comparing control to treated sample using a two-tailed T-test. P values < than 0.05 were considered statistically significant and are marked by an asterisk in Figure 5.

Results

The design of Cerberus constructs

Cerberus is widely considered to be a multifunctional protein that inhibits Nodal, BMPs, Activin A and Wnt activity; however, conflicting findings regarding its function have been reported (1, 13, 14, 15). To clarify the molecular activities of human Cerberus, we expressed a number of constructs as Fc fusion proteins using stably transfected CHO cells, including wild type Cerberus (wtCer-Fc), mutant Cerberus (mutCer-Fc), and short form Cerberus (CerS-Fc) (Fig. 4-1A, B). For wild type Cerberus, the complete wild type human sequence was used. For mutant Cerberus, a putative proprotein convertase processing site (Arg82Gly) and an unpaired Cysteine were modified (Cys206Ala) (16, 17). For short Cerberus, the sequence between signal peptide and a predicted proprotein convertase processing site was deleted (Δ 18-85) and the unpaired Cysteine was mutated (Cys206Ala). Cerberus was fused at the C-terminus to the Fc portion of human IgG1 via a 22-amino acid linker containing a TEV cleavage site (Fig. 4-1B).

Cerberus-Fc fusion proteins were purified from conditioned medium by protein A affinity chromatography followed by SEC (Fig. 4-1C-E). Preparative SEC showed that wtCer-Fc and CerS-Fc were significantly aggregated, whereas mutCer-Fc was almost free of aggregates (data not shown). Monodisperse peaks corresponding to a dimeric species could

be obtained by sequential SEC purification cycles (Fig. 4-1C). To produce the Fc-free forms for SPR and other inhibition studies, we digested purified fusion proteins with TEV. The Fc portion was removed by passing the digested form over a protein A column followed by SEC. Fc-free Cerberus constructs were monodisperse by SEC (Fig. 4-1D). Cerberus elution volumes corresponded to a dimeric form for the full-length constructs, but the elution volume of the CerS construct appeared to be consistent with a monomeric species (Fig. 4-1D).

To determine the dimerization state of Cerberus and the role of its unpaired cysteine, we used SDS-PAGE mobility assays. Molecular weights of Cerberus-Fc constructs were approximately ~ 65-75 kDa under reducing conditions and ~ 130-150 kDa under non-reducing conditions, as expected for the disulfide-linked Fc fusion proteins (Fig. 4-1E, FC). The Fc-free forms migrated as ~ 30-35 kDa proteins on SDS-PAGE both under reducing and non-reducing conditions, demonstrating that human Cerberus, like its homologs PRDC and NBL1, does not form disulfide-linked homodimers (Fig. 4-1E, TEV) (16, 17). Notably, glutaraldehyde cross-linking of the purified Fc-free Cerberus fractions showed that both full-length and short-form Cerberus, like its homologs PRDC and NBL-1, forms non-covalent dimers in solution (Fig. 4-1D) (16, 17).

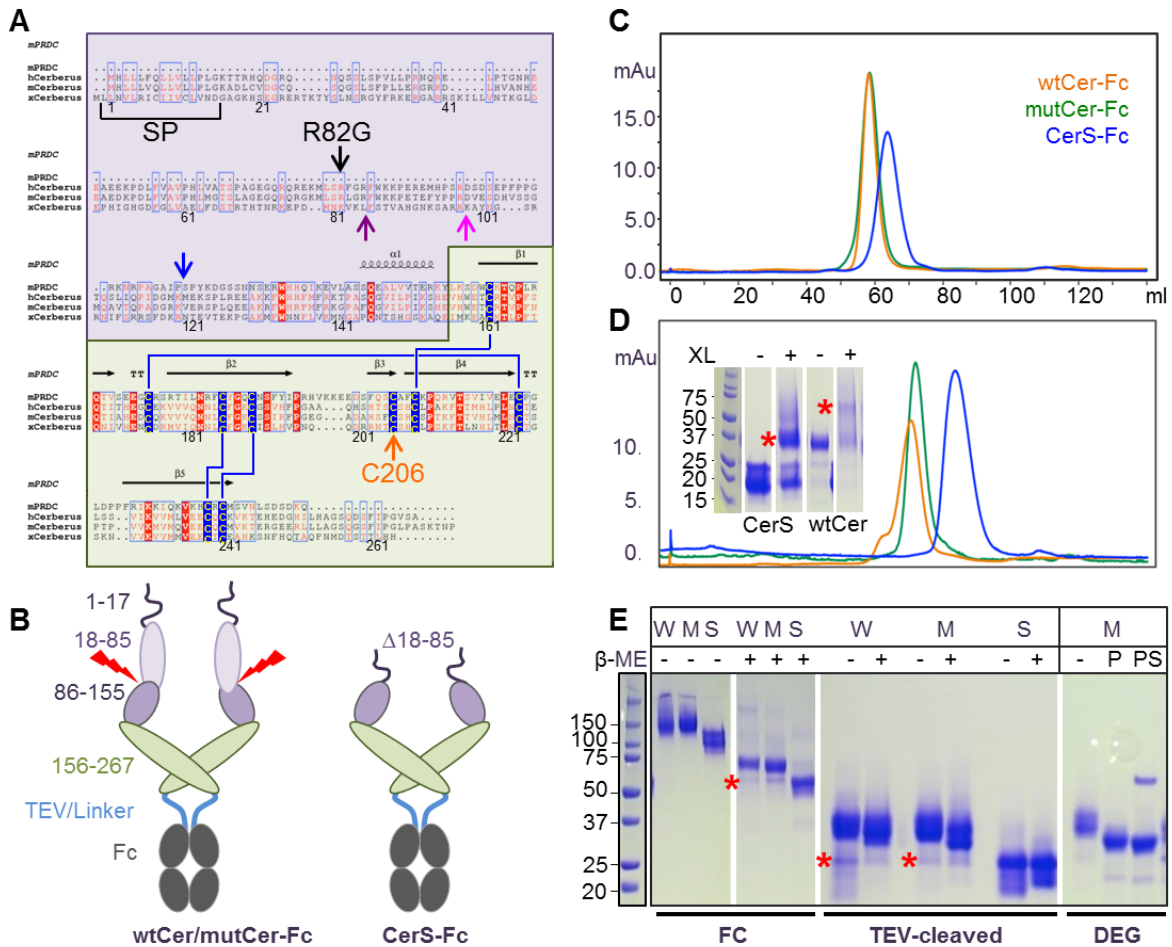


Figure 4-1. Construct design and purification.

(A) Multiple sequence alignment of the DAN family proteins PRDC (mouse), and Cerberus (human, mouse and frog). DAN family proteins are secreted regulators of TGF- β family signaling that have a signal peptide for secretion (SP) and a conserved cystine knot domain (highlighted in green, Cerberus amino acids 156-267). Cerberus has a unique N-terminal region of unknown function (highlighted in purple, Cerberus amino acids 19-155). Cerberus molecules are post-translationally processed and have a predicted proprotein convertase processing site, marked by the purple arrow for mammalian Cerberus and by a blue arrow for frog Cerberus (29), or a proposed processing site marked by a pink arrow (1). Cerberus molecules also have an unpaired Cysteine (Cys206 in human Cerberus, orange arrow). Arginine 82 and Cysteine 206 were mutated for functional analysis. (B) Domain organization of Cerberus and construct design. Cerberus consists of three distinct regions, the cleavable N-terminal region (amino acids 19-85, light purple), the residual N-terminal region (amino acids 86-155, dark purple), and the cystine knot domain (amino acids 156-267, green). Three different constructs were created: Full-length human Cerberus with the wild-type sequence (wtCer-Fc), full-length Cerberus with mutations at Arginine 82 and Cysteine 206 (mutCer-Fc), as well as a short form lacking the N-terminal region (amino acids 18-85) and mutated at Cysteine 206 (CerS-Fc). Cerberus genes were fused at the C-terminus to human IgG1-Fc via

Figure 4-1 (cont'd)

22 amino acid linker containing a TEV cleavage site. **(C)** Purification of wtCer-Fc, mutCer-Fc and CerS-Fc expressed in CHO cells. Following two purification steps, molecules migrate as a single, well-defined peak in a size exclusion chromatographic column. The molecular weight of each protein corresponds to the dimeric species. **(D)** Purification of wtCer, mutCer, and CerS after removal of the Fc domain. All molecules migrate as a single, well-defined peak in a SEC column. For wtCer and mutCer, the molecular weight corresponds to the dimeric species. CerS elutes at a volume that corresponds to a monomeric form, but also forms dimers in solution. The inserted SDS-PAGE shows glutaraldehyde cross-linking of CerS and wtCer. The dimeric forms are highlighted by the red asterisk. For functional studies, only the main peak fractions were used and fractions corresponding to higher molecular weight species were discarded. **(E)** SDS-PAGE gels of purified proteins. The two left panels show non-reducing (- β ME) and reducing (+ β ME) SDS-PAGE gels of the Fc fusion forms (W: wtCer-Fc, M: mutCer-Fc, S: CerS-Fc). Expected molecular weights are 57 kDa for wtCer-Fc, 57 kDa for mutCer-Fc and 49 kDa for CerS-Fc. Higher apparent molecular weights are due to glycosylation. wtCer-Fc and mutCer-Fc have three N-linked glycosylation sites per protomer, two in the Cerberus moiety and one in the Fc moiety. CerS-Fc has two N-linked glycosylation sites per protomer, one in the Cerberus moiety and one in the Fc moiety. Fc fusion constructs form disulfide-linked dimers via the Fc domain. The two right panels show Fc-free Cerberus. The molecular weights of the three cleaved Cerberus constructs correspond to a monomeric form under reducing and non-reducing conditions. Deglycosylation with PNGase F alone (P) or with PNGase F and Sialidase (PS) reduces the molecular weight of mutant Cerberus to the theoretically expected value. The red star designates processed Cerberus.

Cerberus constructs migrated with elevated motility on SDS-PAGE gel and both full-length forms contained degradation products. To clarify the contribution of glycosylation and proteolytic cleavage to SDS-PAGE heterogeneity and elevated molecular weight, we digested mutCer with deglycosylation enzymes (Fig. 4-1E, DEG). Treatment with PNGase F alone decreased the molecular weight of full-length Cerberus to approximately 30 kDa. Simultaneous treatment with PNGase F and Sialidase produced a homogenous band that corresponded to the theoretical molecular weight of full-length Cerberus, which is 28 kDa, indicating that Cerberus is heavily N- and O-glycosylated. Based on SDS-PAGE mobility the degradation product of full-length Cerberus corresponded approximately to the cloned, short-form Cerberus, indicating that Cerberus can be proteolytically processed, and that cleavage

occurs at or near the predicted proprotein convertase processing site (Fig. 4-1E, red star). SEC elution volumes of the short form and the degradation product are the same, indicating that the oligomeric state and apparent molecular weight of the two proteins are the same.

Different forms of Cerberus have similar ligand binding profiles

Co-immunoprecipitation studies have indicated that frog and/or mouse Cerberus bind Nodal, BMP-2, BMP-4 and possibly Activin A (1, 13). By contrast, we previously showed that out of 7 tested TGF- β family ligands (chapter 3), including BMP-2, Activin A, and Nodal, only Nodal bound human Cerberus with significant affinity (1, 13, 15, 18). To investigate more broadly the ligand-binding specificity of human Cerberus, we used a high throughput, SPR-based binding assay. We captured purified wtCer-Fc on a Biacore sensor chip that was cross-linked with an anti-human Fc antibody and we injected 15 different TGF- β family ligands at a concentration that exceeds physiological levels (80 nM) (19, 20, 21). As expected, most of the tested TGF- β family ligands did not bind Cerberus with appreciable affinities, including Activin A, BMP-2, TGF- β 1, TGF- β 2, TGF- β 3, GDF-1, GDF-3, GDF-8, and BMP-9 (Fig. 4-2A) (15). Notably, we discovered three new ligands that bind human Cerberus in addition to Nodal and BMP-4: Activin B, BMP-6 and BMP-7.

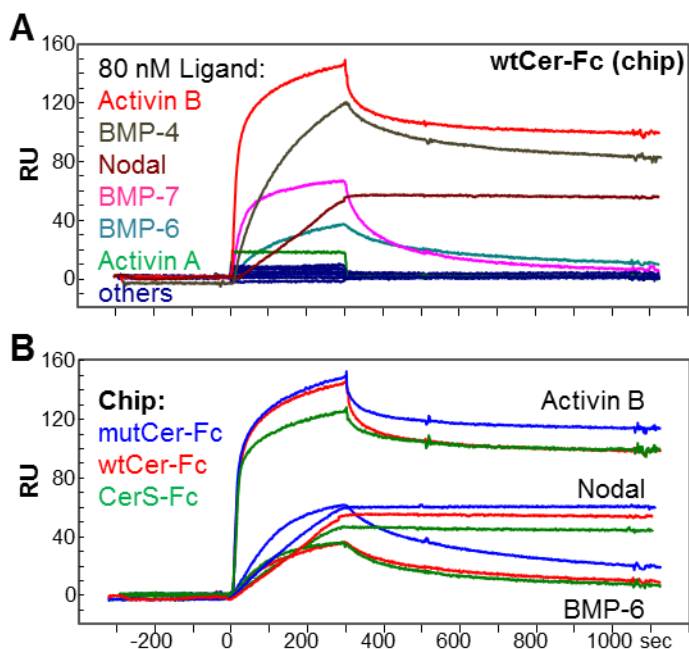


Figure 4-2. Cerberus ligand binding comparison.

(A) Ligand binding comparison of wtCer-Fc. Different ligands were injected over wtCer-Fc at 80 nM concentration. Activin B (red), BMP-4 (brown), Nodal (maroon), BMP-6 (teal) and BMP-7 (pink) bind wtCer-Fc with different affinities. All other tested ligands did not bind Cerberus. (B) Comparison of Activin B, Nodal, and BMP-6 binding to wtCer-Fc, mutCer-Fc, CerS-Fc. Equal amounts of wtCer-Fc, mutCer-Fc and CerS-Fc were immobilized on SPR sensor chip, and 80nM Activin B, Nodal or BMP-6 were injected. wtCer-Fc (red curves), mutCer-Fc (blue curves) and CerS-Fc (green curves) show very similar binding profiles.

Frog Cerberus exists in a long form and a processed, short form. Short form Cerberus is thought to bind and inhibit Nodal, but not other ligands (1). To evaluate the role in ligand binding of the proprotein convertase cleavable N-terminal region and of the unpaired Cysteine (Cys206), we determined the ligand binding profiles of CerS and mutCer using the high throughput, SPR-based binding assay. We captured purified CerS-Fc and mutCer-Fc on a Biacore sensor chip and we injected 15 different ligands at 80 nM concentration as we did for wtCer-Fc (Fig. 4-2A). Intriguingly, we found that ligand binding by CerS-Fc and mutCer-Fc was not significantly different from wtCer-Fc for Activin B, BMP-6 and BMP-7 (Fig. 4-

2B). Thus, the cleavable N-terminus and the unpaired Cysteine of human Cerberus do not appear to have a major, direct role in ligand-binding affinity or specificity.

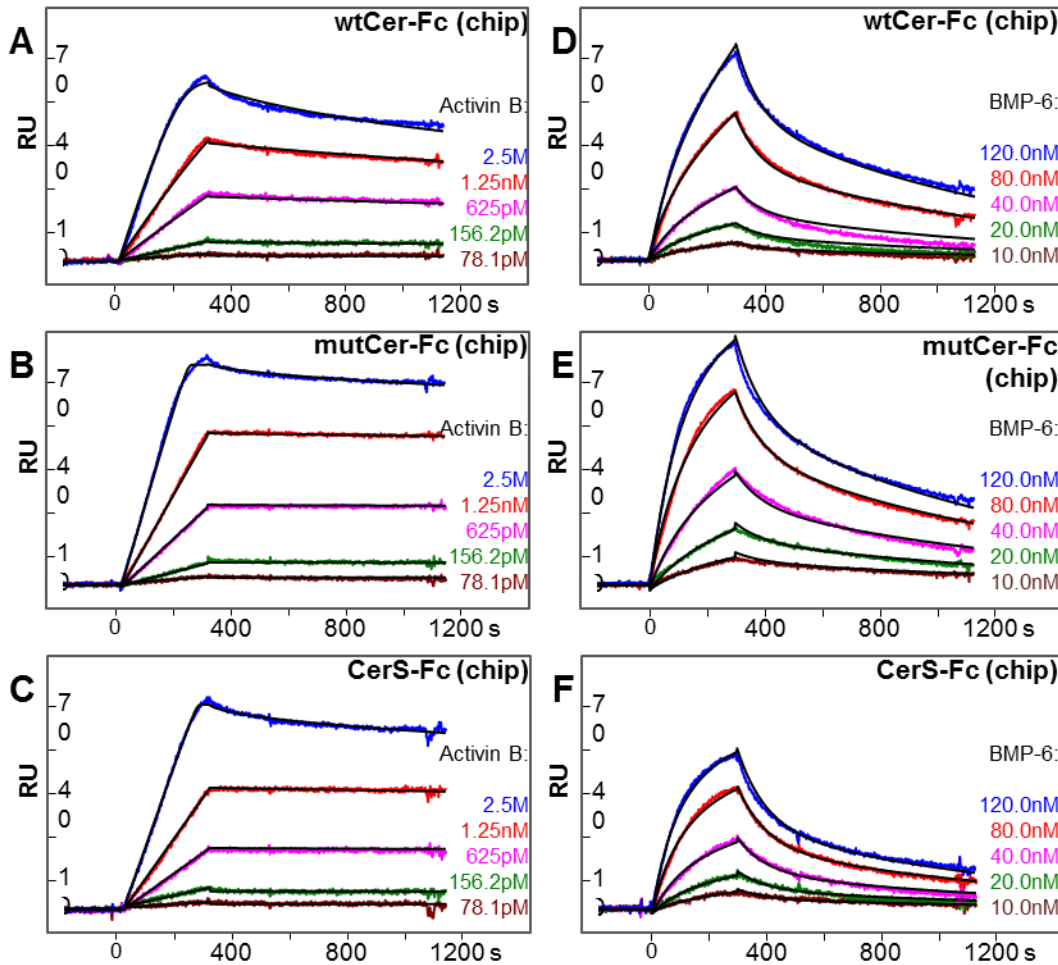


Figure 4-3. Cerberus ligand binding affinities.

(A) wtCer-Fc, (B) mutCer-Fc and (C) CerS-Fc were immobilized on the SPR sensor chip and different concentrations of Activin B were injected as shown. Different Cerberus forms bind Activin B with similar affinities. (D) wtCer-Fc, (E) mutCer-Fc and (F) CerS-Fc were immobilized on the SPR sensor chip and different concentrations of BMP-6 were injected as shown. Different Cerberus forms bind BMP-6 with similar affinities. (A-F) Fitted curves (black lines) are superimposed over all experimental curves.

To determine the binding affinity of the newly discovered Cerberus ligands Activin B, BMP-6 and BMP-7, we captured wtCer-Fc, mutCer-Fc and CerS-Fc on a Biacore sensor

chip and we injected a concentration series for each one of these three ligands (Fig. 4-3, Table 4-1). wtCer-Fc bound Activin B with affinities that are comparable to refolded Nodal ($k_a = 2.3 \times 10^6 \text{ (M}^{-1}\text{s}^{-1}\text{)}$, $k_d = 2.2 \times 10^{-6} \text{ (s}^{-1}\text{)}$, $K_d = 0.096 \text{ nM}$) (Fig. 4-3) (15). The association rate was very fast and the dissociation rate was very slow, as expected for a very strong, picomolar interaction. Binding of BMP-6 and BMP-7 was significantly weaker than Activin B binding to Cerberus. Even at this comparatively weak affinity, BMP-6 and BMP-7 bound Cerberus with several orders of magnitude higher affinity than the frog Cerberus ligands BMP-2 (15). In sum, Nodal, BMP-4 and Activin B are the highest affinity ligands of human Cerberus; however, human Cerberus also binds BMP-6 and BMP-7 with significant affinities.

Table 4-1. Equilibrium dissociation and rate constants

Flow	Chip	$k_a \text{ (M}^{-1}\text{s}^{-1}\text{)}$	$k_d \text{ (s}^{-1}\text{)}$	$K_d \text{ (nM)}$
Activin B	wtCer-Fc	$(2.32 \pm 0.1) \times 10^6$	$(2.23 \pm 0.2) \times 10^{-4}$	0.096 ± 0.01
	mutCer-Fc	$(1.95 \pm 0.3) \times 10^6$	$(3.06 \pm 0.2) \times 10^{-5}$	0.016 ± 0.003
	CerS-Fc	$(1.17 \pm 0.2) \times 10^6$	$(1.66 \pm 0.1) \times 10^{-5}$	0.014 ± 0.002
BMP-6	wtCer-Fc	$(5.54 \pm 1.4) \times 10^4$	$(1.06 \pm 0.2) \times 10^{-3}$	19.1 ± 2.5
	mutCer-Fc	$(6.92 \pm 1.0) \times 10^4$	$(1.02 \pm 0.1) \times 10^{-3}$	14.7 ± 3.6
	CerS-Fc	$(8.20 \pm 0.4) \times 10^4$	$(1.25 \pm 0.1) \times 10^{-3}$	15.2 ± 1.4
BMP-7	wtCer-Fc	$(1.64 \pm 0.2) \times 10^5$	$(2.84 \pm 0.1) \times 10^{-3}$	17.3 ± 0.8
	mutCer-Fc	$(1.26 \pm 0.5) \times 10^5$	$(1.24 \pm 0.1) \times 10^{-3}$	9.8 ± 0.9
	CerS-Fc	$(1.37 \pm 0.2) \times 10^5$	$(2.13 \pm 0.2) \times 10^{-3}$	15.6 ± 1.9

Note: Units are $k_a \text{ (M}^{-1}\text{s}^{-1}\text{)}$, $k_d \text{ (s}^{-1}\text{)}$, $K_d \text{ (nM)}$, $\text{Chi}^2 \text{ (RU}^2\text{)}$, $k_t \text{ (RU / (M*s))}$. N = 3.

Cerberus prevents ligand binding to both type I and type II receptors

Cerberus blocked binding of Nodal to its type I and type II receptors (chapter 3) (1, 13, 15). Inhibition of Nodal binding to the type II receptors ActRIIA and ActRIIB was more efficient than to BMPRII (chapter 3) (15). To validate the mechanism of Cerberus inhibition and to examine its potential for differential regulation, we investigated the effect of the different Cerberus constructs on ligand binding to the type I and type II receptors ActRIIA, ActRIIB, and BMPRII. Receptor-Fc fusion proteins were captured on a Biacore sensor chip that was cross-linked with an anti-human Fc antibody. Activin B and BMP-6 (10 nM and 80 nM, respectively) were preincubated with Fc-free Cerberus at concentrations ranging from 0 nM to 4000 nM. Preassembled ligand-Cerberus complexes were injected over the captured receptors (Fig. 4-4). In this format, Cerberus must be Fc-free to avoid binding of Fc to the anti-human Fc antibody cross-linked sensor chip.

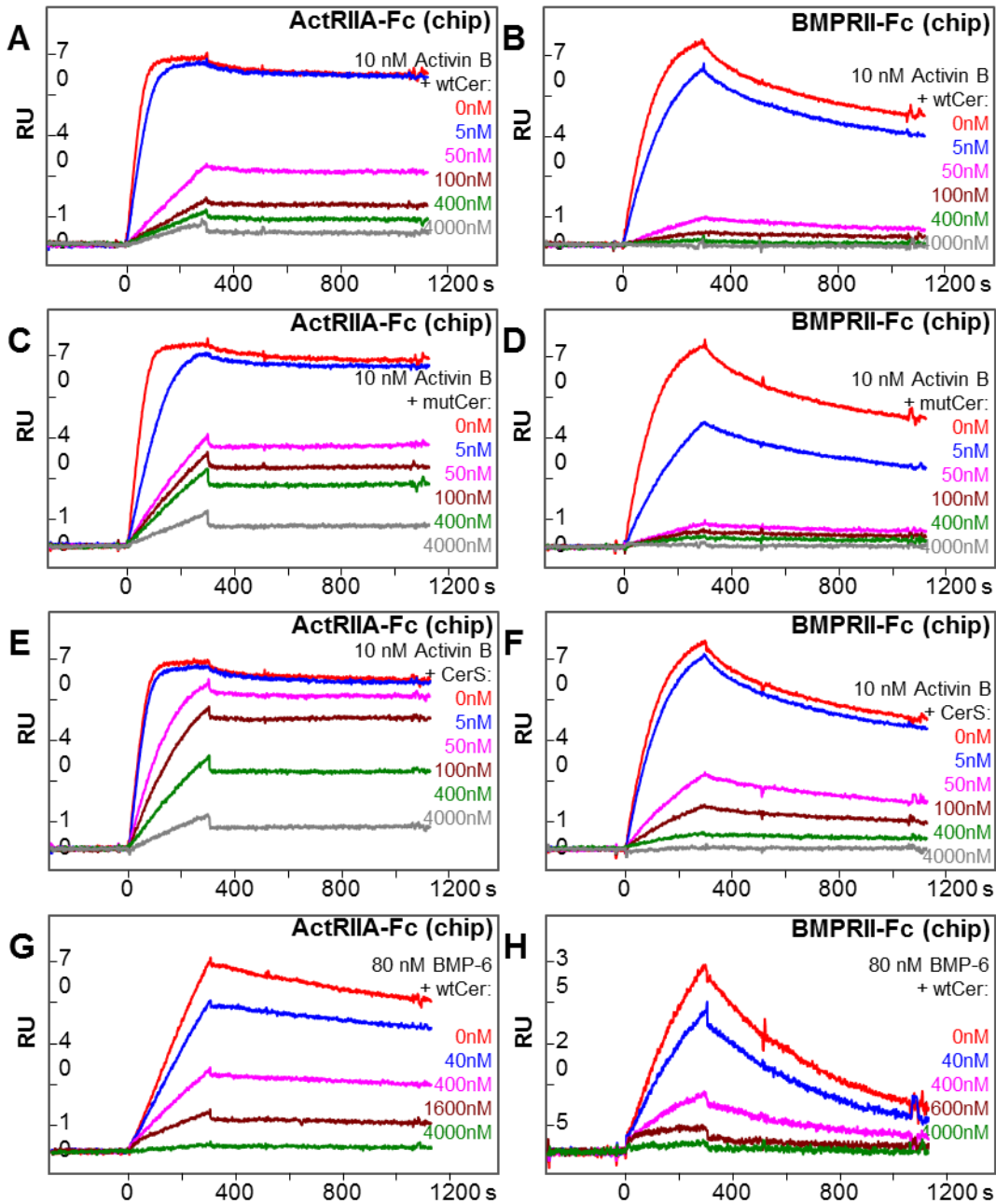


Figure 4-4. Cerberus inhibition of ligand-type II receptor interactions.

wtCer inhibition of (A) Activin B-ActRIIA binding, (B) Activin B- BMPRII binding. mutCer inhibition of (C) Activin B-ActRIIA binding, (D) Activin B-BMPRII binding. CerS inhibition of (E) Activin B-ActRIIA binding, (F) Activin B-BMPRII binding. wtCer inhibition of (G) BMP-6-ActRIIA binding, (H) BMP-6-BMPRII binding. ActRIIA-Fc or BMPRII-Fc was immobilized on the SPR sensor chip. (A-F) 10 nM Activin B was preincubated with 0 nM (red), 5 nM (blue), 50 nM (magenta), 100 nM (brown), 400 nM (green), 4000 nM (grey) wtCer, mutCer or CerS. Preformed Activin B-Cerberus complexes

Figure 4-4 (cont'd)

were injected over the sensor chip. **(G-H)** 80 nM BMP-6 was preincubated with 0 nM (red), 40 nM (blue), 400 nM (magenta), 1600 nM (brown), 4000 nM (green) wtCer. Preformed BMP-6-Cerberus complexes were injected over the sensor chip. **(A-H)** wtCer, mutCer and CerS prevent binding of Activin B and BMP-6 to type II receptors ActRIIA and BMPRII, as seen in the almost complete loss of SPR response at the 4000 nM Cerberus concentration.

As expected, Cerberus prevented Activin B and BMP-6 binding to ActRIIA-Fc, ActRIIB-Fc and BMPRII-Fc in a concentration dependent manner (Fig. 4-4). Inhibition kinetics indicated that Cerberus is a competitive inhibitor of the ligand-type II receptor interaction, further supporting the conclusion that Cerberus binds ligands also by covering the type II receptor binding site (15). However, the different Cerberus constructs did not inhibit ligands equivalently. wtCer strongly inhibited the low picomolar ($K_d \sim 0.01$ nM) interaction between Activin B and the type II receptor ActRIIA (IC_{50} of 26 nM, Fig. 4-4, Table 4-2), whereas mutCer and CerS were less effective (IC_{50} 40 nM and 261 nM, respectively). 50 nM wtCer reduced binding of Activin B to ActRIIA by approximately 60% (Fig. 4-4). By contrast, 50 nM CerS only reduced binding of 10 nM Activin B to ActRIIA by approximately 10%. This trend extends to inhibition of ligand binding to ActRIIB-Fc (data not shown) and BMPRII-Fc (Fig. 4-4, Table 4-2), as well as Nodal. However, as Activin B and BMP-7 binding to BMPRII is weaker than to ActRIIA, inhibition of ligand binding to BMPRII is more effective for all Cerberus forms against these two ligands. By contrast, Cerberus does not completely block binding of Nodal to BMPRII. By itself, Cerberus does not bind ActRIIA, ActRIIB or BMPRII. Taken together, our findings indicate that all Cerberus constructs inhibit ligand binding to type II receptors. mutCer is as effective as wtCer, indicating that the unpaired Cysteine and/or the single point mutation in the proprotein convertase processing site do not contribute significantly to inhibition of the

ligand-type II receptor interaction. By contrast, the cleavable N-terminus appears to have a more direct role in blocking ligand binding to type II receptors, as an approximately 10 fold higher concentration of the short form was needed to inhibit receptor binding. We also evaluated type I receptor inhibition by using BMP-4 only because we currently don't know which type I receptors are bound by Activin B, BMP-6, or BMP-7. We found that wtCer, mutCer and CerS inhibited type I receptor binding equivalently well, showing that the unpaired Cysteine, the single point mutation in the proprotein convertase processing site and/or N-terminal region do not contribute to inhibition of the ligand-type I receptor interaction (data not shown).

Table 4-2. IC₅₀ values for SPR binding inhibition and reporter assays

*SPR-BINDING (IC₅₀ (nM))				
Ligand	Chip	wtCer	mutCer	CerS
Activin B	ActRIIA	26.2 ± 1.7	40.1 ± 2.5	261.0 ± 33.2
Activin B	BMPRII	14.9 ± 4.2	7.4 ± 1.1	28.4 ± 9.6
BMP-6	ActRIIA	319.0 ± 53.4	350.0 ± 96.1	N.D.
BMP-6	BMPRII	156.0 ± 9.2	48.3 ± 3.5	N.D.
**REPORTER-SIGNALING (IC₅₀ (nM))				
Ligand	Cell line	wtCer-Fc	mutCer-Fc	CerS-Fc
Activin B	A-204	34.1 ± 9.4	3.7 ± 1.0	14.8 ± 1.1
BMP-6	HepG2	67.8 ± 24.0	15.8 ± 3.2	49.9 ± 11.8

Note: 5 concentrations of inhibitor were used. *SPR-study was performed in duplicate, **Reporter-gene expression study was performed in quadruplicate.

Cerberus inhibits intracellular SMAD signaling

As Cerberus inhibited the ligand-type II receptor interaction and inhibited Nodal signaling *in vivo* (15, 22, 23, 24), we hypothesized that Cerberus could also inhibit signaling by its newly identified ligands. To test this hypothesis, we used a luciferase reporter gene assay. We transfected A-204 cells with control plasmid and the SMAD3 responsive reporter plasmid or HepG2 cells with the same control plasmid and the SMAD1/5/8 responsive reporter plasmid (25, 26). Transfected A-204 cells were treated with 0.8 nM Activin A or Activin B, and HepG2 cells were treated with 0.8 nM BMP-2 or BMP-6 (25, 26). Both Activin A and Activin B induced luciferase expression with the SMAD3 reporter, and both BMP-2 and BMP-6 induced luciferase expression with the SMAD1/5/8 reporter, as expected (Fig. 4-5). Addition of wtCer-Fc inhibited Activin B and BMP-6 signaling in a concentration dependent manner, but not Activin A or BMP-2. mutCer-Fc and CerS-Fc also inhibited Activin B and BMP-6 signaling, their efficacy was similar to wtCer-Fc. To determine whether the Fc moiety had an impact on signaling inhibition, we also performed this assay with the Fc-free wtCer form. Its effect on signaling was comparable to wtCer-Fc (Fig. 4-5).

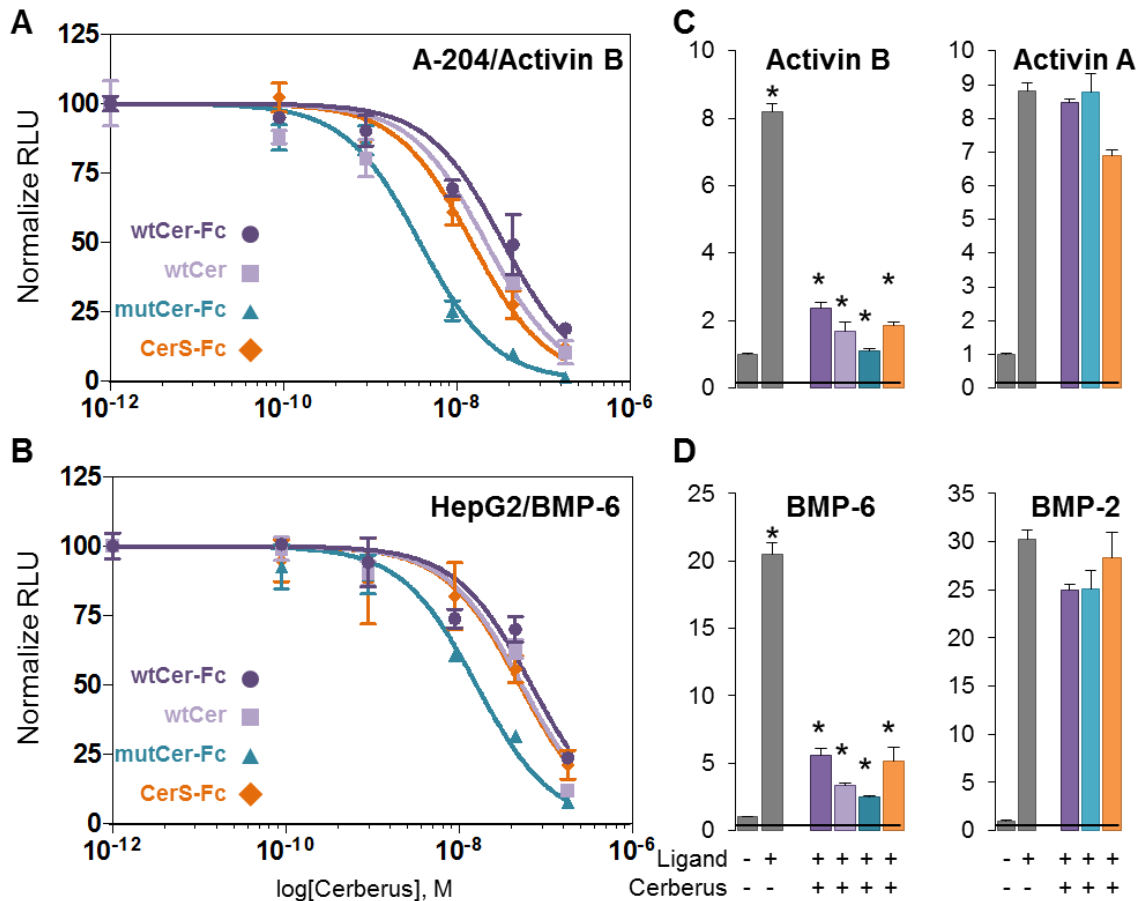


Figure 4-5. Cerberus inhibition of SMAD2/3 and SMAD1/5/8 signaling.

(A) SMAD2/3 signaling inhibition. A-204 cells were transfected with SMAD3 responsive reporter and control plasmids. Cells were treated with 0.8 nM Activin B, and wtCer-Fc (dark purple) / wtCer (light purple), mutCer-Fc (dark blue) or CerS-Fc (dark orange). Cerberus concentrations were 1: 0.089 nM, 2: 0.89 nM, 3: 8.9 nM, 4: 44.5 nM, 5: 178 nM. (B) SMAD1/5/8 signaling inhibition. HepG2 cells were transfected with SMAD1/5/8 responsive reporter and control plasmids. Cells were treated with 0.8 nM BMP-6, and wtCer-Fc (dark purple) / wtCer (light purple), mutCer-Fc (dark blue) or CerS-Fc (dark orange). Cerberus concentrations were 1: 0.089 nM, 2: 0.89 nM, 3: 8.9 nM, 4: 44.5 nM, 5: 178 nM. (C) Single point comparison of SMAD2/3 signaling inhibition by Cerberus in A-204 cells. Cells were treated with 0.8 nM Activin B (left panel) or Activin A (right panel), and 178 nM wtCer-Fc, wtCer, mutCer-Fc, or CerS-Fc. (D) Single point comparison of SMAD1/5/8 signaling inhibition by Cerberus in HepG2 cells. Cells were treated with 0.8 nM BMP-6 (left panel) or BMP-2 (right panel), and 178 nM wtCer-Fc, mutCer-Fc, or CerS-Fc. Signaling was detected as firefly luciferase activity and normalized against renilla luciferase activity. Relative luciferase units (RLU) were calculated by dividing firefly luciferase units (fLU) with renilla luciferase units (rLU). Data are expressed as mean + SE of four independent measurements. Statistically significant differences calculated using a two-tailed T-Test are marked by * (P < 0.05).

Using the luciferase reporter gene expression data, we calculated IC₅₀ for inhibition with the different Cerberus constructs. Overall, IC₅₀ values are in agreement with, but are not identical to IC₅₀ values determined by SPR (Fig. 4-5). One possible reason for the observed differences is that with SPR we determined an IC₅₀ relative to individual receptors. By contrast, in the cell-based assay we determined an IC₅₀ that combines the contributions of all the receptors expressed on the cell surface. As Activin B and BMP-6 interact at least with ActRIIA, ActRIIB and BMPRII, an IC₅₀ determined by SPR should be similar, but cannot be identical to an IC₅₀ determined in a whole cell context, where all three receptors are present at the same time.

Only full-length Cerberus can inhibit migration of MDA-MB-231 breast cancer cells

Long form (xCer-L) and short form (xCer-S) frog Cerberus have distinct biological activities (1). As full-length human Cerberus fused to Fc (wtCer-Fc) inhibited migration of MDA-MB-231 breast cancer cells (15), we undertook to evaluate, using a wound healing assay, how different human Cerberus-Fc fusion constructs inhibit MDA-MB-231 migration (Fig. 4-6A, B). We plated MDA-MB-231 breast cancer cells in an Ibidi culture insert. When cells reached 80% confluence, we removed the insert and replaced culture medium with fresh medium containing 2.5 µg/ml Mitomycin C with or without 17.8 nM wtCer-Fc, mutCer-Fc or CerS-Fc. As expected, the 500 µm gap created by the culture insert completely closed within 24 h in untreated cells (Fig. 4-6, control). By contrast, wtCer-Fc completely prevented wound closure, confirming its ability to suppress MDA-MB-231 migration (Fig. 4-6, wtCer-Fc) (15). mutCer-Fc also had a strong effect on migration, although it was slightly less effective than wtCer-Fc (Fig. 4-6, mutCer-Fc). Strikingly, CerS-Fc lost the ability to suppress migration, allowing greater than 75% wound closure relative to wtCer-Fc (Fig. 4-6, CerS-Fc). To

ascertain that the unpaired Cysteine had no direct role in suppressing MDA-MB-231 migration, we generated a construct that only carried the C206A mutation. This construct was as effective as wtCer-Fc (data not shown), demonstrating that the unpaired Cysteine does not have a prominent role in Cerberus inhibition of breast cancer cell migration. Importantly, the Fc domain did not have an effect on Cerberus activity, as the different Fc-free Cerberus constructs closely paralleled the effect of the corresponding Fc fusion forms (data not shown). Taken together, these findings suggest that the N-terminus of human Cerberus is critical for suppressing MDA-MB-231 cell migration and indicate that the long and short forms could have distinct biological activities, even if ligand binding affinities or the ability to inhibit signaling of the Fc-fusion constructs are not significantly different.

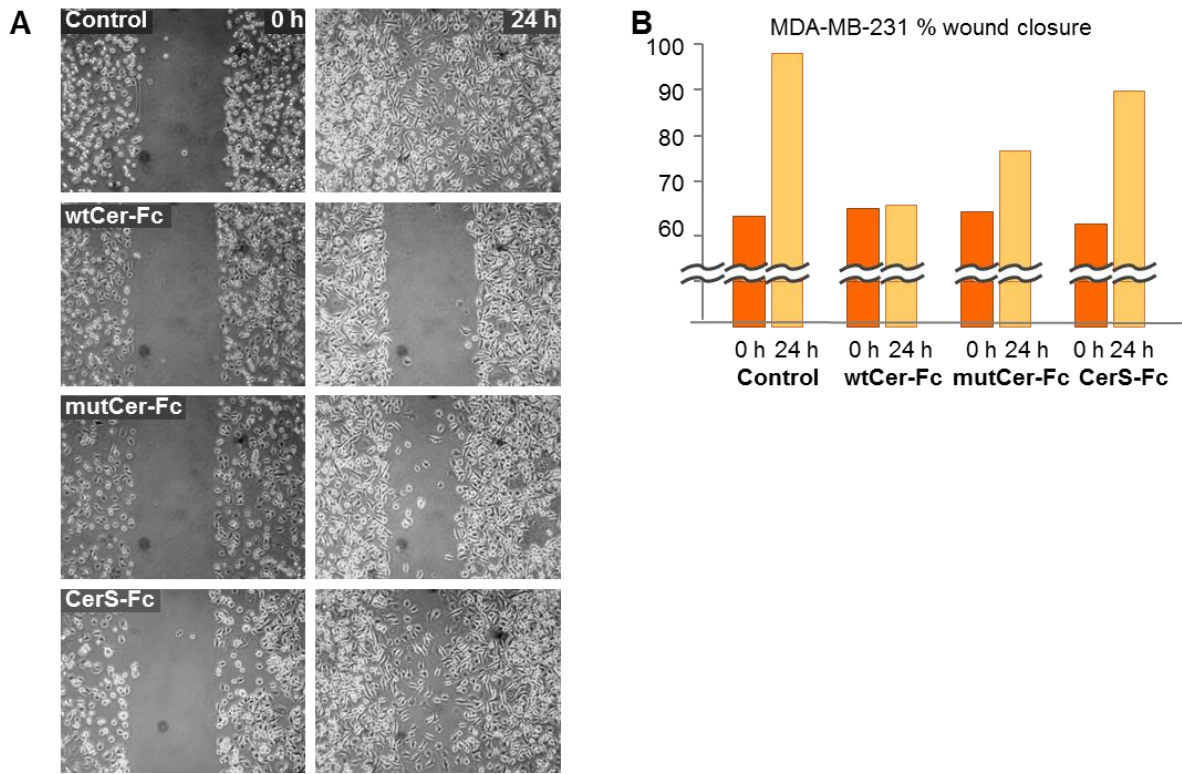


Figure 4-6. Cerberus inhibition of breast cancer cell migration.

(A) Inhibition of MDA-MB-231 wound closure by Cerberus. MDA-MB-231 breast cancer cells were plated in Ibidi insert dishes and grown to 80% confluence. Inserts were removed to create a gap and medium was exchanged with complete medium containing 2.5 $\mu\text{g/ml}$ Mitomycin C and 0 nM (control) or 17.8 nM wtCer-Fc, mutCer-Fc and CerS-Fc. Images were taken after insert removal (0 h) and after 24 h incubation with Cerberus (24 h). (B) Wound closure quantification. Images taken at 0 h and 24 h were analyzed using Wimasis software to quantify cellular migration. The dark orange bar corresponds to image taken at 0 h, the light orange bar corresponds to image taken at 24 h. Control correspond to experiment carried out without Cerberus.

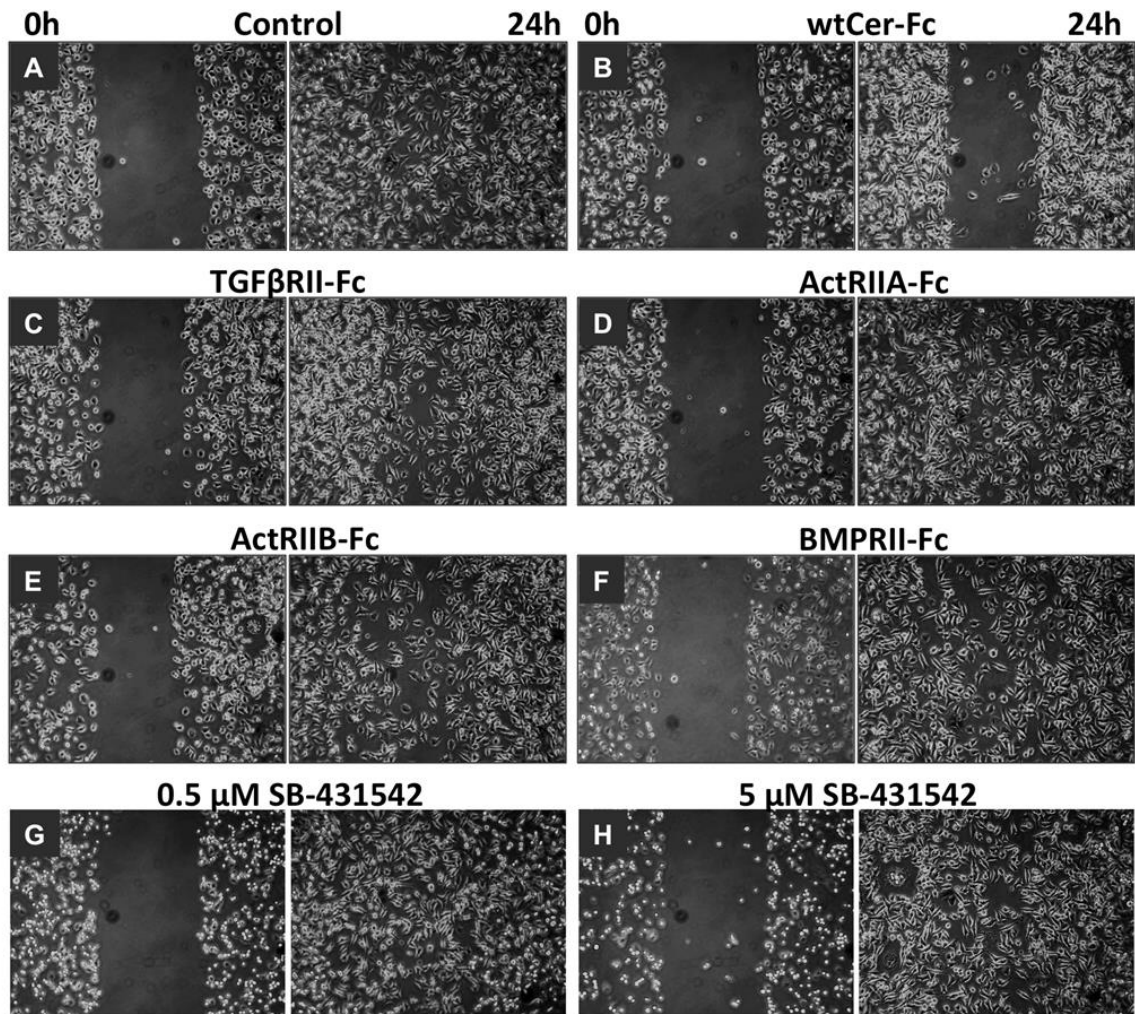


Figure 4-7. The effect of different TGF- β family inhibitor on MDA-MB-231 breast cancer cell migration.

MDA-MB-231 breast cancer cells were plated in Ibidi insert dishes and grown to 80% confluence. Inserts were removed to create a gap and medium was exchanged with complete medium containing 2.5 $\mu\text{g/ml}$ Mitomycin C and (A) 0 mg/ml (control) or 10 mg/ml (approximately 15 nM) (B) wtCer-Fc, (C) TGF β RII-Fc, (D) ActRIIA-Fc, (E) ActRIIB-Fc, (F) BMPRII-Fc, (G) 0.5 μM SB-431542, and (H) 5 μM SB-431542. Images were taken after insert removal (0 h) and after 24 h incubation with inhibitors (24 h).

Discussion

Cerberus is a secreted regulator of TGF- β family signaling that has multiple antagonist activities and that exists in two functionally distinct forms. Which TGF- β family signaling pathways human Cerberus regulates and how the two forms function is poorly understood, as the molecular activities of human Cerberus are yet to be properly defined. As Cerberus is an important regulator of key developmental processes, including head formation and cardiogenesis, and as human Cerberus may play a critical role in adult bone homeostasis, elucidating its function is of considerable biological and biomedical significance. Thus, our goal here was to determine the TGF- β family ligand binding specificity of human Cerberus and to elucidate the function of the N-terminal region, which has a proprotein convertase recognition sequence and is cleaved to produce a processed form with a distinct activity.

Previous studies have indicated that frog Cerberus is an antagonist of the TGF- β family ligands Nodal, BMP-2 and BMP-4 (1). These findings have encouraged the consensus view that every Cerberus from every species is a 'BMP' antagonist (13, 27). However, while we and others have confirmed that human and mouse Cerberus bound and inhibited Nodal, we also discovered that human Cerberus did not bind or inhibit BMP-2 (13, 15). On the other hand, frog Cerberus antagonizes multiple TGF- β family ligands, suggesting that members of the Cerberus family could be promiscuous TGF- β family ligand inhibitors. To better understand the scope of human Cerberus function, we examined whether it could also bind and inhibit multiple TGF- β family ligands. In addition to Nodal and BMP-4, we found that human Cerberus bound Activin B, BMP-6 and BMP-7 with significant affinity, but not BMP-2, or other close homologs of Activin B, including Activin A. Notably, Activin A and Activin B are often considered to be functionally equivalent, and Nodal and Activin A are often used

interchangeably in biological assays. The exquisite specificity of the Cerberus-Activin B and Cerberus-Nodal interactions suggests, however, that Activin A could perform biological functions while Cerberus is proximally expressed in order to inhibit Nodal or Activin B signaling. In sum, we show that TGF- β family signaling regulation by human Cerberus is restricted to a small and specific group of ligands that is different from that reported for frog Cerberus (13, 15). Notably, we suggest that inhibition of Activin B by human Cerberus could play a role in regulating bone mineral density (28).

When frog Cerberus was first characterized, two different forms of the gene product were observed (1). Animal cap cells secreted a soluble protein of 46,000 kDa and a minor form of 33,000 kDa, human 293T cells almost exclusively produced the 33,000 kDa form (1). Notably, the two forms were found to have distinct activities, namely full-length Cerberus antagonized Wnt, Nodal and BMP signaling, whereas the short form only antagonized Nodal signaling (1). We found that CHO cells also produced two forms of human Cerberus, a full-length form and a short form. The two forms also differed by approximately 10-15 kDa. As the short form of Cerberus appears to exist in different species (frog and human), we speculated that post-translational processing could play a role in regulating Cerberus function. Sequence analysis of different Cerberus genes identified a conserved proprotein convertase processing site in mammalian Cerberus (amino acids 80-86 for human Cerberus, Fig. 4-1, RGFR|F; amino acids 125-128 for frog Cerberus, RRSFDKR|N) (29). Remarkably, frog Cerberus also has a predicted proprotein convertase processing-site near the engineered xCer-S N-terminus. As mutation of a key Arginine (Arg81) in the human Cerberus proprotein convertase recognition motif significantly reduced proteolysis, and as a construct lacking the N-terminal sequence produced a biologically active protein that migrated on SDS-PAGE

electrophoresis with a molecular weight corresponding to the processed form, we speculate that the short form of Cerberus can be obtained by pro-protein convertase processing at the predicted pro-protein convertase processing site.

To determine if the two forms of human Cerberus are functionally distinct, we compared their abilities to bind ligands and inhibit signaling. In contrast to frog Cerberus, we found that the two human Cerberus forms bound ligands more or less equally. However, they differed in their ability to block ligand binding to type II receptors. Full-length Cerberus effectively inhibited ligand binding to ActRIIA, ActRIIB and BMPRII, whereas a far higher concentration of the short form was needed to achieve comparable inhibition. On the other hand, both full-length and short form of Cerberus block ligand binding to type I receptor equivalently. As we previously demonstrated in chapter 3 that Cerberus blocked Nodal binding to both type I and type II receptors, and to the co-receptor Cripto-1 (15), we propose that the principal molecular function of the short form Cerberus fragment is to block the type I receptor binding-site. By contrast, the cleavable, N-terminal region does not contribute much to ligand binding-affinity, but improves blockade of the type II receptor binding-site. As the different Cerberus-Fc constructs inhibited signaling equivalently, our findings support the conclusion that inhibition of the ligand-type I receptor interaction is sufficient for Cerberus to inhibit signaling by its cognate TGF- β family ligands. This inhibition directly correlates with ligand binding affinity.

Strikingly, full-length Cerberus profoundly suppressed migration of MDA-MB-231 breast cancer cells, whereas the short form largely lacked this activity. This puzzling finding could indicate that the suppressive effect of Cerberus on aggressive phenotypes of certain human breast cancer cell lines requires simultaneously well inhibition of ligand binding to

both type I and type II receptors (15). Alternatively, the suppressive effect of Cerberus may not be due to inhibition of TGF- β family signaling. Instead, the N-terminal region could have roles beyond the TGF- β family, including inhibition of Wnt signaling (1). However, whether mammalian Cerberus inhibits Wnt signaling is not certain. After the initial characterization of frog Cerberus (1), follow up studies that combined mouse Cerberus and frog Wnt ligands could not reproduce this effect (13). As the N-terminal region of frog and mouse Cerberus share less than 18% sequence identity, we propose that a frog Wnt ligand that interacts with frog Cerberus will not necessarily interact with mouse Cerberus. Thus, whether mammalian Cerberus inhibits Wnt signaling by binding Wnt ligands has neither been demonstrated nor disproved. Our findings that other TGF- β family signaling inhibitors, including the decoy receptors ActRIIA-Fc, ActRIIB-Fc, BMPRII-Fc and TGF β RII-Fc (28, 30, 31), and the small molecule type I receptor kinase inhibitor SB-431542 (32, 33), failed to suppress MDA-MB-231 migration suggests that Cerberus inhibition of aggressive breast cancer cell phenotypes is complex and may also involve signaling pathways that don't belong to the TGF- β family (Fig. 4-7). In future studies we will investigate whether human Cerberus inhibits Wnt ligands or other signaling pathways in aggressive breast cancer cells.

REFERENCES

REFERENCES

1. Piccolo, S., Agius, E., Leyns, L., Bhattacharyya, S., Grunz, H., Bouwmeester, T., and De Robertis, E. M. (1999). The head inducer cerberus is a multifunctional antagonist of nodal, BMP and wnt signals. *Nature* **397**, 707-10.
2. Nolan, K., and Thompson, T. B. (2014). The DAN family: modulators of TGF-beta signaling and beyond. *Protein Science* **23**, 999-1012.
3. Bouwmeester, T., Kim, S., Sasai, Y., Lu, B., and De Robertis, E. M. (1996). Cerberus is a head-inducing secreted factor expressed in the anterior endoderm of Spemann's organizer. *Nature* **382**, 595-601.
4. Foley, A. C., Gupta, R. W., Guzzo, R. M., Korol, O., and Mercola, M. (2006). Embryonic heart induction. *Annals of the New York Academy of Sciences* **1080**, 85-96.
5. Zhu, L., Marvin, M. J., Gardiner, A., Lassar, A. B., Mercola, M., Stern, C. D., and Levin, M. (1999). Cerberus regulates left-right asymmetry of the embryonic head and heart. *Current Biology : CB* **9**, 931-8.
6. Perea-Gomez, A., Vella, F. D., Shawlot, W., Oulad-Abdelghani, M., Chazaud, C., Meno, C., Pfister, V., Chen, L., Robertson, E., Hamada, H., Behringer, R. R., and Ang, S. L. (2002). Nodal antagonists in the anterior visceral endoderm prevent the formation of multiple primitive streaks. *Developmental Cell* **3**, 745-56.
7. Cai, W., Albin, S., Wei, K., Willems, E., Guzzo, R. M., Tsuda, M., Giordani, L., Spiering, S., Kurian, L., Yeo, G. W., Puri, P. L., and Mercola, M. (2013). Coordinate nodal and BMP inhibition directs Baf60c-dependent cardiomyocyte commitment. *Genes and Development* **27**, 2332-44.
8. Foley, A. C., Korol, O., Timmer, A. M., and Mercola, M. (2007). Multiple functions of cerberus cooperate to induce heart downstream of Nodal. *Developmental Biology* **303**, 57-65.
9. Glinka, A., Wu, W., Onichtchouk, D., Blumenstock, C., and Niehrs, C. (1997). Head induction by simultaneous repression of BMP and wnt signalling in *Xenopus*. *Nature* **389**, 517-9.
10. Koromila, T., Dailiana, Z., Samara, S., Chassanidis, C., Tzavara, C., Patrinos, G. P., Aleporou-Marinou, V., and Kollia, P. (2012). Novel sequence variations in the CER1 gene are strongly associated with low bone mineral density and risk of osteoporotic fracture in postmenopausal women. *Calcified Tissue International* **91**, 15-23.

11. Koromila, T., Georgoulis, P., Dailiana, Z., Ntzani, E. E., Samara, S., Chassanidis, C., Aleporou-Marinou, V., and Kollia, P. (2013). CER1 gene variations associated with bone mineral density, bone markers, and early menopause in postmenopausal women. *Human Genomics* **7**, 21.
12. Tang, P. L., Cheung, C. L., Sham, P. C., McClurg, P., Lee, B., Chan, S. Y., Smith, D. K., Tanner, J. A., Su, A. I., Cheah, K. S., Kung, A. W., and Song, Y. Q. (2009). Genome-wide haplotype association mapping in mice identifies a genetic variant in CER1 associated with BMD and fracture in southern Chinese women. *Journal of Bone and Mineral Research* **24**, 1013-21.
13. Belo, J. A., Bachiller, D., Agius, E., Kemp, C., Borges, A. C., Marques, S., Piccolo, S., and De Robertis, E. M. (2000). Cerberus-like is a secreted BMP and nodal antagonist not essential for mouse development. *Genesis* **26**, 265-70.
14. Belo, J. A., Silva, A. C., Borges, A. C., Filipe, M., Bento, M., Goncalves, L., Vitorino, M., Salgueiro, A. M., Texeira, V., Tavares, A. T., and Marques, S. (2009). Generating asymmetries in the early vertebrate embryo: The role of the cerberus-like family. *The International Journal of Developmental Biology* **53**, 1399-407.
15. Aykul, S., Ni, W., Mutatu, W., and Martinez-Hackert, E. (2015). Human cerberus prevents nodal-receptor binding, inhibits nodal signaling, and suppresses nodal-mediated phenotypes. *PLoS One* **10**, e0114954.
16. Nolan, K., Kattamuri, C., Luedeke, D. M., Deng, X., Jagpal, A., Zhang, F., Linhardt, R. J., Kenny, A. P., Zorn, A. M., and Thompson, T. B. (2013). Structure of protein related to DAN and cerberus: Insights into the mechanism of bone morphogenetic protein antagonism. *Structure* **21**, 1417-29.
17. Nolan, K., Kattamuri, C., Luedeke, D. M., Angerman, E. B., Rankin, S. A., Stevens, M. L., Zorn, A. M., and Thompson, T. B. (2015). Structure of neuroblastoma suppressor of tumorigenicity 1 (NBL1): Insights for the functional variability across bone morphogenetic protein (BMP) antagonists. *The Journal of Biological Chemistry* **290**, 4759-71.
18. Hsu, D. R., Economides, A. N., Wang, X., Eimon, P. M., and Harland, R. M. (1998). The *Xenopus* dorsalizing factor gremlin identifies a novel family of secreted proteins that antagonize BMP activities. *Molecular Cell* **1**, 673-83.
19. Harada, K., Shintani, Y., Sakamoto, Y., Wakatsuki, M., Shitsukawa, K., and Saito, S. (1996). Serum immunoreactive activin A levels in normal subjects and patients with various diseases. *The Journal of Clinical Endocrinology and Metabolism* **81**, 2125-30.

20. Suragani, R. N., Cadena, S. M., Cawley, S. M., Sako, D., Mitchell, D., Li, R., Davies, M. V., Alexander, M. J., Devine, M., Loveday, K. S., Underwood, K. W., Grinberg, A. V., Quisel, J. D., Chopra, R., Pearsall, R. S., Sehra, J., and Kumar, R. (2014). Transforming growth factor-beta superfamily ligand trap ACE-536 corrects anemia by promoting late-stage erythropoiesis. *Nature Medicine* **20**, 408-14.
21. Kropf, J., Schurek, J. O., Wollner, A., and Gressner, A. M. (1997). Immunological measurement of transforming growth factor-beta 1 (TGF-beta1) in blood; assay development and comparison. *Clinical Chemistry* **43**, 1965-74.
22. Kumar, A., Novoselov, V., Celeste, A. J., Wolfman, N. M., ten Dijke, P. & Kuehn, and M. R. (2001). Nodal signaling uses activin and transforming growth factor-beta receptor-regulated SMADs. *The Journal of Biological Chemistry* **276**, 656-61.
23. Chen, Y., Lebrun, J. J., and Vale, W. (1996). Regulation of transforming growth factor beta- and activin-induced transcription by mammalian mad proteins. *Proceedings of the Natural Academy of Sciences of the United States of America* **93**, 12992-7.
24. Nakao, A., Imamura, T., Souchelnytskyi, S., Kawabata, M., Ishisaki, A., Oeda, E., Tamaki, K., Hanai, J., Heldin, C. H., Miyazono, K., and ten Dijke, P. (1997). TGF-beta receptor-mediated signalling through SMAD2, SMAD3 and SMAD4. *The EMBO Journal* **16**, 5353-62.
25. Korchynskyi, O., and ten Dijke, P. (2002). Identification and functional characterization of distinct critically important bone morphogenetic protein-specific response elements in the Id1 promoter. *The Journal of Biological Chemistry* **277**, 4883-91.
26. Zawel, L., Dai, J. L., Buckhaults, P., Zhou, S., Kinzler, K. W., Vogelstein, B., and Kern, S. E. (1998). Human SMAD3 and SMAD4 are sequence-specific transcription activators. *Molecular Cell* **1**, 611-7.
27. Walsh, D. W., Godson, C., Brazil, D. P., and Martin, F. (2010). Extracellular BMP-antagonist regulation in development and disease: tied up in knots. *Trends in Cell Biology* **20**, 244-56.
28. Pearsall, R. S., Canalis, E., Cornwall-Brady, M., Underwood, K. W., Haigis, B., Ucran, J., Kumar, R., Pobre, E., Grinberg, A., Werner, E. D., Glatt, V., Stadmeier, L., Smith, D., Sehra, J., and Bouxsein, M. L. (2008). A soluble activin type IIA receptor induces bone formation and improves skeletal integrity. *Proceedings of the Natural Academy of Sciences of the United States of America* **105**, 7082-7.
29. Duckert, P., Brunak, S., and Blom, N. (2004). Prediction of proprotein convertase cleavage sites. *Protein Engineering, Design and Selection* **17**, 107-12.

30. Lee, S. J., Reed, L. A., Davies, M. V., Girgenrath, S., Goad, M. E., Tomkinson, K. N., Wright, J. F., Barker, C., Ehrmantraut, G., Holmstrom, J., Trowell, B., Gertz, B., Jiang, M. S., Sebald, S. M., Matzuk, M., Li, E., Liang, L. F., Quattlebaum, E., Stotish, R. L., and Wolfman, N. M. (2005). Regulation of muscle growth by multiple ligands signaling through activin type II receptors. *Proceedings of the National Academy of Sciences of the United States of America* **102**, 18117-22.
31. Kim, M. Y., Oskarsson, T., Acharyya, S., Nguyen, D. X., Zhang, X. H., Norton, L., and Massague, J. (2009). Tumor self-seeding by circulating cancer cells. *Cell* **139**, 1315-26.
32. Inman, G. J., Nicolas, F. J., Callahan, J. F., Harling, J. D., Gaster, L. M., Reith, A. D., Laping, N. J., and Hill, C. S. (2002). SB-431542 is a potent and specific inhibitor of transforming growth factor-beta superfamily type I activin receptor-like kinase (ALK) receptors ALK4, ALK5, and ALK7. *Molecular Pharmacology* **62**, 65-74.
33. Laping, N. J., Grygielko, E., Mathur, A., Butter, S., Bomberger, J., Tweed, C., Martin, W., Fornwald, J., Lehr, R., Harling, J., Gaster, L., Callahan, J. F., and Olson, B. A. (2002). Inhibition of transforming growth factor (TGF)-beta1-induced extracellular matrix with a novel inhibitor of the TGF-beta type I receptor kinase activity: SB-431542. *Molecular Pharmacology* **62**, 58-64.
34. Baker, J. M., and Boyce, F. M. (2014). High-throughput functional screening using a homemade dual-glow luciferase assay. *Journal of Visualized Experiments* **88**, 50282.

CHAPTER 5 -

TRANSFORMING GROWTH FACTOR- β FAMILY LIGANDS CAN FUNCTION AS ANTAGONISTS BY COMPETING FOR TYPE II RECEPTOR BINDING⁴

⁴The work described in this chapter was published as the following manuscript: Senem Aykul, and Erik Martinez-Hackert. (2016) Transforming Growth Factor- β Family Ligands Can Function as Antagonists by Competing for Type II Receptor Binding. *The Journal of Biological Chemistry* **291**, 10792-10804.

Abstract

Transforming Growth Factor- β (TGF- β) family ligands are pleiotropic cytokines. Their physiological activities are not determined by a simple coupling of stimulus and response, but depend critically on context, i.e. the interplay of receptors, ligands and regulators that form the TGF- β signal transduction system of a cell or tissue. How these different components combine to regulate signaling activities remains poorly understood. Here we describe a ligand-mediated mechanism of signaling regulation. Based on the observation that the type II TGF- β family receptors ActRIIA, ActRIIB and BMPRII interact with a large group of overlapping ligands at overlapping epitopes, we hypothesized high affinity ligands compete with low affinity ligands for receptor binding and signaling. We show Activin A and other high affinity ligands directly inhibited signaling by the low affinity ligands BMP-2, BMP-7 and BMP-9. We demonstrate Activin A functions as competitive inhibitor that blocks the ligand binding epitope on type II receptors. We propose binding competition and signaling antagonism are integral functions of the TGF- β signal transduction system. These functions could help explain how Activin A modulates physiologic signaling during extraordinary cellular responses, such as injury and wound healing, and how Activin A could elicit disease phenotypes such as cancer related muscle wasting and fibrosis.

Introduction

Transforming Growth Factor- β (TGF- β) family signaling pathways play fundamentally important roles in stem cell fate determination, embryonic development, organogenesis, immunity, and cancer (1-3). The basic principles underlying TGF- β family action are well established: A dimeric ligand binds two type I and two type II receptors to

form a hexameric complex, thus initiating a signaling cascade that leads to phosphorylation of SMAD transcription factors, their translocation to the nucleus, and expression of target genes (4-9). Although this simple mechanism completely describes the molecular basis of signaling and response, it fails to explain the complex, sometimes opposite responses elicited by many TGF- β family ligands. For example, some TGF- β family can both inhibit and promote cell growth, both maintain pluripotency and induce differentiation, and both suppress and activate tumor cells. These paradoxical effects have supported the idea that cellular responses to a TGF- β family ligand depend not only on the ligand induced signaling cascade, but also on the cellular context, i.e. the molecular interplay of all the components that form the TGF- β signal transduction system of a particular cell type or tissue (10-14).

In humans, the TGF- β family consists of 33 ligand genes (TGF- β s, Activins, Bone Morphogenetic Proteins/BMPs, Growth and Differentiation Factors/GDFs, Nodal, and Lefty), seven type I receptors, (ALK1–7), five type II receptors (ActRIIA, ActRIIB, BMPRII, TGF β RII, and AMHRII), as well as number of co-receptors, regulators, and intracellular SMAD transcription factors (3, 15). A distinct feature of the family is the promiscuity of its members. Ligands can bind several different receptors, and receptors can bind multiple ligands. Yet ligand-receptor binding affinities vary greatly. Activin A, Activin B, GDF-8, GDF-11, and BMP-10 bind the type II receptors ActRIIA and ActRIIB with very high affinity (16-18). On the other hand, BMP-2 and BMP-4 bind ActRIIA and ActRIIB with low affinity, but they bind type I receptors with high affinity (19, 20). These observations have supported a model of sequential signaling complex assembly where Activins, GDF-8 and GDF-11 first bind type II receptors with high affinity, then recruit low affinity type I receptors (5, 21). By contrast, BMPs and GDFs first bind type I receptors with high affinity,

then recruit low affinity type II receptors (22). Exceptions include BMP-10, which binds both type I and type II receptors with high affinity (9, 23-25).

Significantly, high affinity and low affinity ligands bind the same type II receptors at the same epitope (26, 27). This raises the question, what happens to low affinity BMP or GDF signaling when high affinity ligands like Activin A, GDF-11 or BMP-10 are present at the same time? Thus far, it has been suggested low affinity BMP and GDF signaling is independent of high affinity ligands, because they uniquely utilize BMPRII for signaling (4, 7, 20, 27). But recent studies found Nodal, Activin A, Activin B and BMP-10 bind BMPRII with much higher affinity than most BMPs and GDFs (9, 18, 28, 29), indicating low affinity ligands do not have a dedicated type II receptor. Instead, low affinity ligands use the same type II receptors as high affinity ligands. We therefore hypothesized that high affinity ligands compete with low affinity ligands for type II receptor binding and antagonize low affinity ligand signaling. In this model, high affinity ligands can function both as signal carriers and as signaling regulators that mediate the biological activities of ligands that bind type II receptors with lower affinities.

To test this hypothesis, we examined ligand-type II receptor binding and ligand signaling. Activins and Activin related ligands like GDF-8 and GDF-11 generally bound type II receptors with higher affinity than most BMPs and signaled via the SMAD2/3 pathway. By contrast, BMPs generally bound type II receptors with lower affinity and signaled via the SMAD1/5/8 pathway, as expected. Notably, high affinity ligands directly inhibited SMAD1/5/8 signaling by low affinity ligands, while they activated their canonical SMAD2/3 pathways. Cross-inhibition was not restricted to low affinity ligands. High affinity ligands also inhibited other high affinity ligands. Significantly, cross-inhibition could be prevented

by blocking the Activin A-type II receptor interaction, but not by inhibiting the intracellular signal transduction pathway. These findings thus suggest cross-inhibition is due to competition for type II receptor binding. That ligands can act as antagonists has been suggested for BMP-3 (30-32), Activin A (33), GDF-5 (34) and Inhibin (35-37). We propose that ligand antagonism and signal transduction pathway switching is a general mechanism of TGF- β family regulation and an essential program during extraordinary cellular responses, such as wound healing (38). Cross-inhibition may also help explain how increased TGF- β family ligand expression can lead to pathophysiological responses, such as cancer cachexia (39, 40).

Materials and Methods

TGF- β family ligands

Human Activin B (Q53T31), GDF-8 (O08689), TGF- β 1 (P01137), TGF- β 2 (P61812), TGF- β 3 (P10600), Nodal (Q96S42), GDF-1 (NP_001483), BMP-2 (P12643), BMP-3 (P12645), BMP-4 (P12644), BMP-6 (P22004), BMP-7 (P18075), BMP-9 (Q9UK05), and BMP-10 (O95393) were obtained from R&D Systems or PROMOCCELL, Activin A (P08476) was produced in-house. NCBI-protein accession numbers are shown in parenthesis.

Receptor-Fc constructs

Synthetic genes of human ActRIIA (P27037) and ActRIIB (Q13705) fused to human IgG1-Fc genes were obtained from GeneArt. Human BMPRII (Q13873) and TGF β RII (P37173) were cloned from cDNA (Open Biosystems) and fused to IgG1-Fc by PCR. Receptor-Fc fusion constructs included signal peptide (SP) and extracellular domains (ECD) of human ActRIIA (amino acid 1-120), ActRIIB (amino acid 1-120), TGF β RII (amino acid 1-166), or BMPRII (amino acid 1-136). ECDs were linked at the C-terminus to human IgG1-Fc via a 22

amino acid long linker containing a TEV cleavage site. NCBI-protein accession numbers are shown in parenthesis.

Receptor-Fc purification

Proteins were expressed using CHO cells. Secreted receptor-Fc fusion proteins were captured from condition medium using Protein A affinity chromatography, eluted with 100 mM Glycine, pH 3.0, and directly neutralized by adding 10% v/v 2 M Tris-HCl pH 8.5. Purified proteins were either dialyzed directly into PBS, pH 7.5 and stored at -80 °C, or further purified by SEC in PBS, pH 7.5 and stored at -80 °C. Purity of receptor-Fc fusion proteins was determined by SDS-PAGE under reducing and non-reducing conditions.

Surface plasmon resonance

All experiments were performed using a Biacore 2000, and carried out at 25 °C using HBS-EPS (0.01 M HEPES, 0.5 M NaCl, 3 mM EDTA, 0.005% (v/v) Tween 20, pH 7.4) containing 0.1 % BSA as running buffer. Experimental flow rate was 50 µl/min. For receptor capture, anti-human IgG (Fc) antibody was immobilized on four channels of a CM5 chip using amine-coupling chemistry. 250 response units (RU) of purified ActRIIA-Fc, ActRIIB-Fc, BMPRII-Fc, or TGFβRII-Fc were loaded on the experimental flow channels. A reference channel was monitored to account for nonspecific binding, drift, and bulk shifts. For ligand binding studies, different ligands at a concentration of 80 nM were injected, including Activin A, Activin B, GDF-1, GDF-8, GDF-11, TGF-β1, TGF-β2, TGF-β3, BMP-2, BMP-3, BMP-4, BMP-6, BMP-7, BMP-9, BMP-10 and Nodal. After each binding cycle, the antibody surface was regenerated to base line by injecting MgCl₂. For binding competition studies, anti-BMP-7 monoclonal antibody (MAB3542, R&D Systems) was immobilized on two channels of a CM5 chip using amine-coupling chemistry. 300 response units (RU) of purified

BMP-7 were captured on the experimental flow channel. ActRIIA-Fc (12 nM) preincubated with different amounts of Activin A was injected. After each binding cycle, the antibody-BMP-7 surface was regenerated to base line by injecting $MgCl_2$.

Cell lines

A-204 rhabdomyosarcoma cells (HTB-82) and HepG2 hepatocellular carcinoma cells (HB-8065) were obtained from ATCC. Cells were maintained according to standard ATCC culture conditions. Briefly, A-204 cells were grown in McCoy's 5A medium supplemented with 10% FBS and 1% P/S. HepG2 cells were grown in Eagle's Minimum Essential Medium supplemented with 10% FBS and 1% P/S. Cells were grown at 37 °C under humidified, 5% CO₂ atmosphere. Freshly thawed cells were passaged at least three times before performing assays. A 40 µm cell strainer was used to obtain a uniform, single-cell suspension of HepG2 cells for plating.

Reporter assays

~ 50,000 A-204 or ~ 10,000 HepG2 cells in complete medium were seeded in each well of a 96-well plate and grown overnight. For transfection, solutions containing lipofectamine 2000, assay medium (serum free growth medium supplemented with 0.1% BSA), pGL4.74 [Luc2P/hRluc/TK] vector (control luciferase reporter plasmid, Promega) and SMAD3 responsive reporter plasmid pGL4.48 [luc2P/SBE] or SMAD1/5/8 responsive reporter plasmid pGL3 [luc2P/BRE] were prepared. Transfection medium was removed the following day, and medium was replaced with assay medium, which contained test proteins, including ligands (1-10 nM) and/or the receptor-Fc constructs (0-250 nM). Assay medium containing test proteins was incubated at 37 °C for 1 h before adding to cells. After addition of medium, A-204 cells were incubated for 6 h and HepG2 cells were incubated for 16 h at 37 °C,

luciferase activity was detected using a homemade dual-glow luciferase assay (41). Luminescence was determined using a FluoStar Omega plate reader. Relative luciferase units were calculated by dividing firefly luciferase units with renilla luciferase units. Data are expressed as mean of four independent measurements. Error bars correspond to SE of four independent measurements.

Immunoblotting

~ 8.0×10^4 HepG2 cells were plated in 12-well plates and grown to 80% confluence in complete medium, washed with 1X PBS, starved overnight in serum free medium supplemented with 0.1% BSA (assay medium) and grown for additional 16 h in assay medium with or without treatment. After 16 h incubation at 37 °C, protein lysate was prepared by using ice-cold RIPA lysis buffer (150 mM NaCl, 1% NP40, 0.1% SDS, 0.5% sodium deoxycholate, 50 mM Tris pH 8.0, 1X 'Recom Protease Arrest' protease inhibitor cocktail (G-Biosciences) and 2X 'Phosphatase Arrest' phosphatase inhibitor cocktail (G-Biosciences). Cell lysates were stored at -80 °C. Protein concentration of lysates was determined using Bradford. For Western blot, equal amounts of protein (10 μ g) were separated under reducing conditions on SDS-PAGE and transferred to Hybond-P membranes (GE Healthcare). Membranes were blocked with 5% BSA and incubated with primary antibodies from Cell Signaling at 1:1000 dilution, including anti-phospho-SMAD2 (138D4), anti-SMAD2 (D43B4), anti-phospho-SMAD1/5 (41D10), anti-SMAD4 (9515), and anti- β -Actin (8H10D10), followed by incubation with Horseradish peroxidase conjugated secondary antibody at 1:2000 dilution (7074). WesternBright ECL HRP substrate was used for detection (Advansta). Western blots were visualized by exposing the gel to autoradiography film.

Statistics

Reporter gene assays were performed in quadruplicates and were repeated two to three different times. Statistical analysis was done with GraphPad Prism 6. To determine statistical significance for induction experiments, one-way analysis of variance (ANOVA) and Dunnett's post hoc test were used. For inhibition experiments, two-way ANOVA and Tukey's post hoc test were used. P values < 0.05 were considered statistically significant. A bar marks statistically significant differences in Figure 2, horizontal lines between experimental pairs mark statistically significant differences in Figures 3-6. Light grey lines correspond to SMAD1/5/8 signaling experiments, dark grey lines correspond to SMAD2/3 signaling experiments.

Results

Type II receptors bind multiple ligands with high affinity

Most type II TGF- β receptors bind multiple ligands and many ligands bind multiple type II receptors. Because of this promiscuity, ligand-receptor interactions in the TGF- β family remain poorly defined. To characterize the ligand-binding specificity of the four major type II TGF- β receptors, ActRIIA, ActRIIB, BMPRII and TGF β RII, we used a high throughput, SPR-based binding assay (Fig. 5-1). We captured purified receptor-Fc fusion proteins on a Biacore sensor chip that was cross-linked with an anti-human Fc antibody and injected 16 different ligands at concentrations that exceeded physiological levels (80 nM) (42-44). As anticipated, ActRIIA-Fc and ActRIIB-Fc had similar ligand binding profiles (Fig. 5-1). Both receptors bound Activin A and Activin B with very high affinity as seen in the very fast association and very slow dissociation rates (Fig. 5-1A, B, red and cyan curves). Other ligands that bound both ActRIIA-Fc and ActRIIB-Fc with high affinity included GDF-

8, GDF-11, BMP-6, and BMP-10 (Fig. 5-1 A, B, green, blue, magenta, and maroon curves). However, either their association rates were slower or their dissociation rates were faster than those seen for Activin A or Activin B, resulting overall in a weaker interaction. Important specificity differences between these two highly homologous receptors were seen with BMP-7 and BMP-9, which bound ActRIIA-Fc and ActRIIB-Fc, respectively, with relatively high affinity.

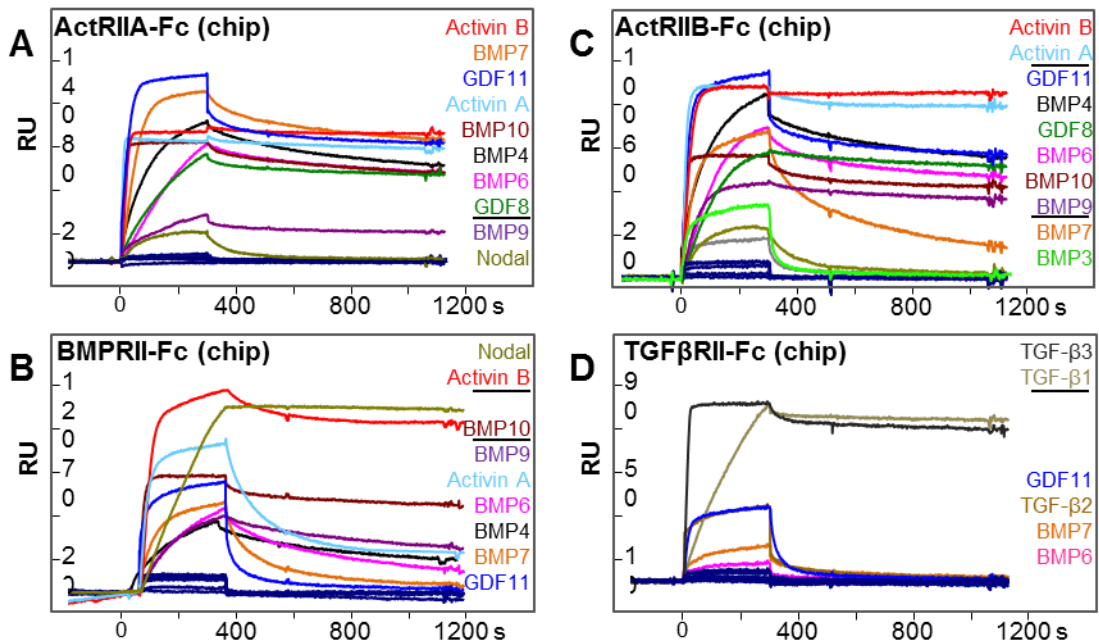


Figure 5-1. Type II receptors bind a range of TGF- β family ligands with high affinity.

250 response units (RU) of protein-A purified (A) ActRIIA-Fc, (B) ActRIIB-Fc, (C) BMPRII-Fc, and (D) TGF β RII-Fc were captured on an SPR sensor chip, and ligands at 80 nM concentration were injected, including Activin A, Activin B, GDF-1, GDF-8, GDF-11, TGF- β 1, TGF- β 2, TGF- β 3, BMP-2, BMP-3, BMP-4, BMP-6, BMP-7, BMP-9, BMP-10, and Nodal. Ligands that bound receptors as determined by a measurable SPR response are shown in relevant panels. Color of binding curve and ligand name are matched. Curves of ligands that did not bind are colored dark blue, their names are not shown.

Table 5-1. Ligand binding to ActRIIA-Fc, single injection

Ligand	k_a ($M^{-1}s^{-1}$),	k_d (s^{-1})	K_d (M)
Activin A	$2.29e^{+6}$	$9.93e^{-5}$	$4.33e^{-11}$
Activin B	$8.42e^{+5}$	$5.16e^{-5}$	$6.13e^{-11}$
BMP-10	$8.02e^{+5}$	$3.06e^{-4}$	$3.81e^{-10}$
GDF-11	$4.15e^{+5}$	$2.38e^{-4}$	$5.73e^{-10}$
BMP-7	$2.23e^{+5}$	$3.53e^{-4}$	$1.59e^{-9}$
BMP-4	$1.17e^{+5}$	$4.11e^{-4}$	$3.51e^{-9}$
GDF-8	$4.84e^{+4}$	$1.82e^{-4}$	$3.77e^{-9}$
BMP-6	$3.21e^{+4}$	$3.37e^{-4}$	$1.05e^{-8}$

Table 5-2. Ligand binding to ActRIIB-Fc, single injection

Ligand	k_a ($M^{-1}s^{-1}$),	k_d (s^{-1})	K_d (M)
Activin B	$4.09e^{+5}$	$2.11e^{-6}$	$5.16e^{-12}$
Activin A	$1.13e^{+6}$	$6.84e^{-5}$	$6.05e^{-11}$
BMP-10	$1.37e^{+6}$	$2.28e^{-4}$	$1.67e^{-10}$
GDF-11	$4.48e^{+5}$	$2.75e^{-4}$	$6.13e^{-10}$
BMP-9	$2.42e^{+5}$	$2.13e^{-4}$	$8.81e^{-10}$
GDF-8	$9.94e^{+5}$	$1.60e^{-4}$	$1.61e^{-9}$
BMP-6	$7.93e^{+4}$	$4.10e^{-4}$	$5.17e^{-9}$
BMP-7	$2.02e^{+5}$	$1.87e^{-3}$	$9.26e^{-9}$

Table 5-3. Ligand binding to BMPRII-Fc, single injection

Ligand	k_a ($M^{-1}s^{-1}$),	k_d (s^{-1})	K_d (M)
BMP-10	$9.13e^{+5}$	$2.10e^{-4}$	$2.30e^{-10}$
Activin B	$3.10e^{+5}$	$1.84e^{-4}$	$5.98e^{-10}$
Nodal	$2.54e^{+4}$	$2.02e^{-5}$	$7.96e^{-10}$
BMP-9	$8.54e^{+4}$	$6.36e^{-4}$	$7.44e^{-9}$
Activin A	$3.10e^{+5}$	$2.79e^{-3}$	$8.96e^{-9}$
BMP-7	$1.05e^{+5}$	$4.08e^{-3}$	$3.90e^{-8}$
BMP-6	$3.68e^{+4}$	$1.64e^{-3}$	$4.45e^{-8}$
GDF-11	$1.35e^{+5}$	$7.18e^{-3}$	$5.33e^{-8}$

Table 5-4. Ligand binding to TGF β RII-Fc, single injection

Ligand	k_a ($M^{-1}s^{-1}$),	k_d (s^{-1})	K_d (M)
TGF- β 3	$1.12e^{+6}$	$1.02e^{-4}$	$9.10e^{-11}$
TGF- β 1	$3.83e^{+4}$	$5.61e^{-5}$	$1.49e^{-9}$

TGF β RII and BMPRII had very distinctive binding profiles. TGF β RII only bound TGF- β 1 and TGF- β 3 with very high affinity, but not TGF- β 2 (Fig. 5-1D, light and dark gray curves) (45, 46). The BMPRII ligand profile was unexpected, as we found it also has high affinity ligands, namely Nodal, Activin B and, to a lesser degree, BMP-10 (Fig. 5-1C, olive green, red, and maroon curves). BMP-9, Activin A, and BMP-6 also associate with BMPRII, but these complexes are much weaker. Notably, some ligands, including GDF-1, BMP-2, BMP-3, and TGF- β 2, did not bind any one of these type II receptors with high affinity. We estimated K_d values based on single injections (Table 5-1, 2, 3, 4). These are comparable to published K_d values determined from multiple injections (9, 16, 45, 46).

Ligands have distinctive, cell-line specific signaling profiles

TGF- β family ligands activate intracellular SMAD signal transduction pathways. Type I receptors determine which SMAD pathway is activated. It is suggested SMAD2/3 pathways are activated by the type I receptors ALK4, ALK5 and ALK7, while SMAD1/5/8 pathways are activated by ALK1, ALK2, ALK3, and ALK6 (47). To characterize the signaling activities of the tested ligands, we used a luciferase reporter gene assay and two different cell lines of human origin, A-204 rhabdomyosarcoma and HepG2 hepatocellular carcinoma cells (Fig. 5-2). Both cell lines expressed the principal TGF- β family receptors (Fig. 5-2A, R2: Genomics Analysis and Visualization Platform (<http://r2.amc.nl>, dataset id GSK950). Cells were transfected with control plasmid pGL4.74 [hRluc] and the SMAD3 responsive reporter plasmid pGL4.48 [luc2P/SBE] or the SMAD1/5/8 responsive reporter plasmid pGL3 [luc2P/BRE] (48, 49). Transfected cells were treated with 1 or 10 nM ligand.

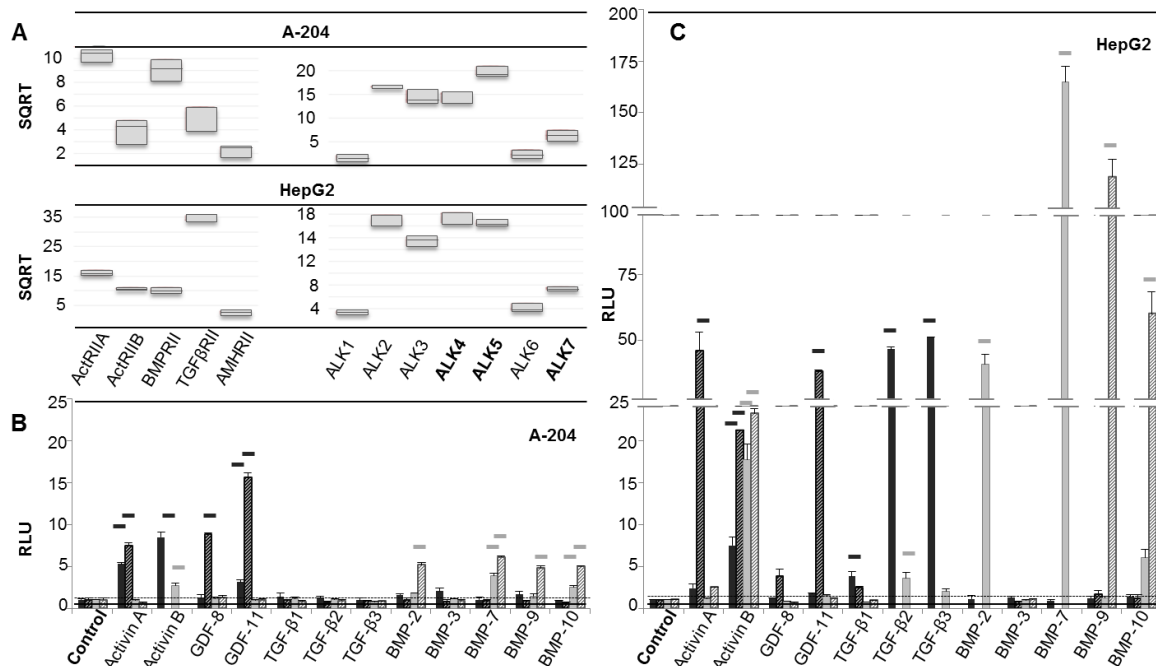


Figure 5-2. TGF-β family signaling activity is cell line dependent.

(A) Microarray data show expression levels of TGF-β family receptors in A-204 rhabdomyosarcoma and HepG2 hepatocellular carcinoma cells (Genomics Analysis and Visualization Platform (<http://r2.amc.nl>), dataset id GSK950). The left panel shows expression of type II receptors, the right panel shows expression of type I receptors. Normalized data is displayed as SQRT transformation. Ligand signaling in (B) A-204 and (C) HepG2 cells. Cells were transfected with control plasmid and SMAD2/3 or SMAD1/5/8 responsive reporter plasmids. Dark grey bars and striped dark grey bars correspond to SMAD2/3 mediated reporter gene expression induced with 1 nM ligand and 10 nM ligand, respectively, light grey bars and striped light grey bars correspond to SMAD1/5/8 mediated reporter gene expression induced with 1 nM and 10 nM ligand, respectively. Relative Luciferase Units (RLU) were calculated as the ratio of luminescence from the experimental reporter to luminescence from the control reporter. Horizontal bars denote statistically significant differences in luciferase activity relative to the ‘no-ligand’ control ($p \leq 0.05$). The base line of the ‘no-ligand’ control is marked by the dotted line.

A-204 cells responded to Activin A, Activin B, GDF-8 and GDF-11, inducing a strong SMAD2/3 mediated response (Fig. 5-2B). By contrast, TGF-βs and BMPs did not induce luciferase gene expression in this cell line. Strikingly, HepG2 cells showed a completely different behavior. Both TGF-βs and BMPs induced a very strong luciferase

signal (Fig. 5-2C). Among BMPs that signal via the type I receptor kinases ALK2, ALK3 or ALK6, BMP-7 mediated SMAD1/5/8 signaling was strongest (165-fold over background) and BMP-2 signaling was weaker (40-fold over background). BMP-3 did not elicit a meaningful luciferase signal (Fig. 5-2B, C). Among BMPs that signal via ALK1, 1 nM BMP-10 elicited a small SMAD1/5/8 signal (6-fold over background), whereas BMP-9 required a 10 nM concentration. However, at this concentration, the BMP-9 signal was very strong (160-fold over background). Both TGF- β 2 and TGF- β 3 induced a strong SMAD2/3 mediated signal at 1 nM concentration. This signal was one order of magnitude greater than the response to TGF- β 1 (Fig. 5-2C, approximately 4-fold over background for TGF- β 1 compared with 45- and 50- fold over background for TGF- β 2 and TGF- β 3, respectively). Intriguingly, TGF- β 2 induced a statistically significant SMAD1/5/8 mediated luciferase signal. This is consistent with previous findings that TGF- β ligands (i.e. TGF- β 1, - β 2 and/or - β 3) can activate SMAD1/5/8 via ALK5 and/or ALK2/ALK3 (50-52). Differences in TGF- β isoform signaling activities may result from differences in type II receptor binding affinities or co-receptor expression.

Responses to Activin A, Activin B, GDF-8 and GDF-11 diverged in HepG2 cells. The SMAD2/3 mediated Activin B response remained constant in both A-204 and HepG2 cells (8-fold over background at 1 nM Activin B). In contrast to A-204 cells, the Activin A response in HepG2 cells was smaller at 1 nM concentration, but could be induced strongly at 10 nM concentration (Fig. 5-2B, C). Interestingly, GDF-8 signaling was reduced relative to A-204 cells, whereas GDF-11 signaling increased significantly (from 16-fold over background in A-204 cells to approximately 40-fold over background in HepG2 cells) (Fig. 5-2B, C). Notably, 1 nM Activin B induced a strong SMAD1/5/8 mediated response in

HepG2 cells, which exceeded the canonical SMAD2/3 response (Fig. 5-2C, 18-fold compared with 8-fold over background).

To explain the differences in signaling, we analyzed expression of TGF- β family components in both cell lines (Fig. 5-2A, <http://r2.amc.nl>, dataset id GSK950). Levels of ActRIIB and TGF β RII are low in A-204 cells. By contrast, HepG2 cells express type II receptors at much higher levels. Notably, TGF β RII expression is so high in HepG2 cells that they rank in the top 8 percentile of 470 cell lines when comparing TGF β RII levels (dataset id gse57083). We suggest differences in ActRIIB and TGF β RII expression could account for significant differences in signaling. But HepG2 cells also express high levels of betaglycan, which helps increase cellular sensitivity to BMPs (53) and enhance responsiveness to TGF- β s (54). We speculate betaglycan could contribute significantly to the divergent signaling activities.

Activin A antagonizes BMP-2 and BMP-7 signaling

As BMPs, GDFs and Activins utilize the same type II receptors for signaling and bind these receptors at the same site (27), we hypothesized high affinity ligands like Activin A could directly inhibit low affinity ligand signaling. To test this hypothesis we first determined by titration the limits of Activin A signaling in HepG2 cells (Fig. 5-3A). The greatest increase in Activin A signaling occurred between 0 and 5 nM concentrations. Beyond that, signaling reached a plateau. Even a 10-fold higher concentration of Activin A (50 nM) did not increase the SMAD2/3 luciferase signal further (Fig. 5-3A). To evaluate cross-inhibition, we incubated Activin A with BMP-2 or BMP-7. Activin A strongly inhibited BMP-2 and BMP-7 mediated SMAD1/5/8 signaling (Fig. 5-3B, C). At a 5-fold excess, Activin A reduced the SMAD1/5/8 signal approximately 7-fold for BMP-2 and 10-fold for BMP-7. Even at

equimolar concentrations, Activin A attenuated the BMP-2 and BMP-7 mediated SMAD1/5/8 responses 4-fold. Notably, Activin A also activated its canonical SMAD2/3 signaling pathway. The SMAD2/3 signal was the same, whether BMP-2 or BMP-7 were present or not (Fig. 5-3A-C). Yet a small, statistically significant residual SMAD1/5/8 signaling activity remained for both BMP-2 and BMP-7 at the highest Activin A concentrations tested (Fig. 5-3B, C).

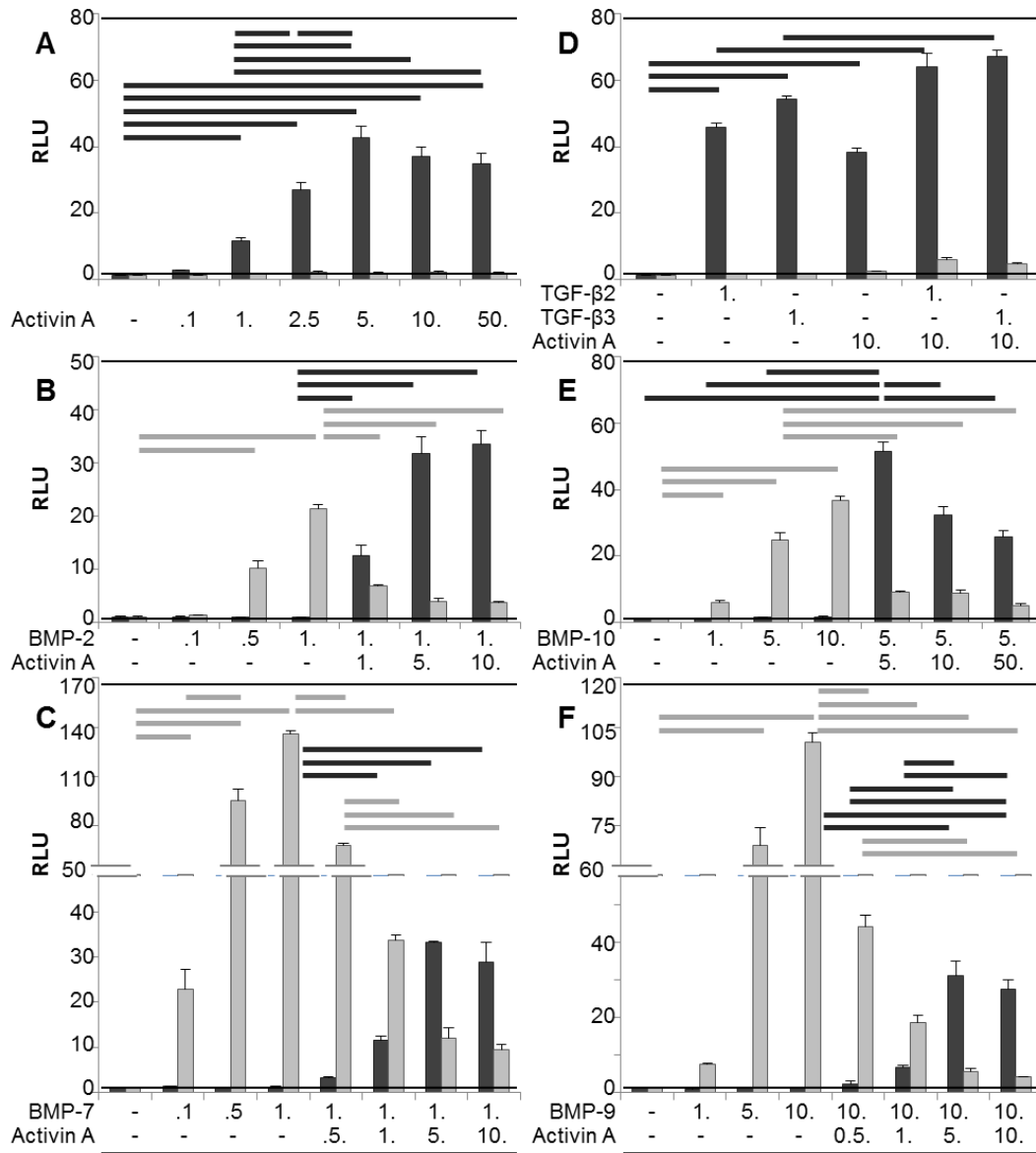


Figure 5-3. Activin A antagonizes BMP signaling.

HepG2 were transfected with control plasmid and SMAD2/3 or SMAD1/5/8 responsive reporter plasmids and treated with various ligands. **(A)** HepG2 cells were treated with 0.1, 1.0, 2.5, 5.0, 10.0, and 50.0 nM Activin A. **(B)** HepG2 cells were treated with 0.1, 0.5, and 1 nM BMP-2. Signaling induced with 1 nM BMP-2 was then inhibited with 1.0, 5.0, and 10.0 nM Activin A. **(C)** HepG2 cells were treated with 0.1, 0.5, and 1 nM BMP-7. Signaling induced with 1 nM BMP-7 was then inhibited with 0.5, 1.0, 5.0, and 10.0 nM Activin A. **(D)** HepG2 cells were treated with 1.0 nM TGF- β 2, 1.0 nM TGF- β 3, and/or 10 nM Activin A. **(E)** HepG2 cells were treated with 1.0, 5.0, and 10.0 nM BMP-10. Signaling induced with 5.0 nM BMP-10 was then inhibited with 5.0, 10.0, and 50.0 nM Activin A. **(F)** HepG2 cells were treated with 1.0, 5.0, and 10.0 nM BMP-9. Signaling induced with 10.0 nM BMP-9 was then inhibited with 0.5, 1.0, 5.0, and 10.0 nM Activin A. Dark grey bars correspond to SMAD2/3

Figure 5-3 (cont'd)

mediated reporter gene expression and light grey bars correspond to SMAD1/5/8 mediated reporter gene expression. Relative Luciferase Units (RLU) were calculated as the ratio of luminescence from the experimental reporter to luminescence from the control reporter. Horizontal light grey lines indicate statistically significant differences in SMAD1/5/8 signaling and horizontal dark grey lines indicate statistically significant differences in SMAD2/3 signaling ($p \leq 0.05$) between relevant experimental pairs.

We performed a similar inhibition experiment with TGF- β 2 or TGF- β 3 (Fig. 5-3D). Activin A did not inhibit the SMAD2/3 mediated TGF- β 2 and TGF- β 3 signals, as expected. Instead, the activities of Activin A and TGF- β 2 or TGF- β 3 were additive (Fig. 5-3D). We also examined if Activin A could inhibit ligands that bind the same type II receptors with high affinity, including BMP-9 and BMP-10 (Fig. 5-3E, F). As we show for BMP-2 and BMP-7, Activin A antagonized signaling by these two ligands, reducing their peak response approximately 2.5-fold for BMP-10 and 25-fold for BMP-9 at equimolar concentrations. Higher concentrations of Activin A further reduced BMP-9 and BMP-10 signaling, but a small SMAD1/5/8 signal remained.

BMP-2 and BMP-7 signaling is antagonized by high affinity ligands

To demonstrate ligand antagonism is not specific to Activin A, we examined BMP-2 and BMP-7 inhibition by other high affinity ligands, including Activin B, GDF-8, GDF-11, BMP-9 and BMP-10 (Fig. 5-4). These ligands also bind ActRIIA-Fc, ActRIIB-Fc and/or BMPRII-Fc to varying degrees: Activin B binds all three receptors, BMP-9 predominantly binds ActRIIB, GDF-8 and GDF-11 bind ActRIIA and ActRIIB, but not BMPRII (Fig. 5-1). Using HepG2 cells and 10 nM ligand concentrations, we confirmed GDF-8 and GDF-11 exclusively signaled via SMAD2/3. Notably, the GDF-11 signal was approximately 10 times greater than the GDF-8 signal (28.9 RLU vs. 3.0 RLU) (Fig. 5-4A). Activin B induced both

SMAD2/3 and SMAD1/5/8 pathways more or less equivalently (18.9 RLU vs. 22.2 RLU) (Fig. 5-4A). BMP-9 and BMP-10 exclusively induced SMAD1/5/8 signaling (Fig. 5-4B).

GDF-8 reduced the BMP-2 signal approximately 2-fold (from 24.7 to 11.5 RLU for BMP-2 and from 145.6 to 70.1 RLU for BMP-7). GDF-11 was more effective and reduced the SMAD1/5/8 signal approximately 4- to 6-fold (from 24.7 to 6.6 RLU for BMP-2 and from 145.6 to 24.4 RLU for BMP-7) (Fig. 5-4A). However, neither ligand inhibited signaling as powerfully as Activin A. The behavior of Activin B was more complex, as it also induced SMAD1/5/8 signaling in HepG2 cells (Fig. 5-4A). The SMAD1/5/8 response was similar whether cells were treated with BMP-2 alone or whether cells were treated with BMP-2 and Activin B. The effect of Activin B on BMP-7 signaling was clearer Activin B reduced the BMP-7 mediated SMAD1/5/8 signal approximately 6-fold (from 145.6 to 27.7 RLU). Notably, the SMAD1/5/8 signal intensity obtained with Activin B alone was virtually the same whether BMP-2 or BMP-7 were present (22.7, 27.7 and 22.2 RLU, respectively). We propose the residual SMAD1/5/8 activity is due to Activin B. In conclusion, GDF-8, GDF-11 and Activin B antagonize BMP-2 and BMP-7 signaling, although they inhibit less effectively than Activin A.

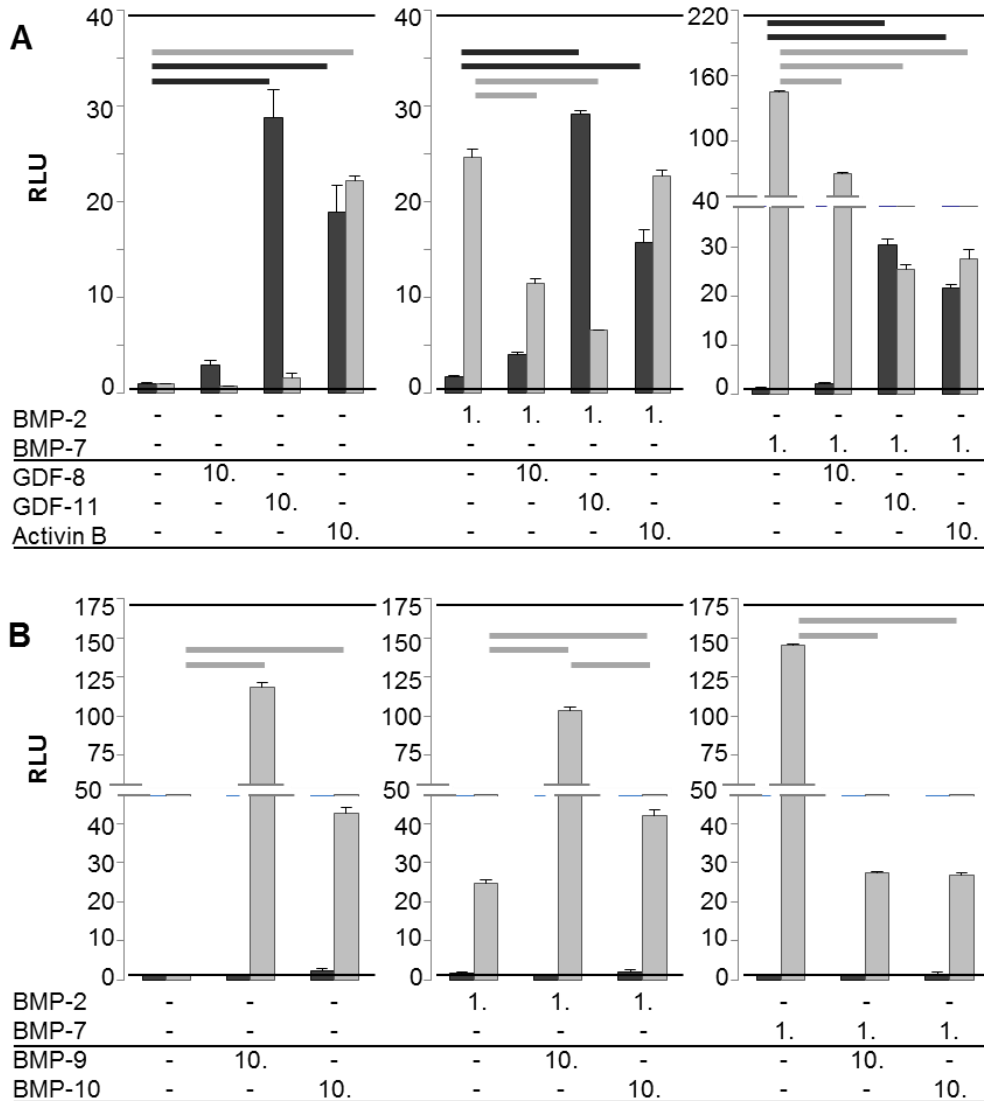


Figure 5-4. Antagonism of low affinity BMP-2 and BMP-7 signaling is common.

Inhibition of BMP-2 and BMP-7 signaling with (A) GDF-8, GDF-11 and Activin B, or (B) BMP-9 and BMP-10. HepG2 were transfected with control plasmid and SMAD2/3 or SMAD1/5/8 responsive reporter plasmids. 1 nM BMP-2 or BMP-7 were added to induce signaling, 10 nM GDF-8, GDF-11, Activin B, BMP-9 or BMP-10 were added for inhibition. Dark grey bars correspond to SMAD2/3 mediated reporter gene expression and light grey bars correspond to SMAD1/5/8 mediated reporter gene expression. Relative Luciferase Units (RLU) were calculated as the ratio of luminescence from the experimental reporter to luminescence from the control reporter. Horizontal light grey lines indicate statistically significant differences in SMAD1/5/8 signaling and horizontal dark grey lines indicate statistically significant differences in SMAD2/3 signaling ($p \leq 0.05$) between relevant experimental pairs.

The behavior of BMP-9 and BMP-10 was intriguing. Their ability to induce a response was nearly indistinguishable whether BMP-2 was present or not (118.7 vs 103.5 RLU for BMP-9 \pm BMP-2 and 42.5 vs 42.2 RLU for BMP-10 \pm BMP-2) (Fig. 5-4B). By contrast, both attenuated a BMP-7 mediated SMAD1/5/8 response. Significantly, the response converged (from 145.6 to 27.3 RLU for BMP-9 and from 145.6 to 26.7 RLU for BMP-10) (Fig. 5-4B). We speculate BMP-9 and BMP-10 override BMP-2 signaling, but remain in a competitive equilibrium with BMP-7 that leads to an attenuated, but defined response.

ActRIIA-Fc and Follistatin, but not SB-431542, inhibit Activin A antagonism

To demonstrate that cross-inhibition is due to ligand-receptor binding-competition, we examined how the extracellular inhibitors ActRIIA-Fc, Follistatin, and the intracellular kinase inhibitor SB-431542 affected Activin A antagonism (Fig. 5-5, 6, 7). We hypothesized ActRIIA-Fc and Follistatin would block Activin A antagonism, as both prevent binding of Activin A to type II receptors and preclude Activin A from competing with BMP-2 or BMP-7 (55). By contrast, SB-431542 would not prevent Activin A antagonism (56, 57), as Activin A would still bind type II receptors and compete with BMP-2 and BMP-7 for type II receptor binding. To test this model, we examined BMP-7 mediated reporter gene expression in A-204 and HepG2 cells (Fig. 5-5A, B), BMP-2 mediated reporter gene expression in HepG2 cells (Fig. 5-6A), and BMP-2 mediated SMAD phosphorylation in HepG2 cells (Fig. 5-6B).

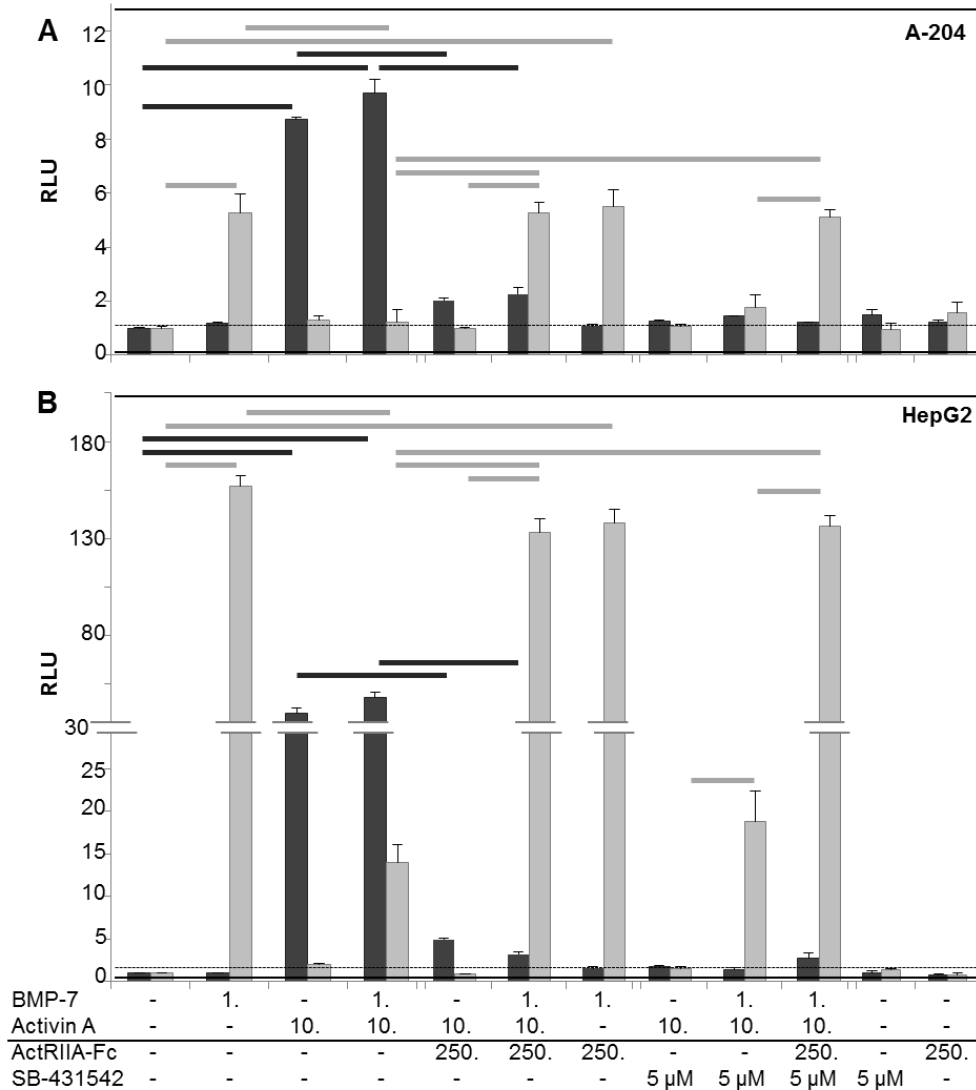


Figure 5-5. The extracellular Activin A signaling inhibitor ActRIIA-Fc rescues BMP-7 activity.

Luciferase reporter gene expression was induced with BMP-7 in (A) A-204, and (B) HepG2 cells transfected with SMAD2/3 or SMAD1/5/8 responsive reporter plasmids. 1 nM BMP-7 was added to induce signaling, 10 nM Activin A was added to antagonize BMP-7 signaling. 250 nM ActRIIA-Fc was used to block binding of Activin A to type II receptors, 5 μM SB-431542 was added to block Activin A mediated kinase activation and SMAD2/3 phosphorylation. Dark grey bars correspond to SMAD2/3 mediated reporter gene expression and light grey bars correspond to SMAD1/5/8 mediated reporter gene expression. Horizontal light grey lines indicate statistically significant differences in SMAD1/5/8 signaling and horizontal dark grey lines indicate statistically significant differences in SMAD2/3 signaling ($p \leq 0.05$) between relevant experimental pairs.

ActRIIA-Fc inhibited SMAD2/3 mediated Activin A signaling, but not SMAD1/5/8 mediated BMP-2 or BMP-7 signaling (Fig. 5-5A, B, 6A). Significantly, Activin A strongly inhibited BMP-7 and BMP-2 signaling when alone, but not when ActRIIA-Fc was also present. (Fig. 5-5A, B, 6A) Likewise, Follistatin inhibited SMAD2/3 mediated Activin A signaling and rescued BMP-7 signaling in the presence Activin A (Fig. 5-7A). But Follistatin also inhibited BMP-7 signaling at high concentrations (58, 59). In sharp contrast to ActRIIA-Fc and Follistatin, SB-431542 did not prevent Activin A antagonism. Activin A reduced BMP-7 and BMP-2 signaling equally whether SB-431542 was added or not (Fig. 5-5A, B, 6A). Importantly, these findings were paralleled by SMAD phosphorylation (Fig. 5-6B), indicating that the response measured by reporter gene expression is directly linked to SMAD mediated signal transduction pathways. Thus, our findings show inhibition of BMP-7 and BMP-2 signaling by Activin A can be rescued by trapping Activin A with ActRIIA-Fc or Follistatin and preventing Activin A-receptor binding. But suppressing signal transduction pathway activation with intracellular kinase inhibitors does not block the Activin A antagonist activity.

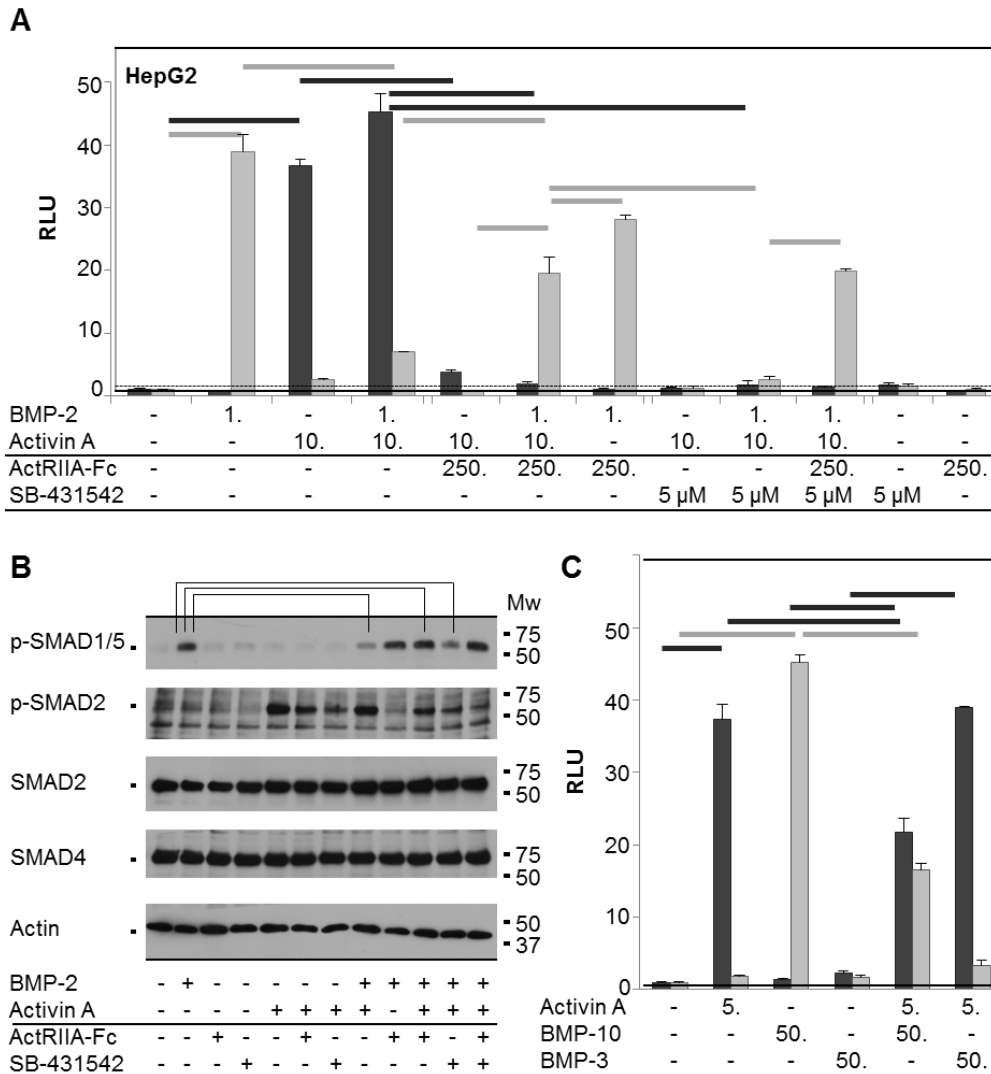


Figure 5-6. Activin A role in BMP-2 signal transduction and inhibition with BMP-10.

(A) Luciferase reporter gene expression was induced with BMP-2 in HepG2 cells transfected with SMAD2/3 or SMAD1/5/8 responsive reporter plasmids. 1 nM BMP-2 was added to induce signaling, 10 nM Activin A was added to antagonize BMP-2 signaling. 250 nM ActRIIA-Fc was used to block binding of Activin A to type II receptors, 5 μ M SB-431542 was added to block Activin A mediated kinase activation and SMAD2/3 phosphorylation. Dark grey bars correspond to SMAD2/3 mediated reporter gene expression and light grey bars correspond to SMAD1/5/8 mediated reporter gene expression. (B) Western blots showing BMP-2 and Activin A mediated SMAD phosphorylation in HepG2 cells. 1 nM BMP-2 was added to induce SMAD1/5/8 phosphorylation, 10 nM Activin A was added to antagonize BMP-2 mediated SMAD1/5/8 phosphorylation, 250 nM ActRIIA-Fc was used to block binding of Activin A to type II receptors, 5 μ M SB-431542 was added to block Activin A mediated kinase activation and SMAD2/3 phosphorylation. (C) HepG2 cells were transfected with SMAD2/3 or SMAD1/5/8 responsive reporter plasmids. 5 nM Activin A was

Figure 5-6 (cont'd)

added to induce signaling, 50 nM BMP-10 or BMP-3 were added to inhibit Activin A mediated SMAD2/3 reporter gene expression. Dark grey bars correspond to SMAD2/3 mediated reporter gene expression. Light grey bars correspond to SMAD1/5/8 mediated reporter gene expression. Horizontal light grey lines indicate statistically significant differences in SMAD1/5/8 signaling and horizontal dark grey lines indicate statistically significant differences in SMAD2/3 signaling ($p \leq 0.05$) between relevant experimental pairs.

Activin A inhibits BMP-7 – ActRIIA binding

To demonstrate directly that Activin A inhibits binding of BMP-7 to type II receptors, we developed a competition SPR binding assay (Fig. 5-7B). We captured BMP-7 on the sensor chip using a cross-linked, BMP-7 specific monoclonal antibody and we flowed ActRIIA-Fc preincubated with different concentrations of Activin A. ActRIIA-Fc (12 nM) bound captured BMP-7 with an association rate that was nearly the same as that determined using our standard setup (data not shown). ActRIIA-Fc binding to BMP-7 decreased with increasing Activin A concentrations and a 4-fold molar excess of Activin A (48 nM) completely inhibited the ActRIIA-Fc – BMP-7 interaction. Thus, Activin A can function as competitive inhibitor of BMP-7 binding to ActRIIA.

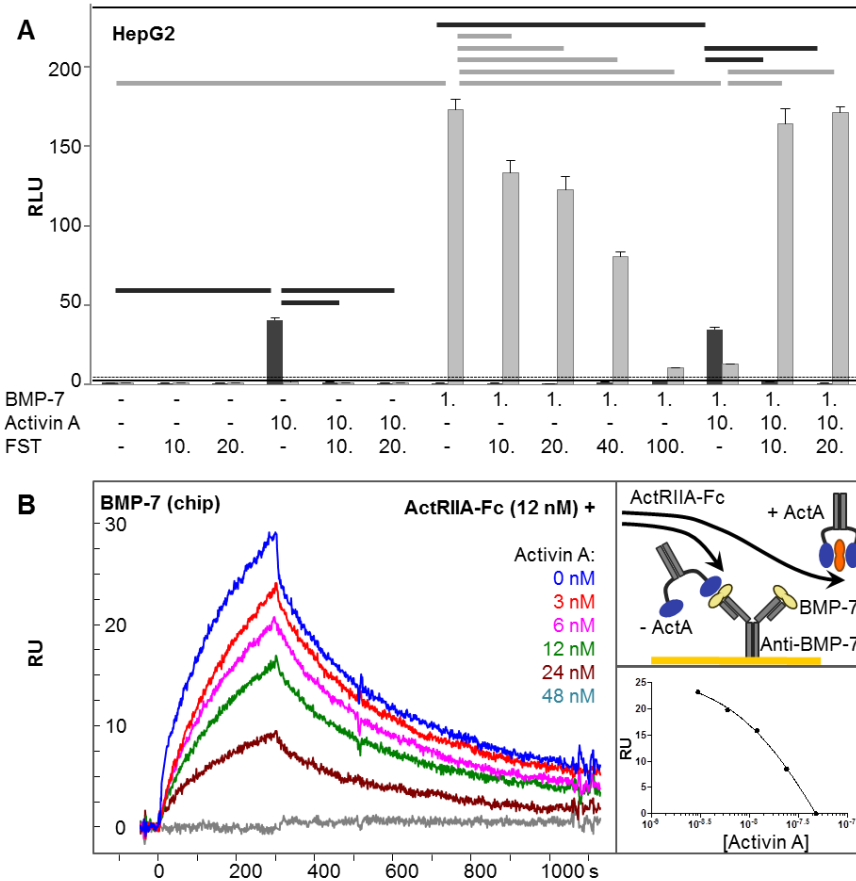


Figure 5-7. Follistatin suppresses Activin A antagonism.

(A) Luciferase reporter gene expression was induced with BMP-7 in HepG2 cells transfected with SMAD2/3 or SMAD1/5/8 responsive reporter plasmids. Follistatin inhibited BMP-7 signaling at high concentrations (40 and 100 nM), but less at lower concentrations (10 and 20 nM). Activin A (10 nM) effectively inhibited BMP-7 signaling. Follistatin (10-20 nM) inhibited Activin A signaling and prevented antagonism of BMP-7. Dark grey bars correspond to SMAD2/3 mediated reporter gene expression and light grey bars correspond to SMAD1/5/8 mediated reporter gene expression. Horizontal light grey lines indicate statistically significant differences in SMAD1/5/8 signaling and horizontal dark grey lines indicate statistically significant differences in SMAD2/3 signaling ($p \leq 0.05$) between relevant experimental pairs. (B) Activin A inhibits binding of ActRIIA-Fc to BMP-7. BMP-7 was captured on the SPR sensor chip using an anti-BMP-7 monoclonal antibody (top right panel). 12 nM ActRIIA-Fc preincubated with 0 nM (blue), 3 nM (red), 6 nM (magenta), 12 nM (green), 24 nM (maroon), 48 nM (grey) Activin A was injected over the sensor chip. Activin A prevented binding of ActRIIA-Fc to BMP-7 in a concentration dependent manner. The bottom right panel shows a dose response curve. RU values were taken at 290 seconds after starting injection of ActRIIA-Fc.

BMP-10 is a weak Activin A antagonist

As the antagonist activity of TGF- β family ligands was not limited to Activin A (Fig. 5-3), we hypothesized some ligands may antagonize Activin A signaling. Previous studies have indicated BMP-3 inhibits Activin A signaling (30-32), and we speculated BMP-10 could potentially antagonize Activin A as it is a high affinity ligand of the three type II Activin A receptors (Fig. 5-1). To test this hypothesis, we examined Activin A mediated reporter gene expression in HepG2 cells and antagonism by BMP-3 and BMP-10 (Fig. 5-6C). Notably, 50 nM BMP-3 did not inhibit signaling by 5 nM Activin A, even after we tested three different BMP-3 samples. On the other hand, a 10-fold excess of BMP-10 reduced the Activin A mediated SMAD2/3 signal about 2-fold (from 37.4 to 21.7 RLU), while Activin A attenuated the BMP-10 mediated SMAD1/5/8 response as expected (from 45.3 to 16.6 RLU). Although BMP-10 antagonism was not as potent as Activin A antagonism, this finding shows Activin A signaling could also be inhibited by some TGF- β family ligands.

Discussion

Our goal was to test the hypothesis that TGF- β family ligands can function as signaling antagonists by competing for type II receptor binding. We showed several TGF- β family ligands directly inhibited signaling by other members of the family. The antagonist activity could be suppressed by blocking the type II receptor binding-site on antagonistic ligands, but not by inhibiting their signal transduction cascade. Moreover, we demonstrated ligand antagonism is mediated by direct competition for receptor binding. We propose ligand antagonism is a common mechanism that can be used to modulate TGF- β family signaling. We speculate the precise combination of ligands available to a cell or tissue will profoundly affects how they read a particular TGF- β family signal (60).

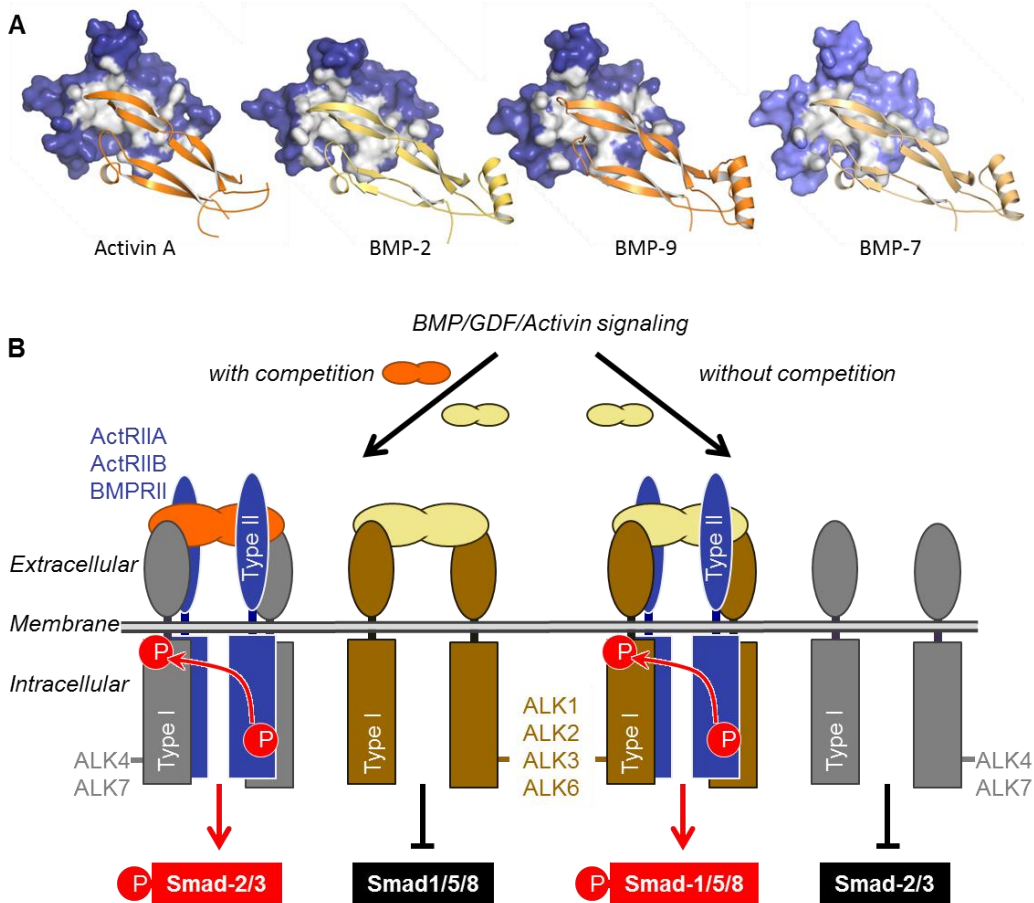


Figure 5-8. Model of ligand antagonism.

(A) Molecular structures of Activin A, BMP-2, BMP-9 and BMP-7 in complex with type II receptors ActRIIA or ActRIIB, based on PDB coordinates 1NYU (74), 2H62 (7), 4FAO (9), and 1LX5 (26) displayed in corresponding orientations. Ligands are shown as orange ribbon diagrams. Type II receptors are shown as molecular surface colored blue with surface atoms that contact ligands colored grey. The ligand binding-site on the type II receptors ActRIIA and ActRIIB is highly conserved (grey surface area). (B) Signaling in the TGF- β family is induced when dimeric ligands (orange/khaki ovals) bind the extracellular domains of type I Activin receptor-like kinases (grey/brown) and type II receptors (blue). Formation of the hexameric ligand-receptor complex leads to phosphorylation of SMAD transcription factors. Ligands that bind type II receptors with high affinity (orange) out-compete ligands that bind type II receptors with lower affinity (khaki) and block low affinity ligand signaling. For example, low affinity ligands, like BMP-2 and BMP-7, induce SMAD1/5/8 phosphorylation via type I receptors ALK2, ALK3, or ALK6 (brown). High affinity ligands like Activin A block BMP-2 and BMP-7 binding to type II receptors, blocking SMAD1/5/8 phosphorylation whilst activating their canonical signaling pathways, i.e. SMAD2/3 phosphorylation via type I receptors ALK4, and ALK7 (grey). Low affinity ligands therefore likely signal only in the absence of high affinity ligands, or when type II receptors are expressed at such high levels that ligand competition is not possible.

An enduring conundrum in the TGF- β field is the promiscuity of its ligand-receptor pairings. This promiscuity is particularly relevant to the ‘Activin receptors’ ActRIIA, ActRIIB, and the ‘BMP receptor’ BMPRII. They interact with a large group of overlapping ligands, including Activins, BMPs, GDFs and Nodal. As these ligands bind receptors at a common site (Fig. 5-8A), we hypothesized that ligands can compete for receptor binding and high affinity ligands can suppress low affinity ligand signaling (Fig. 5-8B). We show the high affinity ligand Activin A effectively inhibited signaling by the low affinity ligand BMP-2, the medium affinity ligand BMP-7 and the high affinity ligands BMP-9 and BMP-10 (Fig. 5-3, 5, 6, 7). The ability to inhibit signaling was not specific to Activin A. GDF-8, GDF-11, BMP-9, BMP-10, and Activin B also inhibited BMP-2 and BMP-7 signaling. However, Activin A was the most powerful BMP-2 and BMP-7 antagonist. Notably, BMP-10 antagonized Activin A signaling with some efficacy. The pervasiveness of competition and antagonism between ligands suggests they are a key feature of the TGF- β family. But they depend on shared receptor utilization, as TGF- β 1 cannot inhibit BMP-6 or BMP-9 signaling (33). We speculate competition and antagonism could play an important role in the biological activities of ligands that are involved in acute biological responses, such as injury, infection, and inflammation (61-63). Thus, by acting as antagonist, Activin A secreted in wound healing could shift the signaling equilibrium from a state that supports tissue homeostasis to a state that leads to regeneration (64-66). Importantly, while Activin A suppressed BMP-2 and BMP-7 mediated SMAD1/5/8 signaling, it also activated its canonical SMAD2/3 signaling pathway, causing a switch in signal transduction pathway utilization.

ActRIIA-Fc, Follistatin and SB-431542 are potent Activin A signaling inhibitors with distinct modes of action. ActRIIA-Fc binds Activin A and shields its type II receptor binding-

site (26). Follistatin binds Activin A and blocks both type I and type II receptor binding-sites (67). SB-431542 inhibits type I receptor kinase activity (57). Activin A trapped by ActRIIA-Fc or Follistatin cannot bind type II receptors. By contrast, Activin A can bind type II receptors when SB-431542 is present. We show ActRIIA-Fc and Follistatin rescued BMP-2 and/or BMP-7 signaling in the presence of Activin A, but SB-431542 did not. The antagonist function of Activin A thus can be suppressed by blocking Activin A binding to type II receptors, but not by inhibiting its signal transduction cascade. As Activin A, BMP-2 and BMP-7 share type II receptors and bind receptors at the same site, we speculated that Activin A is a competitive BMP inhibitor that blocks the weak BMP-type II receptor interaction (Fig. 5-8). Indeed, Activin A prevented BMP-7 binding to ActRIIA *in vitro*, providing direct evidence for a competitive inhibitor function. Notably, binding competition and signaling antagonism are not new concepts in the TGF- β family. Functional antagonism was described for the Activin A/BMP-7 pairing in human embryonic carcinoma cells (30) and for the GDF-8/BMP-7 pairing in C3H10T1/2 cells (68). Inhibin A, an Activin A related ligand that lacks signaling activity, inhibited BMP responses by competing for type II receptor binding (35-37). Binding competition was also proposed for some BMPs together with type II receptors (69), for Activin A combined with type I receptors (70), and for Activin A with BMP-9 (33). We propose that binding-competition and signaling antagonism is a common regulatory mechanism in the TGF- β family enabled by receptor promiscuity and binding site conservation (19).

TGF- β family ligands play critical roles in many human diseases, including cancer, fibrosis, bone loss, and muscle loss (10). It is suggested elevated ligand expression leads to hyper-activation of their canonical signaling pathways and, consequently, to disease onset

and progression (71). However, the ability of a TGF- β family ligand to hyper-activate its signaling pathways can be limited; TGF- β family ligands can have a ‘signaling ceiling’. On the other hand, we found that ‘high affinity’ ligands like Activin A, attenuated or antagonized signaling pathways that were activated by ‘lower affinity’ ligands like BMP-2 and BMP-7. Thus, while hyper-activated signaling could occur in the appropriate context and may be the root cause of a number of diseases, we speculate binding-competition and signaling antagonism between ligands could also play a role in the pathobiology of Activin A and other TGF- β family ligands. Significantly, a recent study indicated Activin A mediated progression of fibrodysplasia ossificans progressive (FOP) by competing for type I receptor binding (70).

Inhibiting Activin A signaling has considerable therapeutic potential. Several approaches have been explored, including blocking the receptor kinase activity with SB-431542, and preventing formation of Activin A-receptor signaling complexes using ActRIIA-Fc (55-57, 72). Both SB-431542 and ActRIIA-Fc inhibited Activin A signaling, as determined by SMAD2/3 phosphorylation and SMAD2/3 mediated luciferase expression. But they differed drastically in their ability to prevent Activin A antagonism. Only extracellular Activin A inhibitors rescued low affinity ligand signaling. As Activin A could either hyper-activate its canonical signaling pathway or antagonize low affinity BMP signaling in disease, our findings indicate selection of an appropriate therapeutic approach to inhibit Activin A signaling should depend on the mechanism of pathogenesis. Even so, extracellular inhibitors that target ligands and prevent receptor binding offer a more defined approach for rescuing the effects of excess ligand in disease.

In sum, we show that high affinity TGF- β family ligands like Activin A compete with low affinity ligands for receptor binding and antagonize low affinity ligand signaling. Several

diseases associate with Activin A overexpression, including inflammation, fibrosis and cancer related muscle wasting (39, 40, 73). How elevated Activin A levels lead to disease is not well understood. It is thought hyper-activated signaling causes pathogenesis. But our findings indicate a second possibility. Namely, ectopic Activin A could antagonize normal signaling, and thus promote disease. Significantly, a recent study indicated Activin A antagonism may be critical for progression of fibrodysplasia ossificans progressiva (70).

REFERENCES

REFERENCES

1. Moustakas, A., and Heldin, C. H. (2009) The regulation of TGF-beta signal transduction. *Development* **136**, 3699-3714.
2. Wrana, J. L. (2013) Signaling by the TGF-beta superfamily. *Cold Spring Harbor Perspectives in Biology* **5**, a011197.
3. Massague, J. (1998) TGF-beta signal transduction. *Annual Review of Biochemistry* **67**, 753-791.
4. Shi, Y., and Massague, J. (2003) Mechanisms of TGF-beta signaling from cell membrane to the nucleus. *Cell* **113**, 685-700.
5. Wrana, J. L., Attisano, L., Wieser, R., Ventura, F., and Massague, J. (1994) Mechanism of activation of the TGF-beta receptor. *Nature* **370**, 341-347.
6. Wrana, J. L., Attisano, L., Carcamo, J., Zentella, A., Doody, J., Laiho, M., Wang, X. F., and Massague, J. (1992) TGF-beta signals through a heteromeric protein kinase receptor complex. *Cell* **71**, 1003-1014.
7. Weber, D., Kotzsch, A., Nickel, J., Harth, S., Seher, A., Mueller, U., Sebald, W., and Mueller, T. D. (2007) A silent H-bond can be mutationally activated for high-affinity interaction of BMP-2 and activin type IIB receptor. *BMC Structural Biology* **7**, 6.
8. Groppe, J., Hinck, C. S., Samavarchi-Tehrani, P., Zubieta, C., Schuermann, J. P., Taylor, A. B., Schwarz, P. M., Wrana, J. L., and Hinck, A. P. (2008) Cooperative assembly of TGF-beta superfamily signaling complexes is mediated by two disparate mechanisms and distinct modes of receptor binding. *Molecular Cell* **29**, 157-168.
9. Townson, S. A., Martinez-Hackert, E., Greppi, C., Lowden, P., Sako, D., Liu, J., Ucran, J. A., Liharska, K., Underwood, K. W., Sehra, J., Kumar, R., and Grinberg, A. V. (2012) Specificity and structure of a high affinity activin receptor-like kinase 1 (ALK1) signaling complex. *The Journal of Biological Chemistry* **287**, 27313-27325.
10. Massague, J. (2012) TGF-beta signalling in context. *Nature Reviews: Molecular Cell Biology* **13**, 616-630.
11. Caja, L., Kahata, K., and Moustakas, A. (2012) Context-dependent action of transforming growth factor-beta family members on normal and cancer stem cells. *Current Pharmaceutical Design* **18**, 4072-4086.
12. Oshimori, N., and Fuchs, E. (2012) The harmonies played by TGF-beta in stem cell biology. *Cell Stem Cell* **11**, 751-764.

13. Wu, M. Y., and Hill, C. S. (2009) TGF-beta superfamily signaling in embryonic development and homeostasis. *Developmental Cell* **16**, 329-343.
14. Heldin, C. H., Landstrom, M., and Moustakas, A. (2009) Mechanism of TGF-beta signaling to growth arrest, apoptosis, and epithelial-mesenchymal transition. *Current Opinion in Cell Biology* **21**, 166-176.
15. Huminiecki, L., Goldovsky, L., Freilich, S., Moustakas, A., Ouzounis, C., and Heldin, C. H. (2009) Emergence, development and diversification of the TGF-beta signalling pathway within the animal kingdom. *BMC Evolutionary Biology* **9**, 28.
16. Sako, D., Grinberg, A. V., Liu, J., Davies, M. V., Castonguay, R., Maniatis, S., Andreucci, A. J., Pobre, E. G., Tomkinson, K. N., Monnell, T. E., Ucran, J. A., Martinez-Hackert, E., Pearsall, R. S., Underwood, K. W., Seehra, J., and Kumar, R. (2010) Characterization of the ligand binding functionality of the extracellular domain of activin receptor type IIB. *The Journal of Biological Chemistry* **285**, 21037-21048.
17. Cash, J. N., Rejon, C. A., McPherron, A. C., Bernard, D. J., and Thompson, T. B. (2009) The structure of myostatin:follistatin 288: Insights into receptor utilization and heparin binding. *Embo Journal* **28**, 2662-2676.
18. Aykul, S., Ni, W., Mutatu, W., and Martinez-Hackert, E. (2015) Human cerberus prevents nodal-receptor binding, inhibits nodal signaling, and suppresses nodal-mediated phenotypes. *PLoS One* **10**, e0114954.
19. Sebald, W., Nickel, J., Zhang, J. L., and Mueller, T. D. (2004) Molecular recognition in bone morphogenetic protein (BMP)/receptor interaction. *Biological Chemistry* **385**, 697-710.
20. Rosenzweig, B. L., Imamura, T., Okadome, T., Cox, G. N., Yamashita, H., ten Dijke, P., Heldin, C. H., and Miyazono, K. (1995) Cloning and characterization of a human type II receptor for bone morphogenetic proteins. *Proceedings of the National Academy of Sciences of the United States of America* **92**, 7632-7636.
21. Attisano, L., Wrana, J. L., Montalvo, E., and Massague, J. (1996) Activation of signalling by the activin receptor complex. *Molecular and Cellular Biology* **16**, 1066-1073.
22. Kirsch, T., Sebald, W., and Dreyer, M. K. (2000) Crystal structure of the BMP-2-BRIA ectodomain complex. *Nature Structural Biology* **7**, 492-496.
23. David, L., Mallet, C., Mazerbourg, S., Feige, J. J., and Bailly, S. (2007) Identification of BMP-9 and BMP-10 as functional activators of the orphan activin receptor-like kinase 1 (ALK1) in endothelial cells. *Blood* **109**, 1953-1961.

24. Scharpfenecker, M., van Dinther, M., Liu, Z., van Bezooijen, R. L., Zhao, Q., Pukac, L., Lowik, C. W., and ten Dijke, P. (2007) BMP-9 signals via ALK1 and inhibits bFGF-induced endothelial cell proliferation and VEGF-stimulated angiogenesis. *Journal of Cell Science* **120**, 964-972.
25. Mitchell, D., Pobre, E. G., Mulivor, A. W., Grinberg, A. V., Castonguay, R., Monnell, T. E., Solban, N., Ucran, J. A., Pearsall, R. S., Underwood, K. W., Seehra, J., and Kumar, R. (2010) ALK1-Fc inhibits multiple mediators of angiogenesis and suppresses tumor growth. *Molecular Cancer Therapeutics* **9**, 379-388.
26. Greenwald, J., Groppe, J., Gray, P., Wiater, E., Kwiatkowski, W., Vale, W., and Choe, S. (2003) The BMP-7/ActRII extracellular domain complex provides new insights into the cooperative nature of receptor assembly. *Molecular Cell* **11**, 605-617.
27. Hinck, A. P. (2012) Structural studies of the TGF-betas and their receptors - insights into evolution of the TGF-beta superfamily. *FEBS Letter* **586**, 1860-1870.
28. Rejon, C. A., Hancock, M. A., Li, Y. N., Thompson, T. B., Hebert, T. E., and Bernard, D. J. (2013) Activins bind and signal via bone morphogenetic protein receptor type II (BMPRII) in immortalized gonadotrope-like cells. *Cellular Signalling* **25**, 2717-2726.
29. Aykul, S., and Martinez-Hackert, E. (2016) New ligand binding function of human cerberus and the role of proteolytic processing in regulating ligand-receptor interactions and antagonist activity. *Journal of Molecular Biology* **428**, 590-602.
30. Piek, E., Afrakhte, M., Sampath, K., van Zoelen, E. J., Heldin, C. H., and ten Dijke, P. (1999) Functional antagonism between activin and osteogenic protein-1 in human embryonal carcinoma cells. *Journal of Cellular Physiology* **180**, 141-149.
31. Gamer, L. W., Nove, J., Levin, M., and Rosen, V. (2005) BMP-3 is a novel inhibitor of both activin and BMP-4 signaling in *Xenopus* embryos. *Developmental Biology* **285**, 156-168.
32. Kokabu, S., Gamer, L., Cox, K., Lowery, J., Tsuji, K., Raz, R., Economides, A., Katagiri, T., and Rosen, V. (2012) BMP-3 suppresses osteoblast differentiation of bone marrow stromal cells via interaction with acvr2b. *Molecular Endocrinology* **26**, 87-94.
33. Olsen, O. E., Wader, K. F., Hella, H., Mylin, A. K., Turesson, I., Nesthus, I., Waage, A., Sundan, A., and Holien, T. (2015) Activin A inhibits BMP-signaling by binding ACVR2A and ACVR2B. *Cell Communication and Signaling* **13**, 27.
34. Klammert, U., Mueller, T. D., Hellmann, T. V., Wuerzler, K. K., Kotzsch, A., Schliermann, A., Schmitz, W., Kuebler, A. C., Sebald, W., and Nickel, J. (2015) GDF-5 can act as a context-dependent BMP-2 antagonist. *BMC Biology* **13**, 77.

35. Wiater, E., and Vale, W. (2003) Inhibin is an antagonist of bone morphogenetic protein signaling. *The Journal of Biological Chemistry* **278**, 7934-7941.
36. Martens, J. W., de Winter, J. P., Timmerman, M. A., McLuskey, A., van Schaik, R. H., Themmen, A. P., and de Jong, F. H. (1997) Inhibin interferes with activin signaling at the level of the activin receptor complex in Chinese hamster ovary cells. *Endocrinology* **138**, 2928-2936.
37. Lebrun, J. J., and Vale, W. W. (1997) Activin and inhibin have antagonistic effects on ligand-dependent heteromerization of the type I and type II activin receptors and human erythroid differentiation. *Molecular and Cellular Biology* **17**, 1682-1691.
38. Werner, S., and Grose, R. (2003) Regulation of wound healing by growth factors and cytokines. *Physiological Reviews* **83**, 835-870.
39. Chen, J. L., Walton, K. L., Winbanks, C. E., Murphy, K. T., Thomson, R. E., Mankanji, Y., Qian, H., Lynch, G. S., Harrison, C. A., and Gregorevic, P. (2014) Elevated expression of activins promotes muscle wasting and cachexia. *FASEB Journal* **28**, 1711-1723.
40. Zhou, X., Wang, J. L., Lu, J., Song, Y., Kwak, K. S., Jiao, Q., Rosenfeld, R., Chen, Q., Boone, T., Simonet, W. S., Lacey, D. L., Goldberg, A. L., and Han, H. Q. (2010) Reversal of cancer cachexia and muscle wasting by ActRIIB antagonism leads to prolonged survival. *Cell* **142**, 531-543.
41. Baker, J. M., and Boyce, F. M. (2014) High-throughput functional screening using a homemade dual-glow luciferase assay. *Journal of Visualized Experiments : JoVE*.
42. Harada, K., Shintani, Y., Sakamoto, Y., Wakatsuki, M., Shitsukawa, K., and Saito, S. (1996) Serum immunoreactive activin A levels in normal subjects and patients with various diseases. *The Journal of Clinical Endocrinology and Metabolism* **81**, 2125-2130.
43. Suragani, R. N., Cadena, S. M., Cawley, S. M., Sako, D., Mitchell, D., Li, R., Davies, M. V., Alexander, M. J., Devine, M., Loveday, K. S., Underwood, K. W., Grinberg, A. V., Quisel, J. D., Chopra, R., Pearsall, R. S., Sehra, J., and Kumar, R. (2014) Transforming growth factor-beta superfamily ligand trap ACE-536 corrects anemia by promoting late-stage erythropoiesis. *Nature Medicine* **20**, 408-414.
44. Kropf, J., Schurek, J. O., Wollner, A., and Gressner, A. M. (1997) Immunological measurement of transforming growth factor-beta 1 (TGF-beta1) in blood; assay development and comparison. *Clinical Chemistry* **43**, 1965-1974.

45. De Crescenzo, G., Pham, P. L., Durocher, Y., and O'Connor-McCourt, M. D. (2003) Transforming growth factor-beta (TGF-beta) binding to the extracellular domain of the type II TGF-beta receptor: receptor capture on a biosensor surface using a new coiled-coil capture system demonstrates that avidity contributes significantly to high affinity binding. *Journal of Molecular Biology* **328**, 1173-1183.
46. Baardsnes, J., Hinck, C. S., Hinck, A. P., and O'Connor-McCourt, M. D. (2009) TbetaR-II discriminates the high- and low-affinity TGF-beta isoforms via two hydrogen-bonded ion pairs. *Biochemistry* **48**, 2146-2155.
47. Schmierer, B., and Hill, C. S. (2007) TGFbeta-SMAD signal transduction: molecular specificity and functional flexibility. *Nature Reviews: Molecular Cell Biology* **8**, 970-982.
48. Korchynskyi, O., and ten Dijke, P. (2002) Identification and functional characterization of distinct critically important bone morphogenetic protein-specific response elements in the Id1 promoter. *The Journal of Biological Chemistry* **277**, 4883-4891.
49. Zawel, L., Dai, J. L., Buckhaults, P., Zhou, S., Kinzler, K. W., Vogelstein, B., and Kern, S. E. (1998) Human SMAD3 and SMAD4 are sequence-specific transcription activators. *Molecular Cell* **1**, 611-617.
50. Liu, I. M., Schilling, S. H., Knouse, K. A., Choy, L., Derynck, R., and Wang, X. F. (2009) TGF-beta-stimulated SMAD1/5 phosphorylation requires the ALK5 L45 loop and mediates the pro-migratory TGF-beta switch. *Embo Journal* **28**, 88-98.
51. Daly, A. C., Randall, R. A., and Hill, C. S. (2008) Transforming growth factor beta-induced SMAD1/5 phosphorylation in epithelial cells is mediated by novel receptor complexes and is essential for anchorage-independent growth. *Molecular and Cellular Biology* **28**, 6889-6902.
52. Wrighton, K. H., Lin, X., Yu, P. B., and Feng, X. H. (2009) Transforming growth factor beta can stimulate SMAD1 phosphorylation independently of bone morphogenic protein receptors. *The Journal of Biological Chemistry* **284**, 9755-9763.
53. Kirkbride, K. C., Townsend, T. A., Bruinsma, M. W., Barnett, J. V., and Blobe, G. C. (2008) Bone morphogenetic proteins signal through the transforming growth factor-beta type III receptor. *The Journal of Biological Chemistry* **283**, 7628-7637.
54. Lopez-Casillas, F., Wrana, J. L., and Massague, J. (1993) Betaglycan presents ligand to the TGF-beta signaling receptor. *Cell* **73**, 1435-1444.

55. Pearsall, R. S., Canalis, E., Cornwall-Brady, M., Underwood, K. W., Haigis, B., Ucran, J., Kumar, R., Pobre, E., Grinberg, A., Werner, E. D., Glatt, V., Stadmeier, L., Smith, D., Seehra, J., and Bouxsein, M. L. (2008) A soluble activin type IIA receptor induces bone formation and improves skeletal integrity. *Proceedings of the National Academy of Sciences of the United States of America* **105**, 7082-7087.
56. Laping, N. J., Grygielko, E., Mathur, A., Butter, S., Bomberger, J., Tweed, C., Martin, W., Fornwald, J., Lehr, R., Harling, J., Gaster, L., Callahan, J. F., and Olson, B. A. (2002) Inhibition of transforming growth factor (TGF)-beta1-induced extracellular matrix with a novel inhibitor of the TGF-beta type I receptor kinase activity: SB-431542. *Molecular Pharmacology* **62**, 58-64.
57. Inman, G. J., Nicolas, F. J., Callahan, J. F., Harling, J. D., Gaster, L. M., Reith, A. D., Laping, N. J., and Hill, C. S. (2002) SB-431542 is a potent and specific inhibitor of transforming growth factor-beta superfamily type I activin receptor-like kinase (ALK) receptors ALK4, ALK5, and ALK7. *Molecular Pharmacology* **62**, 65-74.
58. Amthor, H., Christ, B., Rashid-Doubell, F., Kemp, C. F., Lang, E., and Patel, K. (2002) Follistatin regulates bone morphogenetic protein-7 (BMP-7) activity to stimulate embryonic muscle growth. *Developmental Biology* **243**, 115-127.
59. Iemura, S., Yamamoto, T. S., Takagi, C., Uchiyama, H., Natsume, T., Shimasaki, S., Sugino, H., and Ueno, N. (1998) Direct binding of follistatin to a complex of bone-morphogenetic protein and its receptor inhibits ventral and epidermal cell fates in early *Xenopus* embryo. *Proceedings of the National Academy of Sciences of the United States of America* **95**, 9337-9342.
60. Massague, J. (2000) How cells read TGF-beta signals. *Nature Reviews. Molecular Cell Biology* **1**, 169-178.
61. de Kretser, D. M., O'Hehir, R. E., Hardy, C. L., and Hedger, M. P. (2012) The roles of activin A and its binding protein, follistatin, in inflammation and tissue repair. *Molecular and Cellular Endocrinology* **359**, 101-106.
62. Phillips, D. J., de Kretser, D. M., and Hedger, M. P. (2009) Activin and related proteins in inflammation: not just interested bystanders. *Cytokine and Growth Factor Reviews* **20**, 153-164.
63. Moura, J., da Silva, L., Cruz, M. T., and Carvalho, E. (2013) Molecular and cellular mechanisms of bone morphogenetic proteins and activins in the skin: Potential benefits for wound healing. *Archives of Dermatological Research* **305**, 557-569.
64. Werner, S., and Alzheimer, C. (2006) Roles of activin in tissue repair, fibrosis, and inflammatory disease. *Cytokine and Growth Factor Reviews* **17**, 157-171.

65. Hully, J. R., Chang, L., Schwall, R. H., Widmer, H. R., Terrell, T. G., and Gillett, N. A. (1994) Induction of apoptosis in the murine liver with recombinant human activin A. *Hepatology* **20**, 854-862.
66. Chen, Y. G., Lui, H. M., Lin, S. L., Lee, J. M., and Ying, S. Y. (2002) Regulation of cell proliferation, apoptosis, and carcinogenesis by activin. *Experimental Biology and Medicine* **227**, 75-87.
67. Thompson, T. B., Lerch, T. F., Cook, R. W., Woodruff, T. K., and Jardetzky, T. S. (2005) The structure of the follistatin:activin complex reveals antagonism of both type I and type II receptor binding. *Developmental Cell* **9**, 535-543.
68. Rebbapragada, A., Benchabane, H., Wrana, J. L., Celeste, A. J., and Attisano, L. (2003) Myostatin signals through a transforming growth factor beta-like signaling pathway to block adipogenesis. *Molecular and Cellular Biology* **23**, 7230-7242.
69. Lowery, J. W., Intini, G., Gamer, L., Lotinun, S., Salazar, V. S., Ote, S., Cox, K., Baron, R., and Rosen, V. (2015) Loss of BMPR2 leads to high bone mass due to increased osteoblast activity. *Journal of Cell Science* **128**, 1308-1315.
70. Hatsell, S. J., Idone, V., Wolken, D. M., Huang, L., Kim, H. J., Wang, L., Wen, X., Nannuru, K. C., Jimenez, J., Xie, L., Das, N., Makhoul, G., Chernomorsky, R., D'Ambrosio, D., Corpina, R. A., Schoenherr, C. J., Feeley, K., Yu, P. B., Yancopoulos, G. D., Murphy, A. J., and Economides, A. N. (2015) ACVR1R206H receptor mutation causes fibrodysplasia ossificans progressiva by imparting responsiveness to activin A. *Science Translational Medicine* **7**, 303ra137.
71. Saunier, E. F., and Akhurst, R. J. (2006) TGF beta inhibition for cancer therapy. *Current Cancer Drug Targets* **6**, 565-578.
72. Ruckle, J., Jacobs, M., Kramer, W., Pearsall, A. E., Kumar, R., Underwood, K. W., Seehra, J., Yang, Y., Condon, C. H., and Sherman, M. L. (2009) Single-dose, randomized, double-blind, placebo-controlled study of ACE-011 (ActRIIA-IgG1) in postmenopausal women. *Journal of Bone and Mineral Research* **24**, 744-752.
73. Antsiferova, M., and Werner, S. (2012) The bright and the dark sides of activin in wound healing and cancer. *Journal of Cell Science* **125**, 3929-3937.
74. Thompson, T. B., Woodruff, T. K., and Jardetzky, T. S. (2003) Structures of an ActRIIB:activin A complex reveal a novel binding mode for TGF-beta ligand:receptor interactions. *Embo Journal* **22**, 1555-1566.

CHAPTER 6 –

FUTURE PERSPECTIVES

Discover how Cerberus suppresses breast cancer cell migration and invasion

In chapter 3, we discovered that human Cerberus suppresses migration, invasion and colony formation of triple negative MDA-MB-231 and BT549 breast cancer cell. This effect is unique to Cerberus because other tested TGF- β family inhibitors (at least alone) didn't have this suppressive effect on the tested cell lines (chapter 4). In chapter 3 and 4, we demonstrated that human Cerberus is a specific inhibitor of the TGF- β family ligands Nodal, BMP-4, Activin B and BMP-6. The tested Cerberus responsive breast cancer cell lines overexpress Nodal, BMP-4 and RGMb (one of the RGM co-receptors that has roles in BMP signaling potentiation). It has been also known that Nodal and BMP-4 are overexpressed in several breast cancer types, and both have key roles in breast cancer progression and metastasis. By considering this information, we could hypothesize that Cerberus suppresses migration, invasion and colony formation in MDA-MB-231 and BT-549 by blocking Nodal and/or BMP-4 signaling or RGM potentiated Nodal and/or BMP-4 signaling. In order to test this hypothesis, we need to probe the specific roles of these ligands and in combination with co-receptor by knocking down the expression of them in these two cell lines and by overexpressing them in non-invasive T47D breast cancer cell line or non-invasive mammary epithelial cell line MCF10A. The effect of both knockdown and overexpression of ligands alone and in combination with co-receptor should be tested in signaling, migration and invasion assays to understand which combination contributes to invasive breast cancer cell phenotypes and be affected by Cerberus treatment. These studies will help identify biomarkers associated with breast cancer cell invasion and Cerberus responsiveness, and might reveal new targets for breast cancer treatment.

Establish the effect of Cerberus *in vivo*

In addition to determining the molecular basis of Cerberus effect *in vitro*, it is also critical to expand its function to *in vivo* studies to potentially consider it as a therapeutic agent in the future. The good start point would be testing the function of Cerberus on orthotopic tumor growth and spontaneous metastasis by using Cerberus sensitive human breast cancer cell line MDA-MB-231. By considering the other *in vivo* studies done with similar proteins, up to 10 mg/ml Cerberus-Fc (in PBS) can be injected twice a week to tumor implanted mice. After 4 weeks of treatment (or when tumor volume reaches the maximum limit), the effect of Cerberus on the growth of orthotopic tumors will be determined by analyzing tumor volumes, and the effect of Cerberus on the spontaneous metastasis from orthotopic tumors will be determined by examining the number of lung and liver surface nodules from the organs. This study will provide direct evidence for Cerberus function as a growth, invasion and/or colonization inhibitor at least in one animal model. Furthermore, this study will help understand which step (growth or metastasis) Cerberus is effective on and create the connection with *in vitro* studies.

Determine how EGF-CFC family members recognize TGF- β family ligands

In chapter 2, we showed that EGF-CFC family member Cripto-1 has a dual function. In the soluble form, Cripto-1 prevents the assembly of the signaling complex and antagonizes the downstream signaling, but its membrane-anchored form has a signal potentiating activity. In order to determine how Cripto-1 or other EGF-CFC family members recognize ligands, we need to have structural information. Unfortunately, there is no available crystal or NMR structure of any EGF-CFC family member. This is mostly because these molecules are composed of multiple domains, they are very flexible, and it is hard to obtain the active form

of them and their ligands. Our biochemical studies showed that Cripto-1 binds BMP-4, and Cryptic binds Activin B with high affinity. In order to reveal the basis of EGF-CFC family ligand recognition, the crystallization of Cripto-1 – BMP-4 and Cryptic – Activin B complexes will be tried. This structural study (in combination with mutagenesis studies) will help understand how EGF-CFC family co-receptors recognize TGF- β family ligands and create a correlation with biophysical studies. Because Cripto-1 is overexpressed in many cancer types, it would be very beneficial to obtain Cripto-1 – BMP-4 or Cripto-1 – Nodal structure to create inhibitors targeting the ligand binding surfaces.